UNIVERSITY OF LONDON THESIS

Degree PhD Year 2006 Name of Author POLLARD Patrick John

Genetic and Functional Analysis of Tumourigenesis in Hereditary Leiomyomatosis and Renal Cell Cancer and Hereditary Paragangliomatosis Syndromes

Patrick John Pollard

A thesis Submitted for the Degree of
Doctor of Philosophy in the
University of London

March 2006

Molecular and Population Genetics Laboratory
Cancer Research UK – London Research Institute

ProQuest LLC
789 East Eisenhower Parkway
P.O. Box 1346
Ann Arbor, MI 48106-1346

Abstract

Hereditary leiomyomatosis and renal cell cancer (HLRCC) and hereditary paragangliomatosis (HPGL) are familial cancer syndromes, caused by germline mutations in genes encoding the Tricarboxylic Acid Cycle (TCAC) enzymes fumarate hydratase (FH) and succinate dehydrogenase (SDH) respectively. Both *FH* and *SDH* function as tumour-suppressor genes and the conditions are inherited as autosomal dominant traits. Germline *FH* mutations predispose individuals to develop benign smooth muscle tumours of the skin and uterus (leiomyomas) and renal carcinoma, whilst individuals with mutations in *SDHB*, *-C*, and *–D* develop paragangliomas and phaeochromocytomas. In order to study the genetic and functional consequences of *FH* and *SDH* mutations, and to elucidate mechanisms of tumourigenesis, which are poorly understood, I have undertaken a comprehensive analysis of tumours from both HPGL and HLRCC patients, using gene and protein expression analysis, metabolomic profiling and cytogenetic analysis of HPGL tumours. Tumours from both syndromes over-express hypoxia-inducible factor-alpha (HIF1α), the central signalling protein in hypoxia, and HIF1α-target genes including vascular endothelial growth factor (*VEGF*) and Bcl-2/adenovirus E1B 19 kDa-interacting protein 3 (*BNIP3*). HLRCC and HPGL tumours accumulate the TCAC intermediates succinate and fumarate which have been shown to up-regulate HIF1α *in vitro* by inhibiting the prolyl hydroxylases (PHD) that target HIF1α for proteosomal degradation. Therefore, 'pseudo-hypoxia' - the constitutive expression of HIF1α in normoxic conditions - is likely to contribute largely to the tumourigenesis of HLRCC and HPGL and is most likely to occur as a direct result of accumulation of TCAC intermediates and PHD inhibition. To further investigate the tumourigenesis of HLRCC, I have successfully created a conditional *Fh1* (the mouse homologue of human *FH*) mouse knockout which causes hypertrophy when targeted to smooth muscle. I aim to create further temporal and tissue specific knockouts of *Fh1*, and if these mice develop tumours provide a model of HLRCC for the testing of anti-cancer drugs and therapies.

Dedication

I wish to dedicate this thesis to my parents Brian and Jane Pollard, and to my fiancé Jackie Pickering who have supported and encouraged me with loving care throughout my Ph.D. and to my son Joseph Pollard who has provided me with much happiness and inspiration since his birth in January 2004.

Acknowledgements

I would like to acknowledge my supervisor Professor Ian Tomlinson for his help, support and intellectual input into my Ph.D. during my time in the Molecular and Population Genetics Laboratory. I would also like to acknowledge my second supervisor Dr. Axel Behrens, thesis committee supervisor Professor Gordon Stamp and Graduate student advisor, Nancy Hogg for their advice. I would also like to acknowledge the Research Services at the London Research Institute, notably Richard Poulsom and George Elia (Histopathology), Ken Blight (Electron Microscopy), Bradley Spencer-Dene and Emma Nye (Experimental Pathology), Ian Rosewell, Sunita Varsani-Brown, Alison Martin and the animal technicians (Transgenic Services), Aengus Stuart, Gavin Kelly, Mike Mitchell, Simon Tomlinson and Phil East (Bioinformatics and Biostatistics), Graham Clarke and David Phillips (Equipment Park), Darren Harvey and Matthew Pellowe (Cell Services) and Kimberley Howarth, Andrew Rowan, Angela Jones, Luis Carvajal and Pat Gorman (Molecular Population Genetics Laboratory) for their assistance in experimental techniques and Noel Wortham for his Rasmol modelling. I would like to acknowledge my collaborators, Shirley Hodgson, Yuen-Li Chung, John Griffiths and Julian Barwell (St. Georges Hospital), Simon Olpin (Sheffield Children's Hospital), Pierre Rustin (INSERM, Paris), Helen Cox (Guy's Hospital), and multiple surgeons, genetic Councillors and dermatologists for providing DNA, tumour samples and clinical data. I would like to acknowledge Peter Sheehan for help with the formatting of this thesis

I would also like to acknowledge my close friends: Mark Frigerio, Chris Morris, Jonathan Green and Niall Galbraith who have provided lots of encouragement and moral support during my Ph.D. and the writing of my thesis.

Abbreviations

HLRCC	-	Hereditary Leiomyomatosis and Renal Cell Cancer
HPGL	-	Hereditary Paragangliomatosis
TCAC	-	Tricarboxylic acid cycle (Krebs cycle)
PGL	-	Paraganglioma
PCC	-	Phaeochromocytoma
UL	-	Uterine Leiomyoma
SKL	-	Skin Leiomyoma
RCC	-	Renal Cell Carcinoma
FH	-	Fumarate hydratase
SDHx	-	Succinate Dehydrogenase, x = A,B,C or D subunit
TSC1 / TSC2	-	Tuberous sclerosis 1 / Tuberous sclerosis 2
BHD	-	Birt-Hogg-Dube syndrome
VHL	-	von Hippel-Lindau disease
MEN	-	Multiple Endocrine Neoplasia
ATS-DL	-	Alport syndrome-diffuse leiomyomatosis
RET	-	ret proto-oncogene
VEGF	-	Vascular endothelial growth factor
TSP1	-	Thrombospondin 1
BNIP3	-	BCL2/adenovirus E1B 19kDa interacting protein 3
HIF-1α/β subunit	-	Hypoxia Inducible Factor 1 – alpha subunit / beta
ARNT	-	Aryl hydrocarbon receptor nuclear translocator
EPAS1	-	endothelial PAS domain protein 1 (also called HIF-2α)
EM	-	Electron microscopy
ISH	-	*in situ* hybridisation
IHC	-	Immunohistochemistry
GBM	-	Glomerular basement membranes
CBP	-	cAMP-response-element-binding protein
CREB	-	CREB-binding protein
CTAD	-	Carboxy-terminal transactivation domain
FIH1	-	Factor inhibiting HIF1

NTAD	-	Amino-terminal transactivation domain
ODDD	-	Oxygen-dependent degradation domain
EPO	-	Erythropoietin
FFs	-	Fibrofolliculomas
FLCN	-	Folliculin
RCND	-	Renal cystadenocarcinoma and nodular dermafibrosis
PRT	-	Proximal renal tubules
PEPCK	-	Phosphoenolpyruvate carboxykinase
RET	-	The rearranged during transfection proto-oncogene
RTK	-	Receptor tyrosine kinase
C-cell	-	Calcitonin-producing cell
NF1	-	Neurofibromatosis type I
ROS	-	Reactive oxygen species
Bcl2	-	B-cell leukaemia / lymphoma 2 protein
ETC	-	Electron transport chain
HEK	-	Human embryonic kidney
mtDNA	-	Mitochondrial DNA
ATP	-	Adenosine tri-phosphate
ADP	-	Adenosine di-phosphate
FAD	-	flavin adenine dinucleotide
NAD	-	nicotinamide adenine dinucleotide
COX1	-	Cytochrome oxidase sub-unit 1
PHD	-	Prolyl hydroxylase enzyme
α-KG	-	alpha-ketoglutarate
siRNA	-	small interfering RNA
mTOR	-	mammalian target of rapamycin
PI3K	-	phosphoatidylinositol 3-kinase
SOD	-	superoxide dismutase
FACS	-	Fluorescent-assisted cell sorting
$(\Delta)\Psi_M$	-	(Change) in mitochondrial membrane potential

Contents

Figures

Tables

1 Chapter 1: Introduction

1.1 Cancer predisposition

Individuals differ in their inherited tendency to develop cancer. Major single gene defects that cause early onset cancer have been known for many years from their inheritance patterns, and inherited defects that have weaker effects on predisposition were also expected to exist. Over the recent decade, with the explosion of genomic sequence and molecular profiling, vast advances have been made in understanding the complexity of human malignancies and identifying specific loci that are involved in cancer progression. Many of these loci have key roles in DNA repair, cell-cycle control and cell-death (apoptotic) pathways. The loci are frequently mutated somatically through tumour progression and sometimes also contain inherited mutations. Genetic and quantitative population-genetics analysis provides a framework for understanding the frequency of inherited mutations and the consequences of these mutations for increased predisposition to cancer.

Tumour cells contain many different genes that may be aberrant in structure or copy number and even larger numbers that may be differentially expressed. These aberrant genes can be classified as either oncogenes or tumour-suppressor genes (TSGs).

1.1.1 Oncogenes and Tumour-suppressor genes

Oncogenes are genes that play a normal role in the cell as proto-oncogenes but if they become mutated or amplified (increase in copy number per cell) contribute to the growth of a tumour. Some examples of oncogenes are *RAS* (which encodes a signal transduction molecule), *MYC* (which encodes a transcription factor) and c-*SRC* (which encodes protein tyrosine kinase. An example of a proto-oncogene mutating to become an oncogene is *k-RAS*, where oncogenic activation can arise from mutations in codons 12 and 13 in many adenocarcinomas (Wei, Liang et al. 2005). In colon cancer, codon 12 mutations in *k-RAS* contributes to tumourigenesis by increasing wnt signalling (Li, Mizukami et al. 2005). In tumours, increased copy number of proto-oncogenes (or amplification of chromosomal regions in tumours encompassing proto-oncogenes) is also an important mechanism of oncogene activation in various cancers; for example amplification and over-expression of *l-MYC* in ovarian cancer (Wu, Lin et al. 2003).

TSGs are 'protective' genes that limit the growth of tumours. When TSGs become mutated, they may fail to stop (or contribute towards) the growth of a tumour. An example of a TSG is *BRCA1*, the first breast cancer gene to be mapped (Hall, Lee et al. 1990). In order for mutated TSGs to promote tumour growth, the wild-type allele is frequently lost causing loss of heterozygosity (LOH). This was observed in *BRCA1* mutation carriers with breast cancer (Smith, Easton et al. 1992; Kelsell, Black et al. 1993). In these cases, LOH was a result of loss of part of the wild-type chromosome encompassing *BRCA1*. LOH often occurs by chromosomal loss or deletion, but can also occur as a result of mitotic recombination or non-dysjunction for example in some retinoblastomas (Hagstrom and Dryja 1999).

1.1.2 Cancer predisposition genes and penetrance

Cancer susceptibility genes often vary in penetrance i.e. the likelihood that a mutated allele will result in disease. Many familial cancer genes with high-penetrance mutations have been identified but the contribution of low-penetrance genetic variants to the risk of developing sporadic cancer remains relatively unclear. Knudson's hypothesis (Knudson 1971) and its' molecular confirmation in retinoblastoma (*RB1*) (Figure 1.1) (Friend, Bernards et al. 1986) indicated that cancer predisposition genes were rare, mutated alleles that greatly increased the risk of cancer when inherited through the germline. The result of this was multiple cases of malignancies in families. Genetic linkage and positional cloning was used to identify such genes. RB1 was identified as a key-signalling molecule (Weinberg 1995) as was p53 (encoded by *TP53*), which was subsequently found to function as a germline-inherited tumour predisposition gene (Malkin, Li et al. 1990). High-penetrance alleles have provided fundamental insights into various aspects of cancer biology and include the identification of the Adenomatosis polyposis coli (*APC*) gene, β-catenin and Tcf4 pathway (Kinzler 2002), pathways involved in DNA repair/checkpoint pathways including the products of the breast cancer-associated genes *BRCA1* and *BRCA2* (Venkitaraman 2002) and PTEN; a phosphatase that is implicated in Cowden syndrome in the development of a variety of tumour types (Stambolic, Suzuki et al. 1998; Eng 2002).

The above examples of high-penetrance genes that show Mendelian inheritance are easy to identify, and many of the loci that are associated with a high level of risk have been already identified. However, assessment of the importance of alleles with lower penetrance or later onset is more difficult. For example, most of the familial excess in breast and colorectal cancers is due to unknown genes (Ponder 2001). Even though the remaining familial risk could be due to high-penetrance mutations in as yet unidentified genes, multiple-case cancer families have failed to reveal significant linkage to novel loci. A possible explanation is a polygenic mechanism (Peto 2002) (Pharoah, Antoniou et al. 2002) which proposes that a large number of alleles each conferring a small genetic risk combine additively or multiplicatively to

confer a range of susceptibilities in the population. There are various types of sequence changes that act as low-penetrance alleles such as carcinogen metabolism polymorphisms (e.g. *CYP1A1*) (Drakoulis, Cascorbi et al. 1994), anti-tumour immune response genes (e.g. *TNF1α*) (Demeter, Porzsolt et al. 1997). These would act globally whilst others would affect the local tumour environment through epithelial interactions (e.g. *APOE*) (Slattery, Sweeney et al. 2005) or within the cell metabolically (e.g. *MTHFR*) (Takehara, Kawakami et al. 2005) or through DNA repair or genomic stability (e.g. *CHEK2*) (Meijers-Heijboer, van den Ouweland et al. 2002; Johnson, Junewick et al. 2005)

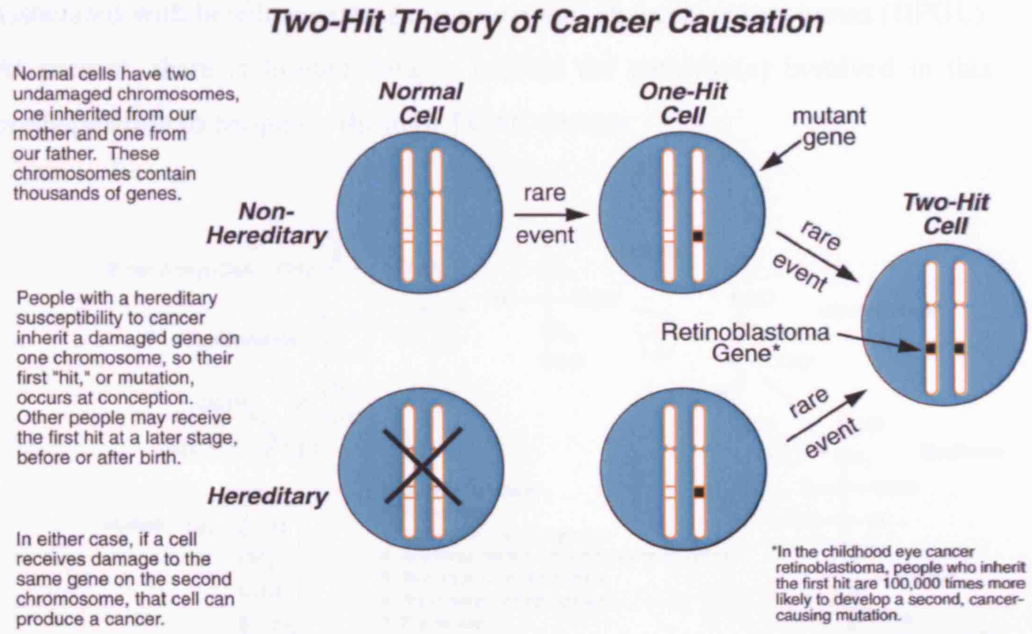

Figure 1.1 Knudson's two-hit theory of cancer causation

Knudson's two-hit theory of cancer causation using the Retinoblastoma gene as an example. This figure was reproduced from (http://www.fccc.edu/research/programs/advisors/knudson/two-hit.html)

1.2 Genes encoding enzymes of the Tricarboxylic Acid Cycle and familial cancer

Recently, heterozygous germline mutations in two enzymes of the tricarboxylic acid cycle (TCAC) have been shown to predispose individuals to tumour development. The two enzymes, Fumarate hydratase (FH) and Succinate dehydrogenase (SDH) (Figure1.2) are ubiquitously expressed, playing a vital role in ATP production through the mitochondrial respiratory chain. Germline mutations in *FH* are associated with hereditary leiomyomatosis and renal cell carcinoma (HLRCC), whilst *SDH* mutations are associated with hereditary paragangliomas and phaeochromocytomas (HPGL). At present, there is limited data to explain the pathway(s) involved in this predisposition to neoplasia through TCAC defects.

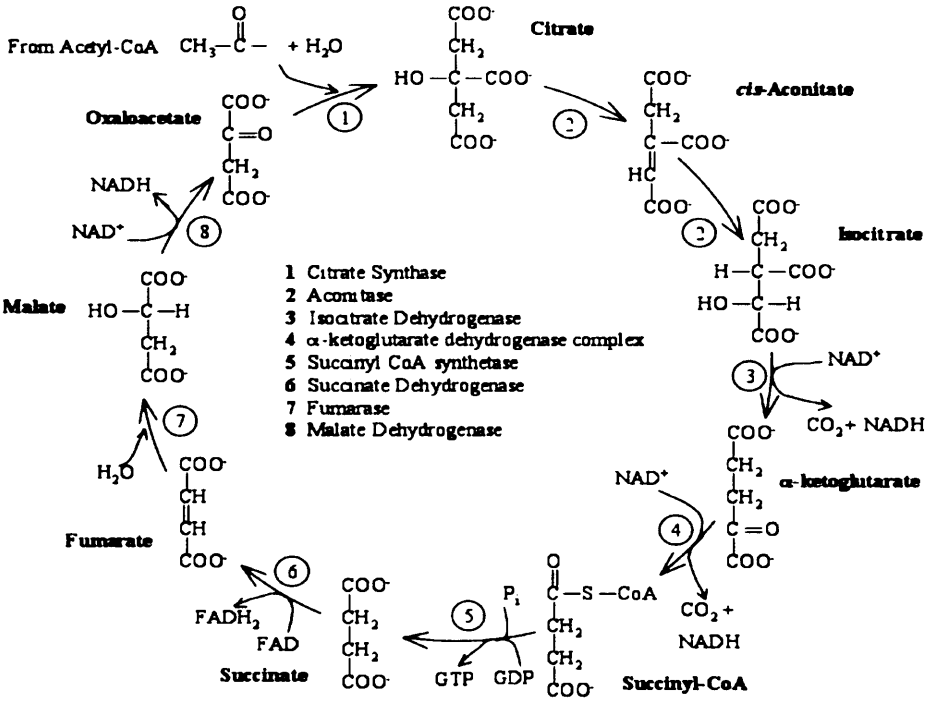

Figure 1.2 The Tricarboxylic Acid Cycle.

The reactions are catalysed by the enzymes as numbered in the diagram. Succinate dehydrogenase (6) and Fumarate hydratase (7) catalyse sequential steps within the cycle.

1.2.1 Hereditary Leiomyomatosis and Renal Cell Cancer

The HLRCC locus was originally defined as the *MCUL1* gene localised to 1q42.3-q43 (Alam, Bevan et al. 2001). The authors undertook a genome wide screen of 11 families segregating dominant transmission of multiple cutaneous and uterine leiomyomas (Figure 1.3). Details of affection status were derived either from personal examination or from histopathology reports and medical records and, wherever possible, were confirmed by histological review of tumours. Fresh-frozen samples were obtained from eight cutaneous leiomyomata from the families. MCUL (multiple cutanous and uterine leiomyomata) was modelled as a dominant trait with a gene frequency of 0.001 and only individuals with skin lesions were classified as affected. Individuals with uterine fibroids but without skin lesions were classified as unknown, to take account of the population prevalence of uterine fibroids and, hence, the relatively high probability of phenocopies from this source. Individuals without skin lesions who married into a family were classified as unaffected and other family members were classified as unknown. The 11 families consisted of 54 affected individuals, and DNA samples were obtained from 44 of these. Skin lesions presented at an age between the early teens and the 4th decade and tended to occur in crops on the trunk and limbs. All patients studied were >18 years old (median 47 years, range 28–91 years). Most patients reported that one or more lesions, especially larger ones, were painful in heat or cold. Between individuals, there was notable variation in the number of skin lesions. Of the 36 females affected by skin leiomyomata, 33 reported a history of fibroids; in all cases, these fibroids were confirmed as multiple lesions, some of which measured only a few millimetres in diameter (Figure 1.3a).

The initial genome screen detected eight regions with two-point LOD scores >1, with a maximum score of 1.84 (recombination fraction [θ] 0.001) at marker D1S547 (1.42.3-q43). Additional typing of markers in these eight regions formally excluded all but the region near D1S547. A maximum two-point LOD score of 2.99 was obtained with marker D1S2785 (θ= 0 04). By means of a sliding map of three markers, multipoint LOD scores were

calculated across the region around D1S547 and D1S2785. The maximum multipoint LOD score obtained was 5.40, for the markers D1S2785–3.2cM–D1S547–0.01cM–D1S404. In family 304 alone, the maximum multipoint LOD score obtained was 3.97 at D1S404, for these same markers.

Haplotype construction showed that, except for pedigree 123, all the families studied were compatible with linkage of MCUL to chromosome 1q42.3-q43. When data from this family were excluded, haplotype analysis placed the MCUL gene within a ~14-cM interval bounded, on the centromeric side, by D1S517 and, on the telomeric side, by D1S2842. Both the critical recombinations defining this region occurred in the large family, 304. As expected, the authors found in the 14-cM region no good evidence of haplotype sharing between families.

Of 33 females with the disease-associated haplotype, 25 (75.8%) had both skin leiomyomata and uterine fibroids, 3 (9.1%) had skin leiomyomata only (although occult fibroids were not excluded), 1 (3.03%) (a member of family 304, who was age 33 years at the time of the study) had uterine fibroids only, and 4 (12.1%) (who were ages 28, 34, 35, and 67 years at the time of the study) were unaffected. One female (a member of family 14) with uterine fibroids did not share the disease-associated haplotype and had developed an unknown number of fibroids during her late 40s; she presumably represented a sporadic case. Of 16 males who had the disease-associated haplotype, 13 (81.3%) had developed skin leiomyomata; the unaffected carriers were ages 33, 35, and 36 years. The disease gene appeared, therefore, to have high penetrance.

The authors observed allelic loss in MCUL tumours indicative of it acting as a TSG. A similar investigation of an MCUL family with 7 affected kindred associated familial cutaneous leiomyomatosis with papillary renal cell cancer (Kiuru, Launonen et al. 2001) and further bioinformatic analysis and screening of transcripts in the minimal region identified mutations in the nuclear-encoded TCAC enzyme *FH* in individuals with leiomyomatosis and the rare Type II papillary renal cell carcinoma; a condition now described as HLRCC (hereditary leiomyomatosis and renal cell cancer) (Tomlinson, Alam

et al. 2002). This study confirmed the tumour-suppressor function of *FH*, showed reduced activity of FH in lymphoblastoid lines from HLRCC patients and low or absent FH activity in tumours from individuals with leiomyomatosis. Further genetic and functional analysis of HLRCC revealed that protein-truncating (nonsense) *FH* mutations are functionally null alleles and disease-associated missense mutations map to highly conserved residues, mostly around the enzymes active site or activation domain (Alam, Rowan et al. 2003). Further studies have identified HLRCC families with aggressive solitary unilateral renal cell cancers of both type II papillary (Toro, Nickerson et al. 2003; Chan, Wong et al. 2005; Wei, Toure et al. 2005) and collecting duct morphology (Toro, Nickerson et al. 2003; Wei, Toure et al. 2005). Occurrence of *FH* mutations in individuals with somatic leiomyomatosis is very rare (Barker, Bevan et al. 2002; Kiuru, Lehtonen et al. 2002) though recently 2 cases of bi-allelic *FH* mutations have been reported in non-syndromic leiomyoma (Lehtonen, Kiuru et al. 2004). Despite the aggressive nature of the renal tumours in HLRCC families, malignancies of leiomyomas i.e. leiomyosarcomas are very rare (Kiuru, Lehtonen et al. 2002).

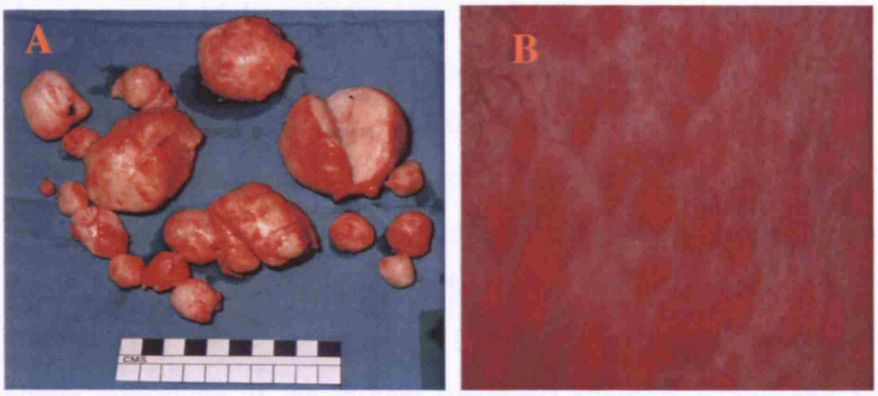

Figure 1.3 Leiomyomata from hereditary leiomyomatosis and renal cell cancer patients.

Uterine leiomyomata (fibroids) (A) are the most common tumours in women during the reproductive years and the most frequent cause for hysterectomy in pre-menopausal women. Symptoms include abnormal uterine bleeding, pelvic pain and reproductive dysfunction. Each square on the ruler is 1cm. Skin leiomyomata (B) are usually 2-20mm (maximum 50mm) and vary from well-circumscribed red nodules to ill defined, flesh coloured papules.

1.2.2 Hereditary Paragangliomatosis

Fumarate hydratase is the second TCAC enzyme to be linked to an inherited family cancer syndrome. Heterozygous germline mutations in genes encoding the three non-catalytic subunits of complex II (SDHB, -C, and –D) have previously been identified in HPGL, where individuals inherit paragangliomas (PGLs) and phaeochromocytomas (PCCs) (Baysal, Ferrell et al. 2000; Niemann and Muller 2000; Astuti, Latif et al. 2001; Baysal 2002; Gimenez-Roqueplo, Favier et al. 2002; Neumann, Bausch et al. 2002; Benn, Croxson et al. 2003; Niemann, Muller et al. 2003). The former are highly vascularised, non-chromaffin tumours most commonly occurring at the bifurcation of the carotid artery (Figure 1.4) whilst the latter are catecholamine-producing, chromaffin tumours arising principally in the adrenal medulla. In HPGL, *SDHD* mutations are associated with multiple, but mostly benign, PGLs and PCCs. *SDHB* mutations are associated with a higher proportion of malignant lesions and a relatively greater risk of PCC (Neumann, Pawlu et al. 2004). *SDHC* mutations appear to be uncommon (Niemann and Muller 2000). Like HLRCC, the 'second hit' in most HPGL tumours associated with *SDHB* and *SDHC* mutations occurs by loss of the wild-type allele. However, *SDHD* associated HPGL is more complex. Affected females were observed not to transmit the disease to their offspring and this was attributed to imprinting i.e. transmission of an already silenced allele thus having no functional effect even if mutated (reviewed in (Niikawa 1997)). This theory is supported by literature showing evidence of mono-allelic expression of the mutant (paternal) allele in a PGL and no apparent LOH at the site of the *SDHD* mutation (Badenhop, Cherian et al. 2001). However, conflicting data has shown bi-allelic expression of *SDHD* in brain, lymphoid and kidney tissues (Baysal, Ferrell et al. 2000) and studies of allelic loss in HPGL suggest that loss of wildtype allele occurs exclusively in the chief cell (predominant cell type of a gland) component of paragangliomas (van Schothorst, Beekman et al. 1998). Another theory is that *SDHD*-associated HPGL occurs as a result of a somatic genetic mechanism targeting both the *SDHD* gene on 11q23 and a paternally imprinted gene on 11p15.5. In this study by Hensen *et al.*, allelic loss was shown to be exclusively maternal

and the authors propose that loss of maternal chromosome 11 (probably through non-disjunction) combined with loss of the wt *SDHD* allele is sufficient to drive tumourigenesis (Hensen, Jordanova et al. 2004). Therefore paternal transmission of HPGL could occur as a somatic genetic mechanism targeting both *SDHD* (11q23) and a paternally imprinted gene (11p15.5), rather than imprinting of *SDHD*.

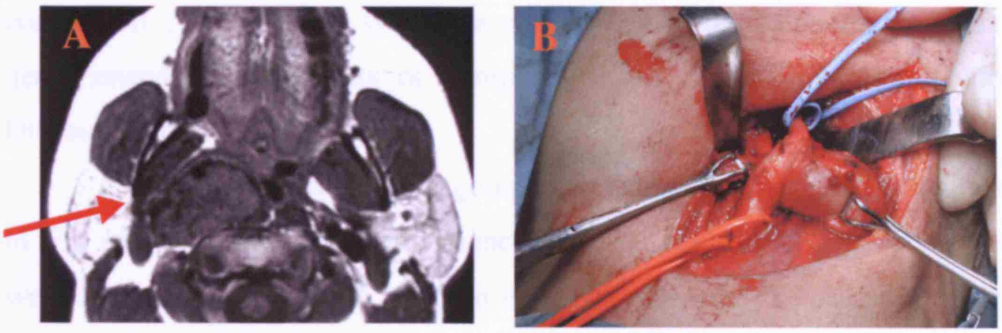

Figure 1.4 Clinical features of HPGL

Magnetic resonance imaging scan (A) and subsequent surgical removal (B) of a carotid body paraganglioma. The tumour in (A) is indicated by the red arrow.

1.3 The recessive disorders Leigh syndrome and fumarase deficiency

Germline heterozygous mutations in *FH* and *SDHB*,-*C* and -*D*, cause HLRCC and HPGL respectively; both genes acting as classical TSGs and are inherited in an autosomal dominant manner. However, there are recessive genetic disorders resulting from homozygous or bi-allelic mutations in both *FH* (FH deficiency) and *SDHA* (Leigh syndrome). The first report of a nuclear-encoded gene mutation causing mitochondrial respiratory chain deficiency in humans was in 1995 and involved the SDHA flavoprotein (Bourgeron, Rustin et al. 1995). The two children with homozygous mutations presented with classic symptoms of the neurologlical disease Leigh Syndrome (Leigh 1951). Leigh syndrome is an early-onset progressive neurodegenerative

disorder with a characteristic neuropathology consisting of focal, bilateral lesions in one or more areas of the central nervous system, including the brainstem, thalamus, basal ganglia, cerebellum, and spinal cord. The lesions are areas of demyelination, gliosis, necrosis, spongiosis, or capillary proliferation. Clinical symptoms depend on which areas of the central nervous system are involved. The most common underlying cause is a defect in oxidative phosphorylation (Dahl 1998), and, as well as genes encoding complex II (SDH), Leigh syndrome can arise from mutations in complex genes encoding components of complexes I, III, IV and V (Schon and DiMauro 2003)

Children born with homozygous or compound heterozygous mutations in *FH* suffer from fumarase deficiency. Clinical features of this syndrome were first described in 1986 by Zinn *et al.* who reported the case of a male infant with mitochondrial encephalopathy at 1 month of age with failure to thrive, developmental delay, hypotonia, cerebral atrophy, lactic and pyruvic acidemia, and fumaric aciduria; the patient died at 8 months of age (Zinn, Kerr et al. 1986). Mitochondria isolated from skeletal muscle showed selective defects in the oxidation of glutamate and succinate, whereas isolated liver mitochondria oxidized these normally. Fumarase activity was virtually absent in mitochondria from both sources. Homogenates of liver and muscle also showed very much reduced fumarase activity, indicating that the cytosolic form of the enzyme was also deficient in these tissues. Organ differences in intramitochondrial accumulation of fumarase were thought to account for the selective oxidative defects observed in skeletal muscle but not in liver mitochondria (Zinn, Kerr et al. 1986). Petrova-Benedict *et al.* reported a case of fumarase deficiency in a 6 month old mentally retarded child with delayed development, microcephaly and hypotonia. In this case, fumarase was deficient in both the mitochondrial and the cytosolic compartments, with the latter more severely affected (Petrova-Benedict, Robinson et al. 1987). Gellera *et al.* described the clinical features of fumarase deficiency in a 7-month old boy who died in a demented state after a clinical course characterized by generalized seizures, psychomotor deterioration, and fumaric aciduria. Again, marked deficiency of both mitochondrial and cytosolic fumarases was found;

in skeletal muscle, brain, cerebellum, heart, kidney, liver, and cultured fibroblasts and anti-fumarase cross-reacting material was present in negligible amounts in these tissues. (Gellera, Uziel et al. 1990). Mutations in *FH* in fumarase deficiency patients were first identified in 1993 by Coughlin *et al.* who identified a homozygous (A265T) mutation in a patient with fumarase deficiency (Coughlin 1993). In 1994, Bourgeron *et al.* identified a homozygous (E319G) mutation in the fumarase gene in 2 patients with progressive encephalopathy associated with fumarase deficiency (Bourgeron, Chretien et al. 1994).

1.4 Association of the mitochondrial genome with cancer

The mitochondrial genome differs from that of the nuclear in many ways (Summarised in Table 1.1). In addition, the polyploidy nature of the mitochondrial genome (up to several thousand copies per cell) is an important feature of mitochondrial genetics and may give rise to either homoplasmy, when all copies of the mitochondrial genome are identical, or heteroplasmy, when there is a mixture of two or more mitocohondrial genotypes. In most individuals there is no evidence of homoplasmy indicating that mtDNA is constantly undergoing mutation, with clonal expansion or loss of either point mutations or deletions (Coller, Khrapko et al. 2001; Taylor, Barron et al. 2003). In heteroplasmy, there is a threshold level of mutation that is important for both the clinical expression of the disease and for biochemical defects.

The only report to date of familial cancer related to a mutation in the mitochondrial genome is the association of multiple symmetric lipomatosis with the A8344G mutation in the tRNA(lys) gene and impairs mitochondrial protein synthesis causing respiratory chain dysfunction.(Gamez, Playan et al. 1998). This mutation is also associated with inherited myclonic epilepsy and ragged-red fibre disease (MERFF) (Shoffner, Lott et al. 1990) However, in this reported case, the proband lacked manifestations of MERFF and the distribution of the mutation was unusual in that the proportion of mutated

mitochondrial genomes was higher in the blood and lipomas than in the muscle tissue.

The presence of somatic mtDNA mutations in solid human tumours was first described in colon cancer and in most cases the mtDNA mutations had accumulated to homoplasmic levels and were absent from the matched 'normal' tissue from the same patient (Polyak, Li et al. 1998). Subsequent studies have identified somatic mtDNA mutations in prostate cancer (Jeronimo, Nomoto et al. 2001), bladder, head and neck and lung primary tumours (Fliss, Usadel et al. 2000), pancreatic cancer (Jones, Song et al. 2001), uterine serous carcinoma (Pejovic, Ladner et al. 2004), and gliobalstoma (Kirches, Krause et al. 2001). As yet, no causal relationship between mtDNA mutations and tumourigenesis has been established, although a recent study of high frequency of somatic mutations on thyroid carcinomas revealed novel mutations in genes located in complex I of the mitochondrial genome. These mutations changed the highly conserved amino acid residues of their corresponding proteins, resulting in severe defect of activity of Complex I (Abu-Amero, Alzahrani et al. 2005). Given that mtDNA mutations are present in the benign multinodular hyperplasia, mutations of mitochondrial genes might be involved in the early stage of tumour development.

FH and SDH are both nuclear-encoded enzymes that function within the mitochondria and it is plausible that mutations in these genes will cause generation of ROS and mtDNA mutations, thereby contributing to the tumourigenesis of HPGL and HLRCC. This will be discussed later (Section 1.10).

Characteristic	Nuclear Genome	Mitochondrial genome
Size	~3.3 x 10^9bp	16,569 bp
DNA molecules / cell	Haploid –23 Diploid – 46	Several 1000's per cell (polyploidy)
Number of genes encoded	~ 20,000 – 30,000	37 (13 polypeptides, 22 tRNAs and 2 rRNAs)
Introns	Very frequent	Absent
Percentage of coding DNA	~3%	~93%
Inheritance Mode	Mendelian inheritance for autosomes and the X chromosome; paternal inheritance for the Y chromosome	Exclusively maternal

Table 1.1 Comparison between the human nuclear and mitochondrial genome.

(Adapted from 'Mitochondrial DNA mutations in human disease' (Taylor and Turnbull 2005)).

1.5 Loss or severe reduction in FH and SDH activity causes tumourigenesis

Both *FH* and *SDH* are arguably unlikely genes to be involved in tumour predisposition due to their vital roles in energy (ATP) production. Nevertheless, both seem to act as classical tumour suppressor loci. Truncating germline mutations have been found in *FH* (Tomlinson, Alam et al. 2002; Toro, Nickerson et al. 2003; Wei, Toure et al. 2005) and in *SDHB, -C* and *-D* (Gimenez-Roqueplo, Favier et al. 2001; Neumann, Bausch et al. 2002; Niemann, Muller et al. 2003) as have whole-gene deletions (Tomlinson, Alam

et al. 2002). Most of these changes clearly abolish protein function. Missense changes are, however, the most common type of germline mutation for all four genes and studies have been undertaken to assess the functional effects of these changes (Alam, Olpin et al. 2005).

The FH enzyme exists as a homotetramer containing four possible catalytic sites involved in conversion of fumarate to malate (Weaver, Levitt et al. 1993; Weaver, Levitt et al. 1995; Weaver and Banaszak 1996). In addition to this, a non-catalytic, regulatory site has been identified, with a substrate affinity 1-2 fold lower than the catalytic site (Beeckmans and Van Driessche 1998). Several lines of evidence show that missense *FH* mutations act to abolish or greatly reduce enzyme function: FH deficiency patients with missense mutations have greatly reduced FH activity, as do MCUL patients with heterozygous germline mutations; tumours from MCUL patients have very low FH activity, owing to loss of the germline wildtype allele in most cases; and most missense changes map to highly conserved residues involved in forming the active site or maintaining protein structure (Figure 1.5) (Alam, Rowan et al. 2003). Some pathogenic missense *FH* mutations are, however, associated with the retention of some catalytic activity, showing that tumourigenesis does not require complete absence of function (Alam, Rowan et al. 2003). Mutations causing severe phenotypic effects are probably under-represented in FH deficiency because they are lethal *in utero*.

Figure 1.5 Mapping of HLRCC (MCUL) and FH deficiency mutations onto the crystal structure of *E. coli* fumC.

(A) Active and activation site residues. (B) HLRCC mutations in relation to active site residues. Both figures show location of mutations within the monomer. Figure reproduced from (Alam, Rowan et al. 2003).

The SDH enzyme exists as a trimer of heterotetramers, each tetramer containing one copy of each of the four subunits, A-D, with each subunit playing an individual role within the protein (Figure 1.6). SDHA is a flavoprotein possessing the catalytic activity to oxidise succinate to fumarate, passing the electron on to the incorporated FAD group. SDHB contains a number of iron-sulphur (Fe-S) clusters, which pass the electrons through the protein towards the ubiquinone molecule bound by the membrane-bound subunits SDHC and SDHD, which also bind a haem b group (Yankovskaya, Horsefield et al. 2003).

The effects of mutations in genes coding for the SDHA and SDHD subunits on the catalytic activity of the enzyme have been studied. Mutations in the SDHA subunit are missense changes and do not result in a complete loss of SDH activity (Bourgeron, Rustin et al. 1995; Parfait, Chretien et al. 2000), perhaps explaining why *SDHA* mutant/wild-type heterozygotes appear not to develop tumours. It seems likely that both missense and protein-truncating *SDHB* and *D* mutations lead to greatly reduced or absent complex II activity (Gimenez-Roqueplo, Favier et al. 2001; Gimenez-Roqueplo, Favier et al. 2002; Douwes Dekker, Hogendoorn et al. 2003). Effects of mutations of *SDHC* on SDH activity have not been as extensively studied, and so the consequences of the mutations are less certain. However, they are probably associated with loss of the wild type allele, resulting in reduced or absent complex II activity.

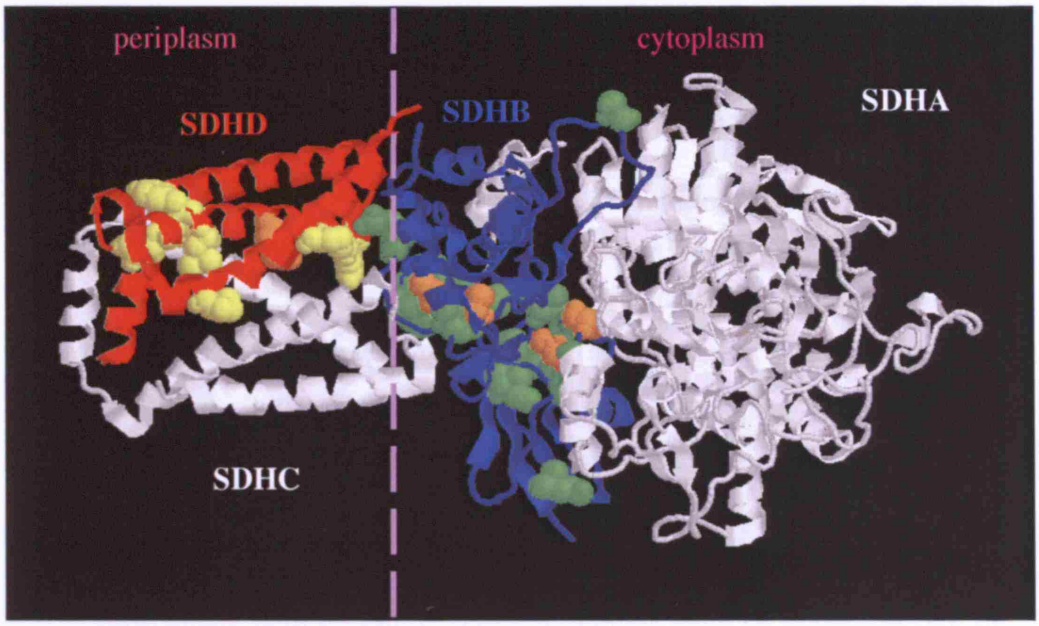

Figure 1.6 Structure of *E. coli* SQR monomer.

SQR SdhA, SdhB, SdhC and SdhD subunits are labelled. The FeS clusters are orange; missense mutations in SdhB and SdhD are green and yellow respectively. The cytoplasm / periplasm boundary is indicated by the dashed line.

1.6 Genotype-phenotype associations for HLRCC and HPGL

There has been no convincing genotype-phenotype association for *FH* and HLRCC and in particular, no specific type of mutation associated with the development of RCCs. *FH* mutations associated with RCC have been 111insA, 138+1G>C, R58P, R58X, L89S, S102X, H153R, c181del2bp, R190C, R190H, R300X, N318K, S376P and Q396P (Tomlinson, Alam et al. 2002; Alam, Rowan et al. 2003; Toro, Nickerson et al. 2003; Kiuru and Launonen 2004; Alam, Barclay et al. 2005; Chan, Wong et al. 2005; Wei, Toure et al. 2005). The presence of modifier genes or environment may explain the cases of renal cancers in HLRCC families. Additionally, UK HLRCC families were selected on the basis of leiomyomata not RCC and this, with the possibility that many may not have been screened for RCC may

account for the apparently increased occurrence of RCC in Finnish and American families.

The phenotype-genotype correlation for *SDH* and HPGL is more complex; each of the four SDH subunits differs in structure and function. Additionally, protein truncating SDH mutations almost certainly cause the whole of complex II to malfunction, whilst the majority of missense *SDHD* mutations probably abrogate quinine or Haem B binding (Yankovskaya, Horsefield et al. 2003). Immuno-electron microscopy has suggested that almost all PGLs resulting from *SDH* mutations show retention of SDHA and loss of SDHB, suggesting that missense mutations cause failure of complex II (Douwes Dekker, Hogendoorn et al. 2003).

Individuals with germline *SDHB* mutations have an increased risk of adrenal PCC and lower risk of carotid body PGL compared with carriers of *SDHD* mutations but the latter are more likely to develop multi-focal tumours (Neumann, Pawlu et al. 2004). *SDHB* mutation carriers may also have increased risk of malignancy especially in extra-adrenal PCCs (Gimenez-Roqueplo, Favier et al. 2003; Neumann, Pawlu et al. 2004). To date, there has only been one report of a *SDHD*-associated malignancy (Milunsky, Maher et al. 2001). Due to the rarity of *SDHC* mutations in HPGL, a similar genotype-phenotype comparison cannot be made. Within *SDHD*, it has been suggested that mutations at the 5' end of the gene are associated with a higher risk of PCC, probably due to the fact that 5' missense mutations only cause partial loss of complex II function (Eng, Kiuru et al. 2003). However, other reports suggesting that all *SD*H-mutant PGLs lose SDHB i.e. all tumour-associated SDH mutations are essentially null alleles (Douwes Dekker, Hogendoorn et al. 2003) conflict with this data and the HPGL genotype-phenotype associations described above.

1.7 *Fumarate hydratase* and *Succinate dehydrogenase* mutations in common cancers

Only a small number of the common cancers have been tested for germline and somatic mutations in *FH* and *SDH*. Breast cancer patients in Finland (n=85) were selected based on positive family or personal history for malignancies associated with HLRCC and screened for germline *FH* mutations, but none were found (Kiuru, Lehtonen et al. 2005). A similar study involving individuals with prostate cancer also revealed an absence of *FH* mutations (Kiuru, Lehtonen et al. 2002). More recently however, a thorough examination of cancer risk and tumour spectrum in Finnish *FH* mutation-positive families was carried out and genealogical and cancer data were obtained from 868 individuals. The overall cancer risk was statistically significantly increased in the age group of 15-29 years, consistent with features of cancer predisposition families in general. *FH* germline mutations were found in 55% of studied individuals. Most RCCs and ULMSs displayed biallelic inactivation of FH, as well as breast and bladder cancers. In addition, several benign tumours including atypical uterine leiomyomas, kidney cysts and adrenal gland adenomas were observed (Lehtonen, Kiuru et al. 2005). A recent screen for somatic *SDHB* mutations in a variety of renal cancers also proved to be negative (Morris, Maina et al. 2004). Changes in mRNA and/or protein expression were not analysed in any of the above studies and therefore cannot be excluded, but it seems that any specific functional effects of *SDH* or *FH* mutations are not selected in the majority of sporadic carcinomas.

1.8 Mechanisms of tumourigenesis in HLRCC and HPGL

SDH and FH catalyse sequential steps of the TCAC (Figure 1.2). Mutations in *FH* or *SDH* predispose primarily to benign tumours, but with an increased risk of malignancy. It is therefore highly plausible that tumourigenesis should occur through some common mechanism, and that the

tissue specificity of each syndrome reflects a different metabolic derangement, which is optimal for tumourigenesis in each cell type. It is true, nevertheless, that the SDH and FH proteins perform very different roles and are structurally dissimilar; and smooth muscle neoplasms cannot be easily compared to PCC. An open mind should therefore be kept as to the possibility that it may be, at least in part, coincidence that *FH* and *SDH* mutations predispose to tumours. It may also be instructive to compare HLRCC and HPGL with other inherited conditions, such as VHL syndrome and tuberous sclerosis, which have certain phenotypic similarities, such as an overlap in tumour spectrum. These conditions and others with similarity to the HLRCC and / or HPGL syndromes are discussed below (Section 1.9), as are the effects of the disruption of these genes in animal models (Section 1.12). Similarities between mechanisms in these other syndromes and tumourigenesis of HLRCC and HPGL will be discussed later (Section 1.10).

1.9 Conditions with similarity to HLRCC and / or HPGL

1.9.1 von Hippel-Lindau syndrome

von Hippel-Lindau (VHL) disease is a dominantly inherited familial cancer syndrome predisposing to a variety of malignant and benign neoplasms, most frequently retinal, cerebellar, and spinal hemangioblastoma, RCC, PCC, and pancreatic tumours. VHL has been classified into subtypes: type 1 (without PCC); type 2 (with PCC) (Neumann 1991), and subsequently further subdivided into type 2A (with PCC); and type 2B (with PCC and renal cell carcinoma) (Brauch, Kishida et al. 1995). VHL type 2C refers to patients with isolated PCC without hemangioblastoma or renal cell carcinoma (Hoffman, Ohh et al. 2001). pVHL functions to regulate HIFα and in hypoxic conditions, the transcriptional co-activators p300 and cAMP-response-element-binding protein (CBP) bind to the carboxy-terminal transactivation domain (CTAD) of HIF1α to activate the transcription of HIF-regulated genes. However, in normoxic conditions, an asparagines residue in the CTAD is hydroxylated by Factor inhibiting HIF1 (FIH1), which prevents this

binding. Proline residues in the oxygen-dependent degradation domain (ODDD) (within the NTAD) are also hydroxylated by egg-laying-defective nine (EGLN) proteins. This facilitates the binding of the pVHL-elongin.cullin-2 complex, which mediates polyubiquitylation, and subsequent proteosomal destruction of HIF1α (Cockman, Masson et al. 2000; Cascon, Ruiz-Llorente et al. 2002; Kaelin 2002) (Figure 1.7). pVHL-defective cells are unable to degrade HIF1α and HIF-inducible mRNA's such as *VEGF*, *CAIX*, (and other angiogenic genes) and *EPO* are constitutively expressed irrespective of changes in ambient oxygen (Maher and Kaelin 1997; Wykoff, Beasley et al. 2000). This explains the high vascularity in tumours in VHL patients. The type of VHL disease, mutation type, molecular defect and clinical manifestation is summarised below (Table 1.2).

The only VHL-associated tumours that occur in HLRCC and HPGL are PCC and RCC so the role of VHL will be discussed only in those tumour types.

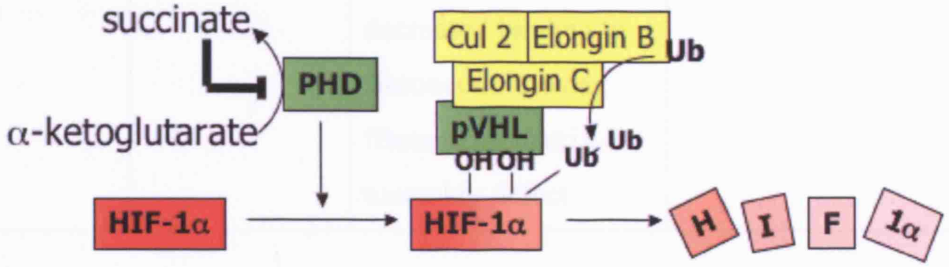

Figure 1.7 pVHL-mediated degredation of HIF-1α

Under normoxic conditions, PHD enzymes hydroxylate two proline residues on HIF-1α. This hydroxylation reaction is oxygen dependent and α-ketoglutarate is converted to succinate. The main PHD to hydroxylate HIF-1α is EGLN3. Increased succinate levels (caused by Krebs cycle blockage) are proposed to inhibit the hydroxylation reaction and therefore cause constitutative HIF-1α expression, termed 'pseudo-hypoxia'. *VHL* mutations also cause pseudo-hypoxia as pVHL cannot bind to HIF-1α and therefore mediate its degradation.

VHL disease type	*VHL* mutation type	Molecular defect	Clinical manifestation
Type I	Loss of *VHL* or a mutation that affects protein folding	Upregulation of HIF1α and HIF-target genes	Haemangioblastomas Low risk PCC RCC
Type 2A	*VHL* missense mutation	Upregulation of HIF1α and HIF-target genes	Haemangioblastomas PCC Low risk RCC
Type 2B	*VHL* missense mutation	Upregulation of HIF1α and-HIF target genes	Haemangioblastomas PCC High risk RCC
Type 2C	*VHL* missense mutation	pVHL retains ability to degrade HIF1α but decreased binding to fibronectin causing fibronectin matrix-assembly defect	Only PCC

Table 1.2 Characteristics of VHL disease

(Adapted from (Kaelin 2002)). Each VHL disease type is associated with specific types of *VHL* mutations types affecting HIF1α regulation and tumour spectrum.

1.9.1.1 Von Hippel-Lindau disease and renal cell carcinoma

VHL is mutated or silenced in >50% of sporadic clear cell RCC (Kaelin 2004). Patients with VHL disease develop neoplastic renal cysts, the epithelial cells of which have lost both copies of the *VHL* gene and can

develop into clear-cell RCC (Zhuang, Bertheau et al. 1995; Lubensky, Gnarra et al. 1996). For the conversion of the cysts to RCCs it is presumed that further genetic alterations are required and several have been described in kidney cancer including chromosomal loss at 3p14, 3p21, 5q, 6q, 10q, 11q, 17p, and 19p (Morita, Ishikawa et al. 1991; Morita, Saito et al. 1991; Foster, Crossey et al. 1994; Thrash-Bingham, Greenberg et al. 1995; Kenck, Bugert et al. 1997). The ongoing requirement for inactivation of *VHL* in RCC cells has been demonstrated by restoration of pVHL in nude mice injected with $VHL^{-/-}$ RCC cells, resulting in suppression of tumour formation (Iliopoulos, Kibel et al. 1995; Gnarra, Duan et al. 1996). Further *in vitro* evidence has demonstrated that reintroduction of pVHL into $VHL^{-/-}$ RCC cells can promote cell-cycle exit, differentiation and correct the over-production of HIF-targets, all of which may impair tumour growth *in vivo* (Chen, Kishida et al. 1995; Iliopoulos, Levy et al. 1996; Siemeister, Weindel et al. 1996; Stratmann, Krieg et al. 1997; Knebelmann, Ananth et al. 1998; Lieubeau-Teillet, Rak et al. 1998; Pause, Lee et al. 1998; Maxwell, Wiesener et al. 1999; Davidowitz, Schoenfeld et al. 2001).

1.9.1.2 Von Hippel-Lindau disease and Phaeochromocytomas

Certain germline *VHL* mutations (see Table 1.2) predispose individuals to develop PCC; however, unlike in RCC, *VHL* mutations are very rare in sporadic PCC. There is no sound explanation for this paradox but in some cases, apparently sporadic PCC have been linked, on further analysis of constitutive DNA from affected individuals, to unsuspected germline *VHL* mutations (Neumann, Berger et al. 1993; Hofstra, Stelwagen et al. 1996; Bender, Gutsche et al. 2000; Neumann, Bausch et al. 2002). It has also been suggested that PCC development in VHL disease requires a field defect i.e. an alteration such as a mutation that involves most or all of the cells in a contiguous region (field), related to VHL hemizygosity (Kaelin 2002). PCC in VHL disease differs from sporadic tumours having an earlier onset (19 years earlier – mean age of diagnosis is 28 years), is often multiple, malignancy is

less frequent and hypertension-realted symptoms are of lower occurrence (Opocher, Conton et al. 2005).

1.9.2 Birt-Hogg-Dube syndrome

Birt-Hogg-Dube syndrome (BHD) is characterised by multiple hamartomas of the hair follicle termed fibrofolliculomas (FFs) (Birt, Hogg et al. 1977). FFs are part of the triad of BHD skin lesions that also includes trichodiscomas (benign tumours of the hair disc) and arcrochordons (skin tags). BHD (also known as FLCN) is inherited in an autosomal dominant manner and has been reported to be associated with renal tumours (Roth, Rabinowitz et al. 1993; Toro, Glenn et al. 1999), spontaneous pneumothorax (Toro, Glenn et al. 1999), colon polyps and colon carcinomas (Hornstein and Knickenberg 1975; Rongioletti, Hazini et al. 1989; Le Guyadec, Dufau et al. 1998). However, more recent data indicates that a diagnosis of BHD confers a 7-fold increased risk of developing renal neoplasia and a 50-fold increased risk of spontaneous pneumothorax but no increased risk of colon polyps or cancer (Zbar, Alvord et al. 2002). Interestingly, there are a variety of histologies associated with BHD renal tumours, including chromophobe RCC, benign renal oncocytoma, clear-cell RCC and Type I papillary RCC (Pavlovich, Walther et al. 2002; Pavlovich, Grubb et al. 2005). The most common form of renal tumour seen in BHD is an oncocytoma-chromophobe hybrid tumour with areas containing both types of histology (Tickoo, Reuter et al. 1999). A mutational hotspot, a C insertion/deletion in exon 11, is frequently mutated in BHD-affected families, renal tumours developing with a higher frequency in C-insertion carriers and also more frequently in individuals who inherit a putative splice-site mutation in intron 9 (Schmidt, Nickerson et al. 2005).

1.9.3 Multiple endocrine neoplasia

Multiple endocrine neoplasia (MEN) syndromes comprise both benign and malignant hormone-secreting tumours and tumours that are not even hormone secreting (Marx 2005). MEN1 and MEN2 are the most striking in terms of hormonal excesses and will be described below due to the overlap with certain tumours in HLRCC and HPGL.

1.9.3.1 Multiple endocrine neoplasia, Type 1

MEN1 is an autosomal dominant hereditary disorder characterized by multiple parathyroid, pancreatic, duodenal, and pituitary neuroendocrine tumours. Non-endocrine mesenchymal tumours, such as lipomas, collagenomas, and angiofibromas have also been reported. *MEN1* encodes a 610-amino-acid protein termed menin which acts as a tumour-suppressor. Over expression of menin in tumour cells partially suppresses the tumour phenotype and LOH at 11q13 is evident in most MEN1 tumours (as well as in many sporadic tumours with a *MEN1* mutation on the other allele) (Marx and Stratakis 2005). *MEN1* germline mutation causes a pleiomorphic multiple neoplasia syndrome and is the gene mutated in the largest range of endocrine tumour types (summarised in Table 1.3)(Heppner, Kester et al. 1997). Leiomyoma (including uterine) have been identified in MEN1 families (Vortmeyer, Lubensky et al. 1999; McKeeby, Li et al. 2001; Ikota, Tanimoto et al. 2004). However the pathogenesis of non-neuroendocrine tumours in MEN1 is unknown and LOH is rare (McKeeby, Li et al. 2001), suggesting that the *MEN1* gene is not a significant contributor to the tumourigenesis of sporadic uterine leiomyomata.

Syndrome	Benign tumours and/or hormonal excess	Malignant tumours and/or hormonal excess	Non-hormonal neoplasia (benign or malignant)
MEN1	Islet non-secreting, pituitary non-secreting, adrenal cortex, parathyroid hormone*, prolactin*, growth hormone*, adenocorticotropic hormone	Foregut carcinoid*, gastrin#, glucagons, vasoactive intestinal polypeptide, pancreatic polypepetide	Angiofibroma, collagenoma, lipoma, leiomyoma, meningioma, ependymoma
MEN2	C-cell cancer (MTC)*, adrenal chromaffin(PCC), calcitonin*, catecholamine* parathyroid hormone	C-cell cancer, adrenal chromaffin (PCC), calcitonin, catecholamine	Neuroma* (MEN2B)

Table 1.3 MEN syndromes and their main characteristics

(Adapted from (Marx 2005)). *Important clinical feature of the syndrome. #Single most important clinical feature in any MEN.

1.9.3.2 Multiple endocrine neoplasia, Type 2 (*MEN2 / RET*)

The *RET* proto-oncogene responsible for this autosomal dominantly inherited cancer syndrome spans 60kb and encodes a protein of ~1100 amino acids which is a transmembrane receptor tyrosine kinase (RTK) (Gschwind,

Fischer et al. 2004; Santoro, Melillo et al. 2004). The commonest phenotypic variant, MEN2A, has a combination of C-cell cancer (also called medullary thyroid cancer), PCC and hyperparathyroidism (see Table 1.3) (Marx 2005). The majority of *RET* mutations in MEN2A occur in 6 cysteins in a small 25-amino-acid domain in the extracellular region (Marx and Simonds 2005). MEN2B differs in that the age of onset of C-cell cancer is much earlier and aggressive than in MEN2A and almost all *RET* mutations are confined to one cytoplasmic amino acid – M918T (Marx 2005).

It is possible that other genetic events in addition to the *RET* germline mutation may trigger tumourigenesis in PCC. In a recent study of patients with germline *RET* mutations, PCCs developed in 5/18 (28%) of carriers with mutations in codon 918, 20/68 (29%) of carriers with mutations in codon 634, 3/21 (14%) of carriers with mutations in codon 618, 2/16 (13%) of carriers with mutations in codon 620, and 2/16 (13%) of carriers with mutations in codon 791. The earliest age of manifestation for each genotype was 22, 18, 29, 22, and 39 years (Machens, Brauckhoff et al. 2005).

Hypermethylation of CpG island promoters are associated with transcriptional inactivation of tumour-suppressor genes in neoplasia. Methylation status of prominent tumour-related genes (*p16*, *PTEN*, *RASSF1 A*, *CDH1*, *MSH2*, *MLH1*, *VHL*, and *TIMP3*) was analysed in sporadic and MEN2 PCC by methylation-specific PCR. Hypermethylation was detected in 48% of PCC for *RASSF1 A*, 36 % for *MSH2*, 16% for *CDH1*, and 8% for *PTEN*. No *VHL*, *MLH1*, and *TIMP3* methylation was observed. Combined methylation of *RASSF1 A* and *p16* was found only in MEN2-related phaeochromocytomas (Dammann, Schagdarsurengin et al. 2005). Therefore, it is possible that epigenetic events, contribute, at least in part to the tumourigenesis of MEN2-related PCC.

1.9.4 Neurofibromatosis type I

Neurofibromatosis type I (NF1) is an autosomal dominant condition caused by mutations of the *NF1* gene. *NF1* comprises 60 exons and is a

tumour-suppressor gene (Legius, Marchuk et al. 1993). Due to its large size (11kb of coding sequence), extensive mutation analysis has been performed and mutations only identified in ~13% of patients with HPGL (Amar, Bertherat et al. 2005). However several point mutations have been found in exon 31 and both LOH and loss of the neurofibromin protein have been observed in PCC from patients with and without *NF1* mutations. (Gutmann, Cole et al. 1994; Lama, Graziano et al. 2004). Differences in PCC phenotype in VHL and NF1 are not very pronounced. However, in VHL, PCC has an earlier onset than in sporadic forms, it is often multiple, and malignancy is less frequent. The mean age of diagnosis is 28 years, the youngest being 5 years old. In NF1 patients, PCC phenotype is similar to sporadic forms, the mean age of PCC onset is ~42 years, ~84% of the patients have solitary adrenal tumours, ~9% have bilateral adrenal disease and ~11.5% have malignant PCC (Opocher, Conton et al. 2005).

1.9.5 Alport syndrome

Alport syndrome (ATS) is the most common inherited disease of the kidney glomerulus, occurs in X-linked and autosomal forms and is characterised by progressive kidney disease with variably associated auditory and ocular abnormalities (Kashtan and Michael 1996). Alport syndrome and diffuse leiomyomatosis (ATS-DL) occurs as rare variant of the X-linked form and presents as proliferation and thickening of the visceral smooth muscle in the gastrointestinal, respiratory and female reproductive tracts and is a cause of considerable morbitity in affected individuals (Garcia-Torres and Orozco 1993). X-linked ATS is caused by mutations in the *COL4A5* and *COL4A6* genes (two of six genes encoding the α1-α6(IV) chains of basement membrane type IV collagen). However only characteristic partial deletions of the *COL4A5-COL4A6* pair cause ATS-DL (Thielen, Barker et al. 2003). The tumours show myocyte abnormities and disorganisation of actin and desmin filaments (Garcia-Torres, Cruz et al. 2000). EM analysis of both sporadic and HLRCC UL has also shown desmin disorganisation (Wortham et al., *in press*).

1.10 HLRCC and HPGL – What links mitochondrial dysfunction and cancer?

The TCAC is an essential and fundamental process involved in the bioenergetics of cells and therefore seems it puzzling as to how its dysfunction leads to the development of tumours. Various models / pathways have been proposed, including decrease in programmed cell death (apoptosis), increased ROS or pseudo hypoxia i.e. activation of HIF and downstream targets in a normoxic state (Pollard, Wortham et al. 2003). However, it is feasible that a combination of the above may contribute to tumourigenesis in HPGL and/or HLRCC. This section will review these pathways and relate existing data to genes and their pathways identified in syndromes which encompass tumour spectra similar to HPGL / HLRCC (see Section 1.9).

The first link between defects in mitochondrial physiology and tumourigenesis was observed during the 1930's when Warburg observed a significant increase in glycolysis and lactate production in the presence of oxygen, without an accompanied increase (or decrease) in oxidative phosphorylation (Warburg 1930; Warburg 1956). This process of aerobic glycolysis has been observed in many tumour cells since this original discovery. Tumours studied with somatic (mostly homoplasmic) mtDNA mutations provided the first genetic evidence to explain aerobic glycolysis in tumour cells (Polyak, Li et al. 1998; Carew and Huang 2002). Even though some evidence suggests that mtDNA may directly promote tumourigenesis (Petros, Baumann et al. 2005), it is still not clear whether mtDNA mutations play a role in tumour development. One possible explanation for the persistent apoptosis inhibiting effect of mitochondrial dysfunction might be the upregulation of glycolysis as an alternative energy producing metabolic pathway. Because of either mtDNA mutations or inactivation of the TCAC, oxidative phosphorylation will occur at sub-optimal levels. This poses a problem for tumour cells due to their increased metabolic requirements — for example, they have increased levels of DNA and protein synthesis. When

oxidative phosphorylation is impaired, glycolytically generated ATP becomes the only other source of energy in tumour cells (Gatenby and Gillies 2004). Once induced, glycolytic enzymes could regulate other cellular processes that include the blocking of apoptosis (Majewski, Nogueira et al. 2004; Kim and Dang 2005). Therefore, by enabling cells to increase glucose metabolism, it is plausible that inactivation of mitochondrial tumour-suppressors might contribute to a persistent anti-apoptotic effect.

The biochemical pathways that may link the mitochondrial dysfunction resulting from *FH* and *SDH* mutations with HLRCC and HPGL respectively are discussed below.

1.10.1 Potential role of apoptosis in HLRCC / HPGL tumourigenenesis

Mitochondria are key regulators in many apoptotic processes (Newmeyer and Ferguson-Miller 2003) and play a central role in bioenergetics. Many apoptogenic proteins are stored in the mitochondria and released in response to the appropriate signal, and during apoptosis mitochondria have the ability to change their shape and bioenergetic performance (Karbowski and Youle 2003).

A theory for the development of tumours as a result of *FH* and *SDH* mutations is therefore that there is a decreased tendency of cells to undergo apoptosis, caused by some form of mitochondrial dysfunction. Leiomyomata are slow-growing tumours with no evidence of hyperproliferation and it may be that a relatively subtle defect in apoptosis leads to a gradual accumulation of cells dependent on the turnover of the tissue involved.

There are thought to be two mechanisms of apoptosis which have mitochondrial involvement. The better-known "energy-dependent" apoptosis utilises B-cell leukaemia / lymphoma 2 (BCL-2) family proteins such as BCL-2-associated X protein (BAX), to form pores in the mitochondrial membranes through which cytochrome C can escape to the cytoplasm to form the apoptosome with Apaf-1 and caspase 9 (McClintock, Santore et al. 2002). The

less well-known "energy-independent" form of apoptosis depends on mitochondrial dysfunction leading to permeability of the mitochondrial membrane and the release of cytochrome C, procaspases, and other pro-apoptotic factors such as endonuclease G (Eng, Kiuru et al. 2003).

As mitochondrial physiology is affected by several 'master regulators' of apoptosis (Downward 2003; Ricci, Munoz-Pinedo et al. 2004), it is possible that TCAC or electron transport chain (ETC) dysfunction may inhibit apoptosis by giving rise to apoptosis resistant cells thus playing a role in the development of tumours. Various studies have been carried out to support this model. For example, SDHC (cybL) was over-expressed in HEK cells and was found to induce apoptosis (Albayrak, Scherhammer et al. 2003). In the same study SDHC deficient CHO cells were found to be defective in response to apoptotic stimuli. Despite the problem of diminishing SDH activity by the over-expression of SDHC, this study was the first to indicate that SDH is a potential regulator of cell death. A more recent implication of SDH as an apoptotic regulator was demonstrated in a transgenic mouse cell line harbouring a Sdhc E69 (Val69Glu) mutation (Ishii, Yasuda et al. 2005). Transient reduction in SDH activity led to increased apoptosis in the culture and mitocohondrial abnormalities including increased size and disorganised cristae. Similar abnormalities have been previously reported: giant mitochondria with paracrystalline inclusions in PGL of urinary bladder (Papadimitriou and Drachenberg 1994); mitochondrial swelling and scant cristae in human PCC (Watanabe, Burnstock et al. 1976); and more recently elevated numbers of tightly packed mitochondria with abnormal morphology in SDHD-linked and sporadic PGLs (Douwes Dekker, Hogendoorn et al. 2003). However, previous literature has shown that mitochondrial have the ability to fuse in order to compensate for their dysfunction (Wakabayashi 1999; Griparic and van der Bliek 2001; Westermann 2002; Mozdy and Shaw 2003). Sdhc E69 cells maintained in culture for 3 months were injected into nude mice and produced tumours after 2 weeks. This provided the first direct *in vivo* evidence of the tumourigenic potential of chronic SDH deficiency in an animal model. The tumour size remained unchanged after 1 month suggesting the formation of benign rather then malignant tumours, resembling

the PGLs that occur in individuals harbouring *SDHC* mutations (Ishii, Yasuda et al. 2005).

Another plausible mechanism for the role of apoptotic failure in the role of HLRCC and HPGL tumourigenesis is that blockage of the TCA cycle resulting from *FH* or *SDH* mutations may cause the accumulation of metabolites from earlier steps of the cycle and other substances such as the amino acids glutamate and glutamine, derived from α-ketoglutarate. Both glutamate and glutamine play an important role in the resistance of cells to apoptosis and also in promoting cell proliferation (Mates, Perez-Gomez et al. 2002). Glutamate has been shown to rescue a breast carcinoma derived cell line (MCF-7) from apoptosis caused by glucose deprivation (Savolainen, Loikkanen et al. 1995), and also to have a proliferative effect in many cell types (Lee, Galoforo et al. 1998). Glutamine has been reported to show anti-apoptotic effects in Jurkat cells via up-regulation of glutathione and Bcl-2 (Chang, Yang et al. 2002). Hence, accumulation of glutamine and glutamate caused by a blockage in the TCA cycle may have the dual effect of cell proliferation plus protection of apoptosis. Increased glutamate concentration has been shown to exhibit a neurotoxic effect (Brecht, Gelderblom et al. 2001) and this may contribute to the encephalopathy observed in patients with FH deficiency and Leigh syndrome.

Recent *in vitro studies* have identified a common mechanism of apoptotic failure in cell lines from patients with germline *NF1*, *c-RET*, *SDH*, and *VHL* mutations, all of which cause familial PCC (Lee, Nakamura et al. 2005). Many of the sympathetic neuronal precursor cells from which PCC derive undergo c-Jun-dependent apoptosis during normal development as nerve growth factor (NGF) becomes limiting. *NF1* encodes a GTPase activating protein (GAP) for the NGF receptor TrkA, and *NF1* mutations promote survival after NGF withdrawal. Lee *et al* found that PCC-associated *c-RET* and *VHL* mutations lead to increased JunB, which blunts neuronal apoptosis after NGF withdrawal (Figure 1.8). The prolyl hydroxylase EglN3 was shown to act downstream of c-Jun and to be specifically required among the three EglN family members for apoptosis in this setting. Moreover, EglN3 proapoptotic activity was shown to require SDH activity because EglN3 is feedback inhibited by succinate. This study suggest that failure of

developmental apoptosis plays a role in PCC pathogenesis in patients with germline mutations in *NF1*, *RET*, *SDH* and *VHL*.

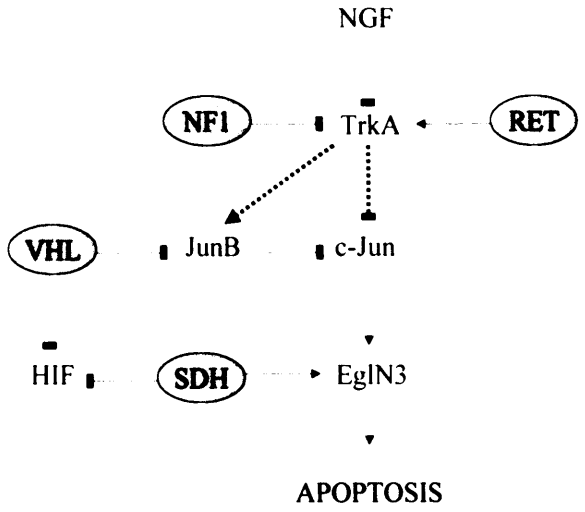

Figure 1.8 Inherited phaeochromocytoma susceptibility genes and neuronal developmental apoptosis pathways.

Germline inactivating mutations in *NF1*, *SDHB*, *SDHD* and *VHL*, and activating *RET* mutations, impair apoptosis associated with NGF withdrawal (adapted from Lee et al (Lee, Nakamura et al. 2005).

1.10.2 Potential role of redox stress in HLRCC / HPGL tuomrigeneis

The main ROS generated by the ETC is superoxide and is formed by a single electron transfer to molecular oxygen. The major sites for ROS generation are reported to be Complex I (NADH-ubiquinone oxidoreductase, and Complex III (ubiquinone-cytochrome c oxidoreductase) (Raha and Robinson 2000). Under normal physiological conditions, Complex II (SDH) is not considered a major site for ROS production. Studies of the *E.coli* SQR, analogous to mitochondrial Complex II suggest a mechanism for ROS production at the FAD site of these enzymes (Yankovskaya, Horsefield et al.

2003). SQR actually catalyses the reverse reaction and is more likely to produce ROS than SDH due to a higher electron density on the FAD thus providing more available electrons for transfer to oxygen (Messner and Imlay 2002). Even though it is possible that *SDH*-mutant tumours block the electron flow within complex II, leading to a build up of electrons on SDHA which may then be transferred directly to oxygen, it is highly unlikely that mutant SDH facilitates a reverse flow of electrons and cause ROS accumulation in HPGL tumours.

Redox studies in HPGL tumours have revealed that the catalytic activity of SDH is virtually undetectable (Gimenez-Roqueplo, Favier et al. 2001; Douwes Dekker, Hogendoorn et al. 2003). It has been suggested that this is probably due to the dissociation of the catalytic domain, comprised of SDHA and B in the tumours (Douwes Dekker, Hogendoorn et al. 2003) and it remains unclear how mutated SDH can catalyse ROS production under normoxic conditions.

Oxidative stress is, however, generally associated with cell death. Recent experiments with *C. elegans* have shown, for example, that a *mev-1* mutation in the cytb L sub-unit causes abnormal energy metabolism and superoxide production, resulting in a shorter life span (Senoo-Matsuda, Yasuda et al. 2001). In the *in vitro* studies linking SDH inactivation to apoptosis, reduction in SDH activity resulted in increased ROS production (Albayrak, Scherhammer et al. 2003; Ishii, Yasuda et al. 2005). Indeed, increased mutagenesis resulting from oxidative damage to nuclear DNA consequently converted the immortal fibroblasts into tumourigenic transformed cells (Ishii, Yasuda et al. 2005). However, despite being an attractive model for mutant-SDH-mediated tumourigenesis, the Sdhc E69 cells only became transformed after 3 months during which time wild-type fibroblasts accumulated tumourigenic potential and gave rise to more malignant tumours (tumours from the Sdhc E69 cells were benign) when injected into nude mice. Knock-down of both *SDHD* and *FH* using siRNA in HEK cells has since shown no evidence of increase ROS (Isaacs, Jung et al. 2005; Selak, Armour et al. 2005).

The strongest association between increased ROS, decreased apoptosis and tumourigenesis has been demonstrated in cells harbouring mtDNA

mutations. A pathogenic mtDNA ATP6 T8993G mutation was introduced into the PC3 prostate cancer cell line through cybrid (trans-mitochondrial hybrids) transfer and tested for tumour growth in nude mice, in order to determine whether mutant tumours had increased ROS and tumour growth rates. The resulting mutant (T8993G) cybrids were found to generate tumours that were 7 times larger than the wild-type (T8993T) cybrids, whereas the wild-type cybrids barely grew in the mice. The mutant tumours also generated significantly more ROS (Petros, Baumann et al. 2005). In a separate study, cybrids were constructed with or without a homoplasmic pathogenic point mutation at nucleotide position 8,993 or 9,176 in the mtDNA ATP synthase subunit 6 gene (*MTATP6*) derived from patients with mitochondrial encephalomyopathy. When the cybrids were transplanted into nude mice, the *MTATP6* mutations conferred an advantage in the early stage of tumour growth. The mutant cybrids also increased faster than wild type in culture. To complement the mtDNA mutations, a wild-type nuclear version of MTATP, whose codons were converted to the universal genetic codes containing a mitochondrial target sequence was transfected into the nucleus of cybrids carrying mutant *MTATP6*. The restoration of MTATP slowed down the growth of tumour in transplantation. Conversely, expression of a mutant nuclear version of MTATP6 in the wild-type cybrids declined respiration and accelerated the tumour growth. These findings showed that the advantage in tumour growth depended upon the MTATP6 function but was not due to secondary nuclear mutations caused by the mutant mitochondria. Apoptosis occurred less frequently in the mutant versus wild-type cybrids in cultures and tumours, indicating that the pathogenic mtDNA mutations seem to promote tumours by preventing apoptosis (Shidara, Yamagata et al. 2005). While the role of ROS in apopotic induction is fairly well established, more investigations are necessary to investigate the potential role of redox stress in promoting tumourigenesis, especially in SDH-deficient tumours (Storz 2005). FH does not play a role in the ETC and therefore there is no direct link with increased free radical production and oxidative damage of DNA. However, accumulation of succinate as a result of TCA cycle blockage could produce similar effects to SDH deficiency.

1.10.3 Potential role pseudo-hypoxia stress in HLRCC / HPGL tumourigenesis

Pseudo-hypoxia i.e. up-regulation of HIF1α and its downstream targets in normoxic conditions, has recently emerged as a different, but not mutually exclusive model for the mechanism by which loss of function of mitochondrial tumour suppressor genes (especially *SDH*) contributes to tumourigenesis. HIF1α over-expression (and up-regulation of HIF1α target genes) occurs in HPGL and HLRCC tumours and also *in vitro* as a consequence of siRNA and biochemical inhibition of FH and SDH (Gimenez-Roqueplo, Favier et al. 2001; Gimenez-Roqueplo, Favier et al. 2002; Isaacs, Jung et al. 2005; Pollard, Briere et al. 2005; Selak, Armour et al. 2005).

HIF, a transcription factor, is a heterodimeric complex comprised of HIF-α and HIF-β subunits (Semenza 2002). Three genes encode the three different α-subunits of HIF (HIF1α, -2α and -3α) and two genes encode the HIF- β subunits (HIF1 β /ARNT1 and ARNT2) (Covello and Simon 2004). The levels of HIF1α proteins are oxygen regulated whilst HIF-β is constitutively expressed. The physiological function of HIF is to promote survival in hypoxic cells by inducing glycolysis (as an anaerobic alternative to oxidative phosphorylation) and inducing angiogenesis in order to supply oxygen and nutrients to hypoxic tissues (Pugh and Ratcliffe 2003). This is especially important in tumours that out-grow their oxygen supply and induction of HIF, therefore, promotes their survival and growth (Covello and Simon 2004). HIF-target genes have one or more HIF-binding sites in their promoter / enhancer region. This specific domain, called the hypoxia response element (HRE), was first discovered in the *EPO* gene and HIF-binding of the *EPO* HRE caused stimulation of transcription of this target gene (Beck, Ramirez et al. 1991).

There is evidence (both *in vitro* and in SDH-deficient tumours) that implicates the role of HIF and oxygen sensing in tumourigenesis. The most common cell type associated with SDH-deficient tumours are the chromaffin producing cells of the adrenal medulla (PCC) and paraganglial cells (extra-

adrenal PCC/PGL). The latter typically occur in the carotid body; an oxygen chemoreceptor situated in the bifurcation of the carotid artery; and are neural crest-derived cells that secrete catecholamines in response to low oxygen tension (Lopez-Barneo, del Toro et al. 2004; Yeo and Roman 2005). In line with this, the penetrance and severity of tumours caused by inherited *SDHD* mutations are increased in populations living at high altitude (Baysal 2004).

Subsets of tumours from both HPGL and HLRCC have some similarity with tumours in individuals with VHL disease (Section 1.9.3). Germline mutations in *SDHB*, *-C*, and *-D* can lead to the development of PCC and RCC, the latter having been identified in *SDHB*-associated HPGL (Vanharanta, Buchta et al. 2004). RCCs have also been identified in HLRCC (Launonen, Vierimaa et al. 2001; Tomlinson, Alam et al. 2002; Toro, Nickerson et al. 2003; Wei, Toure et al. 2005). The histopathology of the RCCs varies; *VHL* and *SDHB*-mutant RCCs are of the clear cell type whereas those identified in HLRCC families are type II papillary or collecting duct morphology. Significantly, all of these tumours are highly vascularised, suggestive of a hypoxic response. There are reports of elevated HIF1α or increased expression of the HIF-target genes *EPAS1* and *VEGF* in SDH-deficient tumours (Gimenez-Roqueplo, Favier et al. 2001; Gimenez-Roqueplo, Favier et al. 2002) and my work, presented in this thesis (Chapter 3), has demonstrated increased expression of *VEGF* and increased vascularity in HLRCC UL in comparison to their sporadic counterparts (Pollard, Wortham et al. 2005), and increased expression of HIF1α in HLRCC RCCs and HPGL PGLs and PCCs (Pollard, Briere et al. 2005). These similarities suggest that a common pathway may, at least in part, be responsible for the tumourigenic effect of these tumour suppressors (*VHL, SDHx, and FH*). Interestingly, germline mutations in *VHL* that are particularly associated with predisposition to PCC do not impair HIF ubiquitylation (Clifford, Cockman et al. 2001; Hoffman, Ohh et al. 2001). It is possible, therefore, that HIF is just one component of a complex network of molecules with effects on cell-autonomous growth and angiogenesis. More recent data based on microarray expression profiling of PCCs showed a clustering of tumours with *SDH* or *VHL* mutations as compared to other mutations (*MEN2*) and sporadic PCC

(Dahia, Ross et al. 2005). A significant signature of this cluster, based on the pattern of gene expression, was the up-regulation of HIF-responsive genes such as *VEGF* and reduced oxidoreducatase activity of VHL- and both SDHB- and SDHD-defective PCC. This evidence suggests that there is a functional link between tumours with *VHL* mutations and those with disrusption of SDHB and –D, and that the oxidoreductase defect (previously not reported in *VHL*-null tumours) is explained by suppression of the SDHB protein.

If pseudo hypoxia is contributing to the tumourigenesis in HPGL and/or HLRCC then it will be very important to determine the biochemical signals linking mitochondrial dysfunction to HIF induction. HIF1α degradation is regulated by pVHL, which binds to and mediates its polyubiquitylation and subsequent proteosomal-mediated degradation. In order for pVHL to bind HIF1α, two proline residues (402 and 564) in the ODDD need to be hydroxylated (Safran and Kaelin 2003) (Figure 1.7). The hydroxylation reaction is catalysed by prolyl hydroxylase (PHD) enzymes, which have a relatively low affinity for oxygen (k_m=230-250μM) and are important intracellular oxygen sensors (Schofield and Ratcliffe 2004). The post-translational hydroxylation of HIF1α is attenuated under hypoxic conditions and therefore pVHL cannot bind, allowing HIF1α to accumulate in the cytosol and translocate to the nucleus where it interacts with HIF1β to form an active transcription factor. The hypothesis that PHD inhibition may connect mitochondrial dysfunction to HIF induction under normoxic conditions, represents a potential mechanistic link between oxygen sensing and *SDH* mutations as mentioned previously. However, in view of the biochemical requirements of PHDs such as the co-substrates; molecular oxygen and α–KG, and co-factors; Fe^{2+} and ascorbate, two models can explain a mitochondrial-to-cytosol signalling pathway connecting mitochondrial dysfunction to PHD inhibition and subsequent HIF1α stabilisation.

As previously mentioned, blocking the succinate-ubiquinone oxidoreductase activity may generate ROS in tumours. Excess accumulation of ROS has been shown to increase HIF1α stabilisation (Moeller, Cao et al. 2004) and additionally H_2O_2 can directly inhibit HIF1α prolyl hydroxylation by oxidising ascorbate and Fe^{2+}(Gerald, Berra et al. 2004).

In contrast, recent data has suggested a role of metabolic signalling in SDH-deficient cells (Selak, Armour et al. 2005). siRNA was used to knockdown *SDHD*, and HIF1α accumulation was observed without any detectable increases in ROS. Adding dimethylsuccinate to the cells mimicked the accumulation of succinate by siRNA and in both cases increased HIF1α was detected. The hypothesis that succinate is a signalling molecule linking SDH inhibition to HIF induction is a plausible theory as succinate is a stable metabolite (unlike the highly reactive, short lived superoxide and H_2O_2), and *in vivo* analysis of HPGL tumours has shown elevated levels of succinate (Briere, Chretien et al. 2004; Pollard, Briere et al. 2005).

A similar *in vitro* study has identified that bi-allelic inactivation of *FH* correlates with HIF1α overexpression (Isaacs, Jung et al. 2005) and fumarate was shown to be a competitive inhibitor for HIF-PHD. Fumarate is chemically similar to succinate but differs structurally due to a double bond between the two central carbon atoms, making fumarate a rigid molecule compared to succinate; however this does not rule out the possibility that it may inhibit PHD. Another explanation may be that blockage of the TCAC causes accumulation of pyruvate and oxaloacetate, both of which can stabalise HIF1α and activate the HIF pathway under normoxic conditions (Dalgard, Lu et al. 2004). There is also the possibility that succinate accumulation in SDH (or FH) – deficient tumours may inhibit other a-KG-dependent hydroxylases. This could lead to a variety of biochemical outcomes and provide a link between mitochondrial dysfunction and tumourigenesis. For example, the collagen PHD, which is less sensitive than HIF-PHD to oxygen deprivation (Hutton, Kaplan et al. 1967) can still be inhibited *in vitro* by succinate (Myllyla, Tuderman et al. 1977).

1.11 Alternative mechanisms of tumourigenesis

The pseudo-hypoxia hypothesis is very plausible and explains the vascularity of HLRCC and HPGL tumours and is very analogous to many aspects of VHL disease and the stabilisation of HIF1α. However, the high incidence of UL and RCC in the Eker rat model (Section 1.12.2) and the increased *VEGF* expression and angiogenesis in these tumours has been shown to be regulated by VHL-independent pathways, namely the TSC2/mTOR pathway (Brugarolas, Vazquez et al. 2003).

TSC2 functions as a GAP toward the small G protein Rheb, through a poorly understood mechanism which controls mTOR, a central regulator of protein translation (Castro, Rebhun et al. 2003; Garami, Zwartkruis et al. 2003; Inoki, Li et al. 2003; Saucedo, Gao et al. 2003; Stocker, Radimerski et al. 2003; Zhang, Gao et al. 2003). In response to growth factor stimulation, PI3K is activated by phosphorylation and recruits AKT (a serine/threonine kinase) to the plasma membrane where it phosphorylates TSC2, inactivating it and facilitating mTOR activation (Dan, Sun et al. 2002; Inoki, Li et al. 2002). Wild-type TSC2 downregulates HIF, and in $TSC2^{-/-}$ cells rapamycin normalises HIF levels, indicating that TSC2 regulates HIF by inhibiting mTOR (Brugarolas, Vazquez et al. 2003). Notably, the mTOR pathway is activated in tumours from TSC patients; in smooth muscle cells in lymphangioleiomyomas (Goncharova, Goncharov et al. 2002), and in RCC (Kenerson, Aicher et al. 2002). An interesting observation is that Rapamycin only partially downregulates *VEGF* expression in $TSC2^{-/-}$ cells thus implying an mTOR-independent link between TSC2 loss and *VEGF* upregulation (Brugarolas, Vazquez et al. 2003).

One suggestion regarding the genotype-phenotype association in HLRCC was the presence of modifier genes that may influence renal carcinogenesis in these families. Interestingly, a recent study on renal carcinogenesis in the Eker rat identified a modifier gene on rat chromosome 5 in a BN-strain which suppressed renal carcinogenesis by 100-fold (Kikuchi, Sudo et al. 2004). However, no such modifier has been identified in humans but there is currently research investigating this (Lehtonen; personal communication).

1.12 Existing animal models of fibroids, renal cancer, paraganglioma and phaeochromoctyoma

1.12.1 *Vhl* targeted mice

Vhl$^{+/-}$ mice develop hepatic blood vessel tumours over time due to stochastic loss of the remaining wild-type *Vhl* allele (Haase, Glickman et al. 2001) and as predicted, these lesions are characterised by increased levels of HIF and its targets. *Vhl* alleles flanked with loxP sites (from herein termed floxed) enabling conditional *Vhl* inactivation in the mouse liver using Cre recombinase cause similar lesions with higher penetrance and shorter latency (Ma, Tessarollo et al. 2003). Interestingly, murine *Vhl* inactivation has not been linked to renal carcinogenesis suggesting that unlike in humans, the mouse kidney is not permissive for tumourigenesis after pVhl loss. Inactivation of murine Vhl in the proximal renal tubules (PRTs), using a combination of floxed *Vhl* and Phosphenolpyruvate carboxykinase (PEPCK) - driven Cre-recombinase only produces a low frequency (4/11, 36.4%) of renal cysts, but no renal tumours by 18 months of age despite reporter mice expressing PEPCK-cre in all S3- and most S1 and S2-segments (>80%) of the PRTs (reviewed (Haase 2005)). Indeed, there is no evidence to suggest that pVhl inactivation is a direct cause of renal cyst formation in these mice. Similarly, renal tumours were not found when β-actin driven Cre-recombinase was used to generate mice which lacked pVhl in a mosaic pattern (Ma, Tessarollo et al. 2003).

1.12.2 *Tsc2* and the Eker rat

Tuberous sclerosis is an autosomal dominantly inherited disorder caused by germline *TSC1* and *TSC2* mutations and is characterised by harmartomatous involvement of many organs; the skin, central nervous system, retina, heart, kidneys, and has an association with RCC. (Gomez 1988).

The Eker rat provides a model of dominantly inherited tumour suppressor-type gene predisposing to the development of renal cell carcinoma and uterine leiomyomas, resulting from a retroviral insertion into the rat *Tsc2* gene (Yeung, Xiao et al. 1994; Kobayashi, Hirayama et al. 1995). Virgin female Eker rats develop UL spontaneously, with a frequency of about 65%. These tumours may be multiple, LOH occurs at a frequency of about 50% and loss of tuberin expression, the protein product of the *Tsc2* gene occurs in ~96% tumours (Hunter, Klotzbucher et al. 2002). The age of onset is 12 months plus although there is a report of a UL in a germline *Tsc2* null mosaic at less than 3 months of age (Kleymenova and Walker 2001). Eker rat UL are similar to HLRCC UL in that they occur at high frequency, are often multiple and are typically benign. Histologically, HLRCC and (sporadic) UL in humans are typically well-differentiated smooth muscle whereas Eker UL are primarily epitheloid (Walker, Hunter et al. 2003). Additionally, no specific chromosomal aberrations have been identified in Eker UL, whilst in HLRCC loss of 1q43 is very common and in sporadic UL translocation involving chromosomes 12q13 (*HMGA2*) and 6p21 (*HMGA1*) and deletion of 7q have been observed (Ligon and Morton 2000).

In contast to humans, *Tsc2* is the primary target for RCC in rodents. The Eker mutation predisposes rats to a high frequency and spontaneous and carcinogen-induced RCC (Walker, Goldsworthy et al. 1992; Hino, Klein-Szanto et al. 1993; Yeung, Xiao et al. 1994; Kobayashi, Hirayama et al. 1995). *Tsc2* knockout mice similarly develop spontaneous RCC (Kobayashi, Minowa et al. 1999; Onda, Lueck et al. 1999) in contrast to *Vhl* knockout mice, which do not develop these tumours (Gnarra, Ward et al. 1997; Haase, Glickman et al. 2001). The main phenotypic difference between the murine RCCs and

human counterparts are that murine tumours are predominantly chromophilic and even though predominantly solid, often have a prominent cystic component (Everitt, Goldsworthy et al. 1992; Wolf, Whiteley et al. 1995). HLRCC RCCs are solid renal lesions with cytological features of amphophillic cytoplasm with large nuclei containing large eosinophillic like-inclusion nuclei (Wei, Toure et al. 2005).

1.12.3 Mouse models of MEN1 and MEN2

Mouse models of *MEN1* have provided information about the tissue-specific consequences of *Men1* loss of function. Conditional knockout of both alleles in the islet β-cells or in the parathyroid cells result in the growth of insulinoma or of parathyroid adenoma (Crabtree, Scacheri et al. 2003; Libutti, Crabtree et al. 2003; Biondi, Gartside et al. 2004) whereas knockout of *Men1* in the hepatocyte has no effect (Scacheri, Crabtree et al. 2004), thus emphasising the tissue-specificity from the menin-null status. The most common tumours in $Men1^{+/-}$ mice are prolactinoma, insulinoma and parathyroid adenoma which develop after nine months of age (Bertolino, Tong et al. 2003; Crabtree, Scacheri et al. 2003). These types of tumour are commonly seen in patients with MEN1 and therefore this is an excellent mouse model. An important difference between mouse and human MEN1 is the development of PCC in $Men1^{+/-}$ mice (7%). In contrasts, incidence is below 1% in humans (Marx 2005).

Mouse models of MEN2 have produced mixed results. Both the short and long isoforms when mutated and overexpressed using the calcitonin promoter produce C-cell cancer; showing variable penetrance (0-98%) which is highly dependent on the germline background of the mice (Michiels, Chappuis et al. 1997; Cranston and Ponder 2003). Expression in mice of the human mutant allele present in MEN2B did not cause any MEN2-like tumour (Skinner, Kalyanaraman et al. 2005), whilst a MEN2B-like murine *Ret* allele when expressed heterozygotes mice caused C-cell hyperplasia and PCC (Smith-Hicks, Sizer et al. 2000).

1.12.4 Mouse models of Alports syndrome

A mouse model of X-linked ATS (not ATS-DL) was generated by targeting a human nonsense mutation, G5X, to the mouse *Col4a5* gene (Rheault, Kren et al. 2004). As predicted for a nonsense mutation, hemizygous mutant male mice were null and heterozygous carrier female mice were mosaic for alpha5(IV) chain expression. Mutant male mice and carrier female mice were viable through reproductive age and fertile. Mutant male mice died spontaneously at 6 to 34 weeks of age, and carrier female mice died at 8 to 45 weeks of age, manifesting proteinuria, azotemia, and progressive and manifold histologic abnormalities of the kidney glomerulus and tubulointerstitium. Ultrastructural abnormalities of the glomerular basement membrane, including lamellation and splitting, were characteristic of human X-linked ATS. Two canine models exist but neither are ATS-DL causing mutations. Affected animals in both models display ultrastructural changes in the GBM but do not have clinically detectable deafness or ocular abnormalities (Kashtan 2002).

1.12.5 Mouse model of NF1

Nf1 knockout mice represent the strongest link between experimental and human neurofibromatosis. For example, PCC (which are very rare in wild mice) occur relatively frequently in *Nf1* targeted mice (Jacks, Shih et al. 1994). $Nf1^{+/-}$ animals do not exhibit the classical symptoms of the human disease, but are highly predisposed to the formation of various tumour types, notably PCC and myeloid leukaemia, both of which occur with increased frequency in human patients. The wild-type *Nf1* allele is lost in approximately 50% of the tumours from $Nf1^{+/-}$ mice *and* $Nf1^{-/-}$ mice and homozygosity leads to abnormal cardiac development and mid-gestational embryonic lethality. Further characterisation of these mice revealed a PCC frequency of 15% in *Nf1* knockout mice with a mixed genetic background but an absence of PCC in inbred mice (Tischler, Shih et al. 1995). Approximately 25% of the tumours

were bi-lateral and all exhibited variable morphology including cells that appeared well differentiated and resembled normal chromaffin cells expressing tyrosine hydroxylase, phenylethanolamine N-methyltransferase (PNMT) and chromogranin A (CGA).

1.12.6 German Shepherd Dogs and BHD.

The only animal models of BHD are German Shephard dogs, which harbour a mutation in exon 7 of canine *Bhd* resulting in hereditary multifocal renal cystadenocarcinoma and nodular Dermatofibrosis (RCND); a previously reported naturally occurring cancer syndrome (Lium and Moe 1985; Moe and Lium 1997), and the Nihon rat (Section 1.12.7). In the former, the disease is characterised by bilateral, multifocal tumours in the kidneys, uterine leiomyomas and nodules in the skin consisting of dense collagen fibres (Lingaas, Comstock et al. 2003).

1.12.7 The Nihon rat and RCC

A novel rat model of hereditary RCC was found in a rat colony of the Sprague-Dawley strain in Japan, and named the "Nihon" rat. In this strain, RCCs (predominantly clear cell type) develop from early preneoplastic lesions, which begin to appear at 4 weeks of age, forming adenomas by the age of 16 weeks (Okimoto, Kouchi et al. 2000). Linkage analysis mapped the RCC gene to rat chromosome 10 (Hino, Okimoto et al. 2001) and subsequently, germ-line mutation in *Bhd* caused by the insertion of a single nucleotide was identified, resulting in a frameshift and producing a stop codon 26 amino acids downstream (Okimoto, Sakurai et al. 2004). LOH of the wild-type allele and depletion of the *Bhd* protein product folliculin in Nihon rat RCC cell lines confirmed the tumour-suppressor function of the *Bhd* gene. However, the mechanism by which *Bhd* acts as a tumour suppressor is yet to

be elucidated and further characterisation of the BHD protein is necessary in humans, canines and rats.

1.12.8 Summary of animal models of PCC/RCC/UL

The use of mice to model human cancer is not necessarily ideal and often the phenotype(s) obtained from knockout models differ from that of human disease and are often background specific. Coupled with this, mice rarely develop invasive or metastatic cancer and most murine neoplasms occur in mesenchymal derived tissue compared to epithelial in humans (Hann and Balmain 2001; Ward and Devor-Henneman 2004). This is evident in the overexpression of *RET* in a mouse model of MEN2 where the penetrance varied from 0% to 98% depending on the background (Marx 2005). The HIF-expressing RCCs resulting from inactivation of *Tsc2* in the Eker rat are analogous to RCCs resulting from mutations in the human *VHL* gene – however abrogation of pVHL in murine renal proximal tubules fails to induce RCC. Interesting, whilst elevated HIF1α is associated with RCC in VHL disease (Kim and Kaelin 2004), HIF2α appears to be the main tumourigenic drive in RCC arising from loss of *Tsc2* in Eker rats (Liu, Poellinger et al. 2003). The *Nf1*-targeted mice (on a mixed background) recapitulated the PCC found in human NF1 patients in that the tumours were of similar morphology and some were bi-lateral. (Tischler, Shih et al. 1995).

1.13 Existing animal models of HLRCC/HPGL

To date, there are no reported mouse models of HLRCC or HPGL involving the germline targeting of *Fh* or *Sdh* that have produced tumours. Subcutaneous injections of the Sdhc E69 fibroblast cell line into nude mice yielded benign tumours (Ishii, Yasuda et al. 2005), however this model does not mimic the tumour-suppressor 'two hit' tumourigenic mechanism in human HLRCC and HPGL.

Sdhd has been knocked out in the germline of mice and unsurprisingly, $Sdhd^{-/-}$ mice were embryonic lethal at E6.5 $Sdhd^{+/-}$ mice showed a general, noncompensated deficiency of SDH activity without alterations in body weight or major physiological dysfunction (Piruat, Pintado et al. 2004). No tumours were observed in $Sdhd^{+/-}$ mice after six months. By floxing *Sdhd*, and crossing with the available Cre-expressing (including inducible) transgenic mouse lines, tissue specific deletion of *Sdhd* could have been achieved, which would have possibly made a better model of the human syndrome and overcome the embryonic lethality of the $Sdhd^{-/-}$ mice.

1.14 Aims and objectives

In order to further our understanding of the roles FH and SDH play in the tumourigenesis of HLRCC and HPGL, various genetic and molecular techniques were employed. These techniques, and the specific issues that were to be addressed, are described in brief below. The results from this work carried out are described and discussed in the relevant results chapters (chapters 3-7).

- To use gene expression profiling of HLRCC fibroids to identify genes involved in hypoxia-related pathways and , and *in situ* techniques to look at markers in HLRCC tumours to substantiate expression data and to see if these same genes/proteins were expressed in HPGL tuomurs
- To use proton NMR to analyse the metabolomic profile of HLRCC and HPGL tumours and also cell lines with bi-allelic mutations from FH deficiency patients to test for Krebs cycle blockage and malfunction
- To carry out a genetic screen for *SDHB*, *-C* and *-D* in individuals with PGL and/or PCC who were already confirmed not to carry mutations in *VHL*, *MEN2* or *NF1*. To try and identify novel mutations and more clinical information relating genotype to phenotype.
- To obtain fresh tumour samples where possible from the above patients and use array-CGH to identify whether the wild-type allele is

lost through chromosomal loss or deletion and also to try and identify new candidate regions in patients that were negative for *SDH* screening.

- To create a mouse model of HLRCC, using ES gene targeting that would enable conditional *Fh1* inactivation using cre-lox technology. Viable mice could then be crossed with specific transgenic mice to knockout *Fh1* in specific tissues. In addition, I intend to make a heterozygous knockout of *Fh1* using the same construct and knock out one copy *in vivo*. These mice will then be analysed for disease development over a time period of 15 months. Heterozygous mice will be inter-crossed to determine if there is an embryonic lethality in the homozygous state and at which stage of embryogenesis, the lethality occurs. Mice crossed with transgenic mice expressing Cre recombinase in smooth muscle and renal cells will be analysed if they develop a phenotype, specifically for benign smooth muscle tumours and renal neoplasms.
- To create a transgenic mouse line expressing Cre recombinas in the uterine myometrium. To date, there is no transgenic line available that solely expresses Cre recombinase in the smooth muscle layer (myometrium) of the uterus. If successful, then the conditional *Fh1* knockout could be crossed with this transgenic line, thus knocking out *Fh1* in the cells where fibroids arise in HLRCC patients.

2 Chapter 2: Materials and Methods

Recipes for standard solutions used in the methods that are not described were made by the media production facility at Clare Hall and are listed at the end of this chapter (2.25).

2.1 Cell Culture methods and maintenance

2.1.1 Human fibroblasts

We received primary culture of FH deficient skin fibroblasts from Dr Simon Olpin (Sheffield Children's Hospital). Cells were stored in liquid nitrogen and thawed by placing immediately into a 37°C water bath for 5 minutes. Cells were then gently pipetted into a 15ml tube containing 10ml of warm (37°C) 10% serum media (E4) and centrifuged at 500g for 2 minutes to pellet the cells. Media was aspirated from the tube and the cell pellet resuspended with 10ml of warm 10% serum media (E4) and added bacterial inhibitors (GIBCO) and transferred to a culture flask (Nunc 153732) at 37°C, 5% CO_2. Cells were fed by aspirating the old media and adding fresh media every 2 days. Cells were passaged when the confluency was greater than 80%. The old media was aspirated and 5ml of 2 x trypsin added to the flask and incubated at 37°c for 5 minutes. The flask was gently tapped on the bench to ensure release of the cells adhered to the flask and 10ml of 10% serum media added to inactivate the trypsin. The cells were then centrifuged at 500g for 5 minutes and the media aspirated. The pellet was resuspended in 10ml of 5% serum media and divided into new flasks according to requirement and 10ml of 10% media added to each flask. Normal skin fibroblasts were obtained from the European collection of cell cultures (ECACC) and maintained and split as described above.

2.1.2 Mouse ES cells

2.1.2.1 Transfection of ES cells

This was carried out at Clare Hall by animal technicians. Embryonic stem cells used in this procedure were of a healthy state, morphologically normal and of a low passage number. Cells were passaged the day prior to being used and medium changed a few hours before harvesting. 3-4 confluent 3.5cm wells are required for each transfection and 4 x 6 well plates of feeders were prepared for each transfection. The ES cells were trypsinised and resuspended in 5ml of ES medium. The cells were counted and adjusted to between $5x10^6$ and $1x10^7$. If there were not enough cells, further wells were trypsinised or if these were not available, the cells were replated at a 1:2 dilution and the transfection carried out. When these cells had reached confluence, they were centrifuged at 1000rpm for 5 minutes. The supernatant was removed and resuspend in 10ml of E4 and this washing step repeated. The supernatant was removed, and the ES cells resuspended in 0.9ml of E4, mixed with the DNA (20μg), transfered into an electroporation cuvette and left for 5 minutes at room temperature. The capacitance and voltage on the electroporator was set to to 500μFD and 0.24 KV, respectively and the cuvette inserted into the electrophorator. After transfection the cell suspension was left for 5 minutes at room temperature. Using a Pasteur pipette, the cell suspension was transferred to 30ml of ES media. 1ml of this solution was plated out to each of the 3.5cm wells of the 4 x 6 well plates which were incubated at 37°C in a 5% CO_2 atmosphere. 24 hours after transfection, the media was changed using ES containing 300μg/ml G418 (see Cell Culture Media). The media was changed daily for up to 10 days when colonies were suitable for picking.

2.1.2.2 Picking colonies

An appropriate number of 96 well plates with feeders were prepared. The plate containing the colonies was washed twice with PBSA then 1ml per well of PBSA added. A 96 well plate containing 25μl of trypsin per well was also prepared. Whilst viewing the colonies under a microscope, a pipette tip was used to transfer in a maximum volume of 10μl PBSAA to the 96 well plate containing trypsin. A sterile pipette tip was used for each colony. Care was taken that only a single colony was seeded per well to avoid a further cloning step. Once picked, the plate was incubated at 37°C for 10 minutes. 25μl of ES media was added to each of the 96 wells. Using fresh tips for each column, the cells were gently disrupted by pipeting the solution up and down, then 50μl of the cell suspension was transferred to the pre-prepared feeder plate, making sure that the cells were put into the corresponding wells. This was repeated for each column of cells until all of the wells had been transferred. The 96 well plates were placed in the incubator and the media changed daily until ready for freezing.

2.1.2.3 Cryopreservation of ES cells in 96 well plates

Once the cells had reached the desired stage of confluence (usually 3-5 days after picking and the media had started to turn yellow) the ES cells were cryopreserved and a duplicate plate prepared for DNA analysis. The required number of 96 well plates were gelatinised, aspirated and 200μl of ES cell media added and placed in the incubator until required. The media for the plate of cells to be stored was changed changed approximately 1-4 hours before carrying out the procedure. Freezing mixture was freshly prepared, and placed in the fridge until required. The plates to be frozen were washed twice with 200μl of PBSA per well. 50μl of prewarmed trypsin/versene was added to each well and incubated for 6 minutes. Once the cells had detached from the plate, 50 μl of ES media was added per well. Using fresh tips for each column,

the cells were gently disrupted by pipetting the solution up and down and 50µl of the cell suspension was transferred to the corresponding wells of the pre-prepared feederless plate. This was repeated for each column of cells and the duplicated plate (DNA plates) were placed into the incubator. 50µl of freezing mixture was added to each of the wells to be frozen. The edges of the plates were sealed with parafilm, coverd with tissue and placde in a -70°C freezer. After 24 hours the plate were stored in liquid nitrogen if required.

2.1.2.4 Generation of chimeric mice

Positive clones were recovered and 10-15 ES cells were injected in blastocysts at E4. The blastocysts were then transferred to pseudo-pregnant CD1 foster female mouse in the uterine horn. The offspring (chimeric mice) were assessed for coat colour contribution (percentage of agouti contribution) and chimeras assessed as having a 70% or more 129 contribution (Agouti) were selected for crossing with C57/BL6 mice.

2.2 DNA extraction

2.2.1 DNA extraction from blood

This was perfomed using the ammonium acetate method. Cell membrane lysis was carried out by thawing 9ml frozen blood samples and transferring the blood to 50ml conical bottom Falcon tubes (Greiner). Ice cold water was added to give the tubes a final volume of 50ml. Tubes were inverted 6 times to mix and centrifuged at 2300rpm for 25 minutes at 4°C (CR412 Jouan). The supernatant was discarded by inverting the tubes gently, taking care not to disturb the pellet. The pellets were then washed with 25ml 0.1% NP-40 (Sigma) and centrifuged at 2300rpm for 20 minutes at 4°C. This step

was repeated and the supernatant discarded and the the tubes inverted over a paper towel. Nuclear lysis was carried by adding 3ml of nuclei lysis buffer (0.32M Sucrose, 10mM Tris-HLC [pH 7.5], 5mM $MgCl_2$, 1% Triton X-100) to the pellets and vortexing the tubes until the pellets were completely resuspended. To degrade proteins, 200µl of 10% SDS and 60 µl of proteinase K solution was added to the tubes and after several inversions were incubated at 55°C for 2 hours. DNA was extracted by adding 1ml of ammonium acetate (saturated), vortexing for 15 seconds, placed in a rack at room temperature for 20 minutes and centrifuged at 2300rpm for 20 minutes at room temperature. DNA was precipitated from the supernatant by transferring to a clean 50ml falcon tube and adding two volumes of ice-cold ethanol. The contents were mixed by gentle inversion and the DNA spooled out using a fine plastic sterile loop. The spooled DNA was incubated in 50ml falcon tubes with 75% ethanol for 1 hour on a rolling platform, transferred to an tube, the supernatant caredully aspirated with a pipette and the DNA pellet allowed to air-dry for 1 hour at room temperature. The DNA was resuspended in 1ml of TE and and a 2µl aliquot removed for quality and concentration determination using the Nanodrop™.

2.2.2 DNA extraction from cell lines

Cells were trypsinised as previously described and pelleted in 50ml falcon tubes by centrifugation at 1000rpm for 10 minutes. The cells were washed twice in PBSA by resuspending using a pipette and then centrifuged at 1000rpm. The PBSA was aspirated and the cell pellet resuspended in 15ml of SE buffer (75mM NaCl, 25mM EDTA [pH 8.0], 1% SDS). RNA was degraded by adding 50µl of of RNAse A (Advanced Biotechnologies) and incubating for 15 minutes at 37°C. Proteinase K was added to a final concentration of 200µgml^{-1} and incubated overnight at 55°C. 4.5ml of pre-warmed (37°C) 5.0M NaCl was added followed by 20ml of chloroform (Merck) and the tubes mixed on a rolling platform for 30 minutes then centrifuged at 2000rpm for 10 minutes. The aqueous layer was transferred to a

new tube, an equal volume of propan-2-ol (BDH) added and mixed for 5 minutes at room temperature to allow DNA precipitation. The DNA was spooled out using a sterile loop and washed in 75% ethanol for 30 minutes. The DNA was pelleted by centrifugation at 2000rpm for 10 minutes, the ethanol eluted using a pipette and the pellet allowed to air-dry for 30 minutes at room temperature. The DNA was resuspended in TE [pH 8.0] and the quality and quantity assessed using the Nanodrop™.

2.2.3 DNA extraction from ES cells (96 well plates)

96 well plates were delivered from Transgenic Services on dry ice and thawed for 30 minutes in a 55°C incubator then allowed to cool to room temperature for a further 30 minutes. The foil seal was carefully removed and 50µl of propan-2-ol added to each well using a multi-channel pipette. The plates were left for 30 minutes at room temperature in order for the DNA to precipitate and centrifuged for 10 minutes at 2000g. The supernatant was carefully poured off by gentle inversion of each plate and 150ml of 75% ethanol added to each well using a multi-channel pipette. The plates were then centrifuged at 2000g for 5 minutes and the supernatant removed by gently inversion of each plate. This washing step was repeated a further twice and then the plates were left at room-temperature for 1 hour in order to air-dry the DNA. To resuspend the DNA, 100µl of TE was added to each well and the plates left overnight on a rocking platform then stored at 4°C for short term or -80°C for long term storage.

2.2.4 Salt/Chloroform DNA extraction from ES cells (flasks)

Between 10^6 and 10^7 cells were centrifuged at 13000g in a falcon tube so that a pellet formed and the media aspirated. The pellet was resuspended in 500µl of DNA buffer. 10µl 10% SDS and 10µl Proteinase K (10mg/ml) were added and the tubes inverted to mix. The lysate was incubated overnight at

55°C and then 150µl 5M NaCl, 650µl chloroform/isoamyl alcohol (96:4) added. The tubes were gently inverted to mix and centrifuged at 13000g for 10 minutes. The upper phase was transferred using a pipette to a fresh tube and the DNA precipitated with 650µl of 100% ethanol. DNA was stored in the ethanol at at -20°C until ready for use.

2.2.5 DNA extraction from mouse tails

Mouse tails arrived from Transgenic Services in tubes on dry ice and were stored at -20°C until required. 400µl of tail buffer with a final concentration of $1mgml^{-1}$ proteinase K (BDH) was added and the tails incubated at 55°C for a minimum of 4 hours and vortexed at least twice during the digestion process. 160µl of NaCl (5.0M) was added to each tube and the tubes placed on a mixer for 2 minutes. The tubes were centrifuged at 13000g for 10 minutes and the supernatant poured into a clean tube. DNA was precipitated by adding 300ml of propan-2-ol and the tubes centrifuged at 13000g for 5 minutes, The supernatant was removed, the DNA pellet air-dried for 15 minutes in a heat block at 55°C and resuspended in 50µl of TE.

2.2.6 DNA (plasmid) extraction from bacteria (*E.coli*)

Plasmid DNA was extracted from bacterial cultures using the maxi-prep kit (Qiagen) according to the manufacturers instructions. In brief, transformed cells were grown in 200ml of LB media + ampicillin ($100\mu gml^{-1}$ final concentration) for 18 hours and then pelleted by centrifugation at 4000g for 20 minutes (Beckman JS25.5). The cells were resuspended in 10ml of buffer P1 by pipetting, then lysed by adding 10ml of buffer P2, inverting 6 times and incubated for 5 minutes at room temperature. 10ml of neutralisation buffer P3 was added and the tubes shaken vigorously and placed in an ice bucket for 20 minutes, inverting 6 times every 5 minutes. The tubes were centrifuged for 30 minutes at 25000g (Beckman JS25.5) and the supernatant

loaded into the purification columns that had been equilibriated with 10ml of buffer QBT. The columns containing the bound DNA were washed twice with wash buffer QC and the DNA eluted with 15ml of elution buffer QF. DNA was precipitated by adding 10.5ml of propan-2-ol to the elute and centrifuging for 30 minutes at 25000g (Beckman JS25.5) at 4°C. The DNA pellet was washed with 15ml of 75% ethanol and air-dried for 30 minutes at room temperature. 500ml of TE was used to resuspend the DNA which was analysed for quality and quantity using the Nanodrop™.

2.2.6.1 Purification of plasmid DNA from bacteria

DNA obtained from maxi-prep that need further purification for transfections or ISH probes was resuspended in total volume of 350µl. An equal volume of phenol:chloroform:isomyl-alcohol (10:10:1) was added and the tubes gently inverted for a minute to ensure mixing. The tubes were centrifuged at 13000g for 10 minutes and the upper aqueous phase carefully removed using a pipette and transferred to a clean tube. A further 350µl of phenol:chloroform:isomyl-alcohol was added and the tubes centrifuged for a further 10 minutes. The supernatant was carefully removed and added to a clean tube with 300µl of chloroform. The tube was gently inverted for 1 minute and then centrifuged at 13000g for 15 minutes. The supernatant was carefully removed using a pipette and transferred to a clean tube. 100µl of 7.5M ammonium acetate was added, the tube vortexed, then 750µl of ice cold 100% ethanol added to precipitate the DNA. The tubes were centrifuged at 13000g for 10 minutes and washed twice with 75% ethanol. After the second wash, the DNA pellet was allowed to air-dry for 1 hour at room temperature and then resuspended in 50µl TE [pH 8.0]. DNA quality and quantity was assessed using the Nanodrop™.

2.2.7 DNA extraction from tissue

DNA was extracted using the DNeasy kit (Qiagen) according to the manufacturers protocol. 25-50mg of tissue was cut up into small pieces using a scapel, placed in a microcentrifuge tube with 180µl of ATL lysis buffer. 20µl of proteinase K solution was added and the samples vortexed and incubated overnight at 55°C. 4µl of RNase A (100mgml^{-1}) was added, the samples vortexed and incubated at room temperature for 5 minutes. 200µl of buffer AL was added and the samples thoroughly vortexed then incubated at 70°C for 10 minutes. 200µl of 100% ethanol was added, the samples vortexed , pipetted into a DNeasy mini spin column and centrifuged for 1 minute at 10000g. The flow-through was discarded and 500µl of AW1 wash buffer added. The samples were centrifuged for a further minute and then the flow-through discarded. This wash step was repeated using AW2 and then the column placed in a clean collection tube, 200µl of TE added and the DNA eluted by centrifuging at 20000g for 3 minutes. DNA quality and quantity was assessed using the Nanodrop™.

2.3 RNA extraction

2.3.1 RNA extraction from cells

Total RNA was isolated from cells using the Genelute mammalian total RNA kit (RTN70, Sigma) according to the manufacturers protocol. In brief, cells were lysed in 500µl of lysis buffer with 5µl of 2-mercaptoethanol by pipetting, transferred to a blue filtration column and centrifuged at 14000g for 2 mniutes. 500µl of 70% ethanol was added to the filtrate and transferred to a binding column and centrifuged for 15 seconds at 14000g. 500µl of wash buffer 1 was added to the column and centrifuged for 1 minute at 14000g. The wash solution was discarded and this step repeated with wash buffer 2. The

RNA was eluted into a new collection tube by adding 100µl of RNase-free water and centrifuging at 14000g for 3 minutes. RNA quality and quantity was assessed by gel electrophoresis and the Nanodrop™. RNA was stored at -70°C.

2.3.2 RNA extraction from tissues

Total RNA was extracted using TRIzol® (Gibco). 100mg of tissue was homogenised by grinding with a motar and pestle in liquid nitrogen and added to 1ml of TRIzol. The samples were incubated in microfuge tubes at room temperature for 5 minutes and 0.2ml of chloroform added. The samples were shaken vigorously for 15 seconds and incubated for a further 3 minutes at room temperature then centrifuged at 12000g for 15 minutes at 4°C. The aqueous phase was transferred to a centrifuge tube and the RNA precipitated by adding 0.5ml of propan-2-ol, incubating at room temperature for 10 minutes then centrifuging at 12000g for 10 minutes at 4°C. The RNA was washed twice with 1ml of 75% ethanol (in RNase-free water) by vortexing, centrifuging for 5 minutes, centrifuging at 8000g at 4°C and removing the ethanol with a pipette. The RNA pellet was air-dried for 10 minutes at room temperature and re-suspended in RNase-free water. RNA quality and quantity was assessed by gel electrohporesis and the Nanodrop™. For further purification the RNA was cleaned up using the Genelute RNA kit (Sigma) as described above. RNA was stored at -70°C.

2.4 cDNA synthesis from RNA

cDNA synthesis was performed using the First Strand cDNA Synthesis kit (Amersham). 1µg of total RNA was added to 11µl of first strand mix, 1 µl of $pd(N)_6$ random-hexamer primers, 1µl DTT solution and nuclease-free water to a total volume of 33µl. The reaction mixture was incubated at 37°C for 1 hour to allow cDNA synthesis.

2.5 cRNA synthesis and labelling for Affymetrix GeneChip™ analysis

The cRNA preparation, hybridisation and analysis techniques were carried out under supervision in Aarhus, Denmark. In brief, 10μg of total RNA was used to generate double stranded cDNA using the Superscript II kit (Invitrogen). The cDNA was cleaned up using the GeneChip Cleanup Sample Module (Affymetrix). cRNA was generated using the BioArray High Yield Transcript Labelling Kit (Enzo). After a clean-up and fragmentation step the arrays were processed and the data normalised and analysed using NetAffx (Affymetrix) and Excel (Microsoft). Full details of the protocols, equipment and probes are available (http://www.affymetrix.com).

2.6 The polymerase chain reaction (PCR)

PCR was used to amplify selected regions of target DNA either for genotyping, SSCP, cloning or sequencing. The sequence of the target DNA was identified using electronic web resources (http://Sanger.ac.uk and http://genome.ucsc.edu/). The 'Primer 3' program was used to design primers (http://frodo.wi.mit.edu/cgi-bin/primer3/primer3_www.cgi) from flanking sequences which were synthesised by the CRUK oligonucleotide service or Sigma. The length of the product was selected depending on the proposed use of the PCR product e.g. cloning 200bp-7kb, SSCP and sequencing, fragments up to 300bp. Primers were designed to anneal to specific sequences in the DNA template and facilitate *in vitro* DNA synthesis from dNTPs catalysed by a thermostable Taq DNA polymerase. PCRs were usually performed in either 25μl or 50μl volumes comprising 25-50ng of DNA template, $Mg2^{+}$ free buffer, $MgCl_2$ (1.5mM to 2mM final concentration depending on primer optimisation), dNTPs (final concentration of 0.1mM) and 1.0 unit of Taq polymerase. The final volume was achieved by adding nuclease-free water. For fragements less than 1.0kb normally the Qiagen PCR kit was used and

primers designed with a T_m of ~60°C. For larger fragments such as homologous arms for mouse targeting constructs, LA-Taq (Takara) was used and the primers were designed with a higher T_m (65-68°C). PCRs were carried out in sealed microtitre plates (Advanced Biotechnologies) in Tetrad PCR machines (MJ Research). A typical PCR reaction consisted of an initial denaturing step of 96°C for 3 minutes, then 30-35 cycles each of 96°C for 30 seconds (denaturing), 55°C (or 2°C below the T_m of the primers) for 1 minute (primer annealing) and 72°C for 1 minute per kb (DNA syntheis) i.e. for a 500bp product – 30s. A final extension step of 72°C for 10 minutes was carried out. When using LA-Taq, the DNA synthesis stage was carried out at 68°C.

2.7 Agarose gel electrophoresis

After the PCR reaction was completed, agarose gel electrophoresis was used for checking for the presence and expected size of the product. Agarose was prepared by boiling a mixture of agarose powder (Gibco) in 1 x TBE at concentrations of 1-3% depending on the size of the DNA fragment. After cooling to 55°C, ethidium bromide was added to a final concentration of 0.25μgml^{-1} in order that the DNA could be visualised under UV light. A gel-casting tray with a comb was used set molten agarose into a gel and after solidifying was placed in a running tank and covered by 1 x TBE. 10μl of PCR product and 3μl of tracking dye (Orange-G) were added to each well and 15μl of 1.0kb DNA ladder also loaded to allow sizing of the fragments. The gel was then electrophoresed at 100-140V for 15-60 minutes depending on the separation required and photographed using a UV transilluminator (260nm) and camera.

2.8 Mutation detection techniques

2.8.1 Single-stranded conformational polymorphism analysis (SSCP)

Nucleotide sequence determines the secondary structure of single stranded DNA which in turn affects the rate of migration of single stranded DNA under non-denaturing conditions through a polyacrylamide gel. Thus sequence differences may be detected as a band of altered mobility on SSCP analysis. Patient DNA samples were PCR amplified to give an optimum product size of 250bp and screened for mutations using SSCP on the PHAST system (Amersham). The PCR products were denatured in an equal volume of 98% de-ionised formamide, 4mM EDTA at 95°C for 5 minutes and then immediately placed on wet ice. 0.3ml of denatured sample were separated on a 12.5% precast acrylamide gel at 250V for 120Vh at 10°C. Gels were manually fixed, stained and developed using a silver stain kit (Amersham). Single strand and double strand DNA mobility patterns of each sample were examined and any samples showing abnormal migration were subsequently analysed using direct sequencing.

2.8.2 Direct sequencing of PCR products

PCR products were first purified using the Qiaquick PCR purification spin columns (Qiagen) according to the manufacturers protocol. This involved the binding of the DNA to the column and adding wash buffer and centrifuging at 13000g to remove excess dNTP's and primers. PCR products were then sequenced using the Applied Biosystems Big Dye terminator (BDT) reaction kit and the 3730 semi-automated DNA analyser.

2.8.3 Sequence analysis

Sequences were analysed using 4 Peaks softwared (Mek and Tosj). Database searching using BLAST (http://www.ncbi.nih.gov/BLAST/) was performed to ensure that the correct region of DNA had been amplified. All sequences were examined by eye to look for heterozygous peaks that might not have been detected by alignment tools. All mutations were confirmed by examining reverse sequence.

2.9 Restriction end digest (RED) cloning of PCR products

RED cloning was used for generating probes for ISH and also for creating mouse targeting constructs. The primers were designed to incorporate restriction enzyme (RE) sites and PCR and gel analysis was carried out as previously described. The vector and the insert were both digested with the appropriate RE and buffer and then loaded onto an agarose gel and electrophoresed for 2 hours at 50 volts. Using a UV transilluminator, the vector and insert DNA were cut out of the gel with a scapel and the DNA purified using the Gel Purification kit (Qiagen). In brief, the gel fragments containing the DNA were dissolved in buffer QG in microfuge tubes at 60°C for 10 minutes with regular vortexing, then loaded onto a Qiaquick column and purified as described for PCR purification. DNA was quantified visually by gel electrophoresis. Ligations were carried out in microfuge tubes. A 5:1 ratio of insert:product was used, 2µl of ligation buffer , 1µl of T4 ligase (NEB) and made up to a volume of 20µl with dH_2O and incubated at room temperature for 1 hour. A control was run in parallal replacing the insert with dH_2O to ensure efficient cutting of the vector. 2µl of the ligation mixture was used for transformation of competent *E.coli* (Invitrogen). 100µl of competent cells were thawed on wet ice for 20 minutes and 50µl added to each falcon tube containing the ligated and the control DNA. The tubes were kept on wet ice for 25 minutes then placed in a 42°C water bath for 30s and immediately

placed back on wet ice for 5 minutes. 1ml of pre-warmed (37°C) SOC media was added to each tube and incubated on a shaking platform at 37°C for 1 hour. 100µl of the culture was pipetted onto a LB+ampicillin (100µgml^{-1}) plate, 10-15 sterile glass beads added and gently shaken to disperse the culture. The beads were removed and the plates incubated at 37°C overnight. The remaining culture was centrifuged at 500g for 5 minutes and the media aspirated. The pellet was resuspended in 100µl of SOC media and plated and incubated as described above. Bacterial colonies were picked from the plates and grown in LB+ampicillin (100µgml^{-1}) media for 18 hours and the DNA extracted using an automated mini-prep machine Biorobot 8000 (Qiagen). The mini-prep DNA was analysed by RE analysis and/or sequencing in order to identify positive clones.

2.10 Sample Collection

Blood, tumour samples; both frozen and paraffin embedded were collected from surgeons and hospitals that were participating in the HLRCC and/or HPGL study. All samples were collected with full ethical approval. When fresh tissue was collected, it was either snap-frozen in liquid nitrogen for future RNA, DNA , protein or enzymatic/metabolite assays or fixed in NBF for 24-36 hours, transferred to 70% ethanol and embedded into paraffin blocks. This was carried out by the histopathology service at the London Research Institute. Mouse tissue was processed similarly, but for β-gal IHC a Zn fixative was used.

2.11 Fumarate hydratase activity assay

FH activity was assayed in mouse ES lines, fibroblast primary cultures from FH deficiency patients and also in control fibroblasts. The assay was carried out by Simon Olpin at the Sheffield Children's Hospital and was based on the modification of the method described by Hatch *et al* (Hatch 1978). The

principle of the assay is that addition of fumarate to a cell will result in malate production, which will depend on the activity of the FH enzyme present. The amount of malate can be measured by adding malic enzyme which will cause formation of pyruvate and conversion of NADP to NAPDH which can be measured by an increase in absorbance at 340nm. This is corrected for the protein concentration of the cell sonicate. The final reaction medium consisted of 10mM fumarate, 25mM Hepes-KOH [pH7.5], 0.2 units of malic enzyme ml^{-1}, 0.27mM NADP, 4mM MgCl2 and 5mM K_2PO_4. The assay was run at least twice for each sample and at 2 different protein concentrations and the final activity was expressed as a percentage of the normal controls.

2.12 Metabolite MRS analysis

For this assay, the extraction of metabolites was carried out by myself and the MRS analysis by the Biomedical Magnetic Resonance group at St Geroge's Hospital. For assessment of succinate and other metabolites, MRS analysis was performed on *FH*-deficient and control fibroblast lines. Medium was removed from each flask and the cells washed twice with 10ml of PBSA. 2ml of 6% perchloric acid (PCA) were added to each flask which was gently rocked for 2 minutes to ensure that all the cells were covered by the PCA. Cells were scraped into a polypropylene tube and placed on ice. An additional 1ml of 6% PCA was used to wash the flask and then added to the tubes which were centrifuged at 10,000 rpm (Beckman) for 15 minutes at 4°C. The supernatant was pipetted into a clean tube and neutralised to pH 7.0 using 1%, 10% KOH and 1% PCA. The protein content of the pellet was determined by the Bradford assay (Biorad). The neutralised solution was further centrifuged at 10,000 rpm for 10 minutes at 4°C and the supernatant pipetted into a clean tube and frozen. For the ^1H MRS studies, the neutralized cell extracts were freeze-dried, reconstituted in D_2O and placed in 5mm NMR tubes. ^1H MR spectra were obtained using a Bruker 600MHz spectrometer (pulse angle 45°; repetition time, 3.5s). The water resonance was suppressed by gated irradiation centered on the water frequency. Sodium 3-trimethylsilyl-2,2,3,3-

tetradeuterpropionate (TSP) was added to the samples for chemical shift calibration and quantification. The pH was re-adjusted to pH 7 prior to ^{1}H MRS.

2.13 Tumour Metabolite analysis

This was carried out at INSERM, Hopital Robert Debre, France. Frozen tumour samples from HLRCC, HPGL and other patients were homogenised in 1ml of extraction buffer (Tris 20mM [pH 7.2], sucrose 250mM, EGTA 2mM, KCl 40mM, bovine serum albumin 1mgml-1). Samples were then centrifuged at 40C for 30 minutes at 16,000g and the supernatant removed. Organic acids were quantified after acidification and ethylacetate extraction using gas chromatography/mass spectrometry according to a standard procedure (Chalmers 1982). The scarcity of the tumour samples and the need to treat each tumour with the optimum technique meant that duplicate analysis was not possible.

2.14 Analysis of oxidative stress

Both of these assays were carried out at Department of Medical Biochemistry and Immunology, University Hospital of Wales.

2.14.1 Superoxide dismutatase (SOD) assay

FH-deficient and control fibroblast cell pellets were re-suspended in 50 mmol/L TRIS buffer containing 0.5% Triton X-100, pH 8.0, and lysed by freeze-thawing. Lysates were centrifuged at 13,000 g for 10 minutes at 4°C. Determination of SOD activity in the cell lysates was performed as previously described (Sandstrom, Granstrom et al. 1995), the method based on the ability of SOD to inhibit the autoxidation of pyrogallol being adapted for use on the

Cobas Fara Autoanalyser (Roche Diagnostic, Welwyn Garden City, UK) using purified SOD from bovine erythrocytes (Sigma, UK) to construct a standard curve for this assay. Lysate protein content was measured using a Pierce BCA protein kit (BCA assay, Pierce, Illinois USA). All data were expressed as units of SOD activity (U) per mg protein. SOD assays were performed in duplicate and protein assays in triplicate.

2.14.2 Glutathione assay

Oxidative stress in *FH*-deficient and control cells was measured using a HPLC method to analyse the oxidation status of the antioxidant glutathione as previously described (Riederer, Sofic et al. 1989).

2.15 Measurement of mitochondrial respiratory enzymes

Assays to measure activites of complex I, II-II and IV were carried out at Neurometabolic Unit, National Hospital, Queen Square, London. Activities of mitochondrial respiratory chain enzymes were measured in *FH*-deficient and control cells as previously described (Complex I (NADH ubiquinone reductase) (Darley-Usmar 1987) Complex II-III (succinate:cytochrome c reductase) (King 1967) and Complex IV (cytochrome oxidase) (Wharton 1967). All respiratory chain activities were expressed as a ratio to citrate synthase activity to allow for mitochondrial enrichment (Shephard 1969).

2.16 Array Comparative Genome Hybridisation (aCGH)

The array construction, hybridisation and analysis were performed as described (Fiegler, Carr et al. 2003; Douglas, Fiegler et al. 2004). In brief, the array was prepared from DOP-PCR (degenerate oligonucleotide primers for

uniform amplification of DNA) amplified DNA from 3452 large insert genomic clones at an average spacing of about 1Mb throughout the genome. DNA from each of the tumours was labelled with Cy5-dCTP. DNA from a pool of normals was used as a control and labelled with Cy-3dCTP. After correcting for background, the log_2 ratio of the fluorescence intensities of tumour (T) to normal (N) was calculated, after normalisation to the remainder of the genome in that tumour. Log_2 T:N ratios of >3SD were taken to indicate gain and ratios of <-3SD were scored as loss, based on previous N:N hybridisations. Copy number changes of the sex chromosomes were not analysed.

2.17 Immunohistochemistry (IHC)

Tumour sections (4μm) were deparaffinized in xylene and rehydrated, and endogenous peroxide was blocked with 3% H_2O_2 (BDH). If antigen retrieval was required, the slides were microwaved or pressure cooked in Sodium citrate buffer (10mM Sodium citrate, 0.05% Tween-20 [pH 6.0] (Table 2.1). Primary antibodies were applied at the appropriate concentrations (Table 2.1) and antibody-antigen binding was detected using biotinylated secondary antibodies raised against the origin of the primary (Vector Laboratories) at a 1:500 dilution This was followed by addition of peroxidase-conjugated streptavidin-biotin complex (Vector Laboratories). Sites of peroxidase activity were demonstrated using 3,3'-diaminobenzidine (Sigma) for until strong staining was observed on the positive control (Table 2.1). Slides were counterstained with haematoxylin for 30s. Omission of primary antibody was used for a negative control.

Antibody	Species/type	Company	Dilution	Antigen retrieval	Positive Control
Laminin	Rabbit polyclonal	Abcam	1:70	Citrate buffer Microwave	Wild-type Embryo (E7.5)
Oct-4	Rabbit polyclonal	Biovision	1:50	Citrate buffer Microwave	Wild-type Embryo (E7.5)
CD34	Mouse monoclonal	Dako	1:50	Citrate buffer Pressure cook	Tonsil
FH	Rabbit polyclonal	Nordic	1:500	Citrate buffer Pressure cook	Liver
Caspase 3	Rabbit polyclonal	R & D	1:500	Citrate buffer Microwave	Mouse Embryo limb (E14)
β-galactosidase	Rabbit polyclonal	Cortex	1:500	No antigen retrieval	Transgenic mouse tissue expressing nuclear β-galactosidase
AMPK	Rabbit monoclonal	Cell-Signalling	1:50	Citrate buffer Microwave	Heart muscle

Table 2.1 Details of antibodies used for IHC

2.17.1 HIF1α IHC

HIF1α staining was carried out using the CSA system (DAKO) as recommended by the manufacturer. In brief, tumour sections (4μm) from fixed, paraffin-embedded were de-paraffinized in xylene, rehydrated and pressure cooked in target retrieval solution (16 psi for 2 mins). Sections were blocked sequentially with avidin, biotin, hydrogen peroxidase and serum-free protein and incubated with the primary antibody (Novus) for 25 minutes. Sections were then treated with anti-mouse link antibody, stepavidin-biotin complex, amplification reagent, streptavidin-peroxidase and positive staining visualised with the addition of substrate chromagen solution (2-3 minutes). Slides were counterstained with haematoxylin for 30s. Omission of primary antibody and non-tumour cells in the same section were used as a negative control and a known HIF1α-positive renal cell cancer, as a positive control. For frozen samples, no antigen retrieval method was used and the sections were fixed in ice-cold acetone for 5 minutes prior to blocking and subsequent staining.

2.17.2 Whole-Mount β-galactosidase staining

This protocol is designed test for β-galactosidase expression in tissue from transgenic mice expressing Cre recombinase. The transgenic mice are crossed to ROSA26 reporter mice that have a floxed stop codon in the 5' region of the *LacZ* gene. Cre recombinase expression removes the stop codon and allows transcription of *LacZ,* the protein product of which can be detected by the chromagenic substrate X-Gal.

Tissue was removed and placed in cold PBSA and a scapel used to carefully remove any fat surrounding the tissue. The tissue was then transferred to cold fix solution (0.4% PFA [PBSA], 0.5mM EGTA, 2mM $MgCl_2$) for 30 minutes at 4°C and rinsed (3 x 15 minutes) at 4°C (2mM $MgCl_2$, 0.02% NP-40, 0.01% Na-deoxycholate). The tissue was placed in stain

solution (5mM potassium ferrocyanide, 5mM potassium ferricyanide, 1mgml^{-1} X-Gal, 0.01% Na-deoxycholate) for 1-2 hours at 37°C or until strong blue colouring was apparent in the positive control.

2.18 In situ hybridisation

In situ hybridisation was carried out using 4μm serial sections from the same formalin-fixed, paraffin-embedded specimens as used for immunohistochemistry. The *VEGF* probe was a gift from Andrew Lee. The plasmid pGEM-3 (Promega) containing cDNA (~204 bases), from a region of *VEGF* common to all four splice variants, was *Hind*III-linearised and transcribed using T7 RNA polymerase. The *thrombospondin 1* (*THSB1*) probe (~630 bases) was generated from *Sal* I-linearised plasmid pCMV-Sport6 (image clone #2262742, (Invitrogen), using T7 polymerase. The *BNIP3* probe was PCR-cloned (445bp) using RED into the *Kpn* I and *Hind* III sites in the vector pGEM-3Z (Promega), linearised with *Eco* RI and transcribed with SP6 RNA polymerase. The murine *Fhl* probes (480bp and 230bp) were also cloned using RED into pGEM-3Z using *Eco* R1 and *Kpn* I. *Kpn* I was used to linearise and T7 polymerase to generate anti-sense RNA. For hybridisation control, a β-actin probe (~414 bases) was generated from *Dra* I-linearised pSP73 (Promega) containing clone hbA-10. ^{35}S-UTP *in situ* hybridisation was performed as described previously (Poulsom, Longcroft et al. 1998) by the ISH service at CRUK. In brief, the sections were de-waxed, taken to water through graded alcohols and digested with proteinase K (20mg/ml) for 10 minutes at 37°C. The sections were hybridized to 1x10^6 cpm of each probe overnight at 55°C. Excess and poorly hybridized probe was destroyed by digestion with RNAse A and stringency washes were carried out to reduce non-specific binding. Slides were dipped in photographic emulsion (Ilford K5) and exposed at 4°C for 10 days before development (Kodak D-19). Patterns of hybridization were studied under dark-field reflected light and signal was scored as absent, weak, moderate, strong or very strong by semi-quantitative observation, by two independent observers (RP, PP).

2.19 Real-time Quantitative PCR (RT-Q-PCR)

Single stranded cDNA was synthesised from RNA as previously described. Gene expression was determined with a real-time *Taq*Man PCR assay using an ABI prism 7700 sequence detector (Applied Biosystems). Probes for analysis of human cDNA (*VEGF*, *TSP1* and *GAPDH* control) and mouse cDNA (*Fh1* and *Gapdh* control) were purchased as Assays-on-Demand with unlabeled PCR primers and *Taq*Man FAM dye-labelled probes (Applied Biosystems). Thermocycling conditions were 2 mins at 50°C and 10 mins of initial denaturation at 95°C, followed by 40 cycles of two-step PCR that consisted of 15s at 95°C and 1 min at 60°C. All reactions were performed in triplicate. Relative expression of *VEGF* and *TSP1* in human leiomyomas and myometrium was calculated as follows. For each of 4 HLRCC leiomyoma and one normal myometrium samples from a single patient, the mean Ct values for *TSP1* and *VEGF* were subtracted from the mean Ct value of *GAPDH* in order to obtain a dCT value. The dCT values for each leiomyoma were subtracted from the corresponding value in the myometrium to obtain a ddCT value. Relative copy number was calculated by the equation 2^{ddCT} for *VEGF* and *TSP1* in each of the 4 leiomyomas. The same method was applied to compare *Fh1* expression in brain, kidney and liver of $Fh1^{+/+}$ and $Fh1^{+/-}$ mice. Calculating the 2^{ddCT} value and using the mean value from the 6 mice used for analysis determined the relative copy number of *Fh1* in each tissue of the mice.

2.20 Western blotting

Levels of protein were characterised using standard Western techniques. Briefly, frozen tumour tissue or cell pellets were homogenised in lysis buffer (7 M urea, 10% glycerol, 10 mM Tris-HCl [pH 6.8], 1% sodium dodecyl sulphate [SDS], 5 mM dithiothreitol [DTT], 0.5 mM phenylmethyl sulfonyl fluoride [PMSF] with 1 $\mu g ml^{-1}$ aprotinin, pepstatin, and leupeptin),

sonicated for 15s (amplitude=30) and centrifuged at 4°C for 20 minutes at 10,000g. The supernatant was assayed for protein concentration (Biorad), denatured in 2x sample buffer (130mM Tris-HCl [pH 8.0], 20% glycerol, 4.6% SDS, 0.02% Bromophenol blue, 2% DTT) and 50μg of total protein electrophoresed through 7.5-12.5% (depending on the Mw of the protein) acrylamide gel (50mA for 2-3 hours) in running buffer (0.25M Trizma base, 1.92M Glycine, 1% SDS), followed by charged transfer to PVDF membrane (Millipore) in transfer buffer (0.05M Trizma base, 1.92M Glycine). Rainbow molecular weight markers (Amersham) were run in parallel in order to assess the transfer efficiency and to size the protein bands during the final analysis. The PVDF membrane was blocked for 1 hour at room temperature (5% Marvel [PBSA] then incubated with the appropriate primary antibody diluted to an optimal concentration in 3% Marvel [PBSA] (including a control antibody) (Table 2.2) for 2 hours at room temperature by gentle rocking. The membrane was washed 5 times in 0.1% Tween-20 [PBSA] for 5 minutes and the appropriate secondary antibody added at 1:2000 dilution in 0.1% Tween-20 [PBSA]. A further 5 washes were carried out followed by a final wash in cold PBSA. Detection of protein was visually observed by treatment of the membrane with enhanced chemi-luminescence reagents (ECL; Amersham Pharmacia Biotech, Amersham, UK) for 1 minute and exposing to film (Kodak) in a dark room. Protein levels were quantitated by densitometry relative to the loading controls.

Antibody	Species/type	Company	Dilution	Positive control
FH	Rabbit polyclonal	Nordic	1:400	HeLa lysate
HIF1α	Mouse monoclonal	Transduction laboratories	1:250	$CoCl_2$ treated HeLa lysate
β-actin	Mouse monoclonal	Sigma	1:2000	None (loading control)
GAPDH	Mouse monoclonal	Abcam	1:5000	None (loading control)

Table 2.2 Details and dilutions of antibodies used in Westerns blots

2.21 Southern blotting

11μg of DNA was digested with the appropriate restriction enzyme (30 units) in a total volume of 40μl overnight at 37°C. 10μl of DNA loading buffer was added and the DNA electrophoresed through a 1% agarose gel for 16 hours at 50V. Molecular weight markers were run in parallel. The gel was photographed under a transilluminator to check sufficient migration. The gel was rinsed in distilled water then gently agitated in depurination buffer (0.125M HCl) for 10 minutes. The gel was rinsed with distilled water and gently agitated in denaturing buffer (1.5M NaCl, 0.5M NaOH) for 30 minutes. After rinsing in distilled water the gel was gently agitated in neutralization buffer (1.5M NaCl, 0.5M Tris-HCl [pH 7.5]) for 30 minutes. These steps were carried out at room temperature. The gel was rinsed with distilled water and transferred overnight to Hybond N+ nitocellulose membrane (Amersham) in transfer buffer (20x SSC). The membrane was placed in a UV Crossslinker (Stratagene) and pre-wet in 2x SSC. Pre-hybridisation solution (6x SSC, 0.25% SDS, 5x Denhardt's (2% BSA, 2% Ficoll™, 2% Polyvinylpyrrolidone), 25μgml-2 salmon sperm DNA) was added to the membrane and incubated at 65°C for 30 minutes in a rotating hybridisation oven. Meanwhile, 100μl of the DNA probe ($1ng\mu l^{-1}$) was denatured at 95oC for 5 minutes and immediately placed on wet ice. 45μl of the probe was added

to a microfuge tube containing a Ready-To-Go™ DNA labelling bead (-dCTP) (Amersham) followed by 5µl of [α-^{32}P]-dCTP (50µCi) (Amersham). Gentle pipetting was used to mix the labelling reactants and pulse centrifugation to remove any air bubbles. The microfuge tube was incubated at 37°C for 20 minutes after which the reaction was stopped by adding 5ml of 0.2M EDTA [pH 8.0]. Unincorporated nucleotides were removed using a ProbeQuant™ G-50 Micro Column (Amersham) as recommended by the manufacturer and the labelled probe denatured at 95°C for 5 minutes then placed on wet ice. The pre-hyb was eluted from the hybridisation tube and replaced with pre-warmed (65°C) hybridisation buffer (same as pre-hyb but with 10% dextran sulphate) and the probe added. Hybridisation was carried out overnight at 65°C in a rotating oven. The membrane was washed (2 x 30 minutes) with low stringency buffer (2x SSC, 0.1% SDS) and then 2 x 30 minute washes with high-stringency buffer (0.2x SSC, 0.1% SDS). The membrane was exposed to film (Kodak) overnight at -80°C, developed and quantitated by signal intensity of specific sized bands.

2.22 Pronuclear injection of transgene DNA

DNA was further purifed using the Elutip-d Minicolumns (Schleicher-Shuell) as recommended by the manufacturer. Eggs were harvested from 1-day pregnant females and transgene DNA injected into male pronuclei. Viable eggs (25) were implanted into female foster mice and offspring were crossed with C57/BL6.

2.23 Mouse Breeding

Mice were bred and housed at Clare Hall Laboratories under strict Home Office guidelines (project licence PPL70/6018). In the event of culling mice for analysis, mice were shipped to the animal unit at the London

Research Institute and culled by using a CO_2 chamber then cranial fracture under the supervision of an animal technician.

2.24 Isolation of mouse embryos

Mice were culled as described and the uteri removed under the supervision of an embryologist. Uteri were placed in cold PBSA and transferred into a petridish. Concepti were removed with the aid of a dissection microscope (Nikon SMZ1500). Gross morphology was observed and photographed using a photo-dissection camera (Nikon DS5M) and selected embryos were fixed as previously described. The histology, H&E and immuno staining was observed and photographed under low and high power (Nikon DXM1200F).

2.25 Solutions and media provided by the Research Services facilities

- **E4 medium (Dulbecco's Modification)**
    - 32g NaCl
    - 22.5g D-Glucose
    - 0.3g Penicillin
    - 0.5g Streptomycin
    - 0.6g Sodium pyruvate
    - 18.5g $NaHCO_3$
    - 2.9g L-Glutamine
    - 10ml KCl (20%)
    - 5ml $CaCl_2$
    - 5ml $MgSO_4$
    - 5ml NaH_2PO_4
    - 5ml $Fe(NO_3)_3$

- 5ml Antimycotic
- 1% Phenol Red
- 250ml amino acids
- Made up to 5L with distilled water
- Flushed with CO_2 unti [pH 7.]
- Filter sterilised and aliquoted (200ml)

- **FHM Media**

  - 95mM NaCl
  - 2.5mM KCl
  - 0.35mM KH_2PO_4
  - 0.2mM $MgSO_4.7H_2O$
  - 10mM Sodium Lactate
  - 0.2mM Sodium Pyruvate
  - 0.2mM Glucose
  - 5.0mM $NaHCO_3$
  - 1.0mM Glutamine
  - 0.01mM EDTA
  - 50mgml^{-1} Penicillin/Streptomycin
  - 1.0mgml^{-1} Phenol Red
  - 20mM HEPES
  - 1.71mM $CaCl_2$

- **ES Media**

  - 200ml E4-Ab-Antimyc
  - 37.5ml FCS ES qualified (15%)
  - 2.5ml Glutamine
  - 2.5ml NEAA (70µl β-mercaptoethanol + 100ml 1 x NEAA)
  - 250µl Gentamicin
  - 25µl LIF (1000 units)

- **G418 Media**

    - 2.5g of G418 dissolved in 25mls of ES media, filter sterilised and aliquoted (5ml) and stored at -20°C.

- **Freezing Media**

General	96 well Plates
90% FCS ESQ	80% ES Media
10% DMSO	20% DMSO

- **DNA Extraction Buffer for cells**

    - 500µl 1M Tris [pH 7.4]
    - 1.8ml 4M NaCl
    - 1.0ml 0.5M EDTA [pH 8.0]
    - Made up to 50ml with dH_2O

- **ES Cell Rederivation Media (10mls)**

    - 7.5mls E4-Ab-Antimyc
    - 2.5mls ESQ FCS (25%)
    - 100µl NEAA
    - 100µl Glutamine
    - 25µl Gentamicin
    - 2µl LIF (2000 units)

- **SOC media**

    - 20g Tryptone
    - 5g Yeast extract
    - 0.6g NaCl
    - 0.2g KCl

- 2g MgCl2
- 2.5g MgSO4
- 3.6g D-glucose
- Dissolved in 1L of dH_2O
- Bottled (100ml) and autoclaved for 15 minutes.

- **LB (L-broth) media/agar**

  - 100g Bacto-Tryptone
  - 50g Yeast extract
  - 100g NaCl
  - Dissolved in dH_20 up to 10L
  - Bottled (400ml) in Duran bottles
  - For L-agar – 6g of agar in each 400ml bottle
  - Autoclaved for 15 minutes.

- **5 x TBE**

  - 54g Tris Base
  - 27.5g Boric acid
  - 20ml 0.5M EDTA [pH 8.0]
  - Made up to 1L with dH_2O and autoclaved

- **Transfer buffer (20x SSC)**

  - 88.23g Tri-sodium citrate
  - 175.32g NaCl
  - Made up to 1L with dH_2O
  - Final [pH 7.8]

- **PBSA**

    - 80g NaCl
    - 2.5g KCl
    - 14.3g Na_2HPO_4
    - Dissolved in 10L of dH_2O
    - Bottled in 400ml Duran bottles and autoclaved for 20 minutes

- **Zinc Fixative**

    - 0.1M Tris Buffer [pH 7.4]
    - 0.5g Calcium acetate
    - 5.0g Zinc acetate
    - 5.0g Zinc chloride
    - Made up to 1L with dH_2O with a final pH of 6.5-7.0

3 Chapter 3. Analysis of FH-deficient tumours and cell lines and SDH-deficient tumours using gene expression analysis immunohistochemistry, in situ hybridisation and metabolomic profiling.

Introduction

Some of the syndromes described in Chapter 1 e.g. VHL disease clearly show activation of the hypoxia pathway in tumours from affected individuals (Kim and Kaelin 2004). Therefore, working on the hypothesis that pseudo-hypoxic drive may at least in part contribute to tumourigenesis of HLRCC and HPGL, we analysed tumours from HLRCC and HPGL patients for over-expression of HIF1α protein and also for HIF1α target genes. Affymetrix™ Genechips were used for micorarray based gene expression analysis to try and identify hypoxia-related genes in HLRCC ULs. As well as analysing components of the hypoxia pathway, we decided to assay reactive oxygen species (ROS) and other components of the respiratory chain in primary fibroblasts with bi-allelic *FH* mutations. These cells and solid tumours from HLRCC and HPGL were subject to metabolomic profiling using ^{1}H-NMR. These further techniques were carried out as we hypothesised that accumulation of TCAC intermediates and not ROS could stabilise HIF1α, and this has subsequently been shown to be the case *in vitro* (Isaacs, Jung et al. 2005; Selak, Armour et al. 2005),

3.1 Expression profiling of HLRCC fibroids

HLRCC is a rare condition and therefore chances of collecting fresh samples are relatively rare. However, we managed to collect 5 ULs and normal myometrium from an HLRCC patient taken fresh from a myomectomy and perform a gene expression microarray experiment. Samples were

collected, stored and RNA extracted as described in the Methods (Section 2.3.2). RNA was labelled and hybridised under the supervision of a technician (Arhus, Denmark). Full details of the experiment are described in the Methods (Section 2.5). Data analysis was carried out using the analysis package GeneSpring (Agilent). Affymetrix probe set summary statistics were generated using the MAS5 algorithm (Affymetrix). The data was median centered to remove systematic bias between chips and reporters flagged as absent in all samples were removed from the analysis. Expression ratios for each reporter were calculated from the mean signal across the tumour samples against the normal signal value. Differential genes were determined by applying a fold change cut-off of 1.9 to the data. A full gene list is in Appendix (ii). Due to the limited sample size (one myometrium control and no duplicate Genechips) the data could not be stringently statistically analysed but we did aim to obtain p-values for differentially expressed genes for testing in a larger set of archival samples. The data were analysed and stored in compliance with MIAME regulations (Brazma, Hingamp et al. 2001) and then combined with more recent Genechip expression data comparing expression profiles of sporadic and HLRCC fibroids (Vanharanta, Pollard et al. 2006). This is discussed in the final discussion and future work (Chapter 8).

The hypothesis for tumourigenesis resulting from *FH* mutations was mitochondrial perturbations resulting in hypoxic signalling, interference with apoptosis or metabolic signalling so we searched initially for genes in this group that were differentially regulated in the tumour samples (Table 3.1). The gene expression analysis identified two genes directly involved in angiogenesis. *VEGF*, a positive regulator of angiogenesis and activated by HIF1α (Forsythe, Jiang et al. 1996), was increased 3.42-fold in HLRCC ULs in comparison to myometrium. *THBS1*, a negative regulator of angiogenesis (Good, Polverini et al. 1990), was decreased in HLRCC UL (0.15-fold). Two other HIF1α target genes (*BNIP3* (3.16-fold) and *CA12* (6.08-fold) were also up-regulated in HLRCC ULs. *BNIP3* codes for a pro-apoptotic protein that is overexpressed in head and neck, pancreatic, ovarian and breast carcinomas (Sowter, Ratcliffe et al. 2001). *CA12* codes for a zinc metalloenzyme that catalyzes the reversible hydration of carbon dioxide and is over-expressed in

VHL-mutant RCC (Tureci, Sahin et al. 1998; Wykoff, Beasley et al. 2000). Analysis of the expression array data identified other genes involved in apoptosis and metabolism (Table 3.1) and these are discussed in Chapter 8.

The overexpression of 3 HIF1α-target genes (*BNIP3*, *VEGF* and *CA12*) in HLRCC ULs supported the hypothesis that *FH* mutations may activate the hypoxia pathway and therefore we used analysed tumours and normal tissue for hypoxia related genes and proteins from HLRCC patients using ISH, IHC and RT-Q-PCR. HPGL tumours were also analysed for up-regulation of hypoxia-related, pro-angiogeneic genes and proteins to investigate whether mutations in *SDHB* and *-D* up-regulated HIF1α and downstream target genes.

Differential expression of genes involved in hypoxia, apoptotic and metabolic pathways in myometrium and uterine leiomyomas from an HLRCC patient.

Gene Title	Gene Symbol	Myo	ULs (Mean)	Uls (mean):Myo Fold Change
carbonic anhydrase XII	*CA12*	189	1151	6.08
NAD(P)H dehydrogenase, quinone 1	*NQO1*	111	562	5.02
vascular endothelial growth factor	*VEGF*	312	1064	3.42
pyruvate kinase, muscle	*PKM2*	519	1720	3.32
vascular endothelial growth factor	*VEGF*	84	267	3.16
BCL2/adenovirus E1B 19kD interacting protein 3	*BNIP3*	164	518	3.16
superoxide dismutase 3, extracellular	*SOD3*	330	961	2.92
nucleolar protein 3 (apoptosis repressor with CARD domain)	*NOL3*	62	175	2.85
cytochrome P450, subfamily I (dioxin-inducible)	*CYP1B1*	173	483	2.74
B-cell CLL/lymphoma 2	*BCL2*	216	557	2.57
glucose-6-phosphate dehydrogenase	*G6PD*	77	189	2.46

fibroblast growth factor receptor 1	*FGFR1*	26	58	2.24
estrogen receptor 1	*ESR1*	43	92	2.14
adrenomedullin	*ADM*	73	157	2.14
fumarate hydratase	*FH*	457	237	0.52
caspase 1, apoptosis-related cysteine protease	*CASP1*	86	44	0.51
thrombomodulin	*THBD*	375	86	0.23
NADPH oxidase 4	*NOX4*	170	37	0.22
thrombomodulin	*THBD*	190	36	0.19
thrombospondin 1	*THBS1*	640	77	0.15

Table 3.1 Differentially expressed genes involved in hypoxia, apoptosis or metabolism in uterine leiomyomas and myometrium from an HLRCC patient.

The mean fold represents the level of expression in the UL compared to the myometrium (myo). Two HIF1α targets; *BNIP3* and *VEGF* were up-regulated 3.16 and 3.42 respectively. *THBS1*, a negative regulator of angiogenesis was down-regulated (0.15 fold). The numbers in columns 3 and 4 are the mean signal across the tissue samples (column 3 = myometrium, column 4 = mean of 5 HLRCC ULs) against the normal signal values from internal controls in the GeneChips. Column 5 is the ratio of signal values of the ULs (mean):myometrium

3.2 HLRCC uterine leiomyomas have increased microvessel compared with sporadic uterine leiomyomas.

We initially decided to investigate angiogenic markers in HLRCC and sporadic leiomyomas. We assayed microvessel density by immunohistochemical staining of vascular endotheilial cells with an antibody to CD34; a human hematopoietic progenitor cell antigen expressed by early normal hematopoietic progenitor cells and vascular endothelial cells (Traweek, Kandalaft et al. 1991). Sample collection and staining protocols are described in the Methods (Sections 2.10, 2.17). The histological features of all tumours and normal tissues were reviewed in order to confirm their origin and to exclude any marked features distinguishing HLRCC and ULs of sporadic origins. No evident differences were found and, in particular, the cellularity of HLRCC lesions, sporadic ULs, and normal myometrium was very similar (Figure 3.1). In order to identify and quantitate microvessels, CD34 IHC was performed on 14 HLRCC ULs, two samples of paired HLRCC myometrium, and 11 sporadic ULs together with 11 samples of paired normal myometrium (Figure 3.1). Vessel numbers as detected by CD34 expression were counted in 20 high-power fields. Vessel density was markedly higher in the HLRCC ULs (mean = 117, range 75–150) than in the HLRCC myometrium (mean = 58, range 53–62), the sporadic ULs (mean = 27, range 16–67), and the normal myometrium (mean = 46, range 34–82) ($c^2_2 = 27.8$, $p = 0.0001$, Kruskal–Wallis test overall). HLRCC leiomyomas had a significantly higher vessel count than HLRCC myometrium ($p = 0.027$, Mann–Whitney test), whereas sporadic ULs actually had fewer vessels than normal myometrium ($p < 0.001$, Mann–Whitney test). The vascularity of HLRCC and normal myometrium did not differ significantly from one another ($p = 0.32$, Mann–Whitney test). CD34 IHC was performed on four SKLs and variable vasculature was observed within the sections. No positive staining was observed in the epidermis and the leiomyomas contained regions of both dense and weak vascularity. We were not able to make a statistical tissue comparison, owing to the small size of the erector pili muscle from which these tumours originate.

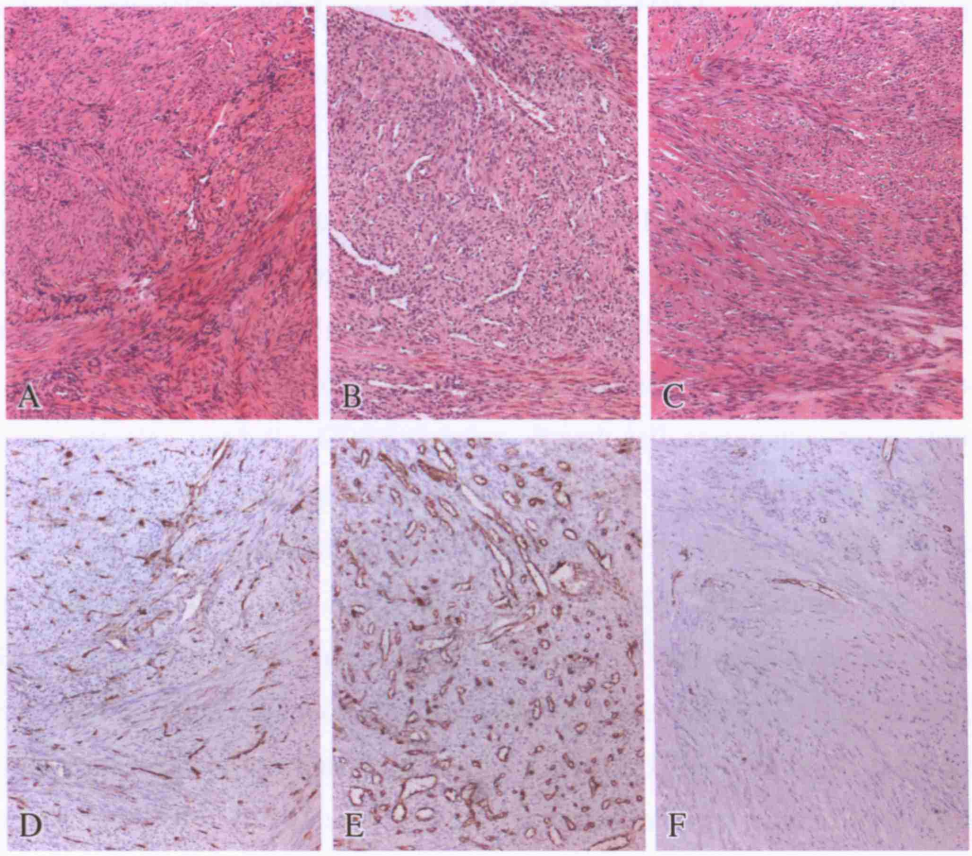

Figure 3.1 Microscopic appearances and CD34 staining of uterine leiomyomas and normal myometrium.

H&E staining reveals similar morphology of (A) normal myometrium, (B) HLRCC UL, and (C) sporadic UL. Representative results are shown of microvessel immunostaining using a CD34 antibody of (D) normal myometrium, (E) HLRCC UL, and (F) sporadic UL (final magnifications x50). Note the increased microvessel density in E and the decreased density in F compared with D.

3.3 Expression analysis of *VEGF*, *THBS1* and *BNIP3* in HLRCC and sporadic leiomyomas.

Given our evidence for hypervascularity in HLRCC tumours, we then tested the expression of various components of the hypoxia and/or angiogenesis pathways. Initially, IHC for EPAS1, a transcription factor involved in the induction of oxygen-related genes, was carried out on the same tissue samples used for CD34 staining. Renal cell carcinomas from three different patients with germline *VHL* mutations were used as a positive control. We did not identify positive staining for EPAS1 in any of the myometrium samples, or in the sporadic or HLRCC leiomyomas. Previous IHC analysis for HIF1α and CAIX, a HIF target, was also negative in the myometrium, and in both the sporadic and the HLRCC ULs (Pollard, unpublished data). We then analysed 11 HLRCC ULs, four HLRCC SKLs, two sporadic ULs, and two myometrium samples for expression of *VEGF* and *THBS1* mRNA; we used ISH because the protein products of these genes are secreted. The *VEGF* promoter contains a HRE and the protein is an angiogenic mitogen involved in the induction of endothelial cell proliferation, inhibition of apoptosis, and permeabilization of blood vessels. *THBS1* suppresses angiogenesis by inducing endothelial cell apoptosis and through indirect effects on growth factor mobilization, but may also have cell autonomous effects. Tumour neovascularization is controlled by a balance of positive effectors (for example, VEGF) and negative effectors (for example, THBS1).

The promoter of the *BNIP3* gene contains a hypoxia response element (HRE) and the expression of this gene is known to be up-regulated in hypoxic states. Its role remains unclear, but it may regulate apoptosis.

ISH was carried out by the Histopathology department at Cancer Research UK and is described in the Methods (Section 2.18). Results were scored under guidance of a histopathologist (Professor R. Poulsom).

3.3.1 HLRCC uterine leiomyomas have increased expression of *VEGF* compared to sporadic leiomyomas

HLRCC ULs exhibited widespread *VEGF* expression, ranging from moderate to very strong (Table 3.2, Figure 3.2). In comparison, the 2 sporadic ULs tested had weak or moderate *VEGF* expression. *VEGF* expression in myometrial tissue from HLRCC and sporadic UL patients was weak. We confirmed the increased *VEGF* expression using RTQ-PCR in 4 HLRCC ULs and 1 myometrium sample from an HLRCC patient (Section 3.4). ISH showed that *VEGF* expression in the SKL samples was weak/moderate and not as wide spread as in the HLRCC ULs. Expression was strongest in the hair follicle and supra-basal epithelial cells. However, we were unable to analyse the level of *VEGF* expression in normal erector pili muscle.

3.3.2 Loss of *THBS1* expression in both HLRCC and sporadic uterine leiomoymas

THBS1 expression, as assessed using ISH, was weak or absent in all UL samples (sporadic and HLRCC) (Table 3.2, Figure 3.3). Myometrium samples exhibited very strong *THBS1* expression evenly distributed throughout the smooth muscle cells. The large decrease in *THBS1* expression in the HLRCC tumour samples was confirmed by RTQ-PCR analysis (Section 3.4.). *THBS1* expression was absent in the 3 SKLs analysed.

3.3.3 *BNIP3* expression is upregulated in HLRCC UL but not in sporadic uterine leiomoymas

ISH showed *BNIP3* expression to mirror that of *VEGF*, with increased mRNA levels only in the HLRCC ULs (Table 3.2, Figure 3.4). The

differences in *BNIP3* expression were statistically significant across the four types of sample (Kruskal–Wallis test, $c^2_2 = 13.7$, $p = 0.0034$).

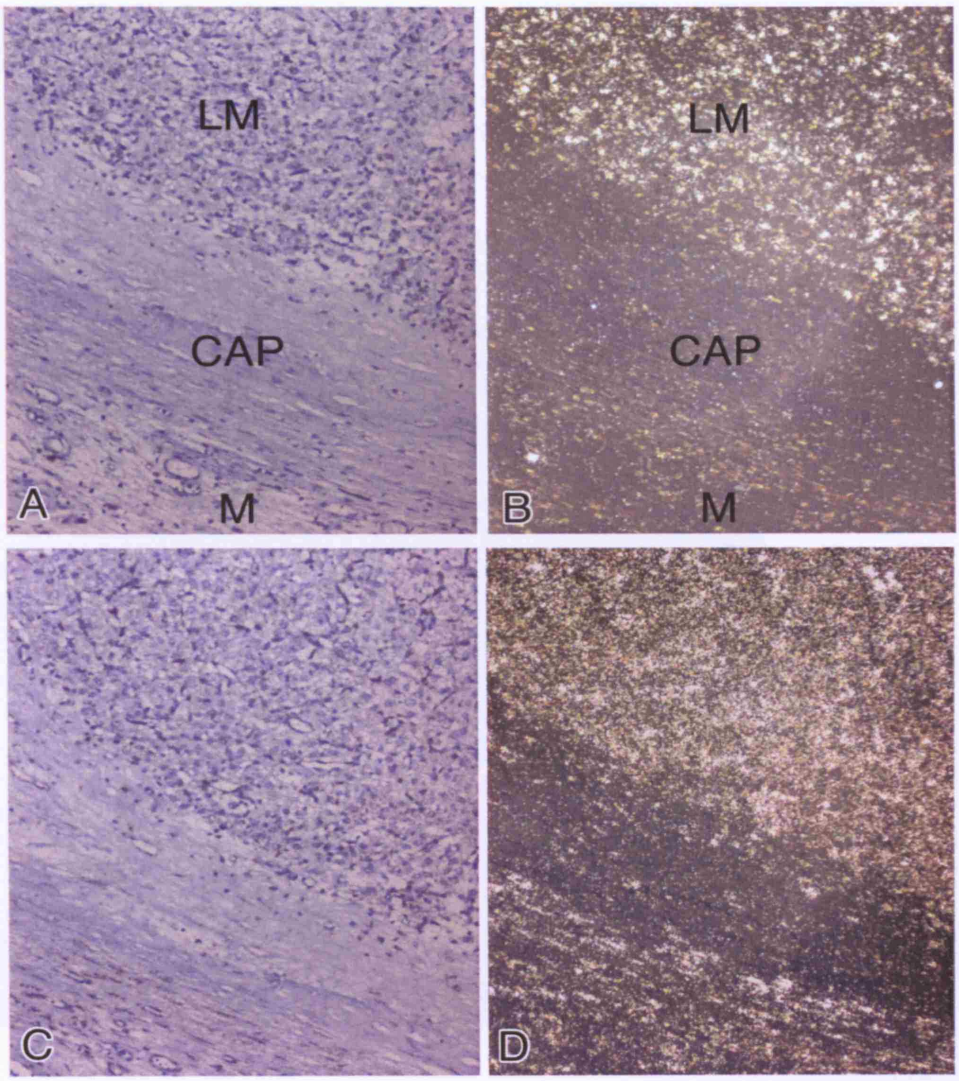

Figure 3.2 Representative *VEGF* expression in HLRCC uterine leiomyomas and normal myometrium by *in situ* hybridisation..

The ISH signals are visualised either under dark field (signal visible as white dots) or bright field illumination (signal visible as black dots) (all x100 magnification). *VEGF* expression is greater in (A,B) HLRCC UL (LM) than the surrounding myometrium (M) and capsule (CAP). β-actin expression is visible in both layers (C,D), with slightly stronger expression in the UL.

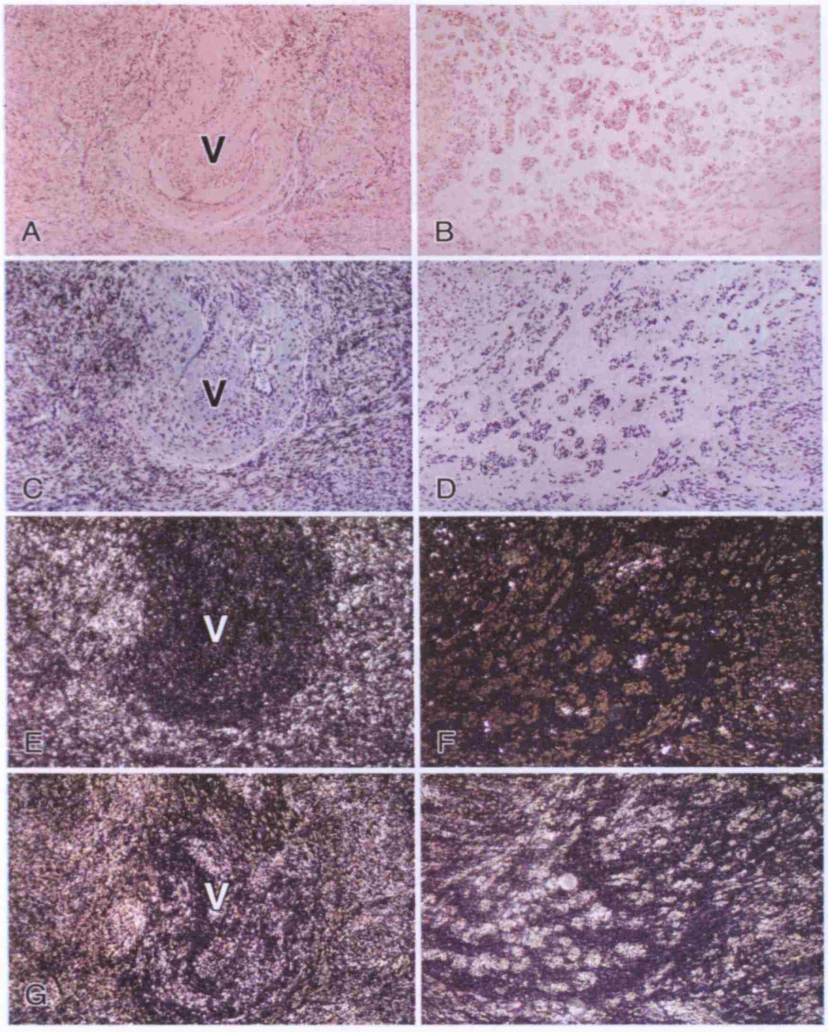

Figure 3.3 *THBS1* expression in HLRCC myometrium and uterine leiomyomas by *in situ* hybridisation.

(A) H&E of myometrium; (B) H&E of leiomyoma; (C, E) *THBS1* expression in myometrium; (D, F) *THBS1* expression in leiomyoma; (G) β-actin expression in myometrium; (H) β-actin expression in leiomyoma (magnifications are x50). There is greatly reduced expression of *THBS1* in the leiomyoma in comparison with the myometrium. β-actin expression is widespread throughout both the myometrium and the leiomyoma. 'V' denotes a blood vessel in the myometrium section.

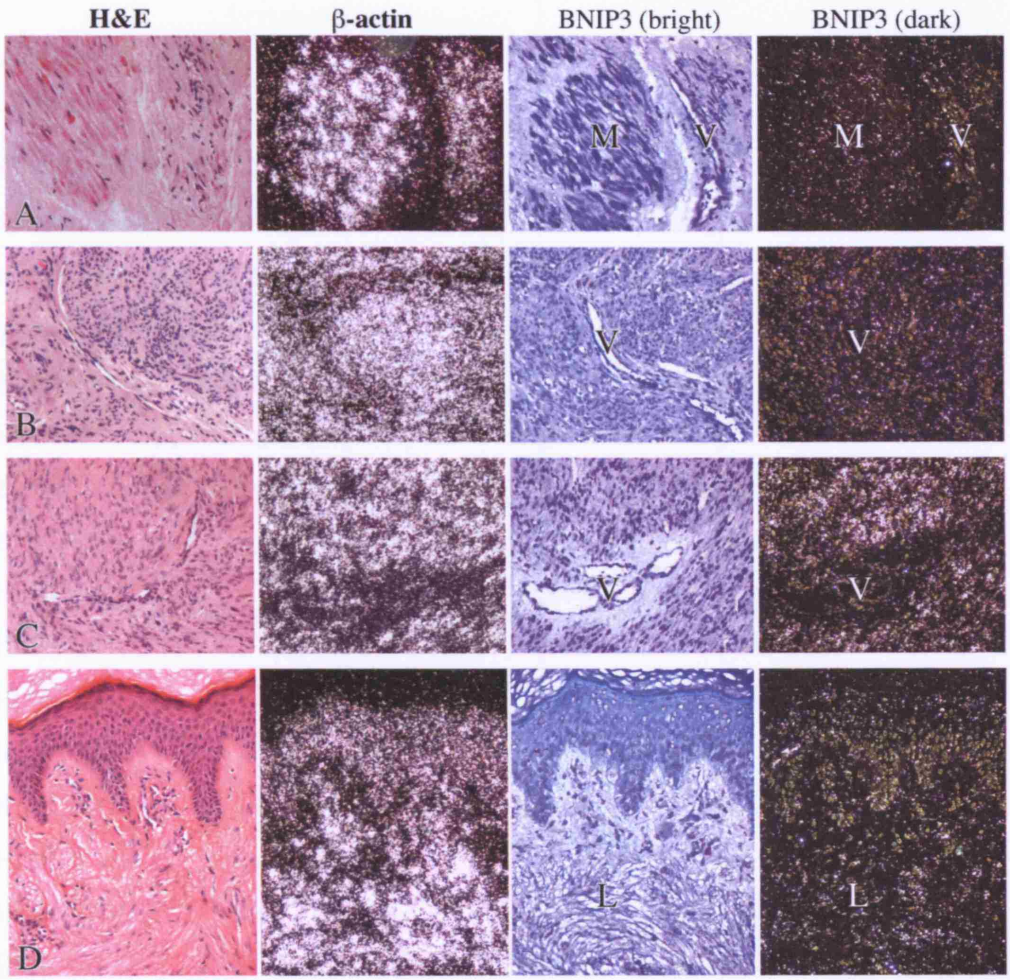

Figure 3.4 *BNIP3* expression in HLRCC myometrium and uterine leiomyomas by *in situ* hybridisation.

(A) Myometrium; (B) sporadic UL; (C) HLRCC UL; (D) SKL. Column 1 = H&E; column 2 = *β*-actin expression (dark field), column 3 = *BNIP3* expression (light field); column 4 = *BNIP3* expression (dark field). In panels A, 'M' denotes the smooth muscle of the myometrium. In panels A, B, and C, 'V' indicates the position of a blood vessel; and in panels D, the SKL is indicated by 'L'.

TISSUE TYPE	PROBE		
	THBS1	*BNIP-3*	*VEGF*
Sporadic UL	-	- / +	++
Sporadic UL	-	-	+
Sporadic UL		-	
Sporadic UL		-	
Myometrium (sporadic)		-	
Myometrium (sporadic)	++++	+ / -	+
Myometrium (sporadic)	++++	-	+
Myometrium (sporadic)		-	
HLRCC UL	-	++	++
HLRCC UL	-		+++
HLRCC UL	+	+++	++++
HLRCC UL		+++	+++
HLRCC UL	+		+++
HLRCC UL	+	+++	++
HLRCC UL	+		+++
HLRCC UL	+	+++	++
HLRCC UL	+	++	++
HLRCC UL	-		+++
HLRCC UL	-		++++
HLRCC SKL	-	+	+
HLRCC SKL	-	++	++
HLRCC SKL		++	++
HLRCC SKL	-	++	++
Myometrium (HLRCC)	++++	+	+
Myometrium (HLRCC)		+ / -	

Table 3.2 Semi quantitative analysis using *in situ* hybridisation for *THBS1*, *BNIP3* and *VEGF*.

Expression of mRNA for *THBS1*, *BNIP3* and *VEGF* was determined using semi quantitative assessment and a five scale scoring system.

3.4 Real-time quantitative PCR (RTQ-PCR) analysis confirms *VEGF* upregulation and and *THBS1* downregulation in HLRCC uterine leiomyomas

RTQ-PCR analysis was carried out as described in the Methods (Section 2.19). In brief, cDNA was synthesised from 450ng of RNA extracted from myometrium and HLRCC fibroids (gross specimens) that were used for the Genechip expression analysis and used as a template for a TaqMan assay (Applied Biosystems). The *VEGF*, *THBS1* and *GAPDH* (control) probes were purchased as 'assays on demand' and were FAM-labelled (Applied Biosystems). All reactions were performed in triplicate.

RTQ-PCR analysis confirmed that *VEGF* expression in HLRCC leiomyomas compared with the surrounding myometrium was increased 1.4 to 3.5 fold (Table 3.2), thus confirming the ISH data.

The large decrease in *THBS1* expression in the HLRCC tumour samples was also confirmed by RTQ-PCR analysis, which showed reduced expression ranging from 0.123 to 0.008-fold.

TISSUE TYPE	Relative Gene Expression (fold change)	
	VEGF	*THBS1*
HLRCC UL 1	3.5	0.035
HLRCC UL 2	1.5	0.123
HLRCC UL 3	1.4	0.015
HLRCC UL 4	1.9	0.008

Table 3.3 Real-time quantitative PCR analyses of *VEGF* and *THBS1* in HLRCC uterine leiomyomas and myometrium.

Relative expression of *VEGF* and *THBS1* in four HLRCC ULs was compared with a matched myometrium sample.

3.5 HIF1α expression in HLRCC uterine leiomyomas, myometrium, and HLRCC renal cell cancers

In order to assess nuclear HIF1α expression in the above tumours, we analysed ten paraffin-embedded UsL, two with surrounding myometrium, one frozen HLRCC type II papillary renal cell cancer and one paraffin embedded HLRCC collecting duct tumour (lymph node metastasis). HIF1α staining was moderate in all of the fibroids studied, although weak/moderate staining was also observed in the surrounding myometrium (Figure 3.5). We had previously shown increased expression of *VEGF* in these lesions, associated with a high density of microvessels (Figures 3.1 and 3.2). In both of the renal cancers, very strong HIF1α staining was observed in each tumour and staining was much weaker in the stromal tissue (Figure 3.6 and 3.7). All of these lesions were found to be highly vascular. We confirmed the HIF1α over-expression by Western blotting in the frozen renal tumour and normal kidney tissue. The 120-kDa band corresponding to HIF1α was consistently only present in the tumour (Figure 3.8), thus verifying the results from the immunohistochemical analysis.

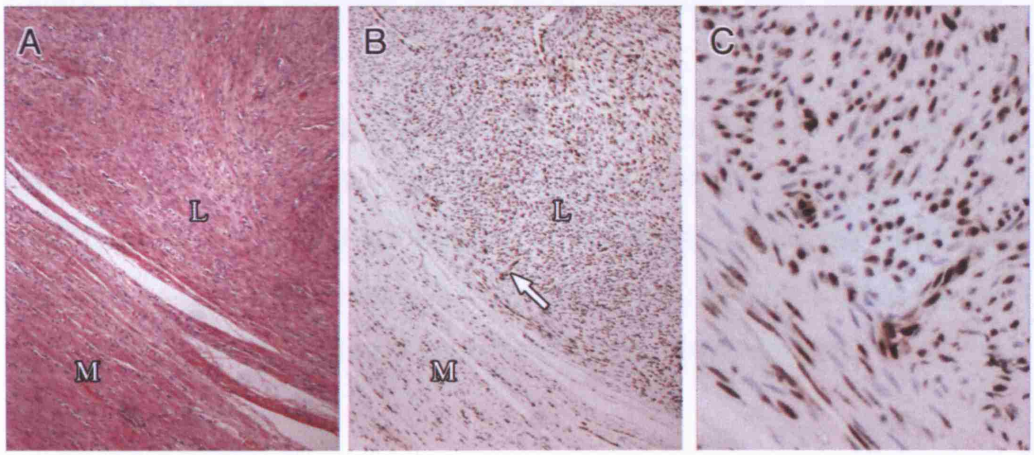

Figure 3.5 HIF1α staining of HLRCC uterine leiomyomas

HIF1α staining of HLRCC UL (L) and surrounding myometrium (M). The H&E stain (A) and HIF1α (B) are both x 100. The arrow in B indicates the area in C (x400). Note nuclear staining of HIF1α is present in the UL, but also some weaker staining is observed in the myometrium.

The sporadic ULs analysed showed weak expression of HIF1α which was variable between samples; this may partly be due to the quality of the tissue blocks as the HIF1α IHC is very sensitive to tissue collection and processing.

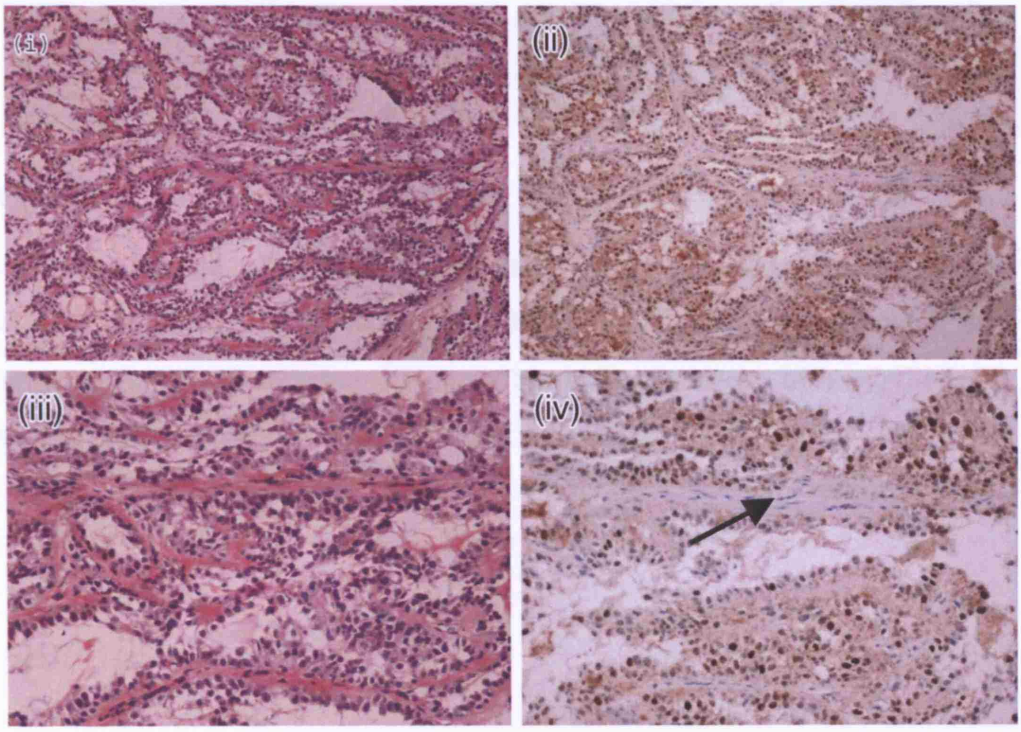

Figure 3.6 HIF1α staining of HLRCC collecting duct renal cancer (metastasis)

A lymph node metastasis from a HLRCC collecting duct renal cancer showing H&E x100 (i), HIF1α x100 (ii), H&E x200 (iii), and HIF1α x200 (iv). There is strong HIF1α staining in the nuclei of tumour cells and negative staining in the stromal tissue (arrowed), well illustrated by the horizontal bands of stromal cells without HIF1α staining in (iv).

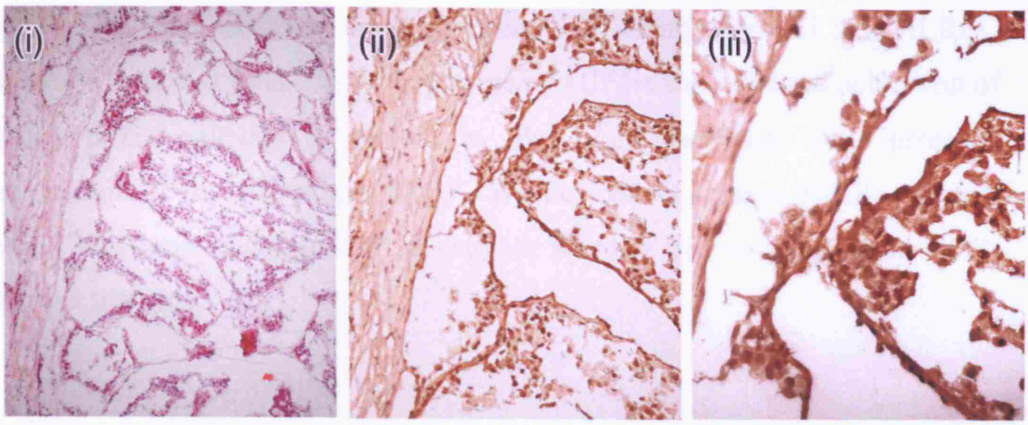

Figure 3.7 HIF1α staining of HLRCC type II papillary renal cancer

A frozen section of a HLRCC papillary type II renal tumour showing H&E x100 (i), HIF1α x100 (ii) and HIF1α x200 (iii). Even allowing for some background staining owing to biotin levels in the kidney, there is strong nuclear expression of HIF1α.

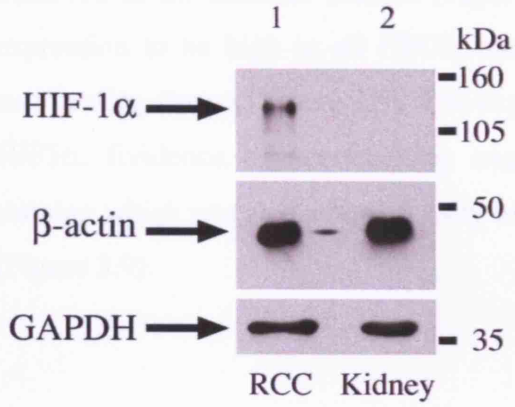

Figure 3.8 HIF1α expression in an HLRCC type II papillary renal tumour by immunoblotting.

Lane 1, total cellular lysate of type II papillary renal cell cancer from HLRCC patient. Lane 2, normal kidney. Bands corresponding to HIF1α (120kDa) and loading controls (GAPDH, 38kDa; β-actin, 44kDa) are arrowed.

The data obtained using IHC and ISH clearly showed that HLRCC tumours (especially RCCs) were expressing HIF1α and indicated activation of the hypoxia pathway as shown by the high vascularity and increased expression of the HIF-target *VEGF*. We decided to analyse HPGL tumours using the same techniques to investigate whether this was similar in *SDH*-mutant tumours.

3.6 *SDH*-mutant tumours strongly express HIF1α, *VEGF* and are highly vascular

We analysed, from HPGL patents, 12 paragangliomas and 4 phaeochromocytomas, including those used for metabolomic analysis (Section 3.7), to test for hypoxic signalling. Strong nuclear expression of HIF1α was observed in all tumours studied (Figure 3.9). Using ISH, we found *VEGF* expression to be high in all HPGL tumours compared with the stroma and surrounding tissues (Figure 3.9). The expression pattern correlated with that of HIF1α. Evidence of the resulting angiogenesis was shown by the CD34 staining which revealed a high density of microvessels throughout the tumours (Figure 3.9).

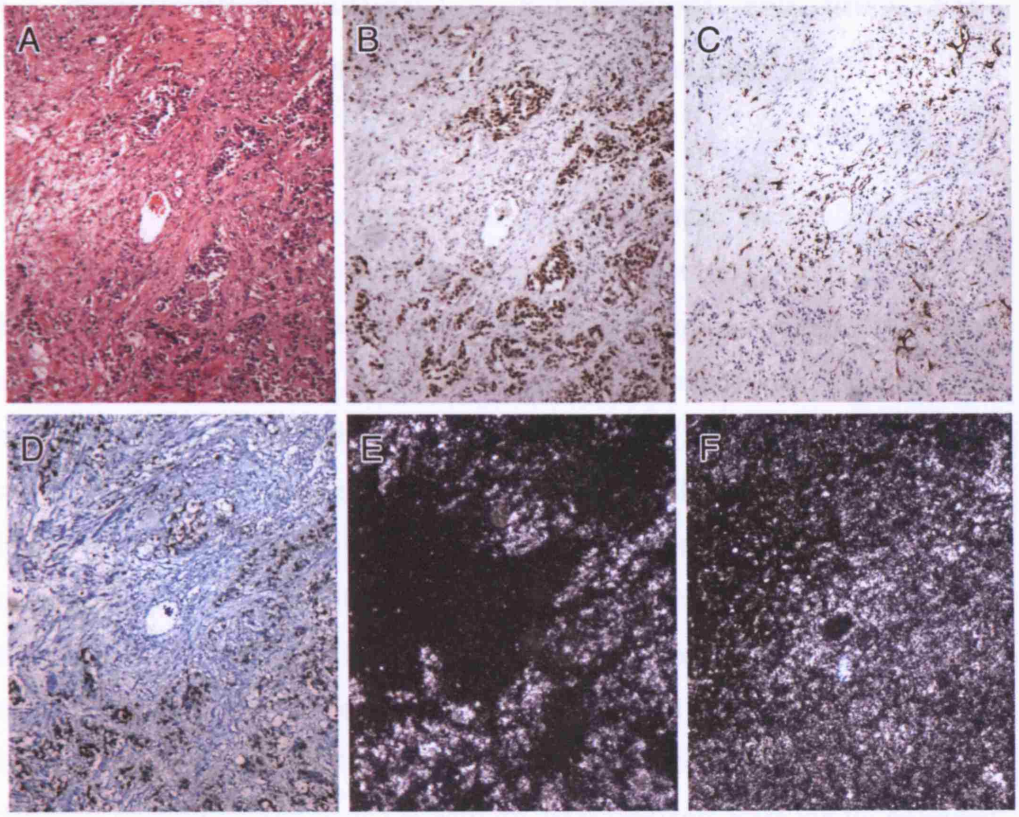

Figure 3.9 Expression of HIF1α, *VEGF* and CD34 staining in HPGL paraganglioma

Representative expression of HIF1α, its target molecule *VEGF* and high vascularity in HPGL paragangliomas. *SDHB* HPGL paraganglioma (x100) showing H&E (A), HIF1α IHC (B), and CD34 IHC (C) and *VEGF* mRNA expression (light field (D) and dark field (E). β-actin mRNA expression was used as a control (F). Note the strong spatial association between the strong nuclear HIF1α staining and *VEGF* expression in the tumour cells within 'Zellballen'. Note also the high density of microvessels shown by the CD34 IHC (C).

3.7 Metabolomic analysis of FH-deficient cell lines, FH-deficient tumours and SDH-deficient tumours

In view of literature linking metabolite accumulation with HIF1α stabilisation, we decided to carry out metabolomic analysis on *FH*-deficient cell lines and tumours, and SDH-deficient tumours in order to test for accumulation of the TCAC cycle intermediates succinate and fumarate. The metabolic procedures are described in the Methods (Sections 2.12, 2.13) and collaborators at St. George's Hospital, London, UK and INSERM, Paris, France carried out the experiments. We also analysed redox stress using a superoxide dismutase (SOD) assay and measured complex I, II-III and IV activity in FH-deficient fibroblasts. These assays were carried out by collaborators at the University of Wales, UK and the National Hospital, London UK and are described in the Methods (Sections, 2.14, 2.15). The FH-deficient fibroblasts and their FH-activity measurements were kindly provided by Dr. S. Olpin at the Sheffield Children's Hospital.

3.7.1 Increased levels of succinate, fumarate and α-ketoglutarate in FH-deficient cells and HLRCC tumours

Metabolomic profiling was initially used to study the effects of *FH* mutations on succinate and fumarate accumulation by analysing skin fibroblasts from 4 patients suffering from the recessive disorder fumarase deficiency. The enzyme activities and bi-allelic *FH* mutations in these patients had been previously determined (Table 3.4). As a control, we used 6 skin fibroblast cell lines from individuals with no apparent disease and no *FH* mutations as determined by direct sequencing. The *FH*-deficient cell lines had significantly higher levels (Table 3.4) of succinate (mean=59.4umol/g protein, median=39.8, range=32-125.9) than the normal cell lines (mean=17.4, median=14.5, range=9.9-29.8). The alpha-ketoglutarate levels were also increased in all of the *FH*-deficiency cells (mean=343.1, median=285.2,

range=170.6-631.5) in comparison with the normal cell lines (mean=132.8, median=129.5, range=65.4-199.1). The method used was not specifically able to detect fumarate in these samples. We then tested for accumulation of succinate and fumarate in four HLRCC fibroids and two normal myometrium samples, one from a HLRCC case and one, a non-HLRCC patient. Each tumour came from a patient with a known germline *FH* mutation and had acquired a 'second hit' by allelic loss. All of the tumour samples showed greatly elevated levels of both succinate and fumarate (Table 3.5). Normal myometrium samples from the HLRCC patient and the non-HLRCC individual showed similar levels for each metabolite. The combined data suggested that bi-allelic *FH* mutations in the HLRCC fibroids severely reduced the conversion of fumarate to malate, resulting in blockage of the Krebs cycle and accumulation of fumarate and, consequently, succinate. The succinate:fumarate ratio was greater than one in the myometria, but typically 0.1-0.2 in the tumours (Table 3.5).

Cell Line	Mutation	Activity (%)
Fhdef1	AAAins435/R58X	1.9
Fhdef2	P131R/exon 2 splice variant	13.0
Fhdef3	R190H/R190H	2.4
Fhdef4	K187R/K187R	6.0

Table 3.4 *FH* mutations and enzyme activity relative to controls in skin fibroblasts from FH deficiency patients

	Succinate	Fumarate	Succinate:fumarate
Myometrium non-HLRCC	6.0	2.0	3.0
Myometrium HLRCC	4.5	0.5	9.0
HLRCC UL 1	88	458	0.19
HLRCC UL 2	70	688	0.10
HLRCC UL 3	98	646	0.15
HLRCC UL 4	93	417	0.22

Table 3.5 Measurement of succinate and fumarate in HLRCC uterine leiomyomas and myometrium

Succinate and fumarate levels (μmol/g protein) in HLRCC ULs and control myometria. Although not significant by the Wilcoxon non-parametric test, a t-test shows both succinate (p=0.0009) and fumarate (p=0.0055) levels to be significantly higher in the tumour samples compared with the normal myometria.

3.7.2 FH-deficient cells do not show notably increased oxidative stress and retain activity of mitochondrial complexes I, II-III and IV

The SOD assay was used on *FH*-deficient fibroblasts (n=2) and control fibroblasts (n=6) (Table 3.6). The former had mean SOD levels of 44.4mU/mg protein (median=44.4, range=38.7-50.1) and the latter showed very similar mean levels of 38.2mU/mg (median=38.0, range=31.3-47.3). A glutathione assay supported absence of oxidative stress; the *FH*-deficient lines had a mean reduced glutathione concentration of 5.52 nmol/mg protein (median=5.52, range=3.30-7.74) and the control lines had a mean of 4.04 (median=3.44, range=1.72=7.34) (Table 3.6). The two *FH*-deficient lines were then tested to determine whether levels of the respiratory chain complexes and/or their abilities to transfer electrons were abnormal compared with the 6 controls. There was no evidence that the levels of functional electron transport chain

proteins were lower in the *FH*-deficient cells than in controls (see Table 3.6 for complex I). Complex II-III activity was 0.096 and 0.010 in the two *FH*-deficient lines (reference 0.070-0.243). Complex IV activity was 0.014 in one *FH*-deficient line, compared with a reference range of 0.007-0.036, and increased in the other at 0.120.

Sample	Succinate (μmol/g)	SOD (mU/mg)	Reduced gluthathione (nmol/mg)	Complex I (μmol/min/mg)
Control 1	17.1	31.3	4.90	0.952
Control 2	9.9	38.3	3.44	0.267
Control 3	11.4	37.7	1.72	0.764
Control 4	24.5	35.7	2.81	0.486
Control 5	29.8	38.7	7.34	0.783
Control 6	11.8	47.3	-	-
Fhdef1	32.6	38.7	7.74	1.72
Fhdef2	125.9	50.1	3.30	0.981
Fhdef3	32.0	-	-	-
Fhdef4	47.0	-	-	-

Table 3.6 Levels of succinate, superoxide dismutase, reduced glutathione, and activities of complex I in *FH*-deficiency cell lines and normal controls.

Electron transport chain activities are shown relative to that of citrate synthase. = not done. Formal statistical analysis is problematic given the small number of samples and lack of information on the underlying distributions, although succinate levels are significantly higher in the *FH*-deficiency patients (p=0.011, Wilcoxon test; p=0.05, t-test). No other significant differences between the two groups of patients exist (p>0.05, Wilcoxon and t-tests, details not shown).

3.7.3 Increased succinate in HPGL tumours

The 6 frozen paragangliomas were analysed using metabolomic profiling in order to determine the succinate and fumarate concentrations. Tumours from patients 2 and 6 with germline *SDHB* mutations had a grossly elevated concentration of succinate compared with the three tumours from the non-HPGL patients (Table 3.7); the succinate:fumarate ratio was increased and positive in these lesions. One *SDHB* tumour from a patient with a germline S100P missense change did not show grossly elevated succinate. These data showed that the *SDHB* mutations in the HPGL tumours could cause accumulation of succinate by impairing enzyme activity. The reason for the failure to detect elevated succinate in one tumour is unclear, but it remains possible that S100P is a non-pathogenic change.

Tumour no.	Germline SDH mutation	Succinate	Fumarate	Succinate:fumarate
1	No	49.7	12.7	3.9
2	Yes	364.5	17.8	20.5
3	No	32.3	3.0	10.8
4	Yes	43.2	12.6	3.4
5	No	40.9	7.0	5.8
6	Yes	517.0	13.9	37.2

Table 3.7 Succinate and fumarate levels in HPGL and non-HPGL paragangliomas.

Meaurements are expressed as μmol/g protein. Owing to sample 4, the differences between HPGL and other tumours are not significantly different (p=0.05), despite the very large increases in succinate in tumours 2 and 6.

3.8 Discussion

The results have demonstrated that bi-allelic *FH* mutations, whether in HLRCC tumours or in cells from fumarase deficiency patients, result in raised levels of both fumarate and succinate. Bi-allelic *SDHB* mutations predominantly cause raised levels of succinate. In addition, the results show that benign and malignant tumours in the HLRCC syndrome exhibit accumulation of the HIF1α protein, the central signalling molecule in the hypoxia pathway. HIF1α also accumulates in HPGL tumours, which result from germline *SDHB* mutations, adding to the existing data showing HIF1α expression in *SDHD*-mutant tumours. The raised levels of HIF1α result in increased expression of HIF-target genes, such as *VEGF*, and in angiogenesis.

There are two reasons that suggest that HIF1α over-expression is a pathological rather than a physiological result of tumour hypoxia. First, there is no spatial association in leiomyomas, renal cancers, paragangliomas or phaeochromocytomas between vessel density as assessed by CD34 expression and HIF1α expression as demonstrated in a *SDHB*-mutant PGL (Figure 3.9). Thus, HIF1α expression is not simply caused by poor vasculature and consequent hypoxia. Second, HIF1α levels are higher in HLRCC fibroids than surrounding myometrium (Figure 3.5), and the expression levels of HIF1α targets; *VEGF*, *THBS1* and *BNIP1*, are higher in HLRCC fibroids than sporadic leiomyomas (Figures 3.2-3.4, Table 3.1). Microvessel density is, however, highest in the HLRCC leiomyomas. Were HIF1α expression to be secondary to hypoxia, we would actually expect lower levels of its own expression and those of its target mRNAs in the more vascular HLRCC tumours. The sporadic fibroids that we analysed showed an anti-angiogenic profile and reduced microvessel density in comparison to their myometrium. This is consistant with existing data (Poncelet, Madelenat et al. 2002; Weston, Trajstman et al. 2003; Poncelet, Fauvet et al. 2004).

Recently, *in vitro* data have shown that RNAi inhibition of *SDHD* and *FH* results in up-regulation of HIF1α (Isaacs, Jung et al. 2005; Selak, Armour et al. 2005). Our data provide evidence that raised succinate and fumarate causes increased HIF1α expression *in vivo*. The model of 'pseudo-hypoxia' both from our data and *the in vitro* studies shows no evidence of increased oxidative stress and a plausible reason could be the inhibition of HIF-PHDs which hydroxylate HIF1α, allowing pVHL to bind and direct proteosomal-mediated degradation of HIF1α. This, however has only been demonstrated in *vitro* (Isaacs, Jung et al. 2005; Selak, Armour et al. 2005) and in order to determine whether the levels of succinate and fumarate required to inhibit HIF-PHDs are physiologically achievable *in vivo*, more experiments are necessary. We have shown that succinate accumulates in both HLRCC and HPGL tumours, but cannot, however, exclude some direct inhibition of prolyl hydroxylases by fumarate in HLRCC as there is evidence to show that other metabolites such as pyruvate and oxaloacetate can stabilise HIF1α (Dalgard, Lu et al. 2004).

The basic mechanism of tumourigenesis in HPGL and HLRCC is therefore likely, at least in part, to be pseudo-hypoxic drive, just as it is in von Hippel-Lindau syndrome. The tumours in all of these syndromes share morphological features, such as high vessel density, and molecular features, such as increased levels of HIF1α. Additionally, recent gene profiling using microarrays has shown that PCCs with *VHL* and *SDHB* and *-D* mutations have reduced oxidoreductase and pro-angiogenic profile in comparison with sporadic tumours and immunohistochemical analysis revealed that PCCs with mutations in these three genes all express very low levels of SDHB protein (Dahia, Ross et al. 2005). These data suggests that HIF1α somehow links hypoxic signalling (via VHL) with mitochondrial signals (via SDH).

The question remains as to why there are different, but overlapping, tumour spectra in the HPGL, HLRCC and VHL syndromes. Although several alternative explanations may exist, the data suggests that the specific genetic defect (in *FH, SDHB, SDHC* or *SDHD*) might cause different levels of HIF1α accumulation with particular effects on cells which require different

physiological responses to hypoxia, leading to the tissue specificity of the lesions in HPGL, HLRCC and VHL disease.

4 Chapter 4: Mutation Screening, Genoype-Phenotype analysis and Comparative Genome Hybridisation analysis of Patients with Paragangliomas and/or Phaeochromocytomas

Introduction

Paragangliomas (PGLs) are rare tumours arising from parasympathetic-associated paraganglia (particularly of the head and neck) or from sympathetic-associated paraganglia such as in the adrenal medulla when they are termed phaeochromocytomas (PCCs).

PGLs and PCCs occur in people with mutations in *NF1*, *MEN2* (*RET*) and *VHL* (Woodward, Eng et al. 1997). More recently, four more predisposition loci were identified, termed PGL1, 2, 3 and 4. After identification of three of the genes, they were found to encode proteins in complex II of the mitochondrial respiratory chain; *SDHD* (PGL1), *SDHC* (PGL3) and *SDHB* (PGL4) (Baysal, Ferrell et al. 2000; Niemann and Muller 2000; Astuti, Latif et al. 2001). The gene at the PGL2 locus has not been identified to date, but linkage analysis has placed it in the 11q13 region (Baysal, Farr et al. 1997). Most mutations in the PGL genes occur in either *SDHB* or *SDHD* (Baysal, Willett-Brozick et al. 2002). The age of diagnosis of PGL and PCC is generally similar for *SDHB* and *–D* carriers but the tumour spectrum and penetrance vary. *SDHB* muation carriers are more likely to have PCC and malignant disease whilst *SDHD* mutation carriers are more likely to have head/neck PGL and multifocal disease (Neumann, Pawlu et al. 2004; Vanharanta, Buchta et al. 2004; Pawlu, Bausch et al. 2005).

In order to further understanding of the prevalence of *SDH* mutations in HPGL (and 'sporadic' PGL/PCC) and any genotype-phenotype association we undertook a mutation screen of 32 patients with PGL or PCC (or both).

Patients with *MEN2*, *VHL* or *NF1* were excluded from the study. We screened individuals with and without family history and, where it was possible to collect fresh tumour material, we used this for aCGH to (a) to test for somatic deletion at the relevant SDH locus (presumably targeting the wild-type allele), and (b) to see if we could detect any other consistent regions of somatic gain or deletion, and thereby to identify the location of genes involved in the pathogenesis of PGL/PCC.

The study was carried out with full ethical approval (MREC no 02/2/106).

4.1 Screen for germline mutations in *SDHB*, *-C* and *–D*

4.1.1 Mutation screen using Single-stranded conformational polymorphism (SSCP) analysis

SSCP analysis was carried out as described in the Methods (Section 2.8.1). Constitutive DNA from each patient was PCR amplified for each exon of *SDHB*, *SDHC* and *SDHD* as described in the methods, and electrophoresed through polyacrylamide gels that were subsequently silver-stained gel so that a direct comparison between patients could be made. Bands were identified that had either migrated through the gel a different distance or produced a different pattern than the others in that group. Where possible, a known mutant DNA was run as a positive control and a known unaffected DNA as a negative control. Where there appeared to be a possibility of a mutation (24 of 576 exons), constitutional DNA from that patient was used for direct sequencing in forward and reverse orientation.

4.1.2 Mutation detection by direct sequencing of DNA

Exons that showed a possible mutation, (n-24) were analysed by direct DNA sequencing (Figure 4.1) as described in the Methods (Section 2.8.2). Data was compiled into a table of comparison with the patients date of birth, age at diagnosis, phenotypic presentation, any other tumour types and whether a mutation had been identified and if so, which gene (Table 4.1).

Patient	Diagnosis	DOB	Family History	Mutation	Previously reported	Malginant	Age at	Other tumours
			Y/N		Y/N	Y/N	Diagnosis	
1	Single PGL	1974	N	none	N/A	N	28	none
2	Bi-lateral PGL	1950	N	SDHD-P81L	Y	N	52	none
3	Single PGL	1928	N	none	N/A	N	70	none
4	Single PGL	1926	N/A	none	N/A	N	49	none
5	Bi-lateral PGL	1947	N	none	N/A	N	55	none
6	Single PGL	1939	N	none	N/A	N	60	none
7	Single PGL	1978	N	none	N/A	N	24	none
8	Single PGL	1935	N	none	N/A	N	61	none
9	Single PGL	1933	N	none	N/A	N	66	none
10	Multiple PGL	1947	N	none	N/A	N	52	none
11	Single PGL	1933	N	none	N/A	N	54	none
12	Single PGL	1919	N	none	N/A	N	60	none
13	Single PGL	1934	N	none	N/A	N	66	none
14	Single PGL	1956	N	none	N/A	N	46	none
15	Multple PGL	1939	Y	SDHD-P81L	Y	N	66	none
16	Multiple PGL	1968	Y	SDHD-P81L	Y	N	34	none
17	Single PGL	1928	Y	SDHB-C196Y	Y	N	72	none
18	Multple PCC	1958	N	SDHB-R90X	Y	Y	20, 40	none
19	Bi-lateral PGL	1941	N	SDHD-H50R	Y	N	56	none
20	Multiple PGL	1963	Y	SDHD-P81L		N	40	none

21	Single PGL	1989	N/A	SDHB-I127S	N	Y	14	none
22	Multiple PGL	1938	Y	SDHD-276delCTA	Y	N	57,67 PGL, 26 PCC	none
23	Single PGL	1970	N	SDHB-I127S	Y	N	34	none
24	Single PGL	1970	Y	SDHB-S100P	N	N	34	Prolactinoma and in mother (S100P) both age 32
25	Single PGL	1960	N	none	N/A	N		none
26	Single PGL	1976	N	none	N/A	N		none
27	Single PGL	1945	N	SDHB-72+1 G>A	Y	N	59	none
28	Single PGL	1963	N	none	N/A	N		none
29	Single PGL	1964	N	SDHB-72+1 G>A	Y	N	59 PGL, 14 PCC	none
30	Single PGL	1946	N	none	N/A	N		none
31	Multiple PGL	1981	Y	SDHD-W5X	Y	N	22 (IPGL)-24 (PGL,PCC)	Father had prostate cancer
32	Single PCC	1994	N	SDHB-S163P	Y	N	9	none but mother S163P asymptomatic - pateranl grandfather RCC - no DNA

Table 4.1 Results of a mutation screen in 32 patients with parangliomas and / or phaeochromocytoma.

The tumour type(s), patient age, age of diagnosis, mutation status are included as obtained from patient records. At the time of completion of the study 2 of the mutations were novel (*SDHB* I127S and S100P). We also investigated any reported malignancy and also if the patients or first-degree relatives had been diagnosed with any other tumours than PGL or PCC. No *SDHC* mutations were found in any of the patients in this study.

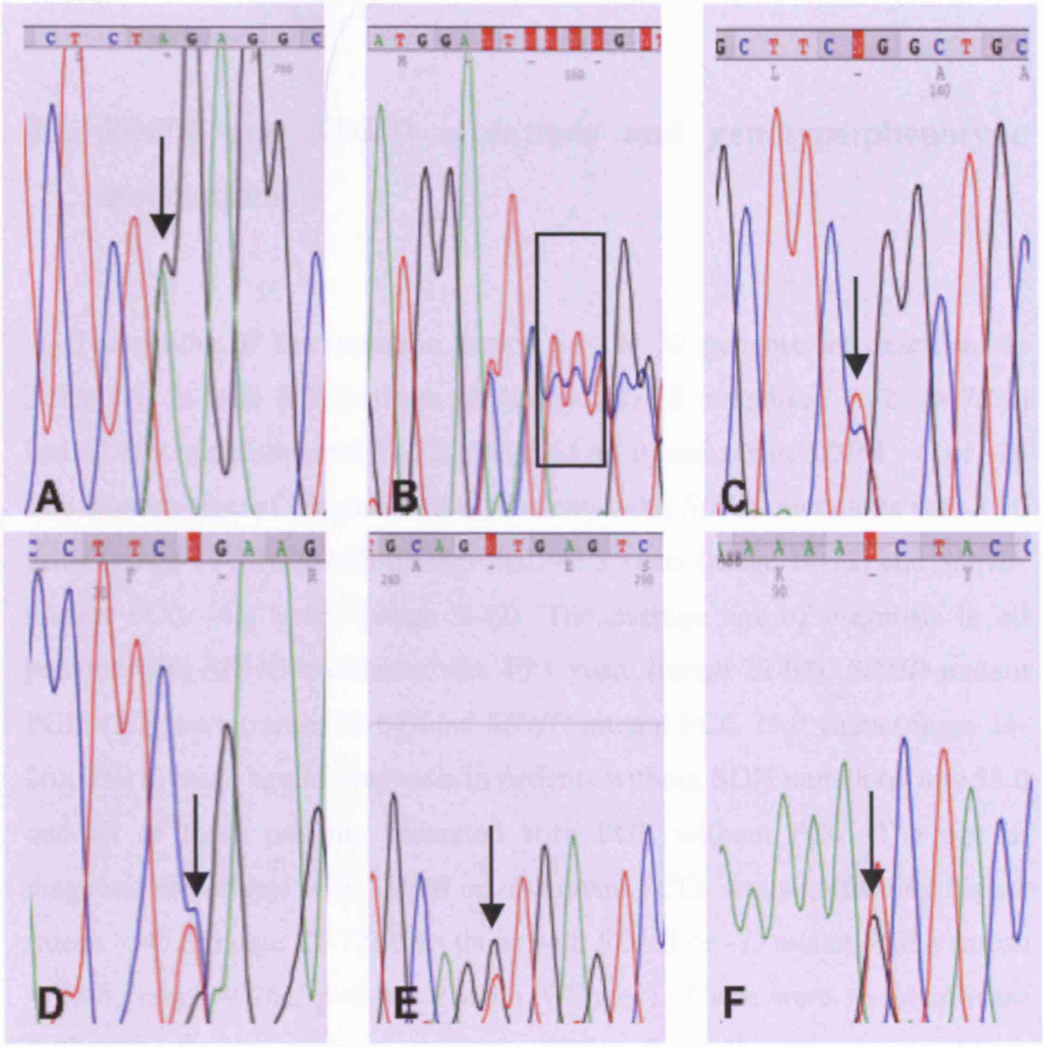

Figure 4.1 Sequencing of DNA from patients with paragangliomas and / or phaeochromocytoma

Direct sequencing of *SDHD* (A-C) and *SDHB* (D-F). These are an example of some of the mutations detected (Table 4.1) and include truncating (nonsense) mutations (A, D), frameshift (B), missense (C, F) and splice site (E). A = *SDHB* W5X, B = *SDHD* 276delCTA, C = *SDHD* P81L, D = *SDHB* R90X, E = *SDHB* 72+1 G>A, F = *SDHB* I127S. Arrows indicate single base pair mutations and the box encompasses the 3 base pair frameshift mutation (B).

4.2 *SDHB* and *SDHD* mutations and genotype:phenotype associations

The results of the mutation screen for the 32 patients are described in Table 4.1. In total 8/32 patients (25%) had *SDHB* mutations, 6/32 (18.75%) had *SDHD* mutations and 18/32 (56.25%) no mutations in *SDHB*, *-C* or *-D*. The average age of diagnosis in all patients with *SDHB* mutations was 35.0 years (range 14-72), *SDHB*-mutant PGL 45.3 years (range 14-72) and *SDHB*-mutant PCC 14.3 years (range 9-42). The average age of diagnosis in all patients with *SDHD* mutations was 40.1 years (range 22-67), *SDHD*-mutant PGL 45.2 years (range 22-67) and *SDHD*-mutant PCC 25.0 years (range 24-26). The average age of diagnosis in patients without SDH mutations was 53.0 and all of these patients presented with PGL without PCC. The age of diagnosis of patients with *SDHB* or *-D* mutant PCCs was significantly higher (mean = 45.3, range 22-72) than those with *SDHB* or *–D* mutant PGLs (mean = 18.6, range 9-26), $p<0.001$ (Mann Whitney). There were no significant differences in the ages of diagnosis within the following groups (Mann Whitney): *SDHB*-mutant PGLs and PCCs (p=0.10); *SDHD*-mutant PGLs and PCCs (p=0.11); *SDHB*-mutant PGLs and *SDHD*-mutant PGLs (p=0.89), and SDHD-mutant PCCs and SDHB-mutant PCCs (p=0.08).

Malignancy in 1 PGL and 1 PCC was reported in 2/8 (25%) of *SDHB* mutation carriers, and 0/6 (0%) of *SDHD* mutation carriers (p=0.30, Fisher's exact). Head and neck PGL occurred in 6/8 (75%) of *SDHB* mutation carriers and 6/6 (100%) of *SDHD* mutation carriers (p=0.30, Fisher's exact). PCC occurred in 3/8 (37.5%) of *SDHB* mutation carriers and in 2/6 (33.3%) of *SDHD* mutation carriers (p=0.70, Fisher's exact). Multi-focal tumours were observed in 1/8 (12.5%) of *SDHB* mutation carriers and 6/6 (100%) in *SDHD* mutation carriers. This was statistically significant (p=0.02, Fisher's exact). There were two cases of other tumour types reported in the patients and first-degree relatives. The *SDHB* S100P mutation was identified in patient 24 and his mother who were both diagnosed with prolactinoma at the age of 32. The father of patient 31 (*SDHD* W5X) was diagnosed with prostate cancer, however, we did not have any DNA or more clinical information on this

person, and prostate cancer is the most common cancer in men in the UK (frequency=11.1%, mean age of diagnosis=72).
(http://info.cancerresearchuk.org/cancerstats/types/prostate/incidence/)

As expected, 7/7 (100%) of patients with family history of PGL/PCC were found to harbour mutations in *SDHB* or *SDHD*. Interestingly 7/25 (28%) of patients with no apparent family history were found to have a mutation in these 2 genes but was not statistically significant (p=0.06, Fisher's exact).

4.3 Array-based Comparative Genome Hybridisation analysis of paragangliomas and phaeochromocytomas

In order to investigate regions of chromosomal loss and gain and possibly identify novel regions that may encompass oncogenes or tumour-suppressor genes, we used aCGH to analyse DNA from frozen tumour material. Tumours were carefully dissected and tissue taken from within the tumour margin for DNA extraction. In total we analysed 7 PGLs (3 x *SDHB*-mutant, 3 x *SDHD*-mutant and 1 sporadic tumours) and 6 PCC (1 x *SDHB*-mutant, 1 x *VHL*-mutant (a positive control with LOH previously shown at 3p25) and 4 sporadic tumours)). DNA extraction, labelling and running and analysing the arrays are described in the Methods (Section 2.16). As laser-capture micro-dissection was not used to isolate tumour specific cells, some normal contamination was expected to occur. Therefore, when processing the data in MS Excel, the graphs of the log2 ratios were scanned by eye to identify regions of chromosomal gain or loss, and the dosage in each region compared with normal:normal hybridisations and regions showing no change in the same tumour using a t-test. These findings are summarised in Table 4.2 and examples of the chromosome plots are shown in Figure 4.2.

Patient	Type	Germline Mutation	Regions of loss (Chromosome and region)	Regions of gain
1	PGL	SDHD P81L	1p (0-77493007)	None
2	PGL	SDHD 276delCTA	1p (0-50284630)	None
3	PGL	SDHD W5X	1p (0-53479583), 19, 22	None
4	PGL	SDHB S100P	1	None
5	PGL	SDHB I127S	1p (0-46577118), 11p, 19	None
6	PGL	SDHB I127S	1p, 11p	1q
7	PGL	None	1, 3, 9, 11p	None
8	PCC	SDHB R90X	1p (0-60703014), 3, 11p, 13p, 17p (0-10156678) 17q (72829398-81236448), 19	1q, 11q, 12
9	PCC	VHL 555insAAA	1p (0-45982179) 3p (0-24114146) 4p (0-13652069), 11p, 19	None
10	PCC	Sporadic	1p, 18p (0-11770775)	None
11	PCC	Sporadic	3, 11	None
12	PCC	Sporadic	1p, 3, 21, 22	1q
13	PCC	Sporadic	1p (944175712-118766121), 3q	None

Table 4.2 Array-based Comparative Genome Hybridisation of paragangliomas and phaeochromcytomas

aCGH (1Mb resolution) analysis of PGL (7) and PCC (6) identifying regions of chromosomal loss and gain in 13 patients with PGLs or PCCs. An entire loss or gain of a chromosome is denoted by the number of the chromosome, loss or gain of an entire arm of a chromosome is denoted by the chromosome number and 'p' or 'q' and specific regions of loss or gain within a chromosome are shown as the specific region of DNA between the midpoint of the clones flanking the specific region. The chromosome locations and clone positions (Mb) were from the Sanger Centre and UCSC (http://www.sanger.ac.uk, http://genome.ucsc.edu/)

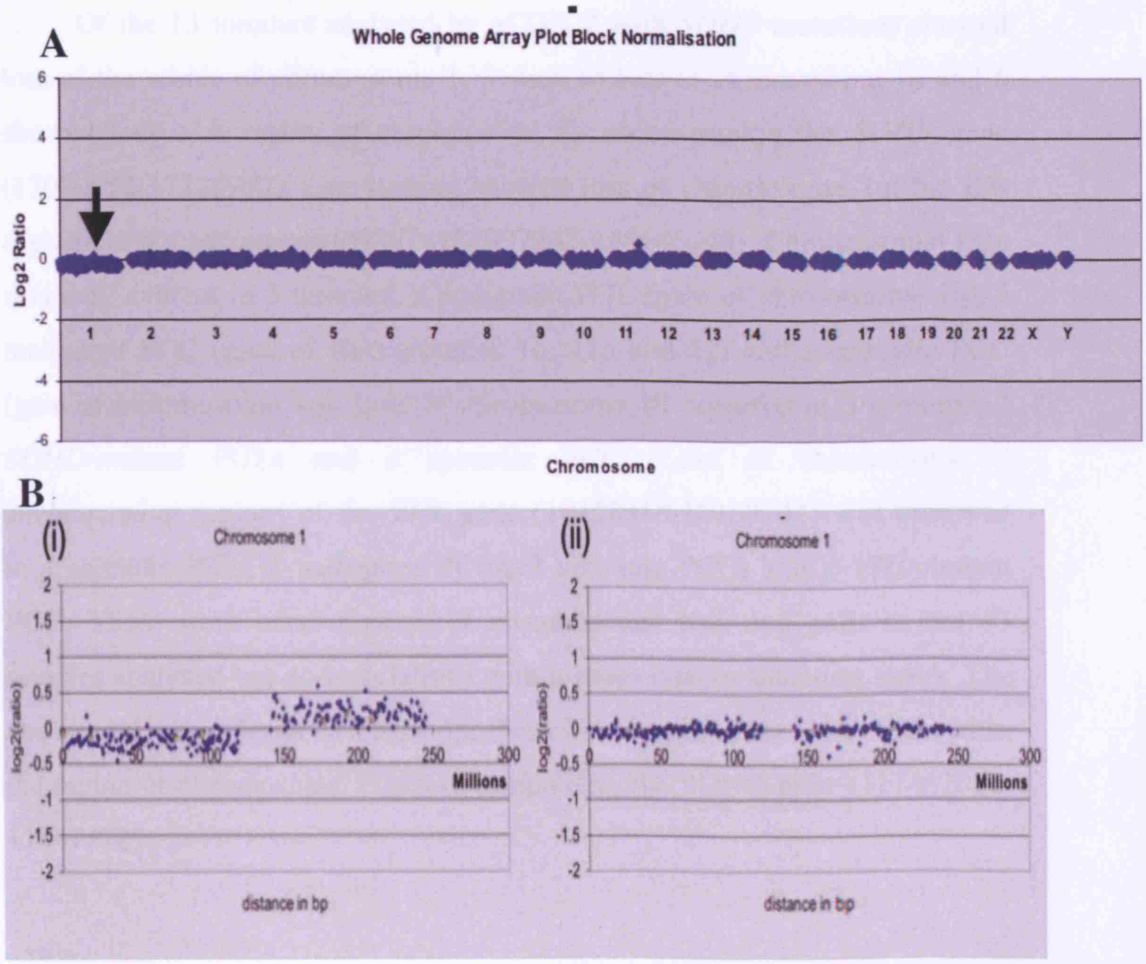

Figure 4.2 Genome plots of aCGH analysis of paragangliomas and phaeochromocytomaas

Whole genome plot of patient 4 with a germline *SDHB* S100P missense mutation (A). The arrow indicates entire loss of chromosome 1 in the PGL. Figure 4.3(B) shows aCGH analysis of chromosome 1 in two patients. The sporadic PCC tumour from patient 12 has lost chromosome 1p and gained chromosome 1q (i). This is evident when compared with the chromosome 1 plot from patient 11 that shows no evidence of loss or gain (ii).

Of the 13 tumours analysed by aCGH 2 with *SDHB* mutations showed loss of the whole of chromosome 1, 3 showed loss of chromosome 1p and 6 showed loss of a region of chromosome 1p encompassing the *SDHB* gene (17090558-17125952). One tumour showed loss of chromosome 1q, but this region did not encompass *SDHC* (158097242-158146049). Chromosomal gain was only evident in 3 tumours, a malignant PGL (gain of chromosome 1q), a malignant PCC (gain of chromosomes 1q, 11q and 12) and a sporadic PCC (gain of chromosome 1q). Loss of chromosome 19 occurred in 3 tumours, 2 *SDHD*-mutant PGLs and a sporadic PCC. Loss of chromosome 3 encompassing regions of the *VHL* gene (10158318-10168744) was observed in a sporadic PGL, 2 malignant PCCs, 2 sporadic PCCs and a *VHL*-mutant PCC. There were other regions of chromosomal loss and gain in the 13 samples analysed but no correlations with tumour type or mutation status. The above analysis is listed in Table 4.2. No chromosomal loss was observed in the region of chromosome 11q23 encompassing the SDHD gene (111462831-111471727).

4.4 Discussion

Patients with PGLs and PCCs have been screened for mutations in *SDHB*, *-C* and *–D*, and where possible, DNA from frozen tumours was analysed using aCGH in order to identify regions of chromosomal loss or gain. The number of patients analysed (n=32 for mutation screening, n=13 for aCGH analysis) were of insufficient size for thorough statistical analysis but the data obtained can be compared with existing literature and more patients recruited for a larger study.

The mutation screen identified one novel *SDHB* mutation (S100P). Interestingly this individual and a first-degree relative both presented with prolactinoma at 32 years and PGL at 34 (see Table 4.1). To our knowledge this is the first reported case of familial prolactinoma in an *SDHB* mutation carrier. Unfortunately, tumour samples were unavailable for either patient, so loss of the wild-type allele could not be confirmed. Previous studies have

reported extra-paraganglial malignancies (e.g. renal cell carcinomas and thyroid papillary carcinomas) in *SDHB* mutation carriers (Neumann, Pawlu et al. 2004; Vanharanta, Buchta et al. 2004). There was no clinical evidence of either of these tumour types in our cohort of patients.

We detected a total of 15 germline *SDH* mutations in the 32 patients screened (46%), [*SDHD* (n=6) and *SDHB* (n=9)]. No germline *SDHC* mutations were detected, but these mutations seem extremely rare (Niemann and Muller 2000; Baysal, Willett-Brozick et al. 2002; Niemann, Muller et al. 2003). It cannot be ruled out that some of the patients in this study (and others) had mutations in the susceptibility gene PGL-2, that was mapped to 11q13.1 and remains unidentified (Mariman, van Beersum et al. 1993; Mariman, van Beersum et al. 1995).

SDHD mutation carriers are more likely to develop multiple/bilateral or PGLs (Neumann, Pawlu et al. 2004) and we confirmed this in 7/7 (100%) patients with a germline *SDHD* mutation (see Table 4.1). Malignancy is more common in *SDHB* mutation carriers, especially in PCC (Neumann, Pawlu et al. 2004), and to date there is only one report of an *SDHD*-associated malignancy (Benn, Gimenez-Roqueplo et al. 2005). In fitting with this, the only malignancies in our patient cohort were found in *SDHB* mutation carriers (1 PGL and 1 multiple PCC – see Table 4.1).

The large ranges of mean age of onset of *SDH*–mutant and sporadic PCC and PGL (Section 4.3) meant that no significant genotype/phenotype association was found, but notably all three of the patients presenting with PCC and/or PGL under the age of 20 had germline *SDHB* mutations (see Table 4.1). These data and previous reports of early onset (and aggressive) *SDHB*-mutant tumours (Benn, Croxson et al. 2003; Vanharanta, Buchta et al. 2004) could perhaps be explained by *SDHB* mutations impairing the assembly of the catalytic complex of SDHA and SDHB, thus leaving only complexes of the structural SDHC and SDHD moieties (Eng, Kiuru et al. 2003). This is further discussed in Chapter 8 (Discussion and Future Work). Also, *SDHB*-mutant tumours may undergo more cytogenetic changes and thus aCGH was used to analyse a variety of tumours for chromosomal aberrations and additionally to try and identify novel regions of chromosomal loss in sporadic

tumours that may indicate a region containing a PGL/PCC tumour-suppressor gene.

The aCGH did not identify any consistent region of loss or gain that has not been previously reported. Loss of chromosome 1p in PCC is a frequent event (Opocher, Schiavi et al. 2003) and there was no correlation between mutation or tumour type and loss of chromosome 1p in the tumours analysed. Gain of chromosome 1q was evident in 1 PGL (malignant) and 2 PCC (1 of which was malignant). The malignant PCC from a patient with a *SDHB* R90X germline mutation showed gain of chromosome 11q, which has been reported as a frequent event in malignant PCC (Cascon, Ruiz-Llorente et al. 2005). The study by Cascon *et al.* also identified a novel region of loss in chromosome 8p22-23 in 62% of PCCs and 33% of the PGLs that they analysed. We did not detect this in our 13 tumours but it remains possible that this candidate region may be linked to development of both PCC and PGL.

Further aCGH analysis of PGLs and PCCs and correlating chromosomal changes with the tumour type and specific germline mutation would possibly identify more candidate regions related to the development of these tumours. PGLs and PCCs contain 2 cell types, chief cells and substanticular cells, both of which derive from a common neural crest precursor (Heath 1991). Analysis of PGLs has shown that they can be diploid, tetraploid, aneuploid, and polyploid, and whereas the chief cells are reported to be the neoplastic component of PGLs and lose the wild-type *SDHD* allele, the substanticular cells have been shown to be diploid (Douwes Dekker, Corver et al. 2004). Therefore to obtain higher quality data by employing aCGH to analyse chromosomal aberrations in PGLs laser micro-dissection and determination of tumour ploidy for each tumour would have to be a major consideration.

5 Chapter 5: Generation of a mouse model of HLRCC

Introduction

HLRCC is a relatively rare family cancer syndrome and therefore opportunities to collect fresh tumour samples are limited. In order to further our understanding of the mechanisms of tumourigenesis and molecular pathogenesis of this syndrome we decided to attempt to create a mouse model of HLRCC by targeting *Fh1* the mouse homologue of human *FH*. To date, this gene has not been targeted in the mouse. We presumed that due to the vital role of *FH* in oxidative metabolism that a homozygous knockout would be lethal and therefore, not wishing to rely on the heterozygous knockout to produce a phenotype, chose to create a conditional model in order that both alleles could be inactivated in a tissue-specific manner. The cre-lox technology available enables the knocking out of genes, which are only excised in tissues expressing the phage-P1 protein Cre recombinase. Cre recombinase facilitates homologous recombination by binding a specific 34bp DNA sequence termed a loxP site and DNA flanked with 2 loxP sites in the same orientation will be deleted by homologous recombination in the presence of Cre recombinase (Hoess, Abremski et al. 1984). It is therefore possible to conditionally knockout genes (or specific exons) by replacing the endogenous copy with a mutated copy (knock-in) or a identical region flanked by loxP sites. Therefore by flanking *Fh1* with loxP sites (from herein called 'floxed') and crossing to strains of mice expressing Cre recombinase in the tissues where HLRCC tumours arise, we aim to mimic the tumour-suppressor function of *FH* in a murine model without adverse systemic effects. We considered making a knock-in *Fh1* mouse by introducing a specific mutation but decided to make a knockout as HLRCC tumours have virtually absent FH activity (Tomlinson, Alam et al. 2002). This chapter will focus on the step-wise construction of the knockout *Fh1* mouse.

5.1 Selection of a targeting vector

The pFLRT-1 eukaryotic targeting vector was chosen (figure 5.1). This vector contains a neomycin resistance cassette for G418 selection in mammalian cells. This is flanked by FRT sequences, which enable the neomycin cassette to be removed in vivo using mice expressing eFlp. The Flp/FRT system excises DNA by homologous recombination between the FRT sites in the presence of Flp recombinase (McLeod, Craft et al. 1986). Therefore, the neomycin cassette which acts as a weak splice acceptor, can not cause any phenotype. The *Bam* HI site is flanked by 2 loxP sites and therefore was used to clone the region of *Fhl* to be deleted. pFLRT-1 contains an ampicillin restistance gene enabling the selective amplification of the targeting construct using bacteria.

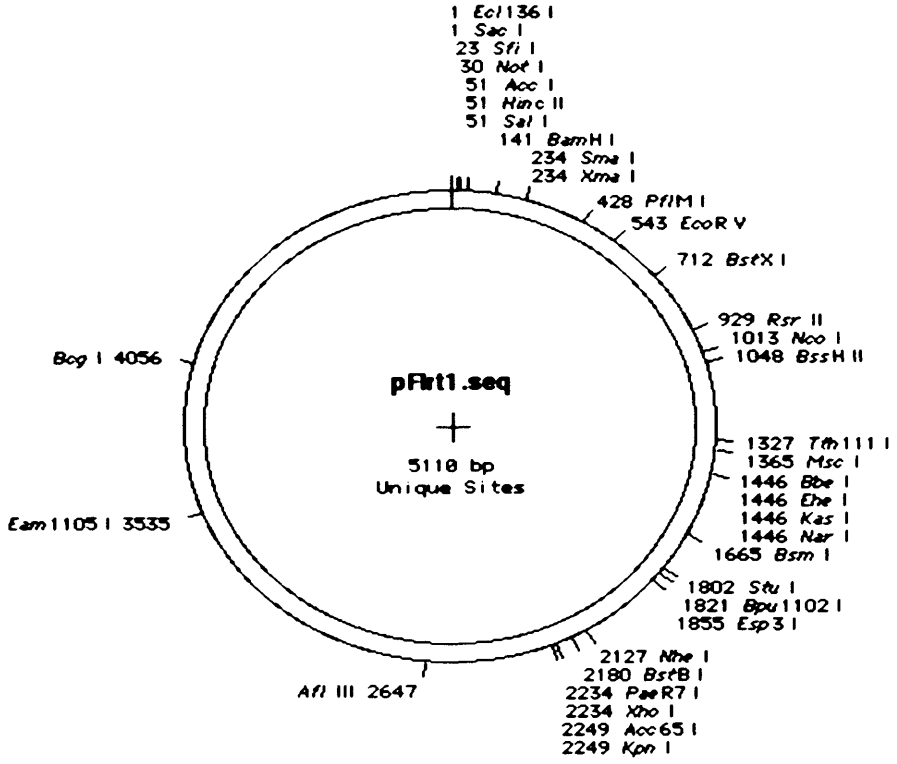

Figure 5.1 Diagram of the pFLRT-1 vector

This diagram indicates the unique restriction enzyme sites in pFLRT and was created using DNA Strider software. The neomycin cassette is between 780-158; the FRT sites are 237-272 and 2134-2168; the loxP sites are 95-125 and 178-208.

5.2 Construct design

Murine *Fh1* (BC006048; 1qH4) is 88% identical to human *FH* (BC003108; 1q43). Murine Fh1 protein (P07954) is 94% homologus to human FH (P97807). We decided to remove a 3.0kb region of *Fh1* encompassing exons 2 and 3 as this region contains both active site residues and the activation domain of the protein in order to maximise the reduction of FH activity (Figure 5.2). This region also contains truncating and missense mutations in humans with HLRCC.

Figure 5.2 Region of *Fh1* to be targeted

Residues highlighted indicate the region to be targeted in the mouse. Residues underlined are active site residues (green) or constitute the activation domain (blue). Known missense (black squares) and truncating (red circles) mutations in humans with HLRCC are also indicated.

5.3 Cloning strategy

The plasmid pFLRT-loxP-FH-loxP was cloned in a 3-step process in the order below due to the required restriction enzyme site usage. To enable efficient homologous recombination in mouse ES cells, 2 flanking 'arms' of homologous DNA (7.2kb long arm 5' and 1.6kb short arm 3') were cloned into pFLRT1 (Figure 5.3). 129 ES mouse DNA was used as template and each PCR was performed using the Advantage II Long Range PCR kit (Clontech) using a GeneAmp thermocycler (ABI). Initial denaturing was for 3 minutes at 96°C, followed by 35 cycles of 30s at 96°C and variable extension at 68°C (see below). A final extension was carried out at 72°C for 10 minutes. The order of cloning was as below.

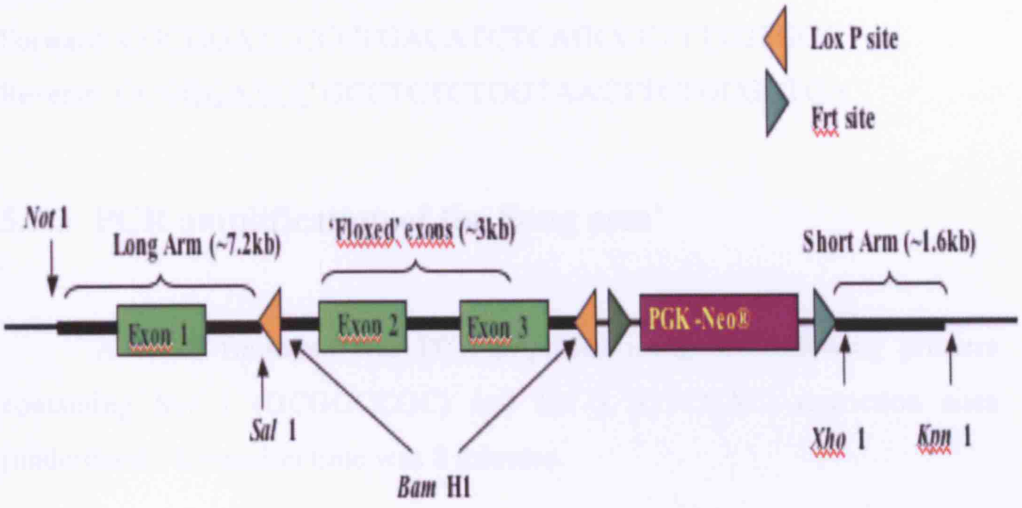

Figure 5.3 Cloning design for ES targeting of mouse *Fh1*

Linear plan of the cloning strategy showing the position of the short, floxed and long arms of homology and the position and orientation of the loxP and FRT sites. The neomycin cassette is in reverse orientation to minimise transcriptional regulation from the PGK promoter.

5.3.1 PCR amplification of the 'short arm'

A 1.6kb fragment was PCR-amplified using the following primers containing *Xho* I (CTCGAG) and *Kpn* I (GGTACC) restriction sites (underlined). Extension time was 2 minutes.

Forward: CCGCTCGAGCTTGAGTCCAGAAATAATTTCCACTG
Reverse: GCCGGTACCGGACAGTGGGGGAAATGAAAAGCA

5.3.2 PCR amplification of the floxed region

A 3.0kb fragment was PCR-amplified using the following primers containing *Bam* H1 (GGATCC) restriction sites (underlined). Extension time was 3 minutes.

Forward: CGCGGATCCCCTGACATCTCAGCCCTTTTGTGGT
Reverse: GCGGGATCC GCCTCTCTGGTAACTTCTGCGGTGA

5.3.3 PCR amplification of the 'long arm'

A 7.2kb fragment was PCR-amplified using the following primers containing *Not* 1 (GCGGCCGC) and *Sal* 1 (GTCGAC) restriction sites (underlined). Extension time was 8 minutes.

Forward:
AAGGAAAAAAGCGGCCGCTGCACCCATGCACACACAGACA
Reverse: TGCGGTCGACTAAGGTGAGAACAACTACACCTAGC

Standard cloning and purification methods were used as described in the Methods (Sections 2.2, 2.9). In brief, each PCR product was cleaned, cut with the appropriate restriction enzyme(s), gel purified and ligated into pFLRT-1 cut with the same enzyme(s). The ligations were transfected into bacteria and

ampicillin resistant positive colonies selected using LB-ampicillin plates. Clones were cultured, DNA extracted and analysed using restriction enzyme analysis and direct sequencing. The final construct was linearised using *Not* 1and purified using phenol-chloroform.

5.4 Transfection of mouse 129 ES cells with pFLRT-loxP-FH-loxP and selection and screening of positive clones

Transfection of the ES cells and G418 selection was carried out by the transgenic mouse facility at Clare Hall laboratories. The procedures are described in the Methods (Section 2.1.2). In brief, colonies were picked, grown to confluence and digested in proteinase K buffer in 96 well plates. DNA was extracted and subject to PCR and Southern analysis

5.5 PCR analysis of positive clones

Primers were designed in order to identify ES clones in which site specific homologous recombination had occurred. Therefore the forward primer was specific to a region of the neomycin cassette and the reverse primer to a region outside the targeting construct. The product size is 1.8kb.

Forward: GTACCGGTTGTTAGTGAAGTAGGTCTCTGCA
Reverse: CTGAGAGCATCATGGAGCTTCTGTAACC

The DNA preparation from the 96 well plates of ES clones produced relatively low quality DNA and therefore a robust DNA polymerase (LA – TAQ, Takara) was used and primers designed with a high T_m. Thermocycling conditions were an initial denaturing step for 3 minutes at 96°C, 35 cycles of: 96°c for 30s, 65°C for 1 minute and 68°C for 3 minutes, then 72°C for 5 minutes.

The expected frequency of positive clones is as low as 1-2% so in order to verify the validity of the PCR reaction, a positive control was cloned into the

Kpn I site (underlined) of pFLRT. This was a modified version of the short arm containing with same DNA sequence but with with an extra 200bp of mouse genomic DNA encompassing the reverse primer sequence of the ES DNA sequencing primers.

Forward: GCCGGTACCTCACTCACCACAGCCTCACAACC
Reverse: GCCGGTACCAACCCAACTGAGCCCACTCACTG

The PCR product was cut, purified and cloned into pFLRT-1 as described for the short arm and confirmed using direct sequencing. The cloned positive control was diluted down to the equivalent of 1 copy number per molecule of genome and used to optimise the PCR conditions. PCR products were electrophoresed through 1.2% agarose gels as described in Methods (Section 2.7) and photographed under UV light (Figure 5.4). A total of 6 positive clones were identified from 288 clones and DNA from these was used for Southern analysis.

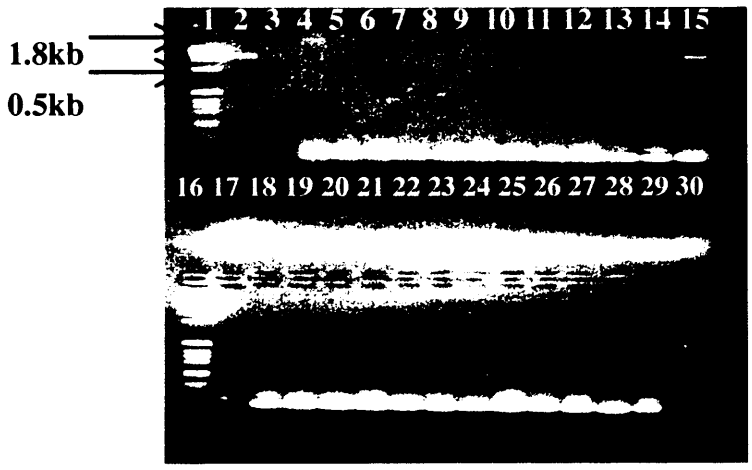

Figure 5.4 PCR screen of transfected ES cells

Photograph of an agarose gel with PCR products from an ES screen. Lane 1 contains DNA ladder, lane 2 the positive control, lanes 3 and 17 a negative control and lanes 4-15 and 18-26 are PCR products from the amplification of DNA from ES clones. Lane 15 contains a positive clone which was further analysed by Southern blotting.

5.6 Southern analysis of positive clones

In order to verify the intergrity of site-specific homologous recombination, Southern analysis was carried out on the positive clones obtained from the PCR screen. A 497bp probe, external to the construct was designed to include the entire sequence of exon 5 and no repetitive elements (Blast, NCBI). The probe was PCR amplified as described in the methods using the following primers:

Forward: CCTTGTAGATTTGTAGCCCTTCCTCTTT
Reverse: AACAAACAAAACATGTAAACGCATGAAC

The Southern screening strategy (Figure 5.5A) was designed such that DNA digested with the restriction enzyme *Xcm* I could be probed to identify wild-type (herein referred to as $Fh1^{+/+}$ (6.8kb fragment), targeted (floxed) *Fh1* (herein referred to as $Fh1^{fl/+}$ (8.2kb) and also Cre-mediated knockout of *Fh1* (herein referred to as $Fh1^{+/-}$ (10.0kb) so that the viability of the loxP sites could be tested in ES culture.

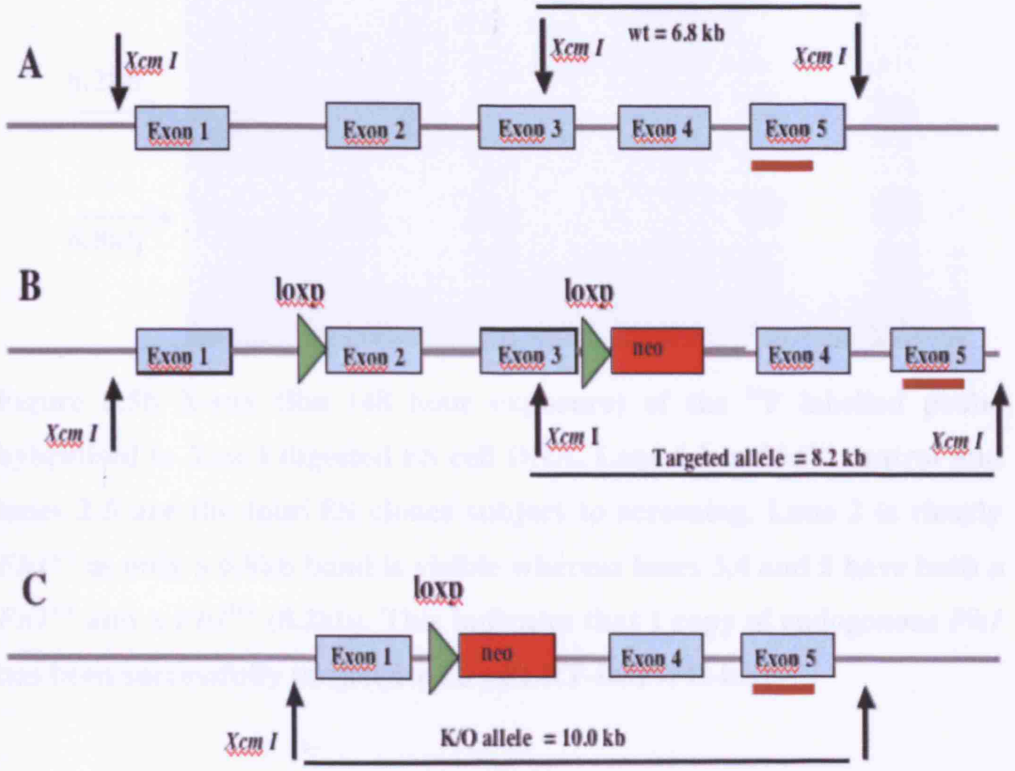

Figure 5.5 Southern analysis of transfected ES clones

In order to verify the ES clones in which the orientation and site specificity of the construct was correct, a specific probe was designed which would hybridise with DNA fragments from *Xcm* I digested DNA. The *Fh1*$^{+/+}$ fragment (A) is 6.8kb, the *Fh1*$^{fl/+}$ (B) 8.2kb and the *Fh1*$^{+/-}$ fragment after recombination of the loxP sites (C) 10.0kb.

We planned to analyse the six ES clones identified as positive from the ES screen. DNA from these clones was extracted at Clare Hall laboratories as described in the Methods (Section 2.2.4). Two clones failed to grow and therefore only four were analysed by Southern blotting. Three of these clones; (4A3, 4E5 and 4C9) were identified as positive and contained a *Fh1*$^{+/+}$ (6.8kb) band and a *Fh1*$^{fl/-}$ (8.2kb) band. (Figure 5.5B.)

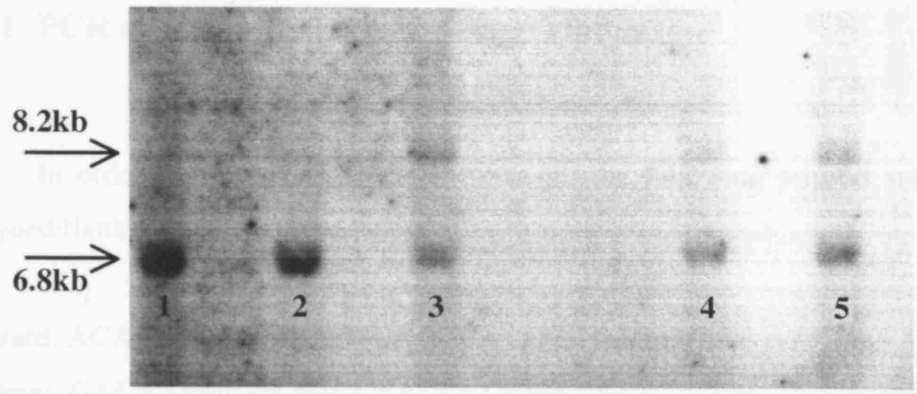

Figure 5.5b X-ray film (48 hour exposure) of the ^{32}P labelled probe hybridised to *Xcm* I digested ES cell DNA. Lane 1 is a $Fh1^{+/+}$ control and lanes 2-5 are the four ES clones subject to screening. Lane 2 is clearly $Fh1^{+/+}$ as only a 6.8kb band is visible whereas lanes 3,4 and 5 have both a $Fh1^{+/+}$ and a $Fh1^{fl/+}$ (8.2kb). This indicates that 1 copy of endogenous *Fh1* has been successfully targeted with pFLRT-loxP-FH-loxP.

5.7 Cre transfection of positive clones

In order to ensure that the loxP sites would function successfully *in vivo* ES cultures from clones 4A3, 4C9 and 4E5 were transfected with the Cre expression plasmid pMC1-CRE. This was carried out by the transgenic facility at Clare Hall and is described in the Methods (Section 2.1.2.1). 192 sub-clones were selected for each and grown up, and DNA was extracted as described in the Methods (Section 2.2.3). An initial PCR screen was performed to identify potential positive clones and then Southern analysis performed as confirmation.

5.7.1 PCR analysis of cre-transfected clones

In order to detect cre-mediated excision, the following primers were designed flanking the loxP sites:

Forward: ACACTAGGCTCAGTCACCCATCCAAAT
Reverse: GACATAGCGTTGGCTACCCGTGATATT

PCR conditions were the same as that described (Section 5.5). The PCR product from *Fh1*$^{+/+}$ DNA was 3.8kb and DNA with successful Cre-mediated excision 0.8kb (Figure 5.6)

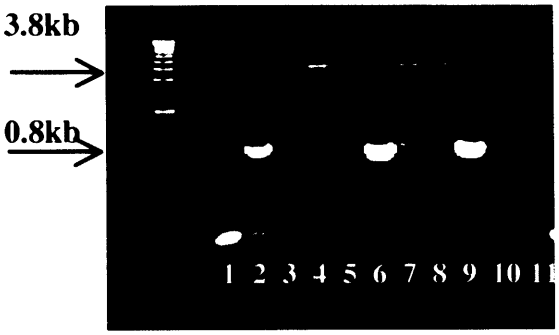

Figure 5.6 PCR screen to assess Cre-mediated excision

PCR genotyping was used to determine in which clones cre-mediated excision had removed the floxed region of *Fh1*. Lanes 1-11 are clones from transfection of 4A3. Excision has clearly occurred in samples 2,6 and 9. The larger *Fh1*$^{+/+}$ band was faint or not present due to the low quality of the DNA extracted in 96 well plates. This probably had an adverse effect on amplification of the larger fragment.

The results of the PCR screen suggests that the loxP sites were recombining in the presence of Cre recombinase and excising exons 2 and 3 of *Fh1*.

5.7.2 Southern analysis of cre-transfected clones

Clones that after the PCR screen had appeared to have undergone Cre-mediated excision were further subject to a Southern screen in order to verify this (Figure 5.7). The procedure was the same as described in section 5.6 of this Chapter. Three clones were selected from each transfection (4A3, 4E5 and 4C9). Two of the 9 clones selected did not grow to the required confluency (1 of 4E5 and 1 of 4C9) so we used DNA from the 7 remaining clones for the Southern blot. The 3 founder clones (4A3, 4E5 and 4C9) were also re-analysed to confirm they were heterozygous for the floxed allele.

Figure 5.7 Southern analysis of founder clones

Southern analysis of founder clones 4A3 (1), 4E5 (2) and 4C9 (3) and founder clones transfected with the cre expression plasmid pMC1-Cre; 4A3 (lanes 5,6,7), 4E5 (lanes 8,9) and 4C9 (lanes 10,11). *Fh1*$^{+/+}$ 129 ES DNA was also probed (lane 1) as a control. The founder clones are confirmed to be heterozygous for the targeted allele as the probe hybridises to both the *Fh1*$^{+/+}$ (6.8kb) and *Fh1*$^{fl/+}$ allele (8.2kb) DNA fragments. The presence of the 10.0kb band in samples 5-11 confirms the PCR screen results and that cre-mediated excision has occurred in the targeted allele. Lane 6 also has a weak 8.2kb band suggesting that the transfection efficiency was not as high as the other samples.

5.7.3 Fumarase activity of *Fh1*$^{+/+}$ and *Fh1*$^{+/-}$ ES cells

Having demonstrated successful gene targeting of *Fh1* and the efficacy of the loxP sites using PCR and Southern analysis, we decided to measure the fumarase activity in pMC-Cre transfected ES cells and compare *Fh1*$^{+/+}$ with *Fh1*$^{+/-}$. Each of the 3 founder clones (Figure 5.7) were transfected with pMC-Cre in parallel with *Fh1*$^{+/+}$ lines and an average reduction of 34.0% in fumarase activity was observed (Figure 5.8). The reduction probably would have been higher if the transfection efficiency had been 100% but we did not carry out a control e.g. eGFP transfection as we felt that the site-specific floxing of *Fh1* would be sufficient to abolish Fh1 activity in *Fh1*$^{-/-}$ cells.

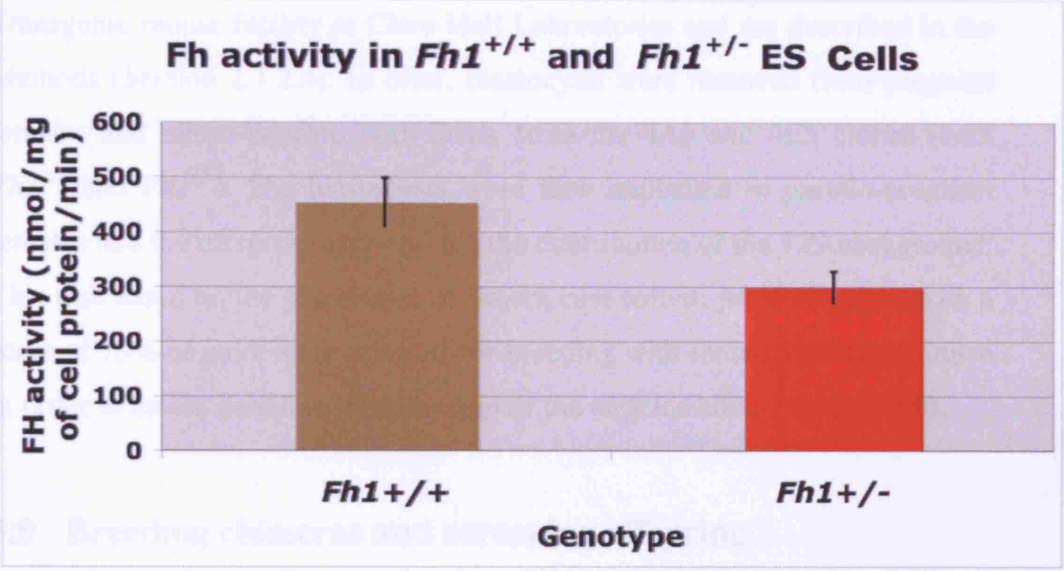

Figure 5.8 Fumarate hydratase activity in *Fh1* targeted ES cells

***Fh1*$^{+/+}$ (n=3) and *Fh1*$^{fl/+}$ ES cells (n=3) were transfected with the Cre recombinase expression plasmid pMC-Cre and fumarase activity measured after 36 hours. *Fh1*$^{+/+}$+ ES cells had higher activity (mean = 453.3, StDev = 45.3) compared with *Fh1*$^{fl/+}$ cells transfected with pMC1-Cre (mean = 299.0, StDev = 29.5); p<0.02 (Students t-test).**

The results so far show that the targeting construct pFLRT-loxP-FH-loxP has been successfully integrated into 129 ES cells; replacing 1 copy of endogenous *Fh1*. Additionally the loxP sites are recombining in the presence of Cre recombinase and excising the floxed exons 2 and 3 of *Fh1* and reducing Fh1 activity in the presence of Cre recombinase. At this stage we decided to generate chimeric mice by blastocyst injection of both the $Fh1^{fl/+}$ and $Fh1^{+/-}$ knockout ES cells.

5.8 Blastocyst injection and generation of chimeras

Blastocyst injection and chimera generation were carried out by the Transgenic mouse facility at Clare Hall Laboratories and are described in the Methods (Section 2.1.2.4). In brief, blastocysts were removed from pregnant females and micro-injected with DNA from the 4A3 and 4E5 clones (both $Fh1^{fl/+}$ and $Fh1^{+/-}$). The blastocysts were then implanted in pseudo-pregnant females and the offspring assessed for the contribution of the 129 background. This was based on the percentage of brown coat colour. Male chimeras with a score of 70% or more were selected for breeding with female C57/BLK6 mice in order to assess germline transmission of the targeted allele (Section 5.9).

5.9 Breeding chimeras and screening offspring

Chimeras were obtained from both the heterozygous floxed clones 4A3 (70%, 75% and 100%) and 4E5 (70%). Unfortunately the blastocyst injections for the $Fh1^{+/-}$ knockout clones were unsuccessful after 2 attempts and no chimeras of sufficient contribution were obtained. Therefore it was decided to knock out *Fh1 in vivo* using the PGK-Cre deleter strain, which express Cre recombinase ubiquitously in all tissues. In order to test for germline transmission, the 100% 4A3 chimera and 70% 4E5 chimera were bred with C57/BLK6 mice. The offspring were assessed for the floxed allele using both a PCR and Southern screen.

5.10 PCR genotype for Chimeras x C57/BLK6

The chimera (4A3) x C57/BLK6 cross produced a litter of 3 mice. Tail clippings were sent from the Transgenic Facility at Clare Hall and DNA extracted as described in the Methods (Section 2,2.5). The genotyping assay and conditions were as previously described (Section 5.5). Two of the mice were positive for the floxed allele (Figure 5.9). The chimera (4E5) x C57/BL-6 cross produced a litter of 4 mice but they were all negative for the floxed allele. A further 2 litters produced no positive offspring and therefore presumed not to transmit through the germline. We decided to proceed with the 4A3 clone and inject the 4C9 clone at a later date.

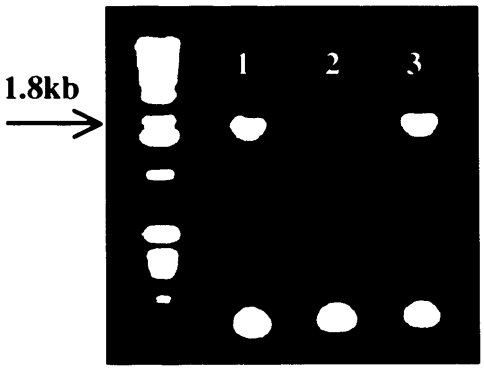

Figure 5.9 PCR genotype to test for germline transmission of the *Fhl1*$^{FL/+}$ allele

PCR genotype confirming germline transmission of the 4A3 founder clone in mice 1 and 3. The 1.8kb band is amplified from the neomycin cassette to 3' of the targeting construct in order to confirm site-specific integration.

5.11 Southern screen for Chimeras x C57/BLK6

A Southern blot (Figure 5.10) was carried out as a confirmatory screen on the DNA used for the PCR screen as previously described (Section 5.6).

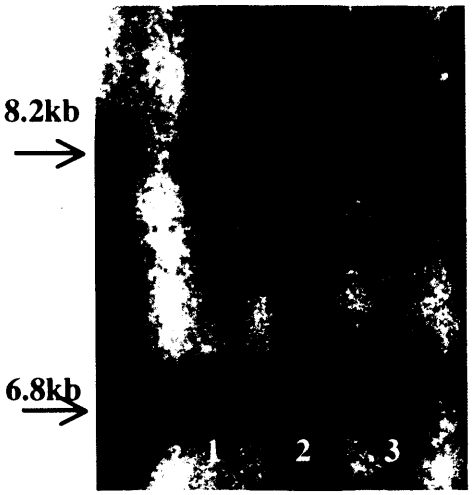

Figure 5.10 Southern analysis to test for germline transmission of the *Fh1*$^{FL/+}$ allele

Southern analysis of the 3 offspring from the chimera (4A3) x C57/BLK6 cross. The presence of the *Fh1*$^{+/+}$ (6.8kb) and *Fh1*$^{fl/+}$ alleles (8.2) bands in mice 1 and 3 confirm the results of the PCR screen and the germline transmission of the 4A3 founder clone. Mouse 2 is *Fh1*$^{+/+}$ as only has the 6.8kb band.

Having confirmed germline transmission of the 4A3 founder clone, positive mice were bred through 3 generations of C57/BLK6 and genotyped using PCR as described above (Section 5.5).

5.11.1 *In vivo* removal of neomycin cassette

In order to ensure that any future phenotype was dependent solely on the knockout of *Fh1* we decided to remove the neomycin cassette from the

Fhl1$^{fl/+}$ mice. The neomycin cassette can act as a weak splice acceptor and additionally there is a chance that the PGK promoter could generate antisense transcripts. The enhanced Flp (eFlp) strain of mice ubiquitously express Flp recombinase which mediates excision of DNA between site specific repeats (FRT sites). The FRT sites flanking the neomycin cassette should recombine and create targeted *Fhl1*$^{fl/+}$ mice without the neomycin cassette.

5.11.2 eFlp mice breeding and genotyping

A breeding pair of eFlp mice on a C57/BLK6 background were kindly provided by Dr. Ralf Adams. Initially to generate a stock they were bred with C57/BLK6 mice and the offspring genotyped by extracting DNA from tails and using a PCR screen to amplify a 0.7kb fragment of the *eFlp* gene (Figure 5.11) using the following primers and annealing temperature of 60°C.

Forward – GTGGATCGATCCTACCCCTTGCG

Reverse – GGTCCAACTGCAGCCCAAGCTTCC

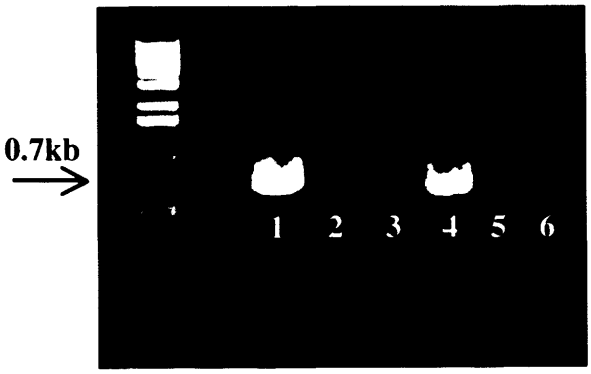

Figure 5.11 PCR genotype of eFLP$^{+/-}$ mice

Mice carrying the eFlp transgene were selected using a PCR screen. Lanes 1 and 4 from are PCR products from *eFlp*$^{+/-}$ micet in this litter as a 0.7kb PCR product can be amplified from their tail DNA. The absence of a PCR product in lanes 2,3 and 5 indicates that these mice are *eFlp*$^{-/-}$. Lane 6 is a negative control.

The 3rd generation *Fhl1*$^{fl/+}$ mice were bred with eFlp positive offspring in order to remove the neomycin cassette *in vivo*. Offspring were tail clipped, DNA extracted and analysed using PCR in order to determine if the excision was successful.

5.11.3 PCR genotype to confirm excision of neomycin cassette

Primers flanking the neomycin cassette were designed to PCR screen the offspring of the eFlp x *Fhl1*$^{fl/+}$crosses. PCR conditions were as previously described in this Chapter (5.12.1).

Foward - GGATCAGGAACCCAGACAAACATGAAT

Reverse - CAGTGGAAATTATTTCTGGACTCAAG

Amplification of the neomycin cassette produced a 2.2kb band and after excision a 0.2kb band (Figure 5.12).

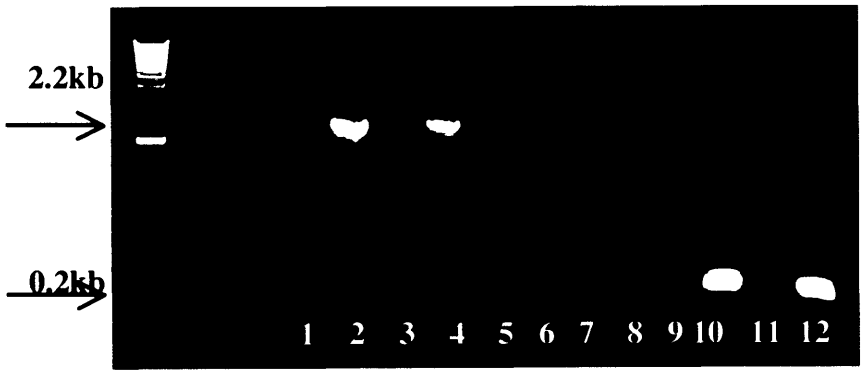

Figure 5.12 PCR screen for eFLP-mediated of the neomycin cassette

PCR screen of DNA from a litter of 11 mice (eFlp$^{+/-}$ x *Fhl1*$^{fl/+}$). The 2.2kb product in lanes 2 and 4 confirms that these mice are *Fhl1*$^{fl/+}$ but still contain the neomycin resistance cassette. Lanes 3,5,6,7,8,9 and 11 with no PCR product confirm that these mice are *Fhl1*$^{+/+}$. The 0.2kb band in lanes 10 and 12 indicate that these mice are *Fhl1*$^{fl/+}$ and that the neomycin cassette has been successfully excised. Lane 1 is a negative control.

After successfully removing the neomycin cassette, the positive mice were bred with C57/BLK6 to create a stock for future experiments and offspring were genotyped with the above primers. All litters were also genotyped for the eFlp transgene and only those mice without the transgene were used for future studies.

5.12 Generation of *Fh1*$^{+/-}$ mice *in vivo*

Humans with HLRCC inherit heterozygous *FH* mutations and therefore it was decided to generate a stock of *Fh1*$^{+/-}$ mice for future analysis.

5.12.1 PGK-cre mice breeding and genotyping

PGK-cre mice were available from Clare Hall Transgenic Laboratories. Initially the 2 males provided were crossed with C57/BLK6 in order to create stock. DNA was extracted from tail clippings and PCR genotyped (Figure 5.13) using the following primers, specific to a region of the Cre recombinase gene and a PCR program with an annealing temperature of 55°C as described in the Methods (Chapter 2, 2.6). An additional set of primers specific to a region of *c-Jun* was used as an internal control.

Cre:

Forward - CGGTCGATGCAACGAGTGATGAGG

Reverse – CCAGAGACGGAAATCCATCGCTCG

c-Jun:

Forward - CTCATACCAGTTCGCACAGGCGGC

Reverse - CCGCTAGCACTCACGTTGGTAGGC

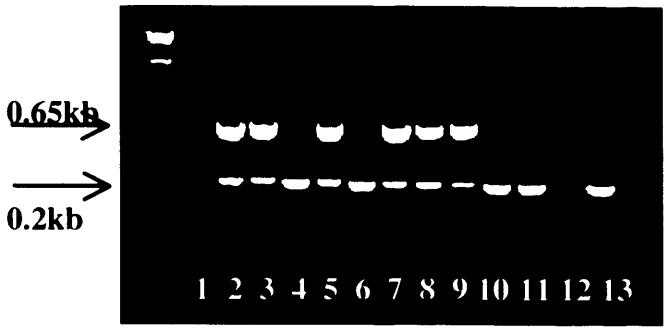

Figure 5.13 PCR genotyping of PGK-cre mice

PCR genotyping was used to determine which mice were carrying the PGK-Cre transgene. The internal PCR control c-Jun was amplified (0.2kb) in all offspring from this litter of 12 mice (lanes 2-13). The 0.65kb band confirming presence of the PGK-cre transgene (lanes 2,3,5,7,8 and 9) confirmed the presence of PGK-Cre in these mice. Lane 1 is a negative control.

We then attempted to create $Fh1^{+/-}$ mice by crossing PGK-$Cre^{+/-}$ mice with $Fh1^{fl/-}$ mice without the neomycin cassette.

5.13 PCR genotype to confirm excision of floxed exons

A PCR screen was designed in order that $Fh1^{+/-}$ mice could be identified. The primers used previously to detect excision could not be used as the reverse primer sequence was in the neomycin cassette. Primers were designed outside the floxed region to amplify a 0.7kb region in $Fh1^{+/-}$ mice (Figure 5.14). DNA was extracted from tail clippings and PCR conditions were used as described above (5.12.1).

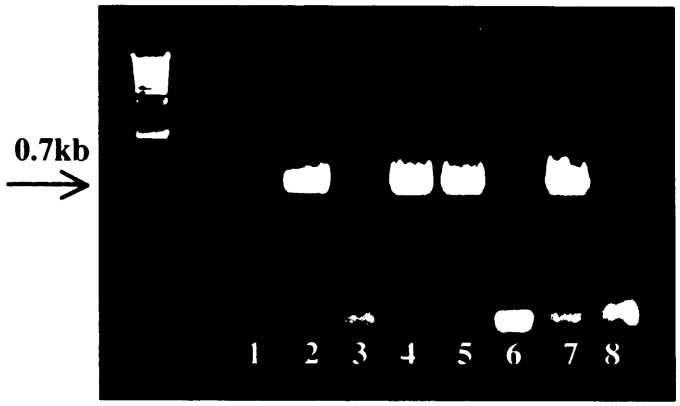

Figure 5.14 PCR genotype to identify *Fhl1*$^{+/-}$ mice

PCR genotype to determine *Fhl1*$^{+/-}$ mice resulting from the *Fhl1*$^{fl/+}$ x PGK-Cre$^{+/-}$ cross. The 0.7kb PCR product in lanes 2,3,5 and 7 confirm that exons 2 and 3 (the floxed region) have been excised by Cre-mediated recombination. The absence of a PCR product in lanes 3,6 and 8 confirms that exons 2 and 3 have not been deleted. Lane 1 is a negative control.

Fhl1$^{+/-}$ mice were bred with C57/BLK6 and the offspring genotyped for both Cre and the null allele. Only *Fhl1*$^{+/-}$ mice without PGK-cre were kept for future work. In order to enable rapid screening of future crosses, a PCR genotype was designed to identify mice which were either *Fhl1*$^{+/+}$, *Fhl1*$^{+/-}$, *Fhl1*$^{fl/+}$, *Fhl1*$^{fl/fl}$ or *Fhl1*$^{-/-}$ (if viable).

5.14 PCR genotype to differentiate between *Fhl1*$^{+/+}$, *Fhl1*$^{fl/+}$ and *Fhl1*$^{+/-}$ mice

A 3 primer PCR screen was designed in order that the genotypes of future crosses could be determined by a single PCR reaction (Figure 5.15A). All reactions were performed with DNA extracted from tail clippings, using PCR program PP55 as described above (5.13.1), and resolved on 2% agarose gels. Genotypes were based on the number and size of specific bands (Figure 5.15B).

Forward – 1 – GCTCAGTCACCCATCCAAAT

Forward – 2 – ACCCTGCTAGGTGTCACCAC

Reverse – 3-- CCTGGCACTGCAGACTACAA

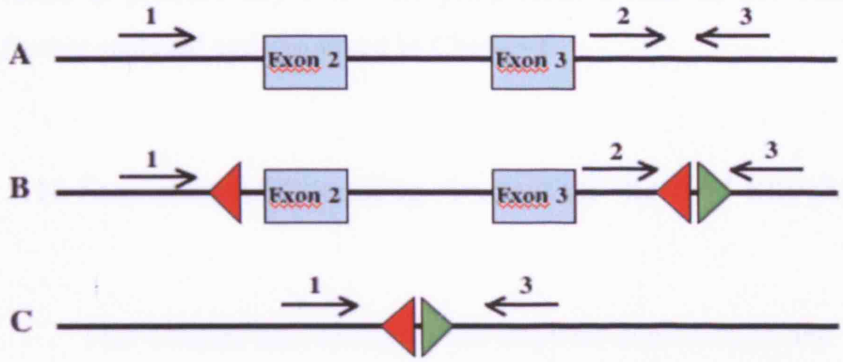

Figure 5.15 PCR genotype screening of Fh1 mice using 3 primers

Figure 5.15A Strategy for 3 primer PCR screen. Three different alleles can be amplified. The wild-type allele (A) amplifies a 0.28kb PCR product (primers 2 and 3), the floxed allele (B) amplifies a 0.49kb PCR product (primers 2 and 3) and the null allele (C) amplifies a 0.44kb PCR product (primers 1 and 3).

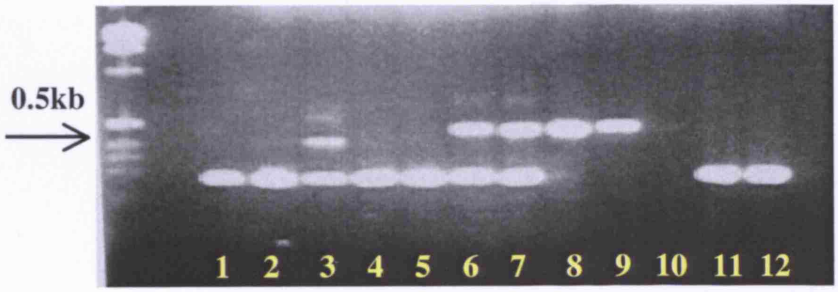

Figure 5.15B Example of genotyping mouse tail DNA using the 3 primer PCR screen. The 0.5kb DNA size marker is indicated. The 0.28kb PCR product in lanes 1,2,4,5,11 and 12 confirm that these mice are *Fh1*$^{+/+}$, the presence of the 0.28kb and the 0.44kb PCR products in lane 3 confirms that this mouse is *Fh1*$^{+/-}$, the 0.28kb and 0.49kb PCR products in lanes 6 and 7 confirms that these mice are *Fh1*$^{fl/+}$, and the 0.49kb PCR product in lanes 8 and 9 confirm that these mice are *Fh1*$^{fl/fl}$. Lane 10 is a negative control.

5.15 Confirmation of homozygous lethality

In order to determine lethality, 10 *Fh1*$^{+/-}$ mice were intercrossed and failed to produce any *Fh1*$^{-/-}$ offspring from a total of 59. This lethality is further analysed and discussed in Chapter 6.

5.16 Summary of breeding strategy of the *Fh1* knockout mouse

This Chapter has described the stepwise construction and validation of an *Fh1* conditional knockout mouse and subsequent crosses. These crosses are summarised below (Figure 5.16) and future work on these mice are described in Chapter 6.

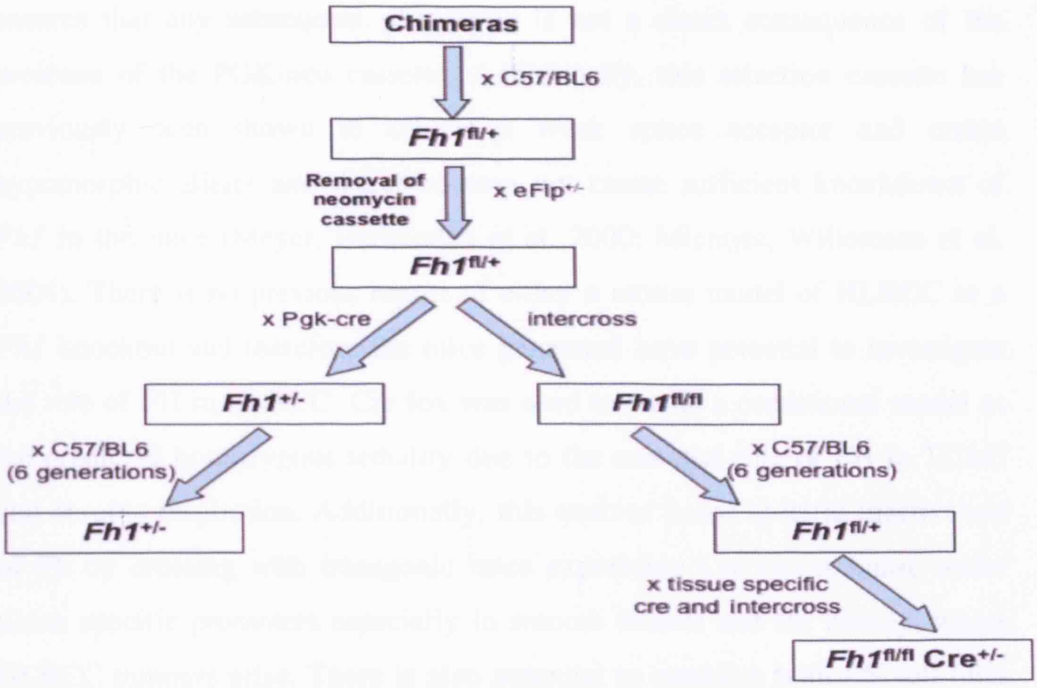

Figure 5.16 Breeding strategy of the *Fh1* knockout mouse

Chimeras were crossed to C57/BL6 and offspring that were positive for the floxed *Fh1* allele were crossed with eFlp mice to remove the neomycin cassette *in vivo*. Hetrozygous knockouts were generated by crossing with PGK-cre mice and then bred through 6 generations of C57/BL6 mice and observed on a weekly basis for any signs of abnormalities. Mice with the floxed *Fh1* allele were also intercrossed and then bred through 6 generations of C57/BL6 mice. These mice were used to create tissue specific knockout of *Fh1* and these studies are described in Chapter 6.

5.17 Discussion

This chapter described the successful design of a conditional *Fh1* knockout mouse using site-specific gene targeting of mouse ES cells and the subsequent generation of chimeric mice that were capable of transmitting the targeted allele through the germline. Additionally, Flp-FRT and Cre-lox technology was successfully used to remove the neomycin resistance cassette and to create heterozygous knockout mice. Removal of the neomycin cassette

ensures that any subsequent phenotype is not a direct consequence of the presence of the PGK-neo cassette. Additionally, this selection cassette has previously been shown to act as a weak splice acceptor and create hypomorphic alleles and therefore may not create sufficient knockdown of *Fh1* in the mice (Meyer, Hernandez et al. 2000; Mientjes, Willemsen et al. 2004). There is no previous report of either a mouse model of HLRCC or a *Fh1* knockout and therefore the mice generated have potential to investigate the role of FH in HLRCC. Cre-lox was used to create a conditional model as we predicted homozygous lethality due to the essential role of FH in TCAC and aerobic respiration. Additionally, this enables tissue specific inactivation of Fh by crossing with transgenic mice expressing Cre recombinase under tissue specific promoters especially in smooth muscle and the kidney, where HLRCC tumours arise. There is also potential to establish both ES cell lines and primary culture cell lines to carry out functional analysis such as measuring Ψ_M, ROS and apoptosis using FACS analysis, investigating HIF and prolyl hydroxylase activity, and testing for energy deficiency using AMPK assays. Of course, if the $Fh1^{+/-}$ or tissue specific $Fh1^{fl/fl}$ $Cre^{+/-}$ mice develop tumours then all of the above assays could be carried out directly on these, but a phenotype can not always be guaranteed by inactivation of tumour-suppressor genes in mice as shown by the *Brca1* knockout (Liu, Flesken-Nikitin et al. 1996). Indeed, the unconditional $Sdhd^{+/-}$ mice had not developed tumours after 8 months (Piruat, Pintado et al. 2004). There are many differences between mice and humans which help account for a lack of phenotype and tumours that do develop in mice are often very different from those in humans (reviewed by M.L. Cooper) (Hooper 1998). These parallels and contrasts between tumour-suppressor gene knockouts in humans and mice is discussed in more detail in Chapter 8. However, the fact that FH activity is virtually absent in HLRCC tumours (Tomlinson, Alam et al. 2002) and that the exons floxed in this mouse model contain both essential active site and activation domain residues should enable abrogation of FH activity in tissues in homozygous floxed mice expressing Cre recombinase in specific tissues, possibly leading to tumourigenesis.

6 Chapter 6: Characterisation and phenotypic analysis of the *Fhl* mouse

Introduction

The successful gene targeting of murine *Fhl* was described in Chapter 5, and confirmed using PCR and Southern analysis. The neomycin cassette was successfully removed in vivo by crossing with eFlp mice and $Fhl^{+/-}$ mice generated *in vivo* by crossing with PGK-Cre. Both $Fhl^{fl/fl}$ and $Fhl^{+/-}$ mice were maintained by breeding with C57/BL6. In order to analyse the functional consequences of the *Fhl* knockout, it was decided to breed sufficient $Fhl^{+/-}$ mice and controls (n=50 for each) to see if at some stage they developed any phenotype, specifically that of HLRCC. A homozygous lethality was predicted, as *Fhl* is an essential housekeeping gene vital for aerobic respiration and we decided to characterise this by inter-crossing $Fhl^{+/-}$ mice, genotyping embryos and carrying out a histological analysis to try and identify the embryonic stage of lethality and any abnormal development. The mouse was designed to be a conditional knockout so that $Fhl^{fl/fl}$ mice were viable and by crossing with transgenic mice expressing Cre recombinase under specific promoters and inter-crossing the offspring, both alleles of *Fhl* could be knocked out in specific tissues thus bypassing the expected embryonic lethality. The most relevant to HLRCC were those expressing Cre recombinase in smooth muscle and renal cells. We applied for 3 strains of transgenic mice expressing Cre recombinase under tissue specific promoters as described below:

- Smooth muscle specific driven by the Myosin Heavy Chain promoter/enhancer elements (herein referred to as Sm-cre). These were a kind gift from Professor M.I. Kotlikoff. The smooth muscle myosin heavy chain (smMHC) promoter was used to direct expression of a

bicistronic transgene consisting of Cre recombinase and enhanced green fluorescent protein (eGFP) coding sequences (Xin, Deng et al. 2002). Animals expressing the transgene display strong fluorescence confined to vascular and nonvascular smooth muscle. Cre recombinase was expressed in all smooth muscles in adult mice, and there was an excellent overlap between expression of the recombinase and eGFP. Initial smooth muscle-specific expression of fluorescence and Cre recombinase was detected on embryonic day 12.5.

- Tubular epithelial cells of the kidney driven by promoter/enhancer elements of Ksp-cadherin (herein referred to as Ksp-cre). These mice were a kind gift from Dr. P Igarashi. Ksp-cadherin is a unique, tissue-specific member of the cadherin family of cell adhesion molecules that is expressed exclusively in tubular epithelial cells in the kidney and developing genitourinary (GU) tract. Transgenic mice carrying 324 bp of the 5' flanking region linked to a GFP reporter gene were produced and exhibited expression exclusively in tubular epithelial cells in the developing kidney and GU tract (Shao, Johnson et al. 2002). Immunoblot analysis showed that the expression of GFP was restricted to the kidney in adult mice.
- Renal collecting ducts of the kidney driven by promoter/enhancer elements of Aquaporin-2 (herein referred to as Aqua2-cre). RT-PCR and immunocytochemistry showed that 14 kb of the human 5'-flanking region conferred specific expression of a nucleus-targeted and epitope-tagged Cre recombinase in the principal cells within the renal collecting duct, in the epithelial cells of the vas deferens, and within the testis of transgenic mice (Nelson, Stricklett et al. 1998).

The Sm-cre line were re-derived onto C57/BL6 and crossed with $Fh1^{fl/fl}$ mice. These were subsequently backcrossed to generate $Fh1^{fl/fl}$ Sm-cre$^{+/-}$ mice (and control littermates) and the phenotype characterised. The advantage of using Sm-cre over other smooth muscle specific strains is that the Sm-cre transgene is not expressed until E12.5 and is strictly confined to smooth muscle (Xin, Deng et al. 2002) whereas the the SM α-actin trangene is highly

expressed in skeletal, heart, and smooth muscle before E13.5 therefore posing a potentially greater chance of embryonic lethality (Mack and Owens 1999).

6.1 *Fh1* mRNA expression of in $Fh1^{+/+}$ and $Fh1^{+/-}$ mice

In order to test whether the $Fh1^{+/-}$ mice had reduced *Fh1* mRNA levels, a real-time PCR Taqman assay was used (Applied Biosystems). The protocols are described in the Methods (Section 2.19). In brief, total RNA was extracted from brain, kidney and liver from both $Fh1^{+/+}$ (n=3) and $Fh1^{+/-}$ (n=3) mice. Single stranded cDNA was synthesised and used as a PCR template. Each cDNA sample was amplified using primers specific to *Fh1* and *Gapdh* (control). All reactions were performed in triplicate. The data was analysed in Excel (Microsoft) and the ratio of *Fh1*:*Gapdh* calculated for each sample (Section 2.19). From the ratios, the level of expression of *Fh1* in the tissues in the $Fh1^{+/-}$ mice in brain, kidney and liver tissue was expressed as a proportion of that of the $Fh1^{+/+}$ mice (Figure 6.1).

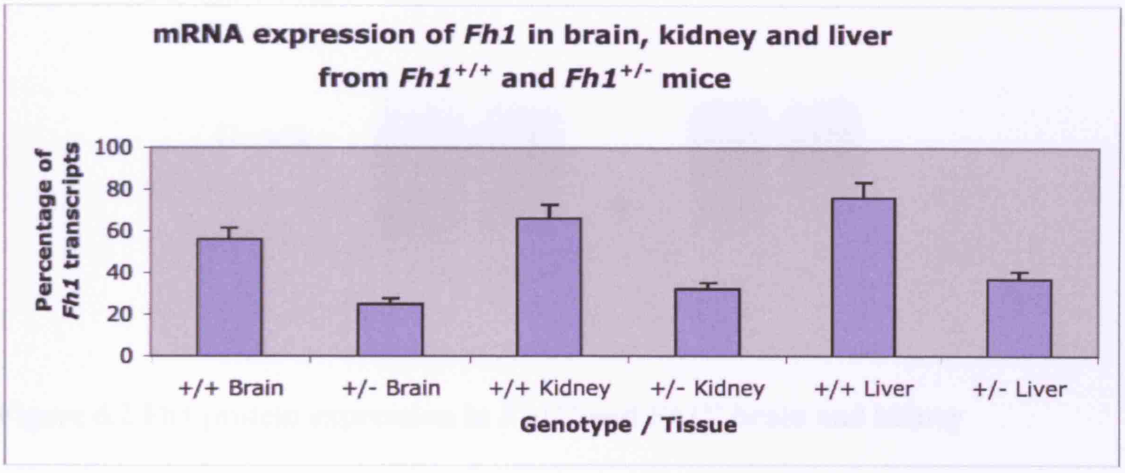

Figure 6.1 Real-time PCR quantitation of mRNA in $Fh1^{+/+}$ and $Fh1^{+/-}$ brain, kidney and liver.

The RT-Q-PCR assay indicates that mRNA levels of *Fh1* are less in tissues from $Fh1^{+/-}$ mice than the $Fh1^{+/+}$ mice (fold decrease in brain = 0.44, in kidney = 0.48 and liver = 0.49). For each experiment $p<0.01$ (t-test). All values of *Fh1* were normalised to *Gapdh*.

6.2 Fh1 Protein expression in *Fh1*$^{+/+}$ and *Fh1*$^{+/-}$ mice

In order to determine if the mRNA reduction in the *Fh1*$^{+/-}$ mice was mirrored at the protein level, immunoblot analysis was preformed on lysate from kidney and liver as described in the Methods (Section 2.20). In brief, total protein was extracted from tissue, the concentration determined, and electrophoresed through acrylamide gels, then blotted with Fh1 and Gapdh (loading control) antibodies as described in Chapter 2 (Section 2.20 and Table 2.2). Fh1 protein was reduced in the *Fh1* $^{+/-}$ kidney and liver tissue (Figure 6.2)

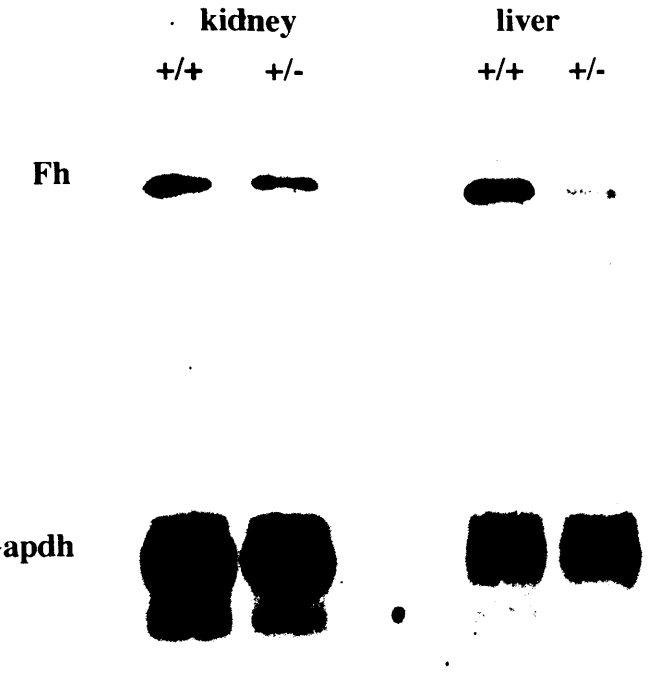

Figure 6.2 Fh1 protein expression in *Fh1*$^{+/+}$ and *Fh1*$^{+/-}$ brain and kidney

Fh protein levels are significantly lower in the *Fh1*$^{+/-}$ mice as demonstrated by the immunoblotting of kidney and liver lysate. Gapdh was used as a loading control.

6.3 Analysis of the embryonic lethality

We mated 10 pairs of *Fhl1*$^{+/-}$ mice (5 pairs from each of the 2 positive clones 4A3 and 4C9 (Section 5.6) and genotyped 59 offspring. 28/59 (47%) were *Fhl1*$^{+/+}$, 31/59 (53%) were *Fhl1*$^{+/-}$ and 0/59 (0%) were *Fhl1*$^{-/-}$; p=5.893e-11 (exact binomial test). Therefore, as predicted *Fhl1*$^{-/-}$ mice are embryonic lethal. It was therefore decided to investigate the stage and cause of lethality by analysing the gross phenotype and using immunohistochemical techniques.

6.3.1 Gross morphology of the *Fhl1*$^{-/-}$ phenotype

All embryo studies were carried out on a minimum of 5 litters from *Fhl1*$^{+/-}$ inter-crosses and the representative data are shown (Figure 6.3). Initially, embryos were studied from *Fhl1*$^{+/-}$ inter- crosses at E10.5. Pregnant females were culled and embryos dissected out and yolk sac removed for genotyping. The embryonic dissection was carried out under close supervision of a mouse developmental biologist (Dr. Spencer-Dene). Two independent primer pairs were used to confirm the genotype of the parents and also that of the offspring by genotyping the yolk sac. At E10.5 the *Fhl1*$^{-/-}$ embryos were virtually reabsorbed and grossly underdeveloped (Figure 6.3). This experiment was repeated 3 times and in each case the *Fhl1*$^{+/+}$ embryos were morphologically indistinguishable form the *Fhl1*$^{+/-}$ embryos.

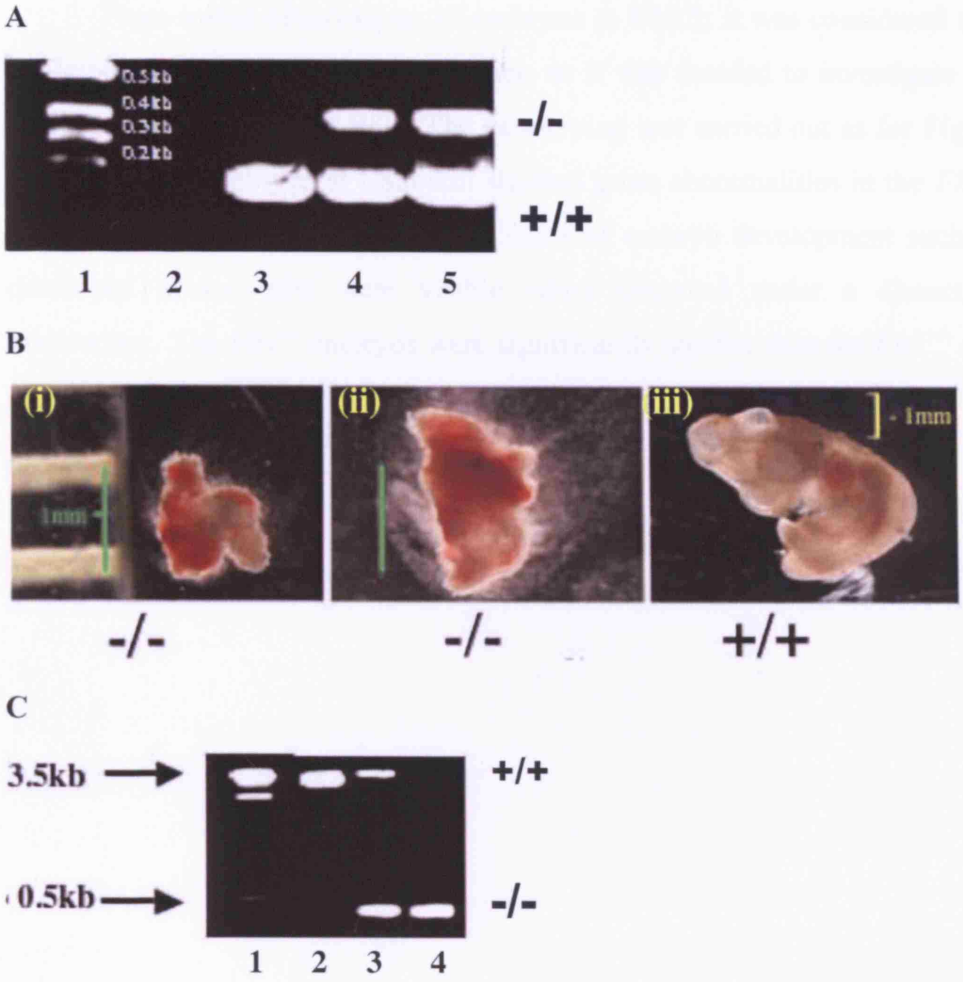

Figure 6.3 Genotyping and morphology of *Fh1*$^{-/-}$ embryos.

The *Fh1*$^{+/-}$ parents were genotyped (A). DNA size markers (lane 1), a negative control (lane 2) and an *Fh1*+/+ mouse (lane 3). The *Fh1*$^{+/+}$ band (180bp) is observed in the *Fh1*$^{+/+}$ control and both the *Fh1*$^{+/-}$ mice (lanes 4 and 5). An additional 400bp band is observed only in the *Fh1*$^{+/-}$ mice (lanes 4 and 5). The *Fh1*$^{-/-}$ embryos (i) and (ii) show gross abnormalities (B) and very retarded growth as indicated by the 1mm size bar. The *Fh1*$^{+/+}$ embryo (iii) is more developed with defined features. The genotyping of the embryos in panel B were confirmed (C) and the 3.5kb *Fh1*$^{+/+}$ band was only present in lane 2 corresponding to embryo (iii) in B and one of the *Fh1*$^{+/-}$ parents (lane 3). The 0.5kb *Fh1*$^{-/-}$ band was only present in the *Fh1*$^{-/-}$ embryos (lane 4, embryo (i) from (B). DNA size markers are in lane 1.

From initial observations of embryos at E10.5, it was considered that the lethality was occurring much earlier, so it was decided to investigate the embryonic morphology at E8.5. The genotyping was carried out as for Figure 6.3. Observing embryos at E8.5 still showed gross abnormalities in the *Fh1*$^{-/-}$ mice (Figure 6.4A-C) and no visible signs of embryo development such as developed neural tube were visible when observed under a dissection microscope. The *Fh1*$^{-/-}$ embryos were significantly smaller than the *Fh1*$^{+/-}$ and *Fh1*$^{+/+}$ embryos.

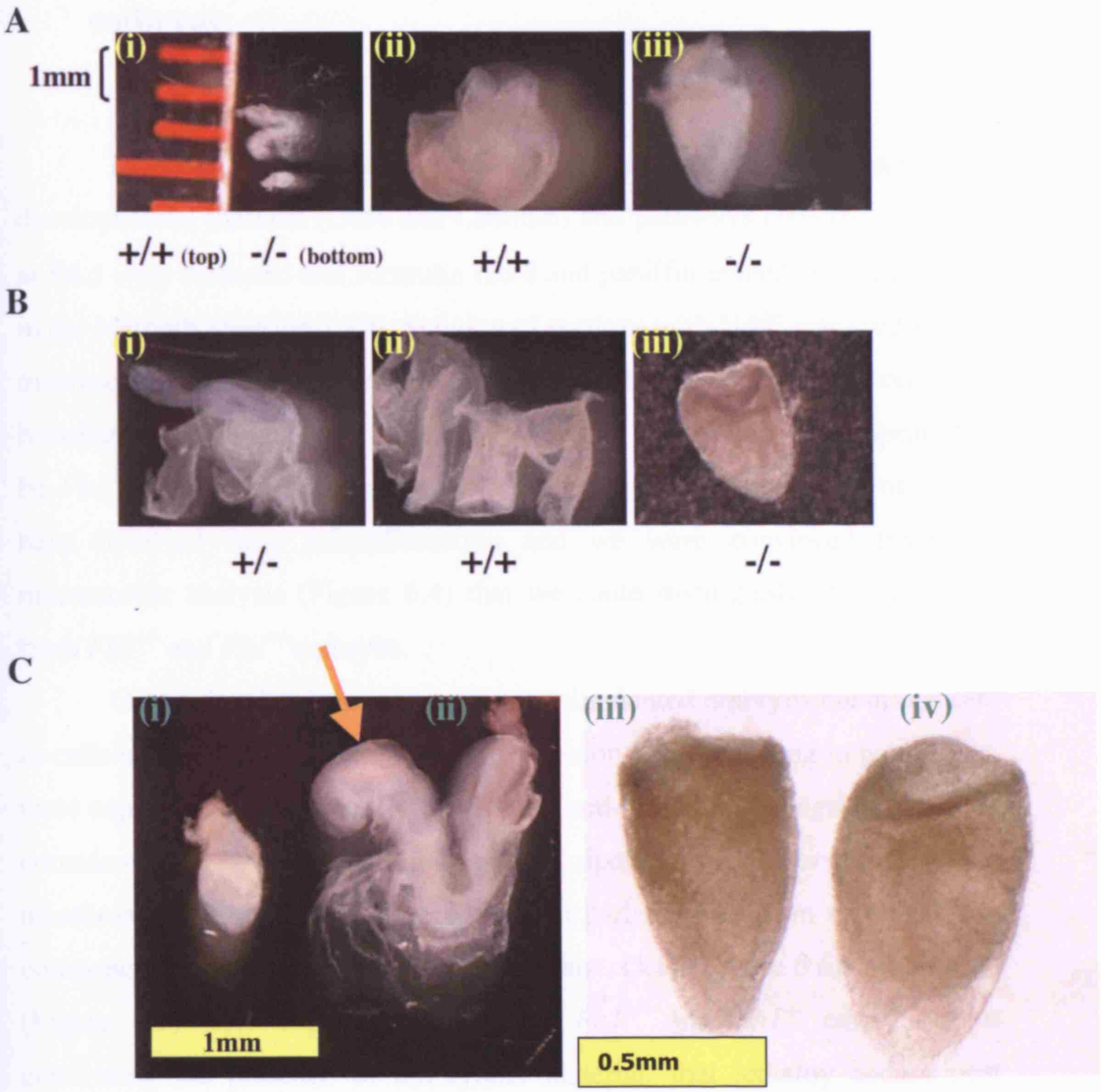

Figure 6.4 Gross morphology of *Fh1*$^{+/+}$, *Fh1*$^{+/-}$ and *Fh1*$^{-/-}$ embryos at E8.5

The *Fh1*$^{-/-}$ embryos are markedly smaller (A). The 1mm rule shows an *Fh1*$^{+/+}$ and *Fh1*$^{-/-}$ embryo and emphasises the difference in size at this stage of development. Panel B indicates that there is no difference in size between the and *Fh1*$^{+/-}$ (i) and *Fh1*$^{+/+}$ (ii) embryos. Panel C highlights the underdevelopment of the *Fh1*$^{-/-}$ embryos (i) The head fold in the *Fh1*$^{+/+}$ embryo (ii) is indicated by the arrow and this is absent in the *Fh1*$^{-/-}$ embryo. The under-developed smaller *Fh1*$^{-/-}$ embryos (iii) and (iv) are shown at higher power (x200). All other pictures are shown at a magnification of x100.

6.4 Histological and immunohistochemical analysis of *Fh1*$^{-/-}$ embryos

In order to confirm loss of Fh1 protein and to investigate other developmental markers (Oct4 and Laminin) and pathways (HIF1α), embryos at E6.5 were dissected and formulin fixed and paraffin embedded as described in the Methods (Section 2.10). Staining of sections with H&E was used so that macroscopically observed gross abnormalities (Figure 6.4) could be confirmed histologically. We analysed 8 litters (56 mice) to ensure that what appeared to be *Fh1*$^{-/-}$ were consistant histologically as genotyping of the embryos would have involved laser microdissection and we were convinced from the macroscopic analysis (Figure 6.4) that we could distinguish *Fh1*$^{-/-}$ embryos from *Fh1*$^{+/-}$ and *Fh1*$^{+/-}$embryos.

Oct4 is localised the epiblast in post-implanted embryos but disappears as cells undergo differentiation, with expression only persisting in germ cells. Oct4 expression is restricted to pluripotent and totipotent lineages and can be considered as a marker of the embryo itself, distinct from the extra-embryonic membrane. Laminin is highly expressed in parietal endoderm cells and key components in the extra-embryonic membrane. Oct4 (Figure 6.6) and laminin (Figure 6.7) were expressed in *Fh1*$^{+/+}$, *Fh1*$^{+/-}$ and *Fh1*$^{-/-}$ embryos thus confirming the presence of embryonic material, that lethality occurs post implantation and that *Fh1*$^{-/-}$ mice survive beyond E4.5. The level of Fh protein was vastly reduced in the *Fh1*$^{-/-}$ embryos as shown by immunohistochemical staining (Figure 6.7) and was additional confirmation that we were in fact looking at genuine homozygous knockouts rather than re-absportions.

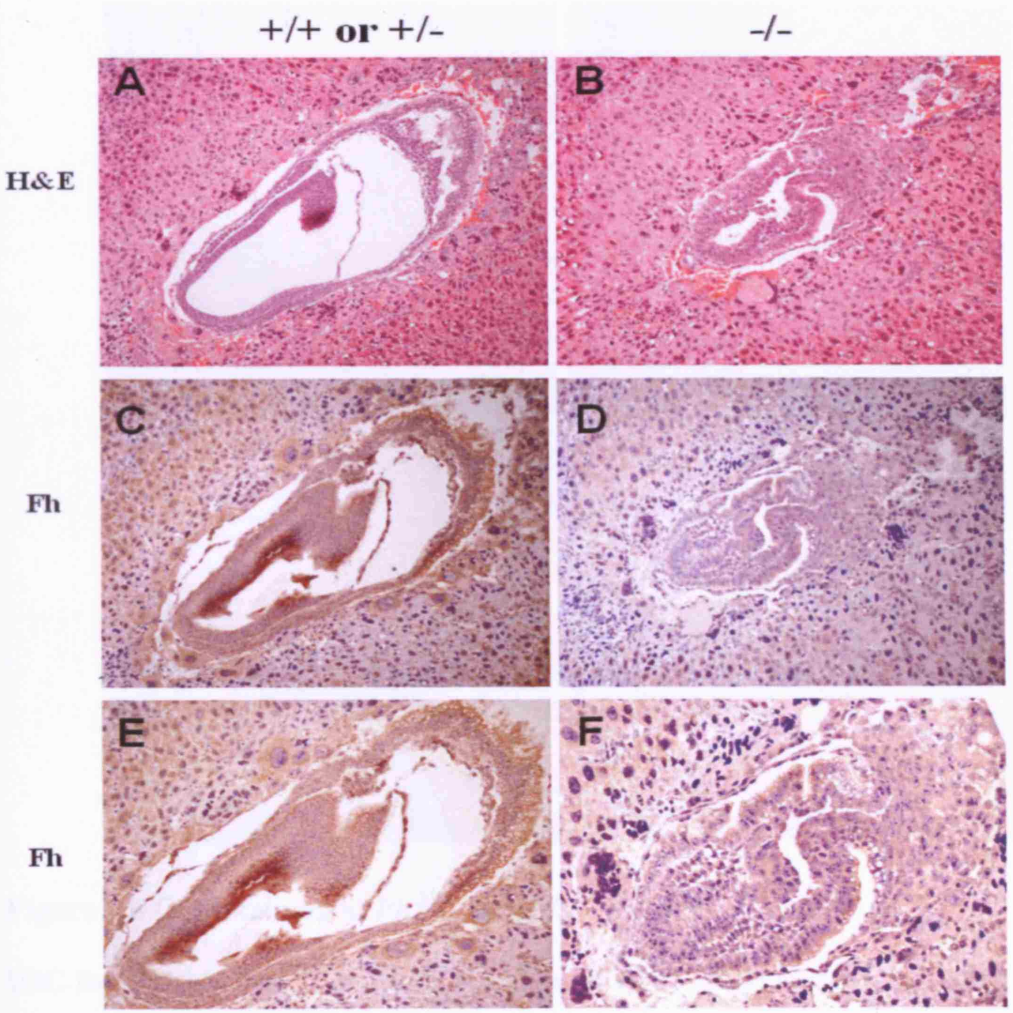

Figure 6.5Histological and immunohistochemcial analysis of embryos at E6.5 generated from inter-crossed *Fh1*$^{+/-}$ mice.

The *Fh1*$^{+/-}$ or *Fh1*$^{+/+}$ embryos (A) are considerably larger and more developed in comparison with the *Fh1*$^{-/-}$ embryos (B) as shown by the H&E staining. Fh protein (brown staning) is present in *Fh1*$^{+/+}$ or *Fh1*$^{+/-}$ embryos (C) but absent from *Fh1*$^{-/-}$ embryos (D). Final magnifications x100 (A-D) and x200 (E and F).

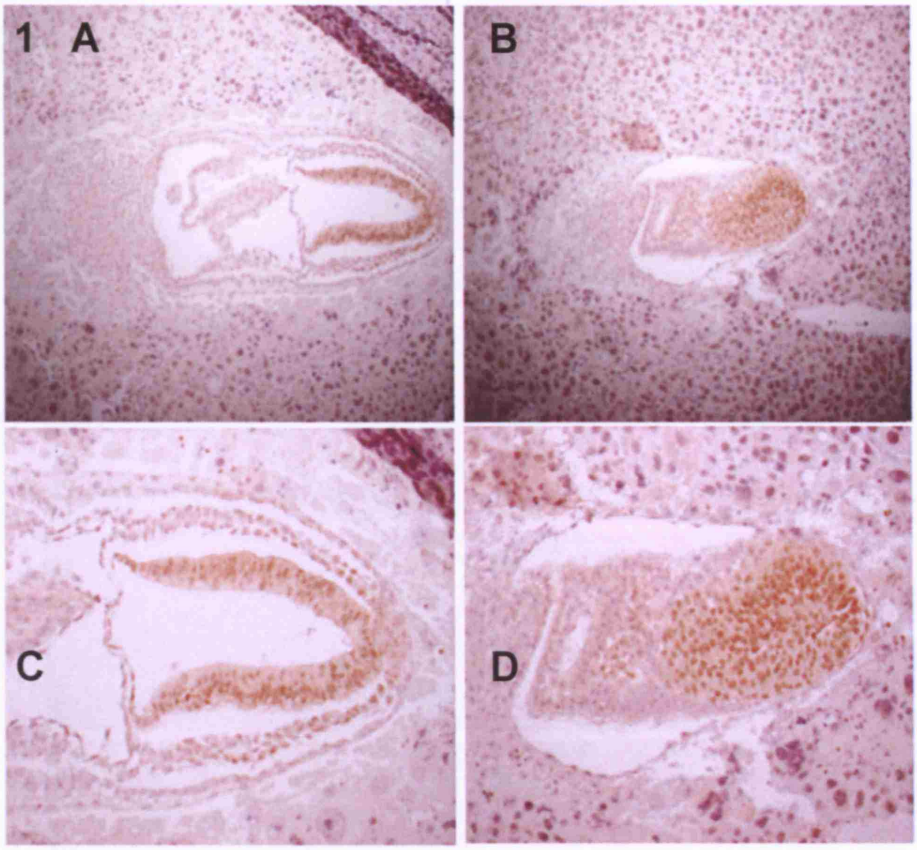

Figure 6.6 Oct4 staining of *Fh1*$^{+/+}$ and *Fh1*$^{-/-}$ embryos

IHC for Oct4 in *Fh1*$^{+/+}$ *or Fh1*$^{+/-}$ (A,C) and *Fh1*$^{-/-}$ (B,D) embryos at E6.5. Oct-4 is expressed only in the embryo and therefore confirms that *Fh1*$^{-/-}$ embryos survive past early embryogenesis. The *Fh1*$^{-/-}$ (B,D) is much less well organised than the normal (A,C) as can be in seen by the more specific staining. Final magnifications are x100 (A,B) and x 200 (C,D).

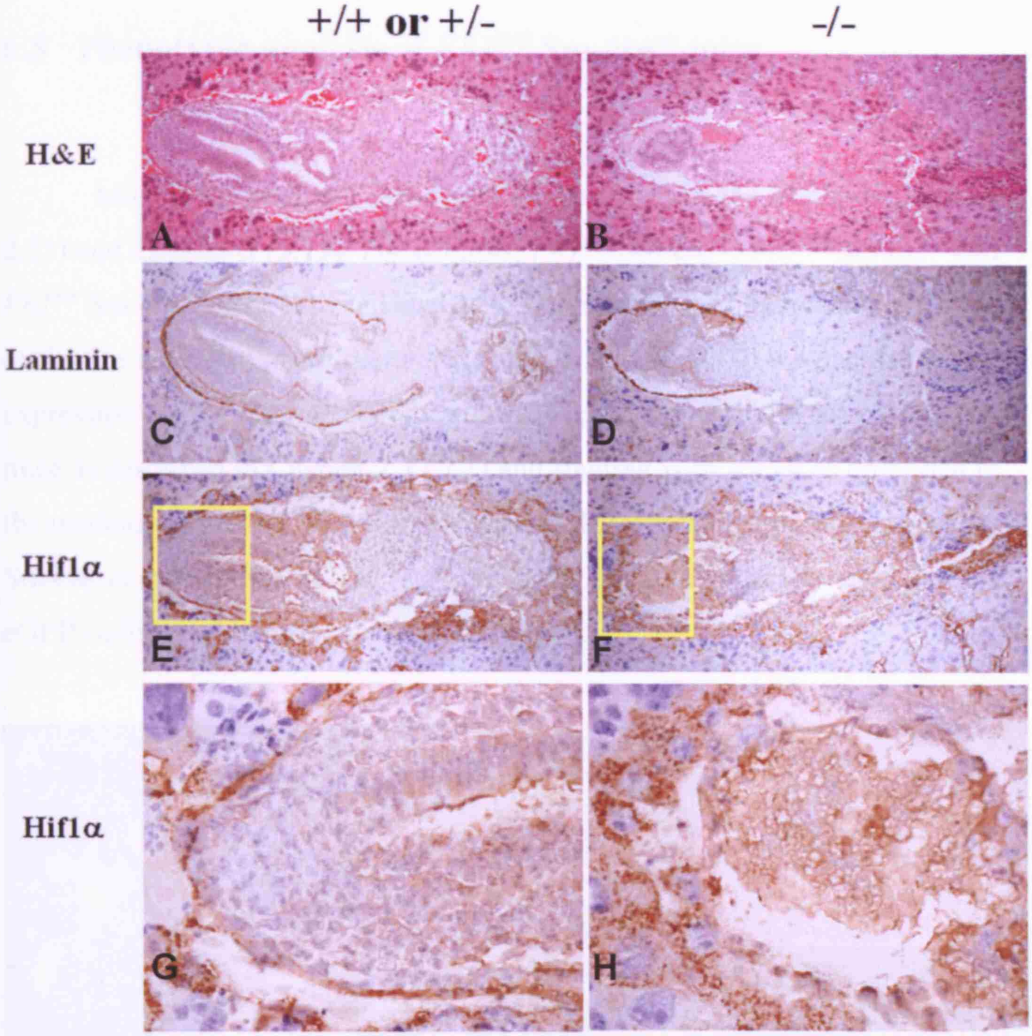

Figure 6.7 Immunohistochemical staining for laminin and Hif1α in *Fh1*$^{+/+}$, *Fh1*$^{+/-}$ and *Fh1*$^{-/-}$ embryos

IHC analyses of laminin and Hif1α in embryos at E6.5 from inter-crossed *Fh1*$^{+/-}$ mice. Gross histology is indicated by H&E staining (A,B). Brown staining identifies the presence of laminin in both *Fh1*$^{+/-}$ or *Fh1*$^{+/+}$ (C) and *Fh1*$^{-/-}$ embryos (D) and confirms that the *Fh1*$^{-/-}$ embryos survive implantation and parietal endoderm forms. Hif1α is moderately expressed in the *Fh1*$^{+/+}$ *or* *Fh1*$^{+/-}$ embryos (G) but highly expressed throughout the *Fh1*$^{-/-}$ embryos (H). This more evident at high power magnification (x400). The yellow boxes (E,F) indicate the region photographed in G (*Fh1*$^{+/+}$ *or* *Fh1*$^{+/-}$ embryos) and H (*Fh1*$^{-/-}$ embryos). All other magnifications are x100.

6.5 Phenotypic analysis of *Fh1*$^{fl/fl}$ Sm-cre$^{+/-}$ mice

Mice were bred and genotyped as described in the Methods (Section 2.23) and Chapter 5 (5.15). For controls, *Fh1*$^{fl/+}$ Sm-cre$^{+/-}$, *Fh1*$^{fl/fl}$ Sm-cre$^{-/-}$ and *Fh1*$^{+/+}$ Sm-cre$^{+/-}$ were kept and analysed. Despite the thorough characterisation of the Sm-cre strain in the literature (Xin, Deng et al. 2002) we decided to test expression in the uterine myometrium by crossing with ROSA26 reporter mice as described in Chapter 7, (7.7.1) and staining with X-Gal as described in the methods (Section 2.17.2) and by using eGFP fluorescent microscopy as the Sm-cre construct has an internal ribosomal entry site (IRES) fused to the eGFP coding region (Xin, Deng et al. 2002).

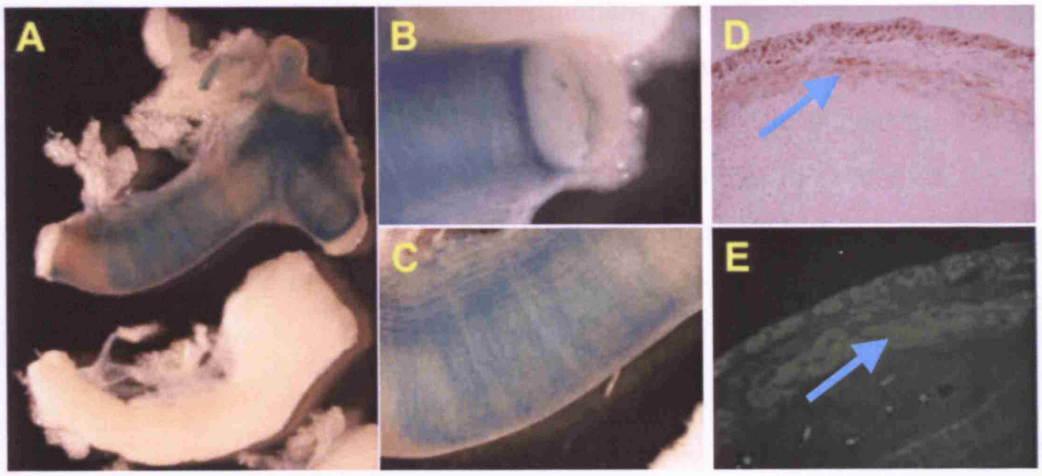

Figure 6.8 Expression of Cre recombinase and eGFP in the myometrium of Sm-Cre$^{+/-}$ mice.

Whole mount X-Gal staining of uteri from Rosa26$^{+/-}$ Sm-cre$^{+/-}$ mice (A-top, B,C) reveals strong blue positive staining compared to the uterus from the Rosa26$^{+/-}$ Sm-cre$^{-/-}$ control mouse (A-bottom). Myometrium specific eGFP expression in the Sm-cre$^{+/-}$ mouse is evident at the microscopic level using both whole-mount IHC (B,C) IHC using an anti-eGFP antibody (D) and fluorescence microscopy (E). The myometrial staining is indicated by the arrow (D,E). Some staining was also observed in the outer epithelial layer (D,E).

6.5.1 *Fhl1*$^{fl/fl}$ Sm-cre$^{+/-}$ mice have distinctly dilated small intestines, smooth muscle hypertrophy and die within six weeks of birth.

After breeding 6 litters of *Fhl1*$^{fl/fl}$ Sm-cre$^{+/-}$ and back-crossing to generate more knockout animals it was noted that all homozygous smooth muscle knockouts died within 6 weeks of birth. Full post-mortem examinations were carried our by a mouse pathologist (Professor G.W. Stamp) on 6 homozygous knockout and 6 control mice (2 each of *Fhl1*$^{fl/+}$ Sm-cre$^{+/-}$, *Fhl1*$^{fl/fl}$ Sm-cre$^{-/-}$ and *Fhl1*$^{+/+}$ Sm-cre$^{+/-}$) to ensure that the phenotype was consistent. The small intestine in the knockout animals showed a distinct dilation immediately after the pyloric junction, with the calibre increased 5-10 fold (Figure 6.9). The muscle wall appeared flaccid and showed little peristaltic activity in the immediate post mortem state. Sections were taken transversely and longitudinally from all levels in the gut from a further 8 mice (4 *Fhl1*$^{fl/fl}$ Sm-cre$^{+/-}$ and 4 controls as described above). The duodenum and jejunum appeared to be predominantly affected, although in several of the older mice (5-6 weeks), the terminal ileum and proximal colon were also dilated.

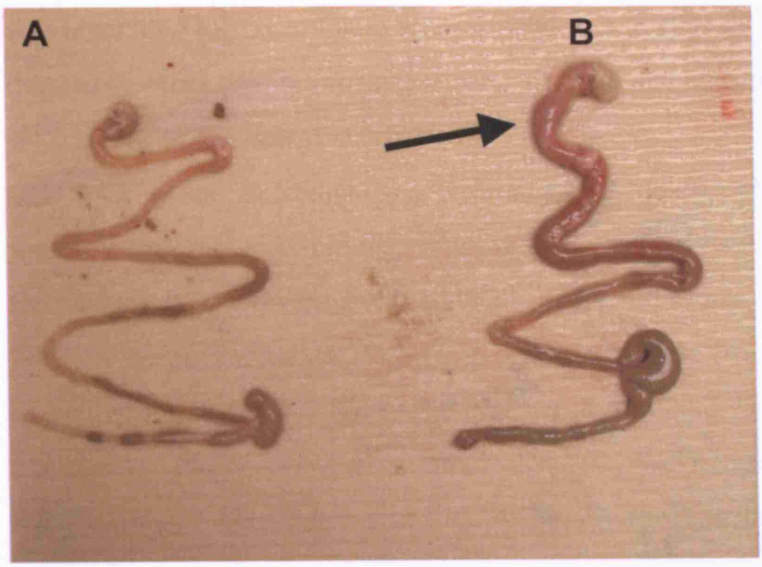

Figure 6.9 Gross morphology of whole guts from *Fh1*$^{fl/fl}$ Sm-cre$^{-/-}$ and *Fh1*$^{fl/fl}$Sm-cre$^{+/-}$ mice

Whole guts taken from 4 week old male mice from the same litter. *Fh1*$^{fl/fl}$ Sm-cre$^{-/-}$ (A) and *Fh1*$^{fl/fl}$ Sm-cre$^{+/-}$ (B). Note the gross dysention notably in the duodenum (arrowed) and ileum and subtler dystension in the terminal ileum and proximal colon.

Histological examination revealed diffuse thickening of the muscularis propria in both the outer longitudinal and inner circular muscle layers. The muscularis mucosae was not affected. Immunostaining for eGFP revealed variably strong staining for GFP in both muscle layers, although in many animals was more intense in the external longitudinal layer (Figure 6.10). In situ hybridisation using a probe for anti-sense *Fh1* as described in the methods (Section 2.18) was used to confirm the absence of *Fh1* transcripts in the muscle layers of the small intestine (Figure 6.10).

The neuronal plexi appeared normal and there was no deficiency in numbers of ganglion cells. This was corroborated by immunostaining for NeuN (data not shown), which highlighted the sympathetic nerve fibres and ganglion cells. There was no excess of cell proliferation or apoptosis in the muscle layers as confirmed by immunostaining for phosphohistone H3 and caspase 3 respectively (data not shown). In a few of the older animals (5-6 weeks of age), there was focal mucosal ulceration in the distal ileum which

was attributed to stasis. There were no changes to suggest inflammatory bowel disease or other primary inflammatory disorder and no atresia or other organic obstruction of the bowel was present.

In order to statistically validate the hypertrophy, microscopy and imaging software (EclipseNet, Nikon) were used to measure the thickness of the muscle layers of the small intestine from transverse sections. At least 20 measurements were taken each from 3 fields of view from 6 different animals (3 control mice ($Fhl^{fl/+}$ Sm-cre$^{+/-}$, $Fhl^{fl/fl}$ Sm-cre$^{-/-}$ and $Fhl^{+/+}$ Sm-cre$^{+/-}$) and 3 knockout ($Fhl^{fl/fl}$ Sm-cre$^{+/-}$) mice Representative sections from which measurements were taken were identified by the histopathologist (Professor G.W. Stamp). For control purposes, measurements were also taken for mucosal thickness and villous length from the same sections. Significant differences between the muscle layer thicknesses in the two groups of mice were tested for using the Mann-Whitney statistical test and smooth muscle hypertrophy was confirmed in the knockout mice (wild-type, mean = 25.04μm, StDev = 5.8; knockout, mean = 55.09μm, StDev = 7.3, $p<0.0001$). There were no statistically significant differences between mucosal thickness (wild-type, mean = 88.89μm, StDev = 12.7; knockout, mean = 93.17μm, StDev = 14.3, $p>0.05$) or villous length (wild-type, mean = 348.93μm, StDev = 25.1; knockout, mean = 350.37μm, StDev = 42.3, $p>0.05$). In order to determine that both the outer longitudinal and inner transverse muscle cells were hypertrophic in the knockout mice, the same counting methods were applied and p-values calculated using the Wilcoxon statistical test. The outer longitudinal muscle layer was thicker in the knockouts (mean = 18.52μm, StDev = 5.3) than wild-type mice (mean = 9.82μm, StDev = 4.1); $p< 0.001$. The inner transverse muscular layer was thicker in the knockout mice (mean = 44.77μm, StDev = 6.8) than in the wild-type (mean = 25.29μm, StDev = 5.1); $p< 0.001$. The hypertrophy observed in both layers is evident when comparing wild-type with knockout (Figure 6.10).

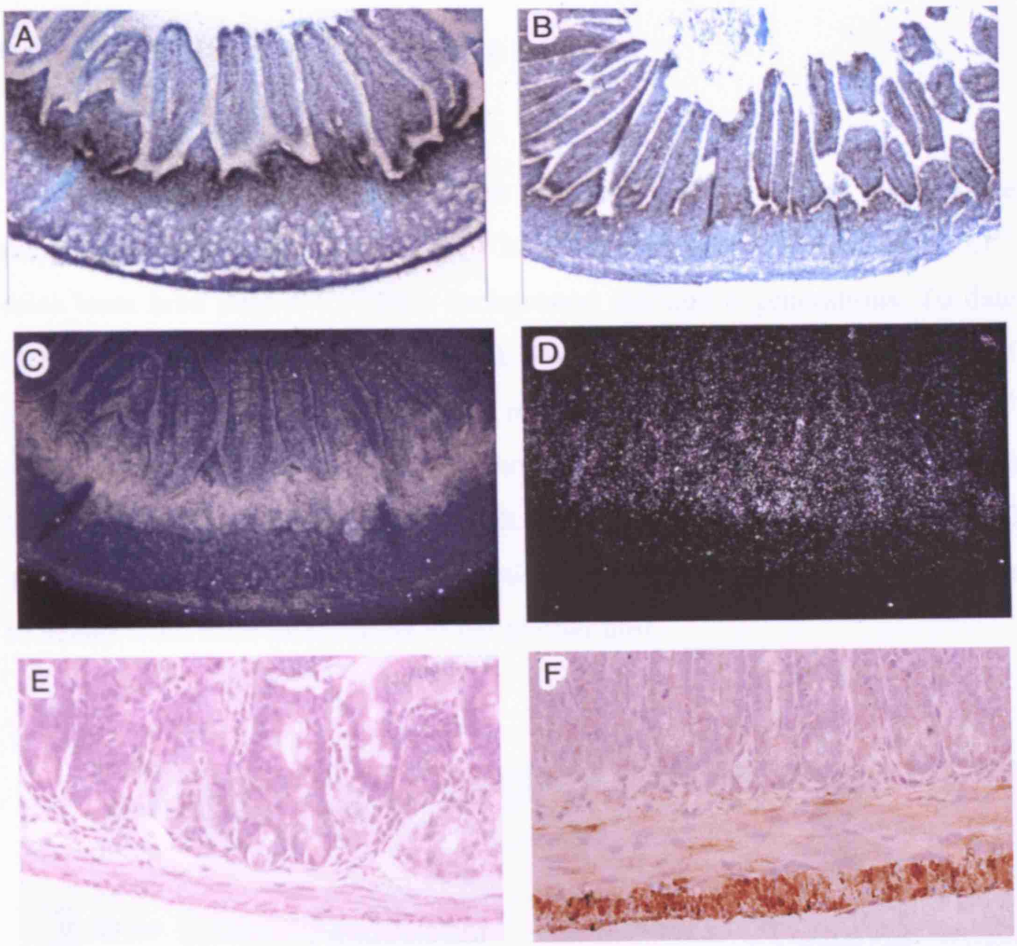

Figure 6.10 ***Fh1 in situ*** **hybridisation and eGFP staining of transverse duodenal sections from** ***Fh1***$^{fl/fl}$ **Sm-cre**$^{-/-}$ **and** ***Fh1***$^{fl/fl}$ **Sm-cre**$^{+/-}$ **mice**

ISH viewed under light (A,B) and dark field (C,D) for ***Fh1*** **in transverse duodenum section from a wild-type (A,C) and knockout (B,D) mouse showing vastly reduced** ***Fh1*** **mRNA expression in the knockout, in both longitudinal and circular muscular layers surrounding the mucosa. The functional effect of knocking out** ***Fh1*** **results in hypertrophy of both (longitudinal and transverse) muscle layers. The wild-type (***Fh1***$^{fl/fl}$ Sm-cre$^{-/-}$) section (E) has no hypertrophy and stains negatively for eGFP (the Sm-cre construct has an IRES-eGFP), whilst the knockout (***Fh1***$^{fl/fl}$ Sm-cre$^{+/-}$) exhibits hypertrophy in both muscle layers and stains positively for eGFP (F). The eGFP staining correlates with loss of** ***Fh1*** **mRNA thus indicating a high recombination efficiency and** ***Fh1*** **knockout in smooth muscle.**

6.6 Aging study of *Fh1* $^{+/-}$ mice

In order to determine whether the *Fh1*$^{+/-}$ mice develop tumours we maintained a stock of 60 mice; 30 *Fh1*$^{+/-}$ mice and 30 C57/BL6. All *Fh1*$^{+/-}$ mice were bred onto a C57/BL6 background through 6 generations. To date (10 months) no mice have become sick. Previously, it was shown that the *Fh1* mRNA and Fh1 protein levels were reduced by roughly 50% in the *Fh1*$^{+/-}$ mice indicating that there was no compensatory mechanism at the transcriptional or translational level. It was decided to weigh all mice at 22 weeks of age (Figure 6.11). Only 24 mice from each group were weighed due to deaths from mite infestations in the animal unit.

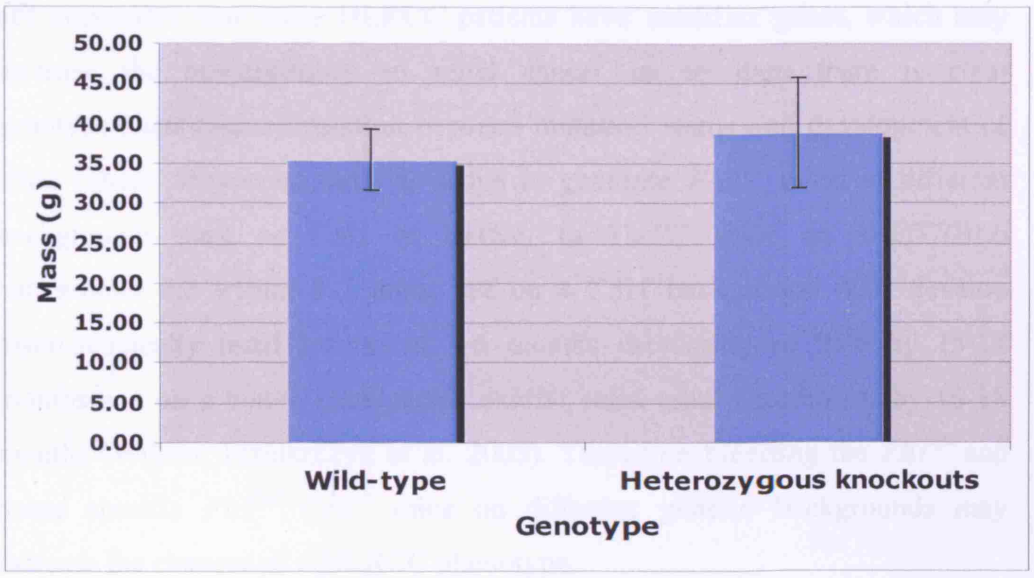

Figure 6.11 Mass of *Fh1*$^{+/+}$ and *Fh1*$^{+/-}$ mice at 22 weeks old

There was no significant difference in body mass between the *Fh1*$^{+/+}$ mice (mean = 35.33g, StDev = 3.8) and *Fh1*$^{+/-}$ mice (mean = 38.59, St Dev = 6.9, $p > 0.05$ for both Wilcoxon and Students T-Test).

6.7 Discussion

Initial analysis of the *Fh1* knockout mouse has revealed that despite about 50% knockdown in mRNA and protein expression, the $Fh1^{+/-}$ mice to date have not developed tumours. However, many mice such as the *Men1* knockout (Bertolino, Tong et al. 2003) do not develop tumours until 12-13 months and some tumour-suppressor genes such as *Brca1* when inactivated in mice do not have a tumour phenotype in the heterozygous genotype (Liu, Flesken-Nikitin et al. 1996). As most of the mouse lines used are very inbred, it is likely that some may contain modifier genes which may influence the phenotype such as the modifier of min (*Mom1*) locus in $Apc^{min/+}$ mice which affects intestinal tumour multiplicity (Gould, Dietrich et al. 1996). In fact it is not impossible that some HLRCC patients have modifier genes, which may increase the susceptibility to renal cancer as to date there is clear genotype/phenotype correlation between mutation status and development of renal cancer. However, there is scope to generate $Fh1^{+/-}$ mice on different backgrounds such as C3H or Balb/c. In $Tsc2^{+/-}$ mice on a C57/BL6 background die within 1-2 days, but on a C3H background 40% develop macroscopically renal lesions at 3-6 months increasing to 95% by 15-18 months and on a blab/c background exhibit solid renal carcinomas by 16-18 months (Wilson, Idziaszczyk et al. 2005). Therefore breeding the $Fh1^{+/-}$ and tissue specific $Fh1^{fl/fl}$ $Cre^{+/-}$ mice on different genetic backgrounds may increase the chances of a HLRCC phenotype.

The embryonic lethality was disappointing but predicted; hence we created a conditional knockout model. However, there is potentially a lot of functional *in vitro* data to be obtained and at present we are attempting to generate $Fh1^{-/-}$ blastocyst lines and $Fh1^{fl/fl}$ Sm-$cre^{+/-}$ mouse embryonic fibroblasts (MEFS). These cell lines can be used for functional assays such as FACS analysis to determine with effect of *Fh1* inactivation on apoptosis, superoxide, and $\Delta\Psi_M$ (mitochondrial membrane potential).

In addition to FACS analysis, a more direct investigation into the tumourigenic effect of *Fh1*$^{-/-}$ blastocyst lines can be investigated by injecting these cells into nude mice and comparing tumour formation with that of *Fh1*$^{+/+}$ cells. Tumours derived from these mice could be easily removed and analysed using expression profiling and metabolomic techniques.

The main advantage of the *Fh1* conditional knockout is that it can be crossed with a wide range of tissue specific Cre-expressing transgenic strains. However, as is the case with the Sm-cre cross, the results are not always as predicted and each of the post mortems has been thoroughly examined by the pathologist (Professor G.W. Stamp) and all other small muscle appears normal at the microscopic level. The original paper describing the myosin heavy chain-lac Z fusion transgenic mice showed very intense staining in the small intestine at E19.5 (Madsen, Regan et al. 1998) so maybe a critical threshold of recombination occurred at this developmental stage. However, there is still a functional effect of knocking out Fh1; muscle hypertrophy, and the next stage is to investigate the pathways that lead to this. It may well be related to energy deficiency and therefore will be interesting to compare with human syndromes such as hypertrophic obstructive cardiac myopthay (HOCM) (Caldwell, Calkins et al. 1996) and hypertrophic pyloric stenosis (Deluca 1993). Physiological analysis and electron microscopy may reveal if the muscle is failing to relax or contract, and the potential analysis of levels and/or activity of gene expression and proteins in potential pathways in related syndromes will be discussed in Chapter 8.

The other tissue specific crosses (Aqua2-Cre and Ksp-Cre) which both express in renal cells are too young to analyse at the moment, though the *Fh1*$^{fl/fl}$ Ksp-Cre$^{+/-}$ and *Fh1*$^{fl/fl}$ Aqua2-Cre$^{+/-}$are healthy at 4 months old. However, even though hopefully the long-term effect of the double knockouts will result in malignancy, it is possible that the animals may die from organ failure so it is important to assess other options available.

One option is to use an inducible Cre strain such as Cre-ER (Indra, Warot et al. 1999). There are an increasing number of transgenic mice expressing Cre-ER under various promoters and as well as being tissue specific, expression of Cre recombinase is reliant on the administration of tamoxifen. This would overcome any 'leaky' expression during development

so that knockout of *Fh1* could be induced in mature adult mice. This may even overcome the early death in the $Fh1^{fl/fl}$ Sm-$cre^{+/-}$ mice.

Another option would be to generate large numbers of $Fh1^{fl/fl}$ mice and administer Cre recombinase either cutaneously or via injection into specific organs. This has shown to be effective in mice where adenoviral-cre has been used to infect organs (Sakai, Mitani et al. 1995).

In summary whereas the $Fh1^{+/-}$ mice have not developed a phenotype to date, conditional inactivation in smooth muscle has provided evidence that knocking out *Fh1* causes smooth muscle hypertrophy. $Fh1^{-/-}$ mice die at E6-E6.5 most probably due to developmental delay possibly caused by energy deficiency as Fh1 is a TCAC enzyme and plays a vital role in ATP production. The $Fh1^{-/-}$ embryos survive implantation and are capable of producing parietal endoderm as shown by the Oct4 and laminin immunohistochermistry.

In order to try and knockout *Fh1* in the uterine myometrium where HLRCC fibroids originate, we therefore attempted to make a transgenic cre-expressing mouse, specific to the myometrium. This is described in Chapter 7.

7 Chapter 7: Creation of the CaBP9K-Cre transgenic mouse and analysis of Cre recombinase expression

Introduction

In order to try to simulate the tumour-suppressor function of *FH* in the mouse, it is preferable to be able to conditionally inactivate both alleles in the tissue(s) where tumours form in humans. The *Fh1* mouse described in chapter 5 was designed and constructed so this would be possible. There were many Cre-expressing strains available but not one that was specific to the uterine myometrium. Literature analysis revealed that one group (Romagnolo, Cluzeaud et al. 1996) had identified a region of the rat Calbindin-D9k gene (herein referred to as CaBP9k) and upstream elements that conferred expression to the uterine myometrium of mice. The rat Calbindin-D9K (CaBP9K) gene is an intracellular calcium binding protein thought to be involved in intracellular calcium homeostasis, is mainly expressed in intestine, uterus, and lung and is regulated in a complex tissue-specific manner (Christakos, Gabrielides et al. 1989).

Previously a region (-117 to +331) of the CaBP9k was shown to express simian virus large T antigen and chloramphenicol acetyl transferase (CAT) in the uterine myometrium, so we decided to clone this region of rat CaBP9K into a Cre-expressing plasmid and use this to create a transgenic mouse line called CaBP9K-Cre.

7.1 Vector design

We used the Cre expression plasmid pBS185 (kind gift from Dr. Behrens). pBS185 (Figure 7.1) contains the major immediate early promoter from human cytomegalovirus (hCMV) and a modified Cre recombinase gene with a T to G transversion in the -3 position relative to the AUG translation

start that is shown to increase the translational proficiency of the Cre transcript (Sauer and Henderson 1990). It also contains a segment of the mouse metallothionein-I gene (MT-I) including the polyadenylation site to ensure export of mRNA from the mucleus and a pUC18-based replicon that encodes the β-lactamase gene to provide selection for ampicillin resistance in *E. coli.*

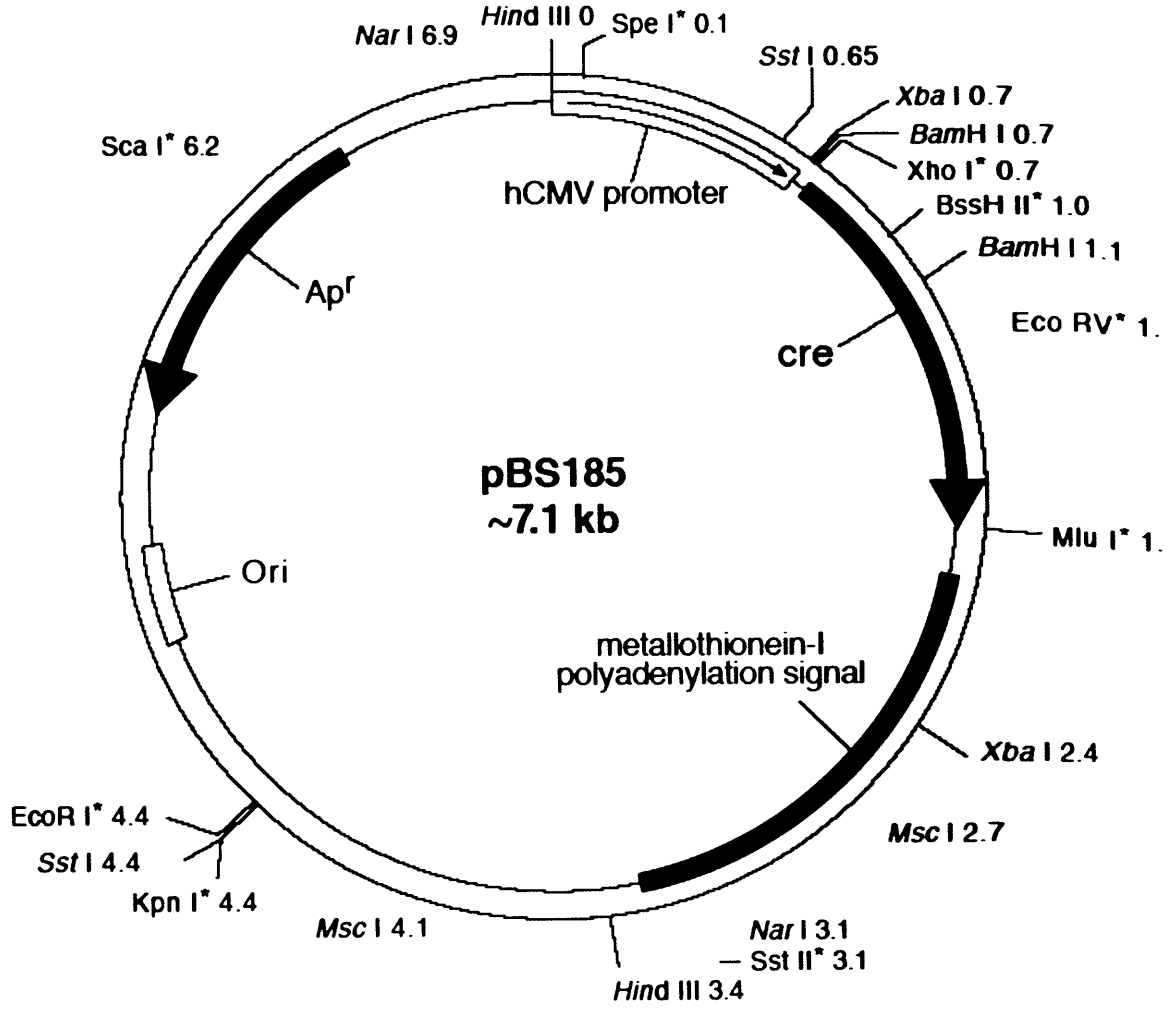

Figure 7.1 Map of of the cloning vector pBS185

Restriction sites indicated with '*' are unique. The plasmid contains the hCMV promoter (0.0-0.7kb), the phage P1 Cre coding region (0.7-2.2kb), the MT-1 polyA signal (2.2-4.4kb) and a segment of pUC18 (4.4-7.1kb) including the origin of replication and ampicillin resistance.

7.2 Cloning strategy

DNA was extracted from rat liver as described in the methods, and a 487bp fragment PCR amplified using the following primers incorporating *Xho* I restriction sites (underlined).

Forward - 5' - CCGCTCGAGTCTTAAGCTTGGTCTCAGA - 3'

Reverse - 5' - GGCCTCGAGTGCTGTAATTTGGGAAGA –3 '

The reverse primer stopped 6 bases short of the ATG initiation codon in exon 2 of CaBP9K. The PCR product was ligated into the *Xho* I site of pBS185 (Figure 7.2), sequenced and amplified as described in the Methods (Sections 2.6 and 2.8.2).

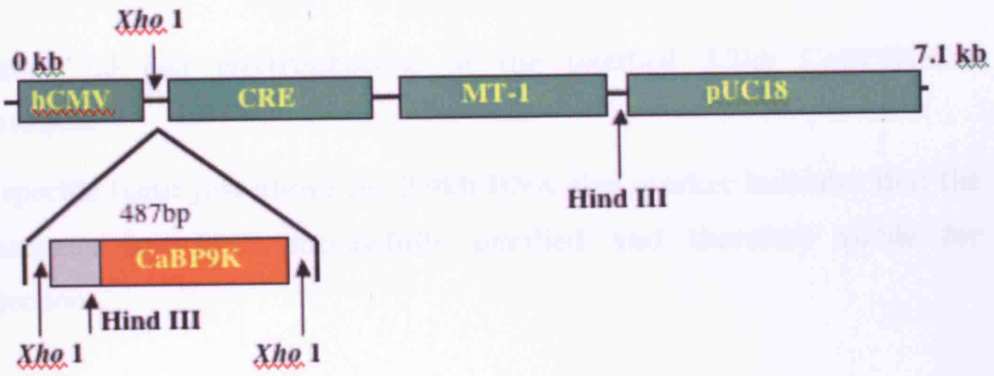

Figure 7.2 Cloning strategy for CaBP9K-Cre

The *Xho* I fragment of rat CaBP9K when cloned into pBS185 in the correct orientation to give pBS185-CaBP9K-Cre. This construct may be digested with *Hind* III to produce a 3.2kb transgene containing the CaBP9k regulatory elements (-117 to +335), the Cre coding region and the MT-1 polyA signal.

7.3 Transgene purification

pBS185-CaBP9K-Cre was cut with Hind III and the 3.2kb fragment gel-purified as described in the Methods (Section 2.9). 100ng of DNA was then electrophoresed through 1.2% agarose to confirm the size and purity (Figure 7.3) and 10μg was sent to Clare Hall Laboratories for pro-nuclear injection.

Figure 7.3 Gel electrophoresis of the purified 3.2kb CaBP9K-Cre transgene

A specific band just above the 3.0kb DNA size marker indicates that the transgene has been successfully purified and therefore viable for injection.

7.4 Pronuclear injection of CaBP9K-Cre

The Transgenic Facility at Clare Hall Laboratories performed an additional DNA purification step and carried out pronuclear injections of the CaBP9K transgene. These procedures are fully described in the Methods (Section 2.22).

7.5 Genotyping offspring

We were sent 95 tail clips from the offspring of the injected females. DNA was extracted as described in the Methods (Section 2.2.5) and PCR genotyped for the Cre transgene, using duplexed with primers specific to c-Jun as an internal control. This assay was carried out as described in Chapter 5 (Section 5.12.1). A total of 6 Cre-positive mice were identified from this screen (Figure 7.4A).

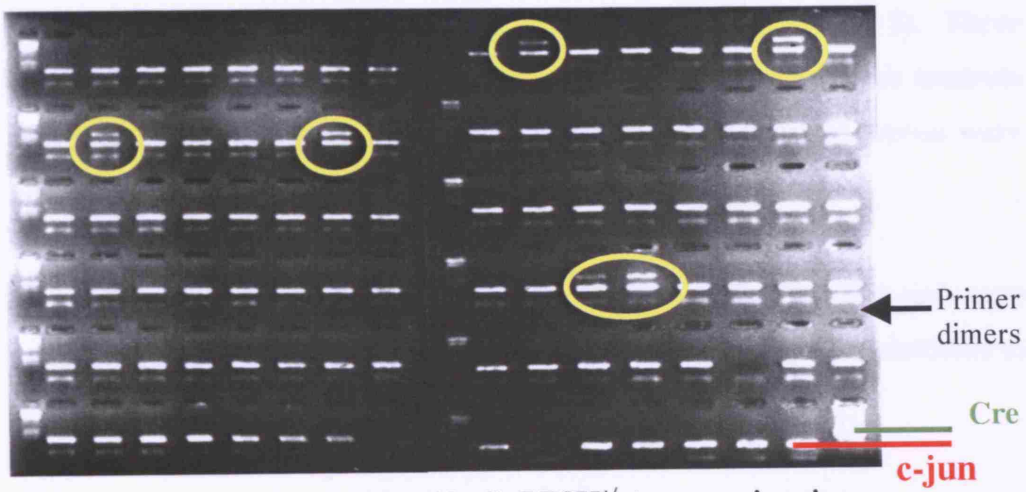

Figure 7.4 PCR screen to identify CaBP9K$^{+/-}$ transgenic mice

Figure 7.4A PCR screen of 95 mouse tails identified six mice (circled) with the Cre transgene (upper band, 0.65kb). The lower (0.2kb) band is c-jun and should be present in each sample. Primer dimers are also present in some PCR products (arrowed).

The PCR reactions were independently repeated with positive and negative controls and the result confirmed (Figure 7.4B).

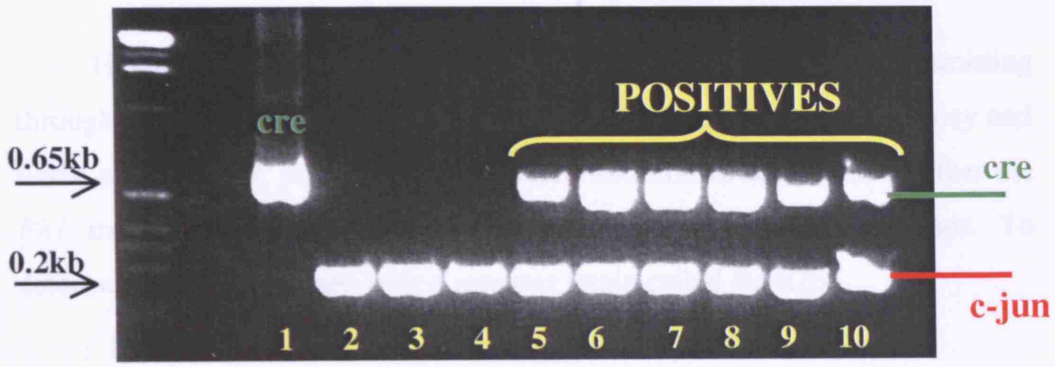

Figure 7.4B Confirmatory PCR genotype of CaBP9K-Cre positive mice. pBS185-CaBP9K-Cre was used as a positive control (lane 1). Three negative samples from the original screen were used as negative controls (lanes 2, 3 and 4). The 6 positive samples from the original screen were also amplified (lanes 5-10).

The 6 positive mice were founder lines for CaBP9K-Cre and were assigned the following codes so that analysis of the offspring was attributed to the specific founder line:

FL:4627B.4
FL:4625A.5
FL:4630A.7
FL:4630A.9
FL:4627B.1
FL:4627A.4

7.6 Confirmation of transmission of CaBP9K-Cre

The 6 founder lines were bred to C57/BL6 mice at Clare Hall Laboratories. The offspring were PCR genotyped as described above and a proportion of offspring from each founder line was found to carry Cre, confirming the transmission of the CaBP9K-Cre transgene. We then tested each line for tissue specific expression of Cre recombinase.

7.7 Analysis of CaBP9K expression in the uterus

Having successfully generated 6 lines of mice carrying, and transmitting through the germline, the CaBP9K-Cre transgene, we tested the efficiency and tissue specificity of potential Cre-mediated excision to determine whether the *Fh1* mouse should be crossed with any of the CaBP9K-Cre lines. To determine this, we crossed with a reporter strain called Rosa26.

7.7.1 Rosa26 reporter strain as an indicator of Cre recombinase expression

In order to test the expression of Cre recombinase in the uterus, we crossed the CaBP9K-cre mice from each founder line with a reporter strain of mice called Rosa26. These mice are homozygous for a β-galactosidase gene, preceded by a stop codon flanked by loxP sites (Soriano 1999) (Figure 7.5). A total of 84 mice were generated (2 litters from each founder CaBP9K x Rosa26$^{+/+}$) and 48 of these (57%) were positive for CABP9K-Cre.

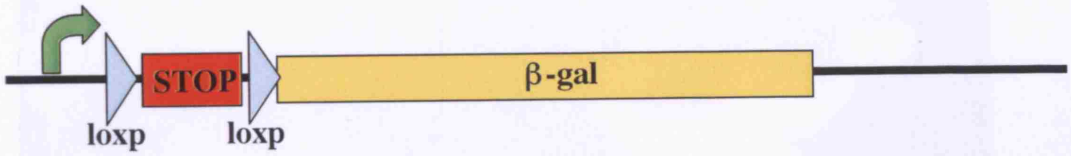

Figure 7.5 Rosa26 mice as a reporter strain for Cre recombinase activty

Rosa26 reporter mice only express β-galactosidase when Cre-mediated excision removes the floxed stop codon 5' to the β-gal coding sequence. The presence of β-gal protein in tissues can be detected by the chromagenic substrate X-gal.

7.7.2 Whole-mount X-gal staining of uteri from CaBP9K-Cre mice

In order to test for Cre expression, uteri were stained with X-gal. All procedures are described in the Methods (Section 2.17.2). In brief, female CaBP9K-Cre mice were housed together for 6 weeks in order that their menstrual cycles were synchronised. Mice were culled following Home Office guidelines, uteri were removed under the supervision of staff from the Experimental Pathology Laboratory and divided into 2 equal sections, one which was fixed and stained in X-gal solution. We analysed uteri from 6 female mice from each founder line; 3 CaBP9K-Cre$^{+/-}$ Rosa26$^{+/-}$ and 3 CaBP9K-Cre$^{-/-}$ Rosa26$^{+/-}$. After carrying out a full analysis, we were unable to differentiate between β-gal expression in the CaBP9K-Cre$^{+/-}$ Rosa26$^{+/-}$ and the CaBP9K-Cre$^{-/-}$ Rosa26$^{+/-}$ mice (Figure 7.6).

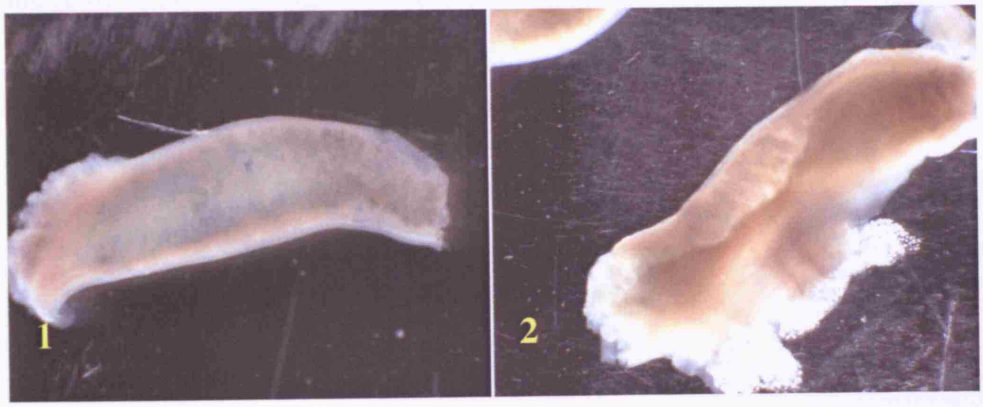

Figure 7.6 X-Gal staining of uteri from CaBP9K-Cre and wild-type mice

Positive staining is shown by the blue colour. No staining was visible after 4 hours. After 6 hours, positive staining appeared in both wild type (1) and CaBP9K-Cre positive (2) mice. This was probably due to endogenous bacteria in the uteri of the mice. This figure is representative of the results from each founder line.

In order to confirm this negative result, we used the other half of the uteri to make tissue sections, which were stained using both X-gal and a β-gal

antibody. The sections were further divided into 2, as different fixing techniques were required (Zinc and PFA).

7.7.3 X-gal staining of frozen sections of CaBP9K-Cre and wild type uteri

Preparation of frozen sections and H & E staining were carried out by the Experimental Pathology Laboratory and representative sections containing myometrium were prepared from each founder line and stained with X-gal as described in the methods (2.17.2). Slides were observed every 30 min. After 4 hours, blue staining was apparent on both the CaBP9K-Cre$^{+/-}$ Rosa26$^{+/-}$ and CaBP9K-Cre$^{-/-}$ Rosa26$^{+/-}$slides (Figure 7.7). However, this was localised to vessels in the endometrium; there was no myometrial staining and therefore was attributed to background resulting from residual bacteria. This result was the same in all offspring from each founder line.

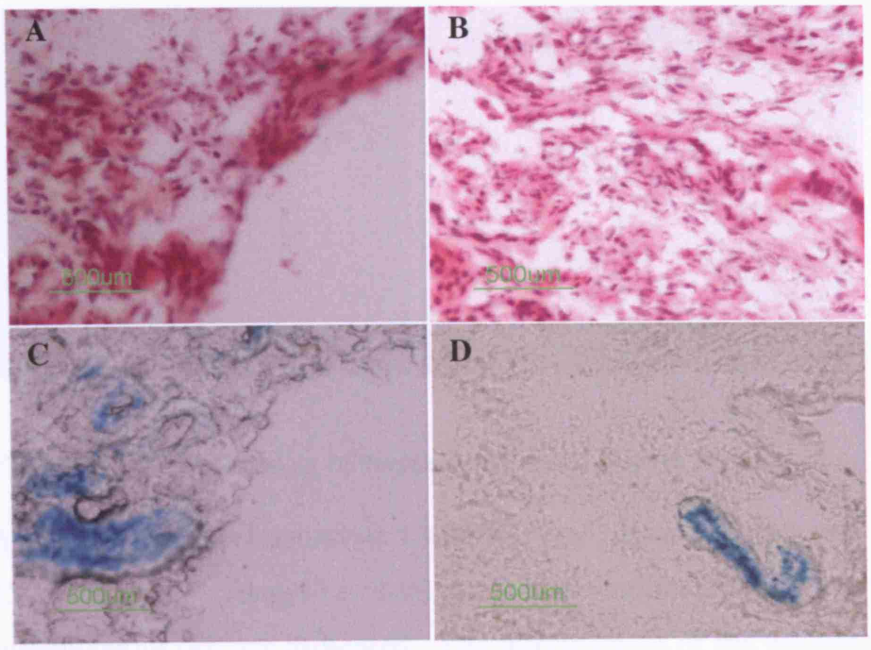

Figure 7.7 X-gal staining of frozen sections of mouse uterus

Sections were stained with H & E (A = CaBP9K-Cre$^{+/-}$ Rosa26$^{+/-}$, B = CaBP9K-Cre$^{-/-}$ Rosa26$^{+/-}$) and X-gal (C = CaBP9K-Cre$^{+/-}$ Rosa26$^{+/-}$, D = CaBP9K-Cre$^{-/-}$ Rosa26$^{+/-}$). Positive staining is evident in both C and D in the endometrial blood vessels.

7.7.4 β-gal immunohistochemistry on paraffin-embedded uterus samples

The tissue histology of the frozen sections was poor so more uteri were removed, fixed in a Zinc based fixative as described above), embedded in paraffin and 5μm sections were cut. and A β-gal antibody used for immunohistochemistry. This was carried out by the Experimental Pathology Laboratory and is described in the methods. As before, positive staining was observed in the endometrial vessels but also in the wild-type uterus (Figure 7.8).

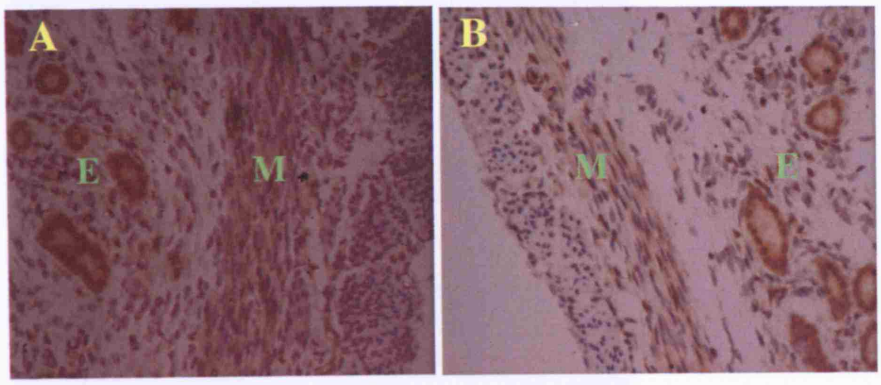

Figure 7.8 β-gal staining of tissue sections of mouse uterus

β-gal IHC was performed on CaBP9K-Cre$^{+/-}$ Rosa26$^{+/-}$ (A) and CaBP9K-Cre$^{-/-}$ Rosa26$^{+/-}$ (negative control). The endometrial layer (E) and myometrium (M) are indicated. The microvessels of the endometrium are positive for β-gal as is evident from the brown staining.

7.8 Sporadic mammary tumour

We observed a mammary tumour in one of the CaBP9K-Cre$^{+/-}$ transgenic mice (Figure 7.9). This was attributed to be a sporadic tumour as was not observed in any of the other progeny. The post-mortem and histopathology analysis were carried out in the Experimental Pathology Laboratory by Professor G.W. Stamp.

Figure 7.9 A sporadic mammary tumour in a female CaBP9K-Cre$^{+/-}$ transgenic mouse

The arrow indicates the tumour.

7.9 Discussion

Despite creating a transgenic mouse line expressing Cre recombinase under the control of regulatory elements of the rat CaBP9K promoter, we failed to drive uterine myometrium-specific expression. The -117 to +331 rat CaBPK9 region has previously been shown to express in the myometrium (Romagnolo, Cluzeaud et al. 1996). Transgenes may not express efficiently when integrated into genomic sites with high chromatin content, but 6 independent founder lines were tested and each failed to express. This particular project could be adapted to try and induce myometrial expression, either by modifying the construct, or by administering additional hormones to the mice such as oestrogen, which increases expression of CaBP9K (Blin, L'Horset et al. 1995; Romagnolo, Cluzeaud et al. 1996).

The use of oestrogen administered directly to the mice may also induce expression of Cre-recombinase and the licence could be suitably amended to administer oestrogen either in drinking water or slow-release subcutaneous implants. Additionally (though not proven to be hormone dependent)

pregnancy may be natural method of increasing endogenous oestrogen and therefore further breeding of the 6 founder lines would be a feasible option. The growth of fibroids in humans has shown to be oestrogen dependent (Maruo, Ohara et al. 2004) and therefore administering oestrogen to *Fh1*$^{+/-}$ mice may be sufficient to initiate fibroid growth.

The mammary tumour described occurred in only one of 84 mice (48 of which were positive for CABP9K-Cre) and therefore appeared to be sporadic and not a direct consequence of the transgene. Additionally, sporadic mammary tumours occur in approximately 1% of C57/BL6 female mice (Hoag 1963).

In summary, a CaBP9K-Cre transgenic mouse was successfully generated but failed to express Cre recombinase in the uterine myometrium. The design of the construct was based on the previously reported work of Romagnolo et al. (Romagnolo, Cluzeaud et al. 1996) who reported myometrium specific expression of CAT using the -117 to +331 region of CaBP9K. There is scope for future work such as modifying the construct by cloning in increasingly large DNA fragments encompassing more upstream regulatory elements of the CaBP9K gene. These constructs could then be cloned into luciferase-expressing vectors such as pGL3 (Promega) and transfected into myometrial derived primary cultures to test for expression. This could also be combined with oestrogen treatment of the cells and from this it may be possible to determine the optimal size upstream fragment to drive expression. Of course, problems can arise as primary cultures often are technically more difficult to transfect and also, even if expression is observed this does not rule out that the more upstream elements will drive expression in other tissues as demonstrated by CAT reporter assays in CaBP9K (-4400 to + 365) transgenic mice (Romagnolo, Cluzeaud et al. 1996).

8 Chapter 8: Discussion and Future Work

The aim of this thesis was to further the current understanding of the genetic and functional consequences of mutations in genes encoding the TCAC enzymes FH and SDH in HLRCC and HPGL respectively. Tumours from individuals from both of these relatively recently discovered family cancer syndromes have been subject to metabolite, gene and protein expression analysis, and additionally, tumours from HPGL patients analysed for somatic chromosomal copy number changes using aCGH. In order to help further our understanding of HLRCC and provide a possible therapeutic model, a conditional *Fh1* knockout mouse of has been constructed, the first murine model of germline *Fh1* inactivation.

The hypothesis that pseudo-hypoxic drive largely contributes to the tumourigenesis in both HLRCC and HPGL seems a very plausible explanation. Indeed, initial comparisons with VHL disease, which has a tumour spectrum overlapping with both HLRCC (RCC) and HPGL (PCC and RCC), suggested a role for HIF1α mediated signalling. The *VHL* tumour-suppressor is a key mediator in the hypoxic response, targeting HIF1α for ubiquitin-mediated degradation under normal oxygen conditions (Kaelin 2003). Indeed, HIF1α has been shown to play a critical role in the oncogenic effects resulting from *VHL* mutations in specific cellular contexts (Kondo, Yao et al. 2002). There is no direct evidence that *FH* and *SDH* mutations dysregulate pVHL directly, but, *in vitro* studies have shown that accumulation of succinate and fumarate by both biochemical and siRNA knockdown of *FH* and *SDH*, stabilise HIF1α by inhibtion of the PHD enzymes (Isaacs, Jung et al. 2005; Selak, Armour et al. 2005). Interestingly, these studies indicate that knockdown of *FH* and perhaps more surprisingly of *SDH*, due to its role in the electron transport chain, does not increase the cellular levels of oxygen free radicals. However, the main flaw of these *in vitro* studies is that they cannot provide evidence that the levels of succinate and fumarate required to stabilise

HIF1α are physiologically obtainable in humans. Additionally, the analogues used (di-methyl derivatives) to increase cellular uptake mean that the actual intracellular levels cannot be accurately determined.

In order to investigate the effect of *FH* and *SDH* mutations on the accumulation of TCAC intermediates *in vivo*, gas chromatography and MRS were used so that a direct comparison could be made between normal tissue, sporadic tumours and familial tumours harbouring a TCAC enzyme mutation. Indeed, analysis showed a marked increase in fumarate and succinate in both HLRCC tumours (in comparison with normal myometrium) and also in primary cultured fibroblasts from FH-deficiency patients with bi-allelic *FH* mutations (compared to control skin fibroblasts). PGLs from HPGL patients also showed increased levels of succinate and a higher succinate:fumarate ration than sporadic counterparts suggesting that TCAC blockage occurs in both HLRCC and HPGL. The HIF1α protein was highly expressed in tumours from both syndromes, but there was also high expression in some non-familial PGLs suggesting that other mechanisms of HIF-dysregulation may play a role in the tumourigenesis of sporadic PGLs. The PGLs analysed were carotid body tumours, and the oxygen-sensing role of this chemoreceptor may well help, in part, to account for this observation. Further larger studies will be necessary to determine if there is a correlation between HIF1α levels and mutation status.

The increase in microvessel density and angiogenic profile of HLRCC fibroids was an interesting observation as previous reports of sporadic fibroids had defined an anti-angiogenic profile (Weston, Trajstman et al. 2003). The microarray analysis identified increased expression of four HIF-target genes in HLRCC fibroids; *VEGF* (3.16-fold), *BNIP3* (3.16-fold), *CA12* (6.08-fold) and *ADM* (2.14-fold). *CA12* and *ADM* are both strongly induced by hypoxia in tumour cell lines and are linked to carcinogenesis (Garayoa, Martinez et al. 2000; Wykoff, Beasley et al. 2000). Our subsequent *in vivo* analysis of HLRCC fibroids is further evidence that pseudo-hypoxia is a pathological and not a physiological phenomena as the latter would have suggested an increase in HIF-expression and angiogenesis in the less vascular sporadic fibroids, resulting from a lower oxygen supply. This hypothesis is further corroborated

by the CD34 staining of HPGL tumours, where there is no spatial association between the microvessels and expression of HIF1α protein and *VEGF* mRNA. The microarray experiment also identified differential expression of genes involved in apoptosis and energy metabolism. *BCL2* and *NOL3* (anti-apoptotic) and, paradoxically, *BNIP3* (pro-apoptotic) were all up-regulated (2.57-fold, 2.85-fold and 3.16-fold respectively). *CASP1* (pro-apoptotic) was down-regulated (0.51-fold). The increased expression of *BNIP3* may well be explained by HIF-mediated transcription, whereas decreased expression of *CASP1* and increase in *BCL2* and *NOL3* expression may be consequence of the tumour cells promoting self-survival. To gain more insight into the differential expression of genes in HLRCC ULs, sporadic ULs and myometrium, microarray data obtained in this experiment was combined with that from a study in Finland and expression profiles of 11 myometrium, 15 sporadic ULs and 7 *FH* mutant ULs determined (Vanharanta, Pollard et al. 2006). The HLRCC fibroids showed significant increase in expression of carbohydrate metabolism-, glycolysis-, iron homeostasis- and oxidoreduction-related genes including some identified in our study: *NQO1* and *PKM2* (Table 3.1). Genes with lower expression in HLRCC fibroids belonged to groups such as extracellular matrix and cell adhesion (including *THSB1*), muscle development and cell contraction. The HIF-target genes *BNIP3* and *CA12* were also over-expressed in HLRCC ULs.

The angiogenic profile of HPGL tumours that the data (Chapter 3) demonstrates is also evident in recent literature. Microarray gene expression profiling and immunohistochemical analysis found that PCCs with *SDHB*, *-C*, *-D* or *VHL* mutations had a profile that distinguished them PCCs arising from germline mutations in *RET* and *NF1* (Dahia 2006). The *VHL* and *SDH*-mutant tumours had an increased angiogenic and reduced oxidoreductase gene expression profile. The oxidoreductase deficiency had never been reported in *VHL*-null tumours and the authors attributed this effect to suppression of SDHB protein, which by using immunohistochemical analysis was shown to be severely diminished in *VHL* and *SDHB*, *-C* and *–D* mutant PCCs. Therefore this *in vivo* evidence suggests a role for HIF1α-mediated signaling, linking hypoxia (via VHL) and oxidoreductase (via SDHB). In contrast, *in vitro* data

suggests a possible role of JunB (a VHL target) and a 2-oxoglutarate-dependent oxygenase (SM-20/EglN3/PHD3) in the tumourigenesis of PCCs. The proposed common pathway for *NF1*, *RET*, *VHL*, and *SDHB*, *-C* and *-D*-associated PCCs is that mutations in all of these genes may cause a reduction in SM-20/EglN3/PHD3-mediated apoptosis of developing neural-crest cells at the time during development when nerve growth factor (NGF) is limiting. Additionally, mutations in *VHL* (including those in VHL-type 2C) are shown to abrogate the efficiency of pVHL-mediated inhibition of JunB (Lee, Nakamura et al. 2005) (Maxwell 2005). The identification of SM-20 as a 2-oxoglutarate-dependent oxygenase, with succinate being an end-product of the reaction, and the clear *in vitro* evidence that this enzyme is required for apoptosis after NGF withdrawel (Lee, Nakamura et al. 2005) provide more evidence of the role of SDH in tumourigenesis of PCC as proposed by Selak and colleagues (Selak, Armour et al. 2005).

Future work will be undertaken, primarily *in vivo* analysis of PCCs, using ISH and IHC to analyse expression of *JunB* and HIFα isoforms, such as HIF2α (EPAS1), and correlation with expression of candidate target genes in order to try and elucidate role of HIF in PCC tumourigenesis. The roles of the HIF1α and HIF2α subunits have been investigated only in VHL-related RCC and derived cell lines (Raval, Lau et al. 2005). This study demonstrated that in VHL-defective RCC cells, the protumourigenic genes encoding CCND1, TGFα, and VEGF respond specifically to HIF2α and that the proapoptotic gene encoding BNIP3 responds positively to HIF1α and negatively to HIF2 α, indicating that HIF1α and HIF2 α have contrasting properties in the biology of RCC. In keeping with this, differential effects were observed on the growth of RCC as tumour xenografts, with HIF1α retarding and HIF2α enhancing tumour growth, thus indicating HIFα isoform-specific transcriptional selectivity (Raval, Lau et al. 2005).

The conflicting data describing mechanisms of tumourigenesis in PCC in individuals with germline mutations in *VHL*, *RET*, *NF1*, *SDH* and *MEN*, (Lee, Nakamura et al. 2005; Maxwell 2005) (Dahia 2006) is probably due to biological differences between *in vitro* i.e. using cell lines and *in vivo* techniques. Analysis of mutant cell lines does not take into consideration the

tumour microenvironment and also any secreted hormones that may be involved in the pathogenesis of PCC. Additionally, the use of siRNA does not guarantee 100% knockdown of the target gene and is often used in cells that are not of the same derivation of the tumour, (for example 293 cells were used in the siRNA knockdown of SDHD (Selak, Armour et al. 2005)). Additionally, transfection reagents have a range of cytotoxic effects (Kiefer, Clement et al. 2004), and some vectors used to generate stably transfected cell lines expressing siRNA can induce an interferon response due to the retroviral elements in the vector (Bridge, Pebernard et al. 2003). The *in vivo* techniques such as ISH and IHC employed in this study allow specific proteins to be assayed for expression and therefore indicate the potential pathways involved in tumourigenesis.

Microarray-based gene expression analysis alone is insufficient to provide significant insights into early events of tumourigenesis as the data provides an overall expression signature of the tumour, many of which could be secondary effects. However, in the cases of PCC tumourigenesis, parallel studies using both gene expression profiling and aCGH on the same tumour samples may provide a more comprehensive platform on which to analyse tumourigenesis and also candidate predisposition genes. To date separate studies of PCCs using aCGH (Cascon, Ruiz-Llorente et al. 2005) and gene expression profiling (Dahia 2006) have provided novel insights into changes in chromosomal copy numbers and expression profiles in PCC but such studies would be more informative if the same tumours were analysed by both techniques.

The germline sequencing and aCGH study we carried out on PGLs and PCCs (Chapter 4) could therefore be used as a base for future work incorporating a greater number of samples and combining the aCGH data with gene expression analysis. This approach has already been implemented in studying a region of chromosome 7q, which is frequently lost in non-HLRCC ULs (Vanharanta, Wortham et al. 2005). With a greater number of samples available, more functional work will be carried out to investigate the genotype: phenotype associations in HLRCC and HPGL. In HPGL the genotype: phenotype associations are clearer than in HLRCC; in the latter there is no convincing evidence of an association, and in particular, no specific

mutation seems to be associated with the development of RCC (Tomlinson, Alam et al. 2002; Alam, Rowan et al. 2003; Toro, Nickerson et al. 2003; Kiuru and Launonen 2004; Alam, Olpin et al. 2005; Chan, Wong et al. 2005; Wei, Toure et al. 2005). *SDHB* mutations pose a higher risk of PCC, malignancy and renal cancer than *SDHD* mutations, whereas *SDHD* mutations are strongly associated with multiple PGLs (Astuti, Hart-Holden et al. 2003; Neumann, Pawlu et al. 2004; Vanharanta, Buchta et al. 2004). However, there are still mutation-specific types and distributions that remain unclear. Missense mutations are relatively more common in *SDHB* and truncating mutations more frequent in *SDHD* suggesting that the SDHB protein is under greater structural constraint than the SDHD protein (Bayley, Devilee et al. 2005). This may be explained by the weaker conservation of SDHD, thus allowing more non-deleterious missense changes and requiring frameshift and truncating mutations to produce a pathogenic effect. *SDHD* mutations are found evenly distributed over the four exons while *SDHB* mutations are concentrated in certain exons (notably exon 2), including the Fe-S clusters and are entirely absent from exon 8 (Bayley, Devilee et al. 2005).

The germline *SDHD* P81L mutation has only been reported in individuals presenting with PGL and there is only one report of this mutation in a PCC, which was somatic change (Gimm, Armanios et al. 2000). P81L is reported to be a founder mutation in the US population (Baysal, Willett-Brozick et al. 2002), but a more likely explanation may be frequent C>T transitions that occur at methylated CpG nucleotides (Perry and Carrell 1989) and the P81L CpG site has previously been shown to be methylated (Badenhop, Cherian et al. 2001). Future studies on specific mutations and how they may affect genotype: phenotype associations in HPGL and HLRCC will be carried out. Despite the technical and biological flaws of using *in vitro* cell-based assays mentioned above, cloning of cDNA with specific mutations such as *SDHD* P81L, and over-expressing the protein in relevant cell types and then comparing the expression profile, proteome and metabolic profile of the mutant cells with wild-type controls may provide evidence of the primary events resulting from the mutation. This approach may be prove to be more informative than simply using siRNA approach, especially in the case of

HLRCC where missense mutations are thought to reduce fumarase activity through a dominant negative effect i.e. only 1/16 functional homo-tetramers will be formed if an individual has a heterozygous germline missense change (Alam, Rowan et al. 2003). Therefore we propose to clone dominant negative mutants of *FH* (e.g. R58X, R58P) and express in both smooth muscle- and renal-derived cell lines for analysis as described above.

The aim of this thesis was to identify tumourigenic mechanisms in HPGL and HLRCC, but the overall aim in the field of cancer research is to take the data obtained from the 'bench' to the 'bedside' so that affected individuals can receive specific therapy to combat cancer. If cancer is diagnosed at an early stage then the prognosis is generally better. Therefore, genetic screening of individuals that may harbour mutations in cancer predisposition genes, such as *SDH*, as described in Chapter 4, may enable earlier detection of disease. However, for patients to receive treatment for cancer, it is first necessary to test new anti-cancer drugs or therapies using clinical trials. Phase II trials examine preclinical cancer models including *in vitro* cell lines, the murine allograft and human / murine xenografts. Xenograft mouse models are widely used as exemplified above where a *VHL*-mutant RCC was grafted into nude mice (Raval, Lau et al. 2005). However, even though some new anti-cancer drugs show highly effective anti-cancer treatment using transplantable tumours in mice, pre-clinical results are often followed by the failure of the drug in clinical trials (Kerbel 2003). This is partly due to the many variables in xenograft experiments which impact on outcome such as the site of implantation, growth properties of the xenograft and size when treatment is initiated, agent formulation, route of administration and dose, and the selected endpoint for assessing activity. There are also instances where the model is inappropriate as a likely predictor of clinical outcome e.g. inhibitors of the metastatic process and anti-angiogenic strategies as the vasculature is of murine origin (Kelland 2004). Due to the scepticism about the use of xenograft models for early stage *in vivo* preclinical testing, a shift has occurred towards developing and using spontaneous mouse tumours arising in transgenic and / or knockout mice. These mice are engineered to recapitulate various genetics alterations thought to be causative of specific

types of respective human cancers. Therefore, we decided to conditionally target *Fh1* (the mouse homologue of *FH*) in the mouse germline using Cre-lox technology (Chapter 5), aiming to create a mouse model of HLRCC and provide a model for analysis of tumourigenesis and for future testing of potential drugs or therapies.

The $Fh1^{-/-}$ mice were embryonic lethal as were the previously reported $Sdhd^{-/-}$ mice (Piruat, Pintado et al. 2004). This is unsurprising as the TCAC enzymes encoded by both of these genes are vital for ATP production via mitochondrial respiration and humans with bi-allelic FH mutations generally survive for a short time, if at all. The advantage of the *Fh1* knockout is that it can be conditionally induced in a tissue-specific manner and therefore crosses were made with transgenic mice expressing Cre recombinase in smooth muscle and renal cells (Chapter 6). The $Fh1^{+/-}$ mice have not yet developed tumours at 8 months of age, but many mouse models such as $Men1^{+-/}$ do not develop tumours until between 9-13 months of age (Bertolino, Tong et al. 2003; Crabtree, Scacheri et al. 2003). Future work with the $Fh1^{+/-}$ mice will involve crossing onto different gentic backgrounds as this evidently can affect both the penetrance and phenotype as shown by the *Men2* and *Tsc2* knockouts (Michiels, Chappuis et al. 1997; Cranston and Ponder 2003) (Onda, Lueck et al. 1999) and the Eker rat model of RCC (Kikuchi, Sudo et al. 2004). It would be very interesting if $Fh1^{+/-}$ mice on a specific genetic background developed renal tumours, as this would suggest the presence of a modifier gene and would warrant further investigation; indeed it is possible that RCC pathogenesis in HLRCC patients involves a modifier gene and this may explain why a genotype: phenotype association has not been demonstrated.

The smooth muscle hypertrophy in the upper GI tract of the $Fh1^{fl/fl}$ Sm-$Cre^{+/-}$ mice is the first functional *in vivo* evidence of complete abrogation of Fh1 in smooth muscle. Despite the Sm-Cre mice expressing Cre recombinase in both vascular and non-vascular smooth muscle, whole-mount staining of the embryos (E18.5) with β-gal clearly shows highest expression in the duodenum and jejunum (Madsen, Regan et al. 1998). There is a lot of scope for future work on these mice in order to determine the mechanisms and pathways involved. A comprehensive IHC / ISH analysis of HIF1α and HIF-

target genes would be a logical starting point, as would metabolomic profiling of the hypertrophic muscle. Electron microscopy would enable high-powered imaging and comparison of mitochondrial morphology and muscle contraction bands in the smooth muscle of the wild-type and knockout mice. Physiological studies using agonists such as capsaicin (a sensory nerve stimulant) to test the ability of the muscle to relax will be employed in order to determine how dysfunctional the muscle is in the knockout mice.

Even though the HIF pathway evidently contributes to the tumourigenesis of HLRCC, it cannot be ruled out that other pathways may be involved. The Eker rat with a germline *Tsc2* mutation develops both ULs and RCCs (Yeung, Xiao et al. 1994; Kobayashi, Hirayama et al. 1995) although, in contrast to humans, *Tsc2* is the primary target for RCC in rodents, as demonstated by the increase RCC but not mesenchymal tumours by adminstistration of a carcinogen targeting both renal epithelia and mesenchymal cells in Eker rats (Walker, Goldsworthy et al. 1992; Hino, Klein-Szanto et al. 1993; Yeung, Xiao et al. 1994; Kobayashi, Hirayama et al. 1995). In humans, TSC2 regulates *VEGF* through mTOR-dependent and -independent pathways and TSC2 loss results in the accumulation of HIF1α and increased expression of HIF-responsive genes including *VEGF* (Brugarolas, Vazquez et al. 2003). AKT, an upstream inhibitor of TSC2 regulates multiple steps in glycolysis via post-transcriptional mechanisms that include localization of the glucose transporter, GLUT1, to the cell surface and maintenance of hexokinase function in the absence of extrinsic factors (Rathmell, Fox et al. 2003). AKT can also induce VEGF expression via a HIF-independent pathway (Pore, Liu et al. 2004). Therefore, bearing in mind that glucose metabolism and glycolysis prevail in the absence of TCAC function, we will investigate the expression patterns of genes and proteins of this pathway in the intestinal smooth muscle of the knockout mice by using IHC / ISH and possibly microarray-based expression and protein expression analysis.

Parallels between the AKT / TSC2 pathway and tumourigenesis can be drawn with HLRCC. Malignancy is very uncommon in the smooth muscle leiomyomas, whereas the renal cancers tend to be solitary and aggressive

(Kiuru, Lehtonen et al. 2002; Pore, Liu et al. 2004). Amongst other explanations, this could be due to higher endogenous levels of HIF1α in the kidney, due to its role in oxygen sensing and EPO production (Le Hir, Eckardt et al. 1991), therefore the HIF-dysregulation resulting from *FH* mutations may be sufficient to reach a threshold of HIF1α to initiate tumourigenesis. This threshold may not be reached in smooth muscle cells with *FH* mutations and therefore the vascularity and angiogenic profile in leiomyomas could be a result of *VEGF* induction, but in a HIF-independent manner, possibly linked to the AKT / TSC2 / MTOR pathway and increased glucose metabolism due to the high energy levels required for muscle contraction. This pathway and its molecular link with several inherited human diseases, including VHL disease is summarised below (Figure 8.1).

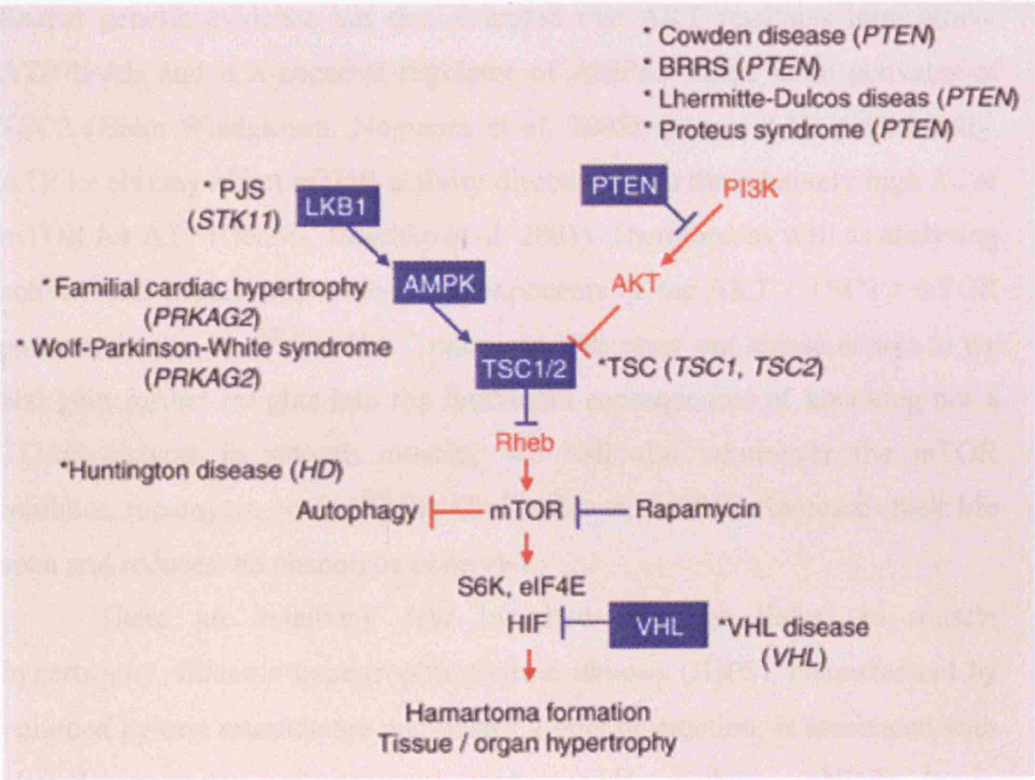

Figure 8.1 The molecular link between several inherited human diseases. Reproduced from (Inoki, Corradetti et al. 2005). Red colouring indicates a molecule or regulation event that is positively involved in mTOR signalling; blue colouring indicates molecules or regulation events that are negatively involved in mTOR signalling. These targets of mTOR include direct and indirect substrates of mTOR; other signalling

pathways also regulate many targets of mTOR.

Initially, due to the expected energy deficiency in the *Fh1*$^{fl/fl}$ Sm-Cre$^{+/-}$ mice, studies will be carried out to confirm the AMP:ATP ratios in the smooth muscle of the jejunum and to test for AMP-activated protein kinase (AMPK) activation. AMPK serves as an energy-sensing protein kinase that is activated by a variety of metabolic stresses that lower cellular energy levels (Hardie and Carling 1997), and when activated, AMPK modulates a network of metabolic pathways that result in net increased substrate oxidation, generation of reduced nucleotide cofactors, and production of ATP. AMPK is activated by a high AMP:ATP ratio and phosphorylation on threonine 172 by an upstream kinase (Hawley, Davison et al. 1996). There is conflicting evidence of the exact roles of AKT, mTOR, TSC2 and AMPK in regulation of cellular ATP levels. Recent genetic evidence has demonstrated that AKT regulates intracellular ATP levels and is a negative regulator of AMPK, which is an activator of TSC2 (Hahn-Windgassen, Nogueira et al. 2005) (Figure 8.1). Additionally, ATP levels may affect mTOR activity directly due to the relatively high K_m of mTOR for ATP (Dennis, Jaeschke et al. 2001). Therefore, as well as analysing activity and protein expression of components of the AKT / TSC2 / mTOR pathway in the *Fh1*$^{fl/fl}$ Sm-Cre$^{+/-}$ mice, we will carry out kinase assays to try and gain further insights into the functional consequences of knocking out a TCAC enzyme in smooth muscle. We will also administer the mTOR inhibitor, rapamycin, to *Fh1*$^{fl/fl}$ Sm-Cre$^{+/-}$ mice to see if this increases their life span and reduces the phenotype observed.

There are relatively few inherited disorders linked to muscle hypertrophy. Infantile hypertrophic pyloric stenosis (IHPS), characterized by enlarged pyloric musculature and gastric-outlet obstruction, is associated with altered expression of neuronal nitric oxide synthase (nNOS) (Saur, Vanderwinden et al. 2004). Hypertrophic cardiomyopathy (HCM) is a relatively common genetic disease, generally with a benign, (though variable) prognosis and more than two hundred different mutations have been described in HCM, in 12 different genes, mostly encoding sarcomere proteins (Brito and Madeira 2005). Mutations in the γ2 subunit of AMPK cause HCM (Figure 8.1)

and this provides evidence for the central role of energy compromise in disease pathogenesis (Blair, Redwood et al. 2001), and *in vitro* studies indicate that inhibition of protein synthesis by pharmacological activation of AMPK may be a key regulatory mechanism by which hypertrophic growth can be controlled (Chan, Soltys et al. 2004). AMPK is a heterotrimeric complex consisting of a catalytic (α) subunit and two regulatory subunits (β and γ) (Hardie and Carling 1997) and as deleterious alleles have not been identified in other AMPK subunit isoforms (Oliveira, Ehtisham et al. 2003), the mutations affecting γ2 subunit are likely to confer a specific alteration of AMPK function of particular importance in the myocardium. This is evident in transgenic mice expressing the R302Q mutation that exhibit a HCM phenotype and loss of cardiac AMPK activity (Sidhu, Rajawat et al. 2005).

Further *in vitro* and *in vivo* work will be undertaken with the *Fh1* conditional knockout mouse in order to investigate the functional consequences of loss of Fh1 and also to investigate possible genetic interactions with other genes / pathways. These are summarised below:

- Generation of $Fh1^{-/-}$ ES and smooth muscle cell lines.

The generation of ES lines will provide an excellent *in vitro* tool for studying downstream effects of knocking out *Fh1*. The advantage over siRNA would be that there would be 100% knockout, readily available heterozygote and wildtype controls and no toxic effects of reagents. Cell lines will be made by inter-crossing either $Fh1^{+/-}$ mice or $Fh1^{fl/fl}$ x $Fh1^{+/-}$ mice. FACS analysis will be used to measure ROS, apoptosis and ψM, and microarrray-based gene expression analysis used to determine differential expression of mRNA profiles between $Fh1^{+/-}$ and $Fh1^{+/+}$ cells. $Fh1^{fl/-}$ ES cells will be transfected with the Cre recombinase expressing plasmid pMC1-Cre and specific proteins / genes identified from above assayed for expression. This combined with the FACS and metabolite analysis, and using a series of time courses post-transfection may indicate the primary events that occur after inactivation of the Fh1 enzyme. The above analyses will also be used in primary cultures derived from the intestinal smooth muscle cells from $Fh1^{fl/fl}$

Sm-Cre$^{+/-}$ mice. This may indicate tissue-specific effects of the knockout and FACS analysis will be used to enable specific isolation of the smooth muscle cells expressing Cre recombinase as the Sm-cre construct contains an IRES-eGFP cassette.

A further investigation of the tumourigenic potential of *Fh1*$^{-/-}$ ES cells will be undertaken, by injecting *Fh1*$^{-/-}$ ES cells into nude mice (in parallel with *Fh1*$^{+/+}$ ES cells controls). The resulting teratomas will be analysed for histology, metabolic and angiogenic markers.

- Investigating genetic interactions of *Fh1* with other mutant mice.

Germline *FH* mutations increase the risk of cancer and bi-allelic inactivation of FH has recently been reported in breast and bladder cancer (Lehtonen, Kiuru et al. 2005). Somatic *FH* mutations have not been extensively screened for in cancers other than in HLRCC. We therefore plan to cross the *Fh1*$^{+/-}$ mice with characterised knockout mice in order to see if there is any acceleration of tumourigenesis, thus indicating genetic and / or functional interaction. *Fh1*$^{+/-}$ mice will be crossed with Apc$^{+/min}$ mice (Su, Kinzler et al. 1992), *K-Ras* mice that acquire a somatic activating mutation at codon 12 (Johnson, Mercer et al. 2001), and *Lkb1*$^{+/-}$ mice (Miyoshi, Nakau et al. 2002). The latter of these crosses should prove to be very interesting due to the role of LKB1 in the AKT / TSC2 / MTOR pathway and functioning in tumour development (Mak and Yeung 2004). Also, this will help to further investigate if forced glycolysis promotes tumourigenesis.

- Inducible knockout of *Fh1*.

The main drawback of creating tissue specific knockouts is that the transgene expression often occurs during embryogenesis, and even though embryonic lethality can be by-passed, it may be that knocking out a vital 'housekeeping' gene such as *Fh1* in a specific organ may impair cause impaired function and development, most probably due to energy deficiency, which could eventually lead to the death of the mice before tumours will form. Therefore, there are two approaches that we plan to implement in order to

overcome this potential problem. Firstly, we plan to use inducible Cre-strains that have Cre recombinase fused to two mutant estrogen-receptor ligand-binding domains (MerCreMer), thus requiring induction via administration of tamoxifen. This has been demonstrated by temporally regulated and tissue-specific gene manipulations in the adult and embryonic heart (Sohal, Nghiem et al. 2001). The unsuccessful attempt at creating a transgenic mouse expressing Cre recombinase in the myometrium (Chapter 7) will be revisited. Initially, increasingly larger DNA fragments containing the CaBP9K enhancer elements will be cloned into luciferase vectors and transfected into myometrial cell lines treated with oestrogen in order to establish the optimum region of DNA to create a transgene. This will then be cloned into a vector expressing MerCreMer and transgenic mice generated that when backcrossed with $Fh1^{fl/fl}$ mice will enable temporal and myometrium-specific knockout of *Fh1* in adult female mice.

The second or possibly alternative method that we plan to employ is *in vivo* adenovirus-mediated Cre recombinase transduction into the myometrium and kidney (renal tubules and collecting ducts) of $Fh1^{fl/fl}$ mice. This method has been successfully employed in many tissues / organs such as endometrial glands and prostate (Beauparlant, Read et al. 2004; Leow, Wang et al. 2005). This technology can potentially complement the limitations such as the availability of cell-type specific or temporally-regulated promoters, and the complication of genetic background differences.

In summary, this thesis has provided the first *in vivo* evidence that HIF-1α, HIF-target genes and angiogenesis play key roles in the tumourigenesis of HLRCC and that tumours from both HLRCC and HPGL patients accumulate the TCAC intermediates succinate and fumarate. The mutation screening of patients with apparently sporadic or familial PGL / PCC for mutations in *SDH,* and the identification of mutations in *SDHB* and *–D*, further enforces the need for genetic counselling and screening of affected individuals. This also is the first report of a germline conditional *Fh1* knockout and by employing the techniques discussed above, I aim to use this mouse to create a model of HLRCC, which can in future be used for the testing of therapeutic agents that can improve treatment of individuals with HLRCC.

9 Chapter 9: References

Abu-Amero, K. K., A. S. Alzahrani, et al. (2005). "High frequency of somatic mitochondrial DNA mutations in human thyroid carcinomas and complex I respiratory defect in thyroid cancer cell lines." Oncogene **24**(8): 1455-60.

Alam, N. A., E. Barclay, et al. (2005). "Clinical features of multiple cutaneous and uterine leiomyomatosis: an underdiagnosed tumour syndrome." Arch Dermatol **141**(2): 199-206.

Alam, N. A., S. Bevan, et al. (2001). "Localization of a gene (MCUL1) for multiple cutaneous leiomyomata and uterine fibroids to chromosome 1q42.3-q43." Am J Hum Genet **68**(5): 1264-9.

Alam, N. A., S. Olpin, et al. (2005). "Missense mutations in fumarate hydratase in multiple cutaneous and uterine leiomyomatosis and renal cell cancer." J Mol Diagn **7**(4): 437-43.

Alam, N. A., A. J. Rowan, et al. (2003). "Genetic and functional analyses of FH mutations in multiple cutaneous and uterine leiomyomatosis, hereditary leiomyomatosis and renal cancer, and fumarate hydratase deficiency." Hum Mol Genet **12**(11): 1241-52.

Albayrak, T., V. Scherhammer, et al. (2003). "The tumour suppressor cybL, a component of the respiratory chain, mediates apoptosis induction." Mol Biol Cell **14**(8): 3082-96.

Amar, L., J. Bertherat, et al. (2005). "Genetic testing in pheochromocytoma or functional paraganglioma." J Clin Oncol **23**(34): 8812-8.

Astuti, D., N. Hart-Holden, et al. (2003). "Genetic analysis of mitochondrial complex II subunits SDHD, SDHB and SDHC in paraganglioma and phaeochromocytoma susceptibility." Clin Endocrinol (Oxf) **59**(6): 728-33.

Astuti, D., F. Latif, et al. (2001). "Gene mutations in the succinate dehydrogenase subunit SDHB cause susceptibility to familial pheochromocytoma and to familial paraganglioma." Am J Hum Genet **69**(1): 49-54.

Badenhop, R. F., S. Cherian, et al. (2001). "Novel mutations in the SDHD gene in pedigrees with familial carotid body paraganglioma and sensorineural hearing loss." Genes Chromosomes Cancer **31**(3): 255-63.

Barker, K. T., S. Bevan, et al. (2002). "Low frequency of somatic mutations in the FH/multiple cutaneous leiomyomatosis gene in sporadic leiomyosarcomas and uterine leiomyomas." Br J Cancer **87**(4): 446-8.

Bayley, J. P., P. Devilee, et al. (2005). "The SDH mutation database: an online resource for succinate dehydrogenase sequence variants involved in pheochromocytoma, paraganglioma and mitochondrial complex II deficiency." BMC Med Genet **6**: 39.

Baysal, B. E. (2002). "Hereditary paraganglioma targets diverse paraganglia." J Med Genet **39**(9): 617-22.

Baysal, B. E. (2004). "Genomic imprinting and environment in hereditary paraganglioma." Am J Med Genet C Semin Med Genet **129**(1): 85-90.

Baysal, B. E., J. E. Farr, et al. (1997). "Fine mapping of an imprinted gene for familial nonchromaffin paragangliomas, on chromosome 11q23." Am J Hum Genet **60**(1): 121-32.

Baysal, B. E., R. E. Ferrell, et al. (2000). "Mutations in SDHD, a mitochondrial complex II gene, in hereditary paraganglioma." Science **287**(5454): 848-51.

Baysal, B. E., J. E. Willett-Brozick, et al. (2002). "Prevalence of SDHB, SDHC, and SDHD germline mutations in clinic patients with head and neck paragangliomas." J Med Genet **39**(3): 178-83.

Beauparlant, S. L., P. W. Read, et al. (2004). "In vivo adenovirus-mediated gene transduction into mouse endometrial glands: a novel tool to model endometrial cancer in the mouse." Gynecol Oncol **94**(3): 713-8.

Beck, I., S. Ramirez, et al. (1991). "Enhancer element at the 3'-flanking region controls transcriptional response to hypoxia in the human erythropoietin gene." J Biol Chem **266**(24): 15563-6.

Beeckmans, S. and E. Van Driessche (1998). "Pig heart fumarase contains two distinct substrate-binding sites differing in affinity." J Biol Chem **273**(48): 31661-9.

Bender, B. U., M. Gutsche, et al. (2000). "Differential genetic alterations in von Hippel-Lindau syndrome-associated and sporadic pheochromocytomas." J Clin Endocrinol Metab **85**(12): 4568-74.

Benn, D. E., M. S. Croxson, et al. (2003). "Novel succinate dehydrogenase subunit B (SDHB) mutations in familial phaeochromocytomas and paragangliomas, but an absence of somatic SDHB mutations in sporadic phaeochromocytomas." Oncogene **22**(9): 1358-64.

Benn, D. E., A. P. Gimenez-Roqueplo, et al. (2005). "Clinical presentation and penetrance of Pheochromocytoma/ Paraganglioma syndromes." J Clin Endocrinol Metab.

Bertolino, P., W. M. Tong, et al. (2003). "Heterozygous Men1 mutant mice develop a range of endocrine tumours mimicking multiple endocrine neoplasia type 1." Mol Endocrinol **17**(9): 1880-92.

Biondi, C. A., M. G. Gartside, et al. (2004). "Conditional inactivation of the MEN1 gene leads to pancreatic and pituitary tumourigenesis but does not affect normal development of these tissues." Mol Cell Biol **24**(8): 3125-31.

Birt, A. R., G. R. Hogg, et al. (1977). "Hereditary multiple fibrofolliculomas with trichodiscomas and acrochordons." Arch Dermatol **113**(12): 1674-7.

Blair, E., C. Redwood, et al. (2001). "Mutations in the gamma(2) subunit of AMP-activated protein kinase cause familial hypertrophic cardiomyopathy: evidence for the central role of energy compromise in disease pathogenesis." Hum Mol Genet **10**(11): 1215-20.

Blin, C., F. L'Horset, et al. (1995). "Contrasting effects of tamoxifen and ICI 182 780 on estrogen-induced calbindin-D 9k gene expression in the uterus and in primary culture of myometrial cells." J Steroid Biochem Mol Biol **55**(1): 1-7.

Bourgeron, T., D. Chretien, et al. (1994). "Mutation of the fumarase gene in two siblings with progressive encephalopathy and fumarase deficiency." J Clin Invest **93**(6): 2514-8.

Bourgeron, T., P. Rustin, et al. (1995). "Mutation of a nuclear succinate dehydrogenase gene results in mitochondrial respiratory chain deficiency." Nat Genet **11**(2): 144-9.

Brauch, H., T. Kishida, et al. (1995). "Von Hippel-Lindau (VHL) disease with pheochromocytoma in the Black Forest region of Germany: evidence for a founder effect." Hum Genet **95**(5): 551-6.

Brazma, A., P. Hingamp, et al. (2001). "Minimum information about a microarray experiment (MIAME)-toward standards for microarray data." Nat Genet 29(4): 365-71

Brecht, S., M. Gelderblom, et al. (2001). "Caspase-3 activation and DNA fragmentation in primary hippocampal neurons following glutamate excitotoxicity." Brain Res Mol Brain Res **94**(1-2): 25-34.

Bridge, A. J., S. Pebernard, et al. (2003). "Induction of an interferon response by RNAi vectors in mammalian cells." Nat Genet **34**(3): 263-4.

Briere, J. J., D. Chretien, et al. (2004). "Respiratory chain defects: what do we know for sure about their consequences in vivo?" Biochim Biophys Acta **1659**(2-3): 172-7.

Brito, D. and H. Madeira (2005). "Malignant mutations in hypertrophic cardiomyopathy: fact or fancy?" Rev Port Cardiol **24**(9): 1137-46.

Brugarolas, J. B., F. Vazquez, et al. (2003). "TSC2 regulates VEGF through mTOR-dependent and -independent pathways." Cancer Cell **4**(2): 147-58.

Caldwell, C. R., Jr., J. B. Calkins, Jr., et al. (1996). "Hypertrophic obstructive cardiomyopathy (HOCM)." J Ark Med Soc **92**(12): 629-32.

Carew, J. S. and P. Huang (2002). "Mitochondrial defects in cancer." Mol Cancer **1**: 9.

Cascon, A., S. Ruiz-Llorente, et al. (2002). "Identification of novel SDHD mutations in patients with phaeochromocytoma and/or paraganglioma." Eur J Hum Genet **10**(8): 457-61.

Cascon, A., S. Ruiz-Llorente, et al. (2005). "A novel candidate region linked to development of both pheochromocytoma and head/neck paraganglioma." Genes Chromosomes Cancer **42**(3): 260-8.

Castro, A. F., J. F. Rebhun, et al. (2003). "Rheb binds tuberous sclerosis complex 2 (TSC2) and promotes S6 kinase activation in a rapamycin- and farnesylation-dependent manner." J Biol Chem **278**(35): 32493-6.

Chalmers, R. A. (1982). Organic Acids in Man. London, Chapman and Hall.

Chan, A. Y., C. L. Soltys, et al. (2004). "Activation of AMP-activated protein kinase inhibits protein synthesis associated with hypertrophy in the cardiac myocyte." J Biol Chem **279**(31): 32771-9.

Chan, I., T. Wong, et al. (2005). "Familial multiple cutaneous and uterine leiomyomas associated with papillary renal cell cancer." Clin Exp Dermatol **30**(1): 75-8.

Chang, W. K., K. D. Yang, et al. (2002). "Glutamine protects activated human T cells from apoptosis by up-regulating glutathione and Bcl-2 levels." Clin Immunol **104**(2): 151-60.

Chen, F., T. Kishida, et al. (1995). "Suppression of growth of renal carcinoma cells by the von Hippel-Lindau tumour suppressor gene." Cancer Res **55**(21): 4804-7.

Christakos, S., C. Gabrielides, et al. (1989). "Vitamin D-dependent calcium binding proteins: chemistry, distribution, functional considerations, and molecular biology." Endocr Rev **10**(1): 3-26.

Clifford, S. C., M. E. Cockman, et al. (2001). "Contrasting effects on HIF-1alpha regulation by disease-causing pVHL mutations correlate with patterns of tumourigenesis in von Hippel-Lindau disease." Hum Mol Genet **10**(10): 1029-38.

Cockman, M. E., N. Masson, et al. (2000). "Hypoxia inducible factor-alpha binding and ubiquitylation by the von Hippel-Lindau tumour suppressor protein." J Biol Chem **275**(33): 25733-41.

Coller, H. A., K. Khrapko, et al. (2001). "High frequency of homoplasmic mitochondrial DNA mutations in human tumours can be explained without selection." Nat Genet **28**(2): 147-50.

Coughlin, E. M. C., R. A.; Slaugenhaupt, S. A.; Gusella, J. F.; Shih, V. E.; Ramesh, V (1993). "Identification of a molecular defect in a fumarase deficient patient and mapping of the fumarase gene." Am. J. Hum. Genet. **53 (suppl.)**: A896.

Covello, K. L. and M. C. Simon (2004). "HIFs, hypoxia, and vascular development." Curr Top Dev Biol **62**: 37-54.

Crabtree, J. S., P. C. Scacheri, et al. (2003). "Of mice and MEN1: Insulinomas in a conditional mouse knockout." Mol Cell Biol **23**(17): 6075-85.

Cranston, A. N. and B. A. Ponder (2003). "Modulation of medullary thyroid carcinoma penetrance suggests the presence of modifier genes in a RET transgenic mouse model." Cancer Res **63**(16): 4777-80.

Dahia, P. L. (2006). "Evolving concepts in pheochromocytoma and paraganglioma." Curr Opin Oncol **18**(1): 1-8.

Dahia, P. L., K. N. Ross, et al. (2005). "A HIF1alpha regulatory loop links hypoxia and mitochondrial signals in pheochromocytomas." PLoS Genet **1**(1): 72-80.

Dahl, H. H. (1998). "Getting to the nucleus of mitochondrial disorders: identification of respiratory chain-enzyme genes causing Leigh syndrome." Am J Hum Genet **63**(6): 1594-7.

Dalgard, C. L., H. Lu, et al. (2004). "Endogenous 2-oxoacids differentially regulate expression of oxygen sensors." Biochem J **380**(Pt 2): 419-24.

Dammann, R., U. Schagdarsurengin, et al. (2005). "Frequent promoter methylation of tumour-related genes in sporadic and men2-associated pheochromocytomas." Exp Clin Endocrinol Diabetes **113**(1): 1-7.

Dan, H. C., M. Sun, et al. (2002). "Phosphatidylinositol 3-kinase/Akt pathway regulates tuberous sclerosis tumour suppressor complex by phosphorylation of tuberin." J Biol Chem **277**(38): 35364-70.

Darley-Usmar, V. M., Rickwood, D. and Wilson, M.T. (1987). Mitochondria: a practical approach, IRL Press, London.

Davidowitz, E. J., A. R. Schoenfeld, et al. (2001). "VHL induces renal cell differentiation and growth arrest through integration of cell-cell and cell-extracellular matrix signaling." Mol Cell Biol **21**(3): 865-74.

Deluca, S. A. (1993). "Hypertrophic pyloric stenosis." Am Fam Physician **47**(8): 1771-3.

Demeter, J., F. Porzsolt, et al. (1997). "Polymorphism of the tumour necrosis factor-alpha and lymphotoxin-alpha genes in chronic lymphocytic leukaemia." Br J Haematol **97**(1): 107-12.

Dennis, P. B., A. Jaeschke, et al. (2001). "Mammalian TOR: a homeostatic ATP sensor." Science **294**(5544): 1102-5.

Douglas, E. J., H. Fiegler, et al. (2004). "Array comparative genomic hybridization analysis of colorectal cancer cell lines and primary carcinomas." Cancer Res **64**(14): 4817-25.

Douwes Dekker, P. B., W. E. Corver, et al. (2004). "Multiparameter DNA flow-sorting demonstrates diploidy and SDHD wild-type gene retention in the sustentacular cell compartment of head and neck paragangliomas: chief cells are the only neoplastic component." J Pathol **202**(4): 456-62.

Douwes Dekker, P. B., P. C. Hogendoorn, et al. (2003). "SDHD mutations in head and neck paragangliomas result in destabilization of complex II in the mitochondrial respiratory chain with loss of enzymatic activity and abnormal mitochondrial morphology." J Pathol **201**(3): 480-6.

Downward, J. (2003). "Cell biology: metabolism meets death." Nature **424**(6951): 896-7.

Drakoulis, N., I. Cascorbi, et al. (1994). "Polymorphisms in the human CYP1A1 gene as susceptibility factors for lung cancer: exon-7 mutation (4889 A to G), and a T to C mutation in the 3'-flanking region." Clin Investig **72**(3): 240-8.

Eng, C., M. Kiuru, et al. (2003). "A role for mitochondrial enzymes in inherited neoplasia and beyond." Nat Rev Cancer **3**(3): 193-202.

Eng, C. P., R (2002). The Genetic Basis of Human Cancer. New York, McGraw Hill.

Everitt, J. I., T. L. Goldsworthy, et al. (1992). "Hereditary renal cell carcinoma in the Eker rat: a rodent familial cancer syndrome." J Urol **148**(6): 1932-6.

Fiegler, H., P. Carr, et al. (2003). "DNA microarrays for comparative genomic hybridization based on DOP-PCR amplification of BAC and PAC clones." Genes Chromosomes Cancer **36**(4): 361-74.

Fliss, M. S., H. Usadel, et al. (2000). "Facile detection of mitochondrial DNA mutations in tumours and bodily fluids." Science **287**(5460): 2017-9.

Forsythe, J. A., B. H. Jiang, et al. (1996). "Activation of vascular endothelial growth factor gene transcription by hypoxia-inducible factor 1." Mol Cell Biol 16(9): 4604-13.

Foster, K., P. A. Crossey, et al. (1994). "Molecular genetic investigation of sporadic renal cell carcinoma: analysis of allele loss on chromosomes 3p, 5q, 11p, 17 and 22." Br J Cancer **69**(2): 230-4.

Friend, S. H., R. Bernards, et al. (1986). "A human DNA segment with properties of the gene that predisposes to retinoblastoma and osteosarcoma." Nature **323**(6089): 643-6.

Gamez, J., A. Playan, et al. (1998). "Familial multiple symmetric lipomatosis associated with the A8344G mutation of mitochondrial DNA." Neurology **51**(1): 258-60.

Garami, A., F. J. Zwartkruis, et al. (2003). "Insulin activation of Rheb, a mediator of mTOR/S6K/4E-BP signaling, is inhibited by TSC1 and 2." Mol Cell **11**(6): 1457-66.

Garayoa, M., A. Martinez, et al. (2000). "Hypoxia-inducible factor-1 (HIF-1) up-regulates adrenomedullin expression in human tumour cell lines during oxygen deprivation: a possible promotion mechanism of carcinogenesis." Mol Endocrinol **14**(6): 848-62.

Garcia-Torres, R., D. Cruz, et al. (2000). "Alport syndrome and diffuse leiomyomatosis. Clinical aspects, pathology, molecular biology and extracellular matrix studies. A synthesis." Nephrologie **21**(1): 9-12.

Garcia-Torres, R. and L. Orozco (1993). "Alport-leiomyomatosis syndrome: an update." Am J Kidney Dis **22**(5): 641-8.

Gatenby, R. A. and R. J. Gillies (2004). "Why do cancers have high aerobic glycolysis?" Nat Rev Cancer **4**(11): 891-9.

Gellera, C., G. Uziel, et al. (1990). "Fumarase deficiency is an autosomal recessive encephalopathy affecting both the mitochondrial and the cytosolic enzymes." Neurology **40**(3 Pt 1): 495-9.

Gerald, D., E. Berra, et al. (2004). "JunD reduces tumour angiogenesis by protecting cells from oxidative stress." Cell **118**(6): 781-94.

Gimenez-Roqueplo, A. P., J. Favier, et al. (2001). "The R22X mutation of the SDHD gene in hereditary paraganglioma abolishes the enzymatic activity of complex II in the mitochondrial respiratory chain and activates the hypoxia pathway." Am J Hum Genet **69**(6): 1186-97.

Gimenez-Roqueplo, A. P., J. Favier, et al. (2003). "Mutations in the SDHB gene are associated with extra-adrenal and/or malignant phaeochromocytomas." Cancer Res **63**(17): 5615-21.

Gimenez-Roqueplo, A. P., J. Favier, et al. (2002). "Functional consequences of a SDHB gene mutation in an apparently sporadic pheochromocytoma." J Clin Endocrinol Metab **87**(10): 4771-4.

Gimm, O., M. Armanios, et al. (2000). "Somatic and occult germ-line mutations in SDHD, a mitochondrial complex II gene, in nonfamilial pheochromocytoma." Cancer Res **60**(24): 6822-5.

Gnarra, J. R., D. R. Duan, et al. (1996). "Molecular cloning of the von Hippel-Lindau tumour suppressor gene and its role in renal carcinoma." Biochim Biophys Acta **1242**(3): 201-10.

Gnarra, J. R., J. M. Ward, et al. (1997). "Defective placental vasculogenesis causes embryonic lethality in VHL-deficient mice." Proc Natl Acad Sci U S A **94**(17): 9102-7.

Gomez, M. R. (1988). "Varieties of expression of tuberous sclerosis." Neurofibromatosis **1**(5-6): 330-8.

Goncharova, E. A., D. A. Goncharov, et al. (2002). "Tuberin regulates p70 S6 kinase activation and ribosomal protein S6 phosphorylation. A role for the TSC2 tumour suppressor gene in pulmonary lymphangioleiomyomatosis (LAM)." J Biol Chem **277**(34): 30958-67.

Good, D. J., P. J. Polverini, et al. (1990). "A tumour suppressor-dependent inhibitor of angiogenesis is immunologically and functionally indistinguishable from a fragment of thrombospondin." Proc Natl Acad Sci U S A 87(17): 6624-8.

Gould, K. A., W. F. Dietrich, et al. (1996). "Mom1 is a semi-dominant modifier of intestinal adenoma size and multiplicity in Min/+ mice." Genetics **144**(4): 1769-76.

Griparic, L. and A. M. van der Bliek (2001). "The many shapes of mitochondrial membranes." Traffic **2**(4): 235-44.

Gschwind, A., O. M. Fischer, et al. (2004). "The discovery of receptor tyrosine kinases: targets for cancer therapy." Nat Rev Cancer **4**(5): 361-70.

Gutmann, D. H., J. L. Cole, et al. (1994). "Loss of neurofibromin in adrenal gland tumours from patients with neurofibromatosis type I." Genes Chromosomes Cancer **10**(1): 55-8.

Haase, V. H. (2005). "The VHL tumour suppressor in development and disease: Functional studies in mice by conditional gene targeting." Semin Cell Dev Biol.

Haase, V. H., J. N. Glickman, et al. (2001). "Vascular tumours in livers with targeted inactivation of the von Hippel-Lindau tumour suppressor." Proc Natl Acad Sci U S A **98**(4): 1583-8.

Hagstrom, S. A. and T. P. Dryja (1999). "Mitotic recombination map of 13cen-13q14 derived from an investigation of loss of heterozygosity in retinoblastomas." Proc Natl Acad Sci U S A **96**(6): 2952-7.

Hahn-Windgassen, A., V. Nogueira, et al. (2005). "Akt activates the mammalian target of rapamycin by regulating cellular ATP level and AMPK activity." J Biol Chem **280**(37): 32081-9.

Hall, J. M., M. K. Lee, et al. (1990). "Linkage of early-onset familial breast cancer to chromosome 17q21." Science **250**(4988): 1684-9.

Hann, B. and A. Balmain (2001). "Building 'validated' mouse models of human cancer." Curr Opin Cell Biol **13**(6): 778-84.

Hardie, D. G. and D. Carling (1997). "The AMP-activated protein kinase--fuel gauge of the mammalian cell?" Eur J Biochem **246**(2): 259-73.

Hatch, M. D. (1978). "A simple spectrophotometric assay for fumarate hydratase in crude tissue extracts." Anal Biochem **85**(1): 271-5.

Hawley, S. A., M. Davison, et al. (1996). "Characterization of the AMP-activated protein kinase kinase from rat liver and identification of threonine 172 as the major site at which it phosphorylates AMP-activated protein kinase." J Biol Chem **271**(44): 27879-87.

Heath, D. (1991). "The human carotid body in health and disease." J Pathol **164**(1): 1-8.

Hensen, E. F., E. S. Jordanova, et al. (2004). "Somatic loss of maternal chromosome 11 causes parent-of-origin-dependent inheritance in SDHD-linked paraganglioma and phaeochromocytoma families." Oncogene **23**(23): 4076-83.

Heppner, C., M. B. Kester, et al. (1997). "Somatic mutation of the MEN1 gene in parathyroid tumours." Nat Genet **16**(4): 375-8.

Hino, O., A. J. Klein-Szanto, et al. (1993). "Spontaneous and radiation-induced renal tumours in the Eker rat model of dominantly inherited cancer." Proc Natl Acad Sci U S A **90**(1): 327-31.

Hino, O., K. Okimoto, et al. (2001). "A novel renal carcinoma predisposing gene of the Nihon rat maps on chromosome 10." Jpn J Cancer Res **92**(11): 1147-9.

Hoag, W. G. (1963). "Spontaneous Cancer In Mice." Ann N Y Acad Sci **108**: 805-31.

Hoess, R., K. Abremski, et al. (1984). "The nature of the interaction of the P1 recombinase Cre with the recombining site loxP." Cold Spring Harb Symp Quant Biol **49**: 761-8.

Hoffman, M. A., M. Ohh, et al. (2001). "von Hippel-Lindau protein mutants linked to type 2C VHL disease preserve the ability to downregulate HIF." Hum Mol Genet **10**(10): 1019-27.

Hofstra, R. M., T. Stelwagen, et al. (1996). "Extensive mutation scanning of RET in sporadic medullary thyroid carcinoma and of RET and VHL in sporadic pheochromocytoma reveals involvement of these genes in only a minority of cases." J Clin Endocrinol Metab **81**(8): 2881-4.

Hooper, M. L. (1998). "Tumour suppressor gene mutations in humans and mice: parallels and contrasts." Embo J **17**(23): 6783-9.

Hornstein, O. P. and M. Knickenberg (1975). "Perifollicular fibromatosis cutis with polyps of the colon--a cutaneo-intestinal syndrome sui generis." Arch Dermatol Res **253**(2): 161-75.

Hunter, D. S., M. Klotzbucher, et al. (2002). "Aberrant expression of HMGA2 in uterine leiomyoma associated with loss of TSC2 tumour suppressor gene function." Cancer Res **62**(13): 3766-72.

Hutton, J. J., Jr., A. Kaplan, et al. (1967). "Conversion of the amino acid sequence gly-pro-pro in protein to gly-pro-hyp by collagen proline hydroxylase." Arch Biochem Biophys **121**(2): 384-91.

Ikota, H., A. Tanimoto, et al. (2004). "Ureteral leiomyoma causing hydronephrosis in Type 1 multiple endocrine neoplasia." Pathol Int **54**(6): 457-9.

Iliopoulos, O., A. Kibel, et al. (1995). "Tumour suppression by the human von Hippel-Lindau gene product." Nat Med **1**(8): 822-6.

Iliopoulos, O., A. P. Levy, et al. (1996). "Negative regulation of hypoxia-inducible genes by the von Hippel-Lindau protein." Proc Natl Acad Sci U S A **93**(20): 10595-9.

Indra, A. K., X. Warot, et al. (1999). "Temporally-controlled site-specific mutagenesis in the basal layer of the epidermis: comparison of the recombinase activity of the tamoxifen-inducible Cre-ER(T) and Cre-ER(T2) recombinases." Nucleic Acids Res **27**(22): 4324-7.

Inoki, K., M. N. Corradetti, et al. (2005). "Dysregulation of the TSC-mTOR pathway in human disease." Nat Genet **37**(1): 19-24.

Inoki, K., Y. Li, et al. (2003). "Rheb GTPase is a direct target of TSC2 GAP activity and regulates mTOR signaling." Genes Dev **17**(15): 1829-34.

Inoki, K., Y. Li, et al. (2002). "TSC2 is phosphorylated and inhibited by Akt and suppresses mTOR signalling." Nat Cell Biol **4**(9): 648-57.

Isaacs, J. S., Y. J. Jung, et al. (2005). "HIF overexpression correlates with biallelic loss of fumarate hydratase in renal cancer: novel role of fumarate in regulation of HIF stability." Cancer Cell **8**(2): 143-53.

Ishii, T., K. Yasuda, et al. (2005). "A mutation in the SDHC gene of complex II increases oxidative stress, resulting in apoptosis and tumourigenesis." Cancer Res **65**(1): 203-9.

Jacks, T., T. S. Shih, et al. (1994). "Tumour predisposition in mice heterozygous for a targeted mutation in Nf1." Nat Genet **7**(3): 353-61.

Jeronimo, C., S. Nomoto, et al. (2001). "Mitochondrial mutations in early stage prostate cancer and bodily fluids." Oncogene **20**(37): 5195-8.

Johnson, J., J. Junewick, et al. (2005). "Phrenic nerve hemangioblastoma in a von Hippel-Lindau patient." AJR Am J Roentgenol **184**(3 Suppl): S10-1.

Johnson, L., K. Mercer, et al. (2001). "Somatic activation of the K-ras oncogene causes early onset lung cancer in mice." Nature **410**(6832): 1111-6.

Jones, J. B., J. J. Song, et al. (2001). "Detection of mitochondrial DNA mutations in pancreatic cancer offers a "mass"-ive advantage over detection of nuclear DNA mutations." Cancer Res **61**(4): 1299-304.

Kaelin, W. G., Jr. (2002). "Molecular basis of the VHL hereditary cancer syndrome." Nat Rev Cancer **2**(9): 673-82.

Kaelin, W. G., Jr. (2003). "The von Hippel-Lindau gene, kidney cancer, and oxygen sensing." J Am Soc Nephrol **14**(11): 2703-11.

Kaelin, W. G., Jr. (2004). "The von Hippel-Lindau tumour suppressor gene and kidney cancer." Clin Cancer Res **10**(18 Pt 2): 6290S-5S.

Karbowski, M. and R. J. Youle (2003). "Dynamics of mitochondrial morphology in healthy cells and during apoptosis." Cell Death Differ **10**(8): 870-80.

Kashtan, C. E. (2002). "Animal models of Alport syndrome." Nephrol Dial Transplant **17**(8): 1359-62.

Kashtan, C. E. and A. F. Michael (1996). "Alport syndrome." Kidney Int **50**(5): 1445-63.

Kelland, L. R. (2004). "Of mice and men: values and liabilities of the athymic nude mouse model in anticancer drug development." Eur J Cancer **40**(6): 827-36.

Kelsell, D. P., D. M. Black, et al. (1993). "Genetic analysis of the BRCA1 region in a large breast/ovarian family: refinement of the minimal region containing BRCA1." Hum Mol Genet **2**(11): 1823-8.

Kenck, C., P. Bugert, et al. (1997). "Duplication of an approximately 1.5 Mb DNA segment at chromosome 5q22 indicates the locus of a new tumour gene in nonpapillary renal cell carcinomas." Oncogene **14**(9): 1093-8.

Kenerson, H. L., L. D. Aicher, et al. (2002). "Activated mammalian target of rapamycin pathway in the pathogenesis of tuberous sclerosis complex renal tumours." Cancer Res **62**(20): 5645-50.

Kerbel, R. S. (2003). "Human tumour xenografts as predictive preclinical models for anticancer drug activity in humans: better than commonly perceived-but they can be improved." Cancer Biol Ther **2**(4 Suppl 1): S134-9.

Kiefer, K., J. Clement, et al. (2004). "Transfection efficiency and cytotoxicity of nonviral gene transfer reagents in human smooth muscle and endothelial cells." Pharm Res **21**(6): 1009-17.

Kikuchi, Y., A. Sudo, et al. (2004). "Presence of a modifier gene(s) affecting early renal carcinogenesis in the Tsc2 mutant (Eker) rat model." Int J Oncol **24**(1): 75-80.

Kim, J. W. and C. V. Dang (2005). "Multifaceted roles of glycolytic enzymes." Trends Biochem Sci **30**(3): 142-50.

Kim, W. Y. and W. G. Kaelin (2004). "Role of VHL gene mutation in human cancer." J Clin Oncol **22**(24): 4991-5004.

King, T. S. (1967). Methods in Enzymology.

Kinzler, K. W. V., B (2002). The Genetic Basis of Human Cancer. New York, McGraw Hill.

Kirches, E., G. Krause, et al. (2001). "High frequency of mitochondrial DNA mutations in glioblastoma multiforme identified by direct sequence comparison to blood samples." Int J Cancer **93**(4): 534-8.

Kiuru, M. and V. Launonen (2004). "Hereditary leiomyomatosis and renal cell cancer (HLRCC)." Curr Mol Med **4**(8): 869-75.

Kiuru, M., V. Launonen, et al. (2001). "Familial cutaneous leiomyomatosis is a two-hit condition associated with renal cell cancer of characteristic histopathology." Am J Pathol **159**(3): 825-9.

Kiuru, M., R. Lehtonen, et al. (2002). "Few FH mutations in sporadic counterparts of tumour types observed in hereditary leiomyomatosis and renal cell cancer families." Cancer Res **62**(16): 4554-7.

Kiuru, M., R. Lehtonen, et al. (2005). "No germline FH mutations in familial breast cancer patients." Eur J Hum Genet **13**(4): 506-9.

Kleymenova, E. and C. L. Walker (2001). "Determination of loss of heterozygosity in frozen and paraffin embedded tumours by denaturating high-performance liquid chromatography (DHPLC)." J Biochem Biophys Methods **47**(1-2): 83-90.

Knebelmann, B., S. Ananth, et al. (1998). "Transforming growth factor alpha is a target for the von Hippel-Lindau tumour suppressor." Cancer Res **58**(2): 226-31.

Knudson, A. G., Jr. (1971). "Mutation and cancer: statistical study of retinoblastoma." Proc Natl Acad Sci U S A **68**(4): 820-3.

Kobayashi, T., Y. Hirayama, et al. (1995). "A germline insertion in the tuberous sclerosis (Tsc2) gene gives rise to the Eker rat model of dominantly inherited cancer." Nat Genet **9**(1): 70-4.

Kobayashi, T., O. Minowa, et al. (1999). "Renal carcinogenesis, hepatic hemangiomatosis, and embryonic lethality caused by a germ-line Tsc2 mutation in mice." Cancer Res **59**(6): 1206-11.

Kondo, K., M. Yao, et al. (2002). "Comprehensive mutational analysis of the VHL gene in sporadic renal cell carcinoma: relationship to clinicopathological parameters." Genes Chromosomes Cancer **34**(1): 58-68.

Lama, G., L. Graziano, et al. (2004). "Blood pressure and cardiovascular involvement in children with neurofibromatosis type1." Pediatr Nephrol **19**(4): 413-8.

Launonen, V., O. Vierimaa, et al. (2001). "Inherited susceptibility to uterine leiomyomas and renal cell cancer." Proc Natl Acad Sci U S A **98**(6): 3387-92.

Le Guyadec, T., J. P. Dufau, et al. (1998). "[Multiple trichodiscomas associated with colonic polyposis]." Ann Dermatol Venereol **125**(10): 717-9.

Le Hir, M., K. U. Eckardt, et al. (1991). "Structure-function correlations in erythropoietin formation and oxygen sensing in the kidney." Klin Wochenschr **69**(13): 567-75.

Lee, S., E. Nakamura, et al. (2005). "Neuronal apoptosis linked to EglN3 prolyl hydroxylase and familial pheochromocytoma genes: developmental culling and cancer." Cancer Cell **8**(2): 155-67.

Lee, Y. J., S. S. Galoforo, et al. (1998). "Glucose deprivation-induced cytotoxicity and alterations in mitogen-activated protein kinase activation are mediated by oxidative stress in multidrug-resistant human breast carcinoma cells." J Biol Chem **273**(9): 5294-9.

Legius, E., D. A. Marchuk, et al. (1993). "Somatic deletion of the neurofibromatosis type 1 gene in a neurofibrosarcoma supports a tumour suppressor gene hypothesis." Nat Genet **3**(2): 122-6.

Lehtonen, H. J., M. Kiuru, et al. (2005). "Increased risk of cancer in patients with fumarate hydratase germline mutation." J Med Genet.

Lehtonen, R., M. Kiuru, et al. (2004). "Biallelic inactivation of fumarate hydratase (FH) occurs in nonsyndromic uterine leiomyomas but is rare in other tumours." Am J Pathol **164**(1): 17-22.

Leigh, D. (1951). "Subacute necrotizing encephalomyelopathy in an infant." J Neurochem **14**(3): 216-21.

Leow, C. C., X. D. Wang, et al. (2005). "Novel method of generating prostate-specific Cre-LoxP gene switching via intraductal delivery of adenovirus." Prostate **65**(1): 1-9.

Li, J., Y. Mizukami, et al. (2005). "Oncogenic K-ras stimulates Wnt signaling in colon cancer through inhibition of GSK-3beta." Gastroenterology **128**(7): 1907-18.

Libutti, S. K., J. S. Crabtree, et al. (2003). "Parathyroid gland-specific deletion of the mouse Men1 gene results in parathyroid neoplasia and hypercalcemic hyperparathyroidism." Cancer Res **63**(22): 8022-8.

Lieubeau-Teillet, B., J. Rak, et al. (1998). "von Hippel-Lindau gene-mediated growth suppression and induction of differentiation in renal cell carcinoma cells grown as multicellular tumour spheroids." Cancer Res **58**(21): 4957-62.

Ligon, A. H. and C. C. Morton (2000). "Genetics of uterine leiomyomata." Genes Chromosomes Cancer **28**(3): 235-45.

Lingaas, F., K. E. Comstock, et al. (2003). "A mutation in the canine BHD gene is associated with hereditary multifocal renal cystadenocarcinoma and nodular dermatofibrosis in the German Shepherd dog." Hum Mol Genet **12**(23): 3043-53.

Liu, C. Y., A. Flesken-Nikitin, et al. (1996). "Inactivation of the mouse Brca1 gene leads to failure in the morphogenesis of the egg cylinder in early postimplantation development." Genes Dev **10**(14): 1835-43.

Liu, M. Y., L. Poellinger, et al. (2003). "Up-regulation of hypoxia-inducible factor 2alpha in renal cell carcinoma associated with loss of Tsc-2 tumour suppressor gene." Cancer Res **63**(10): 2675-80.

Lium, B. and L. Moe (1985). "Hereditary multifocal renal cystadenocarcinomas and nodular dermatofibrosis in the German shepherd dog: macroscopic and histopathologic changes." Vet Pathol **22**(5): 447-55.

Lopez-Barneo, J., R. del Toro, et al. (2004). "Regulation of oxygen sensing by ion channels." J Appl Physiol **96**(3): 1187-95; discussion 1170-2.

Lubensky, I. A., J. R. Gnarra, et al. (1996). "Allelic deletions of the VHL gene detected in multiple microscopic clear cell renal lesions in von Hippel-Lindau disease patients." Am J Pathol **149**(6): 2089-94.

Ma, W., L. Tessarollo, et al. (2003). "Hepatic vascular tumours, angiectasis in multiple organs, and impaired spermatogenesis in mice with conditional inactivation of the VHL gene." Cancer Res **63**(17): 5320-8.

Machens, A., M. Brauckhoff, et al. (2005). "Codon-specific development of pheochromocytoma in multiple endocrine neoplasia type 2." J Clin Endocrinol Metab **90**(7): 3999-4003.

Mack, C. P. and G. K. Owens (1999). "Regulation of smooth muscle alpha-actin expression in vivo is dependent on CArG elements within the 5' and first intron promoter regions." Circ Res **84**(7): 852-61.

Madsen, C. S., C. P. Regan, et al. (1998). "Smooth muscle-specific expression of the smooth muscle myosin heavy chain gene in transgenic mice requires 5'-flanking and first intronic DNA sequence." Circ Res **82**(8): 908-17.

Maher, E. R. and W. G. Kaelin, Jr. (1997). "von Hippel-Lindau disease." Medicine (Baltimore) **76**(6): 381-91.

Majewski, N., V. Nogueira, et al. (2004). "Hexokinase-mitochondria interaction mediated by Akt is required to inhibit apoptosis in the presence or absence of Bax and Bak." Mol Cell **16**(5): 819-30.

Mak, B. C. and R. S. Yeung (2004). "The tuberous sclerosis complex genes in tumour development." Cancer Invest **22**(4): 588-603.

Malkin, D., F. P. Li, et al. (1990). "Germ line p53 mutations in a familial syndrome of breast cancer, sarcomas, and other neoplasms." Science **250**(4985): 1233-8.

Mariman, E. C., S. E. van Beersum, et al. (1995). "Fine mapping of a putatively imprinted gene for familial non-chromaffin paragangliomas to chromosome 11q13.1: evidence for genetic heterogeneity." Hum Genet **95**(1): 56-62.

Mariman, E. C., S. E. van Beersum, et al. (1993). "Analysis of a second family with hereditary non-chromaffin paragangliomas locates the underlying gene at the proximal region of chromosome 11q." Hum Genet **91**(4): 357-61.

Maruo, T., N. Ohara, et al. (2004). "Sex steroidal regulation of uterine leiomyoma growth and apoptosis." Hum Reprod Update **10**(3): 207-20.

Marx, S. J. (2005). "Molecular genetics of multiple endocrine neoplasia types 1 and 2." Nat Rev Cancer **5**(5): 367-75.

Marx, S. J. and W. F. Simonds (2005). "Hereditary hormone excess: genes, molecular pathways, and syndromes." Endocr Rev **26**(5): 615-61.

Marx, S. J. and C. A. Stratakis (2005). "Multiple endocrine neoplasia--introduction." J Intern Med **257**(1): 2-5.

Mates, J. M., C. Perez-Gomez, et al. (2002). "Glutamine and its relationship with intracellular redox status, oxidative stress and cell proliferation/death." Int J Biochem Cell Biol **34**(5): 439-58.

Maxwell, P. H. (2005). "A common pathway for genetic events leading to pheochromocytoma." Cancer Cell **8**(2): 91-3.

Maxwell, P. H., M. S. Wiesener, et al. (1999). "The tumour suppressor protein VHL targets hypoxia-inducible factors for oxygen-dependent proteolysis." Nature **399**(6733): 271-5.

McClintock, D. S., M. T. Santore, et al. (2002). "Bcl-2 family members and functional electron transport chain regulate oxygen deprivation-induced cell death." Mol Cell Biol **22**(1): 94-104.

McKeeby, J. L., X. Li, et al. (2001). "Multiple leiomyomas of the esophagus, lung, and uterus in multiple endocrine neoplasia type 1." Am J Pathol **159**(3): 1121-7.

McLeod, M., S. Craft, et al. (1986). "Identification of the crossover site during FLP-mediated recombination in the Saccharomyces cerevisiae plasmid 2 microns circle." Mol Cell Biol **6**(10): 3357-67.

Meijers-Heijboer, H., A. van den Ouweland, et al. (2002). "Low-penetrance susceptibility to breast cancer due to CHEK2(*)1100delC in noncarriers of BRCA1 or BRCA2 mutations." Nat Genet **31**(1): 55-9.

Messner, K. R. and J. A. Imlay (2002). "In vitro quantitation of biological superoxide and hydrogen peroxide generation." Methods Enzymol **349**: 354-61.

Meyer, A. J., A. Hernandez, et al. (2000). "Novel mutations of the von hippel-lindau tumour-suppressor gene and rare DNA hypermethylation in renal-cell carcinoma cell lines of the clear-cell type." Int J Cancer **87**(5): 650-3.

Michiels, F. M., S. Chappuis, et al. (1997). "Development of medullary thyroid carcinoma in transgenic mice expressing the RET protooncogene altered by a multiple endocrine neoplasia type 2A mutation." Proc Natl Acad Sci U S A **94**(7): 3330-5.

Mientjes, E. J., R. Willemsen, et al. (2004). "Fxr1 knockout mice show a striated muscle phenotype: implications for Fxr1p function in vivo." Hum Mol Genet **13**(13): 1291-302.

Milunsky, J. M., T. A. Maher, et al. (2001). "Novel mutations and the emergence of a common mutation in the SDHD gene causing familial paraganglioma." Am J Med Genet **100**(4): 311-4.

Miyoshi, H., M. Nakau, et al. (2002). "Gastrointestinal hamartomatous polyposis in Lkb1 heterozygous knockout mice." Cancer Res **62**(8): 2261-6.

Moe, L. and B. Lium (1997). "Hereditary multifocal renal cystadenocarcinomas and nodular dermatofibrosis in 51 German shepherd dogs." J Small Anim Pract **38**(11): 498-505.

Moeller, B. J., Y. Cao, et al. (2004). "Radiation activates HIF-1 to regulate vascular radiosensitivity in tumours: role of reoxygenation, free radicals, and stress granules." Cancer Cell **5**(5): 429-41.

Morita, R., J. Ishikawa, et al. (1991). "Allelotype of renal cell carcinoma." Cancer Res **51**(3): 820-3.

Morita, R., S. Saito, et al. (1991). "Common regions of deletion on chromosomes 5q, 6q, and 10q in renal cell carcinoma." Cancer Res **51**(21): 5817-20.

Morris, M. R., E. Maina, et al. (2004). "Molecular genetic analysis of FIH-1, FH, and SDHB candidate tumour suppressor genes in renal cell carcinoma." J Clin Pathol **57**(7): 706-11.

Mozdy, A. D. and J. M. Shaw (2003). "A fuzzy mitochondrial fusion apparatus comes into focus." Nat Rev Mol Cell Biol **4**(6): 468-78.

Myllyla, R., L. Tuderman, et al. (1977). "Mechanism of the prolyl hydroxylase reaction. 2. Kinetic analysis of the reaction sequence." Eur J Biochem **80**(2): 349-57.

Nelson, R. D., P. Stricklett, et al. (1998). "Expression of an AQP2 Cre recombinase transgene in kidney and male reproductive system of transgenic mice." Am J Physiol **275**(1 Pt 1): C216-26.

Neumann, H. P. (1991). "[The von Hippel-Lindau syndrome]." Dtsch Med Wochenschr **116**(1): 28-34.

Neumann, H. P., B. Bausch, et al. (2002). "Germ-line mutations in nonsyndromic pheochromocytoma." N Engl J Med **346**(19): 1459-66.

Neumann, H. P., D. P. Berger, et al. (1993). "Pheochromocytomas, multiple endocrine neoplasia type 2, and von Hippel-Lindau disease." N Engl J Med **329**(21): 1531-8.

Neumann, H. P., C. Pawlu, et al. (2004). "Distinct clinical features of paraganglioma syndromes associated with SDHB and SDHD gene mutations." Jama **292**(8): 943-51.

Newmeyer, D. D. and S. Ferguson-Miller (2003). "Mitochondria: releasing power for life and unleashing the machineries of death." Cell **112**(4): 481-90.

Niemann, S. and U. Muller (2000). "Mutations in SDHC cause autosomal dominant paraganglioma, type 3." Nat Genet **26**(3): 268-70.

Niemann, S., U. Muller, et al. (2003). "Autosomal dominant malignant and catecholamine-producing paraganglioma caused by a splice donor site mutation in SDHC." Hum Genet **113**(1): 92-4.

Niikawa, N. (1997). "Genomic imprinting relevant to genetic diseases." Southeast Asian J Trop Med Public Health **28 Suppl 3**: 46-57.

Okimoto, K., M. Kouchi, et al. (2000). "A novel "Nihon" rat model of a Mendelian dominantly inherited renal cell carcinoma." Jpn J Cancer Res **91**(11): 1096-9.

Okimoto, K., J. Sakurai, et al. (2004). "A germ-line insertion in the Birt-Hogg-Dube (BHD) gene gives rise to the Nihon rat model of inherited renal cancer." Proc Natl Acad Sci U S A **101**(7): 2023-7.

Oliveira, S. M., J. Ehtisham, et al. (2003). "Mutation analysis of AMP-activated protein kinase subunits in inherited cardiomyopathies: implications for kinase function and disease pathogenesis." J Mol Cell Cardiol **35**(10): 1251-5.

Onda, H., A. Lueck, et al. (1999). "Tsc2(+/-) mice develop tumours in multiple sites that express gelsolin and are influenced by genetic background." J Clin Invest **104**(6): 687-95.

Opocher, G., P. Conton, et al. (2005). "Pheochromocytoma in von Hippel-Lindau disease and neurofibromatosis type 1 Review." Fam Cancer **4**(1): 13-6.

Opocher, G., F. Schiavi, et al. (2003). "Fine analysis of the short arm of chromosome 1 in sporadic and familial pheochromocytoma." Clin Endocrinol (Oxf) **59**(6): 707-15.

Papadimitriou, J. C. and C. B. Drachenberg (1994). "Giant mitochondria with paracrystalline inclusions in paraganglioma of the urinary bladder: correlation with mitochondrial abnormalities in paragangliomas of other sites." Ultrastruct Pathol **18**(6): 559-64.

Parfait, B., D. Chretien, et al. (2000). "Compound heterozygous mutations in the flavoprotein gene of the respiratory chain complex II in a patient with Leigh syndrome." Hum Genet **106**(2): 236-43.

Pause, A., S. Lee, et al. (1998). "The von Hippel-Lindau tumour suppressor gene is required for cell cycle exit upon serum withdrawal." Proc Natl Acad Sci U S A **95**(3): 993-8.

Pavlovich, C. P., R. L. Grubb, 3rd, et al. (2005). "Evaluation and management of renal tumours in the Birt-Hogg-Dube syndrome." J Urol **173**(5): 1482-6.

Pavlovich, C. P., M. M. Walther, et al. (2002). "Renal tumours in the Birt-Hogg-Dube syndrome." Am J Surg Pathol **26**(12): 1542-52.

Pawlu, C., B. Bausch, et al. (2005). "Mutations of the SDHB and SDHD genes." Fam Cancer **4**(1): 49-54.

Pejovic, T., D. Ladner, et al. (2004). "Somatic D-loop mitochondrial DNA mutations are frequent in uterine serous carcinoma." Eur J Cancer **40**(16): 2519-24.

Perry, D. J. and R. W. Carrell (1989). "CpG dinucleotides are "hotspots" for mutation in the antithrombin III gene. Twelve variants identified using the polymerase chain reaction." Mol Biol Med **6**(3): 239-43.

Peto, J. (2002). "Breast cancer susceptibility-A new look at an old model." Cancer Cell **1**(5): 411-2.

Petros, J. A., A. K. Baumann, et al. (2005). "mtDNA mutations increase tumourigenicity in prostate cancer." Proc Natl Acad Sci U S A **102**(3): 719-24.

Petrova-Benedict, R., B. H. Robinson, et al. (1987). "Deficient fumarase activity in an infant with fumaricacidemia and its distribution between the different forms of the enzyme seen on isoelectric focusing." Am J Hum Genet **40**(3): 257-66.

Pharoah, P. D., A. Antoniou, et al. (2002). "Polygenic susceptibility to breast cancer and implications for prevention." Nat Genet **31**(1): 33-6.

Piruat, J. I., C. O. Pintado, et al. (2004). "The mitochondrial SDHD gene is required for early embryogenesis, and its partial deficiency results in persistent carotid body glomus cell activation with full responsiveness to hypoxia." Mol Cell Biol **24**(24): 10933-40.

Pollard, P., N. Wortham, et al. (2005). "Evidence of increased microvessel density and activation of the hypoxia pathway in tumours from the hereditary leiomyomatosis and renal cell cancer syndrome." J Pathol **205**(1): 41-9.

Pollard, P. J., J. J. Briere, et al. (2005). "Accumulation of Krebs cycle intermediates and over-expression of HIF1{alpha} in tumours which result from germline FH and SDH mutations." Hum Mol Genet **14**(15): 2231-9.

Pollard, P. J., N. C. Wortham, et al. (2003). "The TCA cycle and tumourigenesis: the examples of fumarate hydratase and succinate dehydrogenase." Ann Med **35**(8): 632-9.

Polyak, K., Y. Li, et al. (1998). "Somatic mutations of the mitochondrial genome in human colorectal tumours." Nat Genet **20**(3): 291-3.

Poncelet, C., R. Fauvet, et al. (2004). "Prognostic value of von Willebrand factor, CD34, CD31, and vascular endothelial growth factor expression in women with uterine leiomyosarcomas." J Surg Oncol **86**(2): 84-90.

Poncelet, C., P. Madelenat, et al. (2002). "Expression of von Willebrand's factor, CD34, CD31, and vascular endothelial growth factor in uterine leiomyomas." Fertil Steril **78**(3): 581-6.

Ponder, B. A. (2001). "Cancer genetics." Nature **411**(6835): 336-41.

Pore, N., S. Liu, et al. (2004). "Sp1 is involved in Akt-mediated induction of VEGF expression through an HIF-1-independent mechanism." Mol Biol Cell **15**(11): 4841-53.

Poulsom, R., J. M. Longcroft, et al. (1998). "A robust method for isotopic riboprobe in situ hybridisation to localise mRNAs in routine pathology specimens." Eur J Histochem **42**(2): 121-32.

Pugh, C. W. and P. J. Ratcliffe (2003). "Regulation of angiogenesis by hypoxia: role of the HIF system." Nat Med **9**(6): 677-84.

Raha, S. and B. H. Robinson (2000). "Mitochondria, oxygen free radicals, disease and ageing." Trends Biochem Sci **25**(10): 502-8.

Rathmell, J. C., C. J. Fox, et al. (2003). "Akt-directed glucose metabolism can prevent Bax conformation change and promote growth factor-independent survival." Mol Cell Biol **23**(20): 7315-28.

Raval, R. R., K. W. Lau, et al. (2005). "Contrasting properties of hypoxia-inducible factor 1 (HIF-1) and HIF-2 in von Hippel-Lindau-associated renal cell carcinoma." Mol Cell Biol **25**(13): 5675-86.

Rheault, M. N., S. M. Kren, et al. (2004). "Mouse model of X-linked Alport syndrome." J Am Soc Nephrol **15**(6): 1466-74.

Ricci, J. E., C. Munoz-Pinedo, et al. (2004). "Disruption of mitochondrial function during apoptosis is mediated by caspase cleavage of the p75 subunit of complex I of the electron transport chain." Cell **117**(6): 773-86.

Riederer, P., et al. (1989). "Transition metals, ferritin, glutathione, and ascorbic acid in parkinsonian brains." J Neurochem 52(2): 515-20.

Romagnolo, B., F. Cluzeaud, et al. (1996). "Tissue-specific and hormonal regulation of calbindin-D9K fusion genes in transgenic mice." J Biol Chem **271**(28): 16820-6.

Rongioletti, F., R. Hazini, et al. (1989). "Fibrofolliculomas, tricodiscomas and acrochordons (Birt-Hogg-Dube) associated with intestinal polyposis." Clin Exp Dermatol **14**(1): 72-4.

Roth, J. S., A. D. Rabinowitz, et al. (1993). "Bilateral renal cell carcinoma in the Birt-Hogg-Dube syndrome." J Am Acad Dermatol **29**(6): 1055-6.

Safran, M. and W. G. Kaelin, Jr. (2003). "HIF hydroxylation and the mammalian oxygen-sensing pathway." J Clin Invest **111**(6): 779-83.

Sakai, K., K. Mitani, et al. (1995). "Efficient regulation of gene expression by adenovirus vector-mediated delivery of the CRE recombinase." Biochem Biophys Res Commun **217**(2): 393-401.

Sandstrom, B. E., M. Granstrom, et al. (1995). "A comparison of four assays detecting oxidizing species. Correlated reactivity of Fe(III)-quin2, but not Fe(III)-EDTA, with hydrogen peroxide." Biol Trace Elem Res 47: 29-36.

Santoro, M., R. M. Melillo, et al. (2004). "Minireview: RET: normal and abnormal functions." Endocrinology **145**(12): 5448-51.

Saucedo, L. J., X. Gao, et al. (2003). "Rheb promotes cell growth as a component of the insulin/TOR signalling network." Nat Cell Biol **5**(6): 566-71.

Sauer, B. and N. Henderson (1990). "Targeted insertion of exogenous DNA into the eukaryotic genome by the Cre recombinase." New Biol **2**(5): 441-9.

Saur, D., J. M. Vanderwinden, et al. (2004). "Single-nucleotide promoter polymorphism alters transcription of neuronal nitric oxide synthase exon 1c in infantile hypertrophic pyloric stenosis." Proc Natl Acad Sci U S A **101**(6): 1662-7.

Savolainen, K. M., J. Loikkanen, et al. (1995). "Amplification of glutamate-induced oxidative stress." Toxicol Lett **82-83**: 399-405.

Scacheri, P. C., J. S. Crabtree, et al. (2004). "Homozygous loss of menin is well tolerated in liver, a tissue not affected in MEN1." Mamm Genome **15**(11): 872-7.

Schmidt, L. S., M. L. Nickerson, et al. (2005). "Germline BHD-mutation spectrum and phenotype analysis of a large cohort of families with Birt-Hogg-Dube syndrome." Am J Hum Genet **76**(6): 1023-33.

Schofield, C. J. and P. J. Ratcliffe (2004). "Oxygen sensing by HIF hydroxylases." Nat Rev Mol Cell Biol **5**(5): 343-54.

Schon, E. A. and S. DiMauro (2003). "Medicinal and genetic approaches to the treatment of mitochondrial disease." Curr Med Chem **10**(23): 2523-33.

Selak, M. A., S. M. Armour, et al. (2005). "Succinate links TCA cycle dysfunction to oncogenesis by inhibiting HIF-alpha prolyl hydroxylase." Cancer Cell **7**(1): 77-85.

Semenza, G. L. (2002). "HIF-1 and tumour progression: pathophysiology and therapeutics." Trends Mol Med **8**(4 Suppl): S62-7.

Senoo-Matsuda, N., K. Yasuda, et al. (2001). "A defect in the cytochrome b large subunit in complex II causes both superoxide anion overproduction and abnormal energy metabolism in Caenorhabditis elegans." J Biol Chem **276**(45): 41553-8.

Shao, X., J. E. Johnson, et al. (2002). "A minimal Ksp-cadherin promoter linked to a green fluorescent protein reporter gene exhibits tissue-specific expression in the developing kidney and genitourinary tract." J Am Soc Nephrol **13**(7): 1824-36.

Shephard, J. A. (1969). Methods in Enzymology.

Shidara, Y., K. Yamagata, et al. (2005). "Positive contribution of pathogenic mutations in the mitochondrial genome to the promotion of cancer by prevention from apoptosis." Cancer Res **65**(5): 1655-63.

Shoffner, J. M., M. T. Lott, et al. (1990). "Myoclonic epilepsy and ragged-red fiber disease (MERRF) is associated with a mitochondrial DNA tRNA(Lys) mutation." Cell **61**(6): 931-7.

Sidhu, J. S., Y. S. Rajawat, et al. (2005). "Transgenic mouse model of ventricular preexcitation and atrioventricular reentrant tachycardia induced by an AMP-activated protein kinase loss-of-function mutation responsible for Wolff-Parkinson-White syndrome." Circulation **111**(1): 21-9.

Siemeister, G., K. Weindel, et al. (1996). "Reversion of deregulated expression of vascular endothelial growth factor in human renal carcinoma cells by von Hippel-Lindau tumour suppressor protein." Cancer Res **56**(10): 2299-301.

Skinner, M. A., S. Kalyanaraman, et al. (2005). "A human yeast artificial chromosome containing the multiple endocrine neoplasia type 2B Ret mutation does not induce medullary thyroid carcinoma but does support the growth of kidneys and partially rescues enteric nervous system development in Ret-deficient mice." Am J Pathol **166**(1): 265-74.

Slattery, M. L., C. Sweeney, et al. (2005). "Associations between apoE genotype and colon and rectal cancer." Carcinogenesis **26**(8): 1422-9.

Smith, S. A., D. F. Easton, et al. (1992). "Allele losses in the region 17q12-21 in familial breast and ovarian cancer involve the wild-type chromosome." Nat Genet **2**(2): 128-31.

Smith-Hicks, C. L., K. C. Sizer, et al. (2000). "C-cell hyperplasia, pheochromocytoma and sympathoadrenal malformation in a mouse model of multiple endocrine neoplasia type 2B." Embo J **19**(4): 612-22.

Sohal, D. S., M. Nghiem, et al. (2001). "Temporally regulated and tissue-specific gene manipulations in the adult and embryonic heart using a tamoxifen-inducible Cre protein." Circ Res **89**(1): 20-5.

Soriano, P. (1999). "Generalized lacZ expression with the ROSA26 Cre reporter strain." Nat Genet **21**(1): 70-1.

Sowter, H. M., P. J. Ratcliffe, et al. (2001). "HIF-1-dependent regulation of hypoxic induction of the cell death factors BNIP3 and NIX in human tumours." Cancer Res 61(18): 6669-73.

Stambolic, V., A. Suzuki, et al. (1998). "Negative regulation of PKB/Akt-dependent cell survival by the tumour suppressor PTEN." Cell **95**(1): 29-39.

Stocker, H., T. Radimerski, et al. (2003). "Rheb is an essential regulator of S6K in controlling cell growth in Drosophila." Nat Cell Biol **5**(6): 559-65.

Storz, P. (2005). "Reactive oxygen species in tumour progression." Front Biosci **10**: 1881-96.

Stratmann, R., M. Krieg, et al. (1997). "Putative control of angiogenesis in hemangioblastomas by the von Hippel-Lindau tumour suppressor gene." J Neuropathol Exp Neurol **56**(11): 1242-52.

Su, L. K., K. W. Kinzler, et al. (1992). "Multiple intestinal neoplasia caused by a mutation in the murine homolog of the APC gene." Science **256**(5057): 668-70.

Takehara, A., K. Kawakami, et al. (2005). "Prognostic significance of the polymorphisms in thymidylate synthase and methylenetetrahydrofolate reductase gene in lung cancer." Anticancer Res **25**(6C): 4455-61.

Taylor, R. W., M. J. Barron, et al. (2003). "Mitochondrial DNA mutations in human colonic crypt stem cells." J Clin Invest **112**(9): 1351-60.

Taylor, R. W. and D. M. Turnbull (2005). "Mitochondrial DNA mutations in human disease." Nat Rev Genet **6**(5): 389-402.

Thielen, B. K., D. F. Barker, et al. (2003). "Deletion mapping in Alport syndrome and Alport syndrome-diffuse leiomyomatosis reveals potential mechanisms of visceral smooth muscle overgrowth." Hum Mutat **22**(5): 419.

Thrash-Bingham, C. A., R. E. Greenberg, et al. (1995). "Comprehensive allelotyping of human renal cell carcinomas using microsatellite DNA probes." Proc Natl Acad Sci U S A **92**(7): 2854-8.

Tickoo, S. K., V. E. Reuter, et al. (1999). "Renal oncocytosis: a morphologic study of fourteen cases." Am J Surg Pathol **23**(9): 1094-101.

Tischler, A. S., T. S. Shih, et al. (1995). "Characterization of Pheochromocytomas in a Mouse Strain with a Targeted Disruptive Mutation of the Neurofibromatosis Gene Nf1." Endocr Pathol **6**(4): 323-335.

Tomlinson, I. P., N. A. Alam, et al. (2002). "Germline mutations in FH predispose to dominantly inherited uterine fibroids, skin leiomyomata and papillary renal cell cancer." Nat Genet **30**(4): 406-10.

Toro, J. R., G. Glenn, et al. (1999). "Birt-Hogg-Dube syndrome: a novel marker of kidney neoplasia." Arch Dermatol **135**(10): 1195-202.

Toro, J. R., M. L. Nickerson, et al. (2003). "Mutations in the fumarate hydratase gene cause hereditary leiomyomatosis and renal cell cancer in families in North America." Am J Hum Genet **73**(1): 95-106.

Traweek, S. T., P. L. Kandalaft, et al. (1991). "The human hematopoietic progenitor cell antigen (CD34) in vascular neoplasia." Am J Clin Pathol 96(1): 25-31.

Tureci, O., U. Sahin, et al. (1998). "Human carbonic anhydrase XII: cDNA cloning, expression, and chromosomal localization of a carbonic anhydrase gene that is overexpressed in some renal cell cancers." Proc Natl Acad Sci U S A 95(13): 7608-13.

van Schothorst, E. M., M. Beekman, et al. (1998). "Paragangliomas of the head and neck region show complete loss of heterozygosity at 11q22-q23 in chief cells and the flow-sorted DNA aneuploid fraction." Hum Pathol **29**(10): 1045-9.

Vanharanta, S., M. Buchta, et al. (2004). "Early-onset renal cell carcinoma as a novel extraparaganglial component of SDHB-associated heritable paraganglioma." Am J Hum Genet **74**(1): 153-9.

Vanharanta, S., P. J. Pollard, et al. (2006). "Distinct expression profile in fumarate-hydratase-deficient uterine fibroids." Hum Mol Genet **15**(1): 97-103.

Vanharanta, S., N. C. Wortham, et al. (2005). "7q deletion mapping and expression profiling in uterine fibroids." Oncogene **24**(43): 6545-54.

Venkitaraman, A. R. (2002). "Cancer susceptibility and the functions of BRCA1 and BRCA2." Cell **108**(2): 171-82.

Vortmeyer, A. O., I. A. Lubensky, et al. (1999). "Multiple endocrine neoplasia type 1: atypical presentation, clinical course, and genetic analysis of multiple tumours." Mod Pathol **12**(9): 919-24.

Wakabayashi, T. (1999). "Structural changes of mitochondria related to apoptosis: swelling and megamitochondria formation." Acta Biochim Pol **46**(2): 223-37.

Walker, C., T. L. Goldsworthy, et al. (1992). "Predisposition to renal cell carcinoma due to alteration of a cancer susceptibility gene." Science **255**(5052): 1693-5.

Walker, C. L., D. Hunter, et al. (2003). "Uterine leiomyoma in the Eker rat: a unique model for important diseases of women." Genes Chromosomes Cancer **38**(4): 349-56.

Warburg, O. (1930). The Metabolism of Tumours. London, Constable and Co.

Warburg, O. (1956). "On respiratory impairment in cancer cells." Science **124**(3215): 269-70.

Ward, J. M. and D. E. Devor-Henneman (2004). "Mouse models of human familial cancer syndromes." Toxicol Pathol **32 Suppl 1**: 90-8.

Watanabe, H., G. Burnstock, et al. (1976). "Mitochondrial abnormalities in human phaeochromocytoma." Cell Tissue Res **172**(2): 281-8.

Weaver, T. and L. Banaszak (1996). "Crystallographic studies of the catalytic and a second site in fumarase C from Escherichia coli." Biochemistry **35**(44): 13955-65.

Weaver, T. M., D. G. Levitt, et al. (1993). "Purification and crystallization of fumarase C from Escherichia coli." J Mol Biol **231**(1): 141-4.

Weaver, T. M., D. G. Levitt, et al. (1995). "The multisubunit active site of fumarase C from Escherichia coli." Nat Struct Biol **2**(8): 654-62.

Wei, M. H., O. Toure, et al. (2005). "Novel mutations in FH and expansion of the spectrum of phenotypes expressed in families with hereditary leiomyomatosis and renal cell cancer." J Med Genet.

Wei, S., Z. Liang, et al. (2005). "Patterns of K-ras codon 12 and 13 mutations found in pancreatic adenocarcinoma of 30 Chinese patients by microdissection, PCR and direct sequencing." J Gastroenterol Hepatol **20**(1): 67-72.

Weinberg, R. A. (1995). "The retinoblastoma protein and cell cycle control." Cell **81**(3): 323-30.

Westermann, B. (2002). "Merging mitochondria matters: cellular role and molecular machinery of mitochondrial fusion." EMBO Rep **3**(6): 527-31.

Weston, G., A. C. Trajstman, et al. (2003). "Fibroids display an anti-angiogenic gene expression profile when compared with adjacent myometrium." Mol Hum Reprod **9**(9): 541-9.

Wharton, D. C. (1967). Methods in Enzymology.

Wilson, C., S. Idziaszczyk, et al. (2005). "A mouse model of tuberous sclerosis 1 showing background specific early post-natal mortality and metastatic renal cell carcinoma." Hum Mol Genet **14**(13): 1839-50.

Wolf, D. C., H. E. Whiteley, et al. (1995). "Preneoplastic and neoplastic lesions of rat hereditary renal cell tumours express markers of proximal and distal nephron." Vet Pathol **32**(4): 379-86.

Woodward, E. R., C. Eng, et al. (1997). "Genetic predisposition to phaeochromocytoma: analysis of candidate genes GDNF, RET and VHL." Hum Mol Genet **6**(7): 1051-6.

Wu, R., L. Lin, et al. (2003). "Amplification and overexpression of the L-MYC proto-oncogene in ovarian carcinomas." Am J Pathol **162**(5): 1603-10.

Wykoff, C. C., N. J. Beasley, et al. (2000). "Hypoxia-inducible expression of tumour-associated carbonic anhydrases." Cancer Res **60**(24): 7075-83.

Xin, H. B., K. Y. Deng, et al. (2002). "Smooth muscle expression of Cre recombinase and eGFP in transgenic mice." Physiol Genomics **10**(3): 211-5.

Yankovskaya, V., R. Horsefield, et al. (2003). "Architecture of succinate dehydrogenase and reactive oxygen species generation." Science **299**(5607): 700-4.

Yeo, H. and S. Roman (2005). "Pheochromocytoma and functional paraganglioma." Curr Opin Oncol **17**(1): 13-8.

Yeung, R. S., G. H. Xiao, et al. (1994). "Predisposition to renal carcinoma in the Eker rat is determined by germ-line mutation of the tuberous sclerosis 2 (TSC2) gene." Proc Natl Acad Sci U S A **91**(24): 11413-6.

Zbar, B., W. G. Alvord, et al. (2002). "Risk of renal and colonic neoplasms and spontaneous pneumothorax in the Birt-Hogg-Dube syndrome." Cancer Epidemiol Biomarkers Prev **11**(4): 393-400.

Zhang, Y., X. Gao, et al. (2003). "Rheb is a direct target of the tuberous sclerosis tumour suppressor proteins." Nat Cell Biol **5**(6): 578-81.

Zhuang, Z., P. Bertheau, et al. (1995). "A microdissection technique for archival DNA analysis of specific cell populations in lesions < 1 mm in size." Am J Pathol **146**(3): 620-5.

Zinn, A. B., D. S. Kerr, et al. (1986). "Fumarase deficiency: a new cause of mitochondrial encephalomyopathy." N Engl J Med **315**(8): 469-75.

10 Appendices:

10.1 List of publications from the work described in my thesis

1: Vanharanta S, **Pollard PJ**, Lehtonen HJ, Laiho P, *et al.* Distinct expression profile in fumarate-hydratase-deficient uterine fibroids. Hum Mol Genet. 2006 Jan 1;15(1):97-103.

2: **Pollard PJ**, Briere JJ, Alam NA, Barwell J, *et al.* Accumulation of Krebs cycle intermediates and over-expression of HIF1alpha in tumours which result from germline FH and SDH mutations. Hum Mol Genet. 2005 Aug 1;14(15):2231-9.

3: **Pollard P**, Wortham N, Barclay E, Alam A, *et al.* Evidence of increased microvessel density and activation of the hypoxia pathway in tumours from the hereditary leiomyomatosis and renal cell cancer syndrome. J Pathol. 2005 Jan;205(1):41-9.

4: **Pollard PJ**, Wortham NC, Tomlinson IP. The TCA cycle and tumourigenesis: the examples of fumarate hydratase and succinate dehydrogenase. Ann Med. 2003;35(8):632-9. Review.

5: Alam NA, Rowan AJ, Wortham NC, **Pollard PJ**, *et al.* Genetic and functional analyses of FH mutations in multiple cutaneous and uterine leiomyomatosis, hereditary leiomyomatosis and renal cancer, and fumarate hydratase deficiency. Hum Mol Genet. 2003 Jun 1;12(11):1241-52.

10.2 Microarray analysis of gene expression in HLRCC uterine leiomyomata and normal myometrium.

The fold change is the ratio of gene expression of the mean of 5 uterine leiomyomas (UL) to the myometrium (MYO) from an HLRCC patient

Gene Title	Gene Symbol	MYO	MEAN UL	FOLD CHANGE
calpain 6	CAPN6	52	820	15.68
calpain 6	CAPN6	125	1440	11.53
hypothetical protein FLJ20151		40	449	11.12
tumour necrosis factor receptor superfamily, member 21	TNFRSF21	35	344	9.72
collapsin response mediator protein 1	CRMP1	72	644	8.95
G protein-coupled receptor 20	GPR20	91	815	8.94
hypothetical protein		171	1489	8.69
transketolase (Wernicke-Korsakoff syndrome)	TKT	162	1305	8.04

reductase)	AKR1B10	148	1169	7.91
ferredoxin reductase	FDXR	27	187	7.07
KIAA1034 protein		31	216	7.07
solute carrier family 5 (inositol transporters), member 3	SLC5A3	248	1724	6.97
thymidylate synthetase	TYMS	82	566	6.88
diacylglycerol kinase, iota	DGKI	39	244	6.34
activating transcription factor 3	ATF3	90	564	6.26
cyclin-dependent kinase inhibitor 1A (p21, Cip1)	CDKN1A	160	976	6.11
carbonic anhydrase XII	CA12	189	1151	6.08
transketolase (Wernicke-Korsakoff syndrome)	TKT	288	1727	6.00
high-mobility group (nonhistone chromosomal) protein isoforms I and Y	HMGIY	68	384	5.63
stearoyl-CoA desaturase (delta-9-desaturase)	SCD	25	140	5.59
hypothetical protein FLJ21472		49	266	5.47
SRY (sex determining region Y)-box 4	SOX4	149	809	5.41
hypothetical protein FLJ21551		28	147	5.35

synaptosomal-associated protein, 25kD	SNAP25	51	270	5.29
CGI-111 protein		247	1299	5.27
mesenchymal stem cell protein DSC54		42	222	5.24
NAD(P)H dehydrogenase, quinone 1	NQO1	111	562	5.06
NAD(P)H dehydrogenase, quinone 1	NQO1	25	126	4.98
reticulon 1	RTN1	44	213	4.85
prostate differentiation factor		27	132	4.82
sorting nexin 10	SNX10	45	217	4.80
protein kinase C, beta 1	PRKCB1	31	143	4.67
serine protease inhibitor, Kunitz type 1	SPINT1	34	154	4.61
collagen, type XIV, alpha 1 (undulin)	COL14A1	32	147	4.54
Norrie disease (pseudoglioma)	NDP	28	125	4.45
integral membrane protein 3		166	727	4.39
bridging integrator 1	BIN1	89	385	4.33
proprotein convertase subtilisin/kexin type 1 inhibitor	PCSK1N	79	341	4.29
glioma pathogenesis-related protein		39	167	4.26
insulin receptor substrate 1	IRS1	125	531	4.26

BCL2/adenovirus E1B 19kD interacting protein 3	BNIP3	63	268	4.23
carbonyl reductase		77	321	4.19
hypothetical protein FLJ12377		26	109	4.17
solute carrier family 7 (cationic amino acid transporter, y+ system), member 8	SLC7A8	83	344	4.15
protein tyrosine phosphatase, receptor type, U	PTPRU	35	147	4.14
dickkopf homolog 2 (Xenopus laevis)	DKK2	29	117	4.06
tropomodulin	TMOD	162	650	4.01
heme oxygenase (decycling) 1	HMOX1	35	139	3.94
glutamate receptor, ionotropic, N-methyl D-aspartate 2A	GRIN2A	35	137	3.93
eukaryotic translation initiation factor 2, subunit 3 (gamma, 52kD)	EIF2S3	37	144	3.87
integrin, alpha 8	ITGA8	114	438	3.84
37 kDa leucine-rich repeat (LRR) protein		73	281	3.83
insulin-like growth factor binding protein 5	IGFBP5	67	255	3.79
bridging integrator 1	BIN1	222	839	3.79
endothelin receptor type A	EDNRA	200	756	3.79

cytoplasmic polyadenylation element binding protein		33	124	3.75
KIAA0215 gene product		44	165	3.74
synaptosomal-associated protein, 25kD	SNAP25	61	226	3.73
hypothetical protein FLJ11539		45	165	3.71
twist homolog (acrocephalosyndactyly 3; Saethre-Chotzen syndrome) (Drosophila)	TWIST	41	152	3.70
apolipoprotein E	APOE	75	278	3.68
bromodomain adjacent to zinc finger domain, 2A	BAZ2A	31	111	3.63
hypothetical protein MGC12904		31	111	3.60
tropomodulin	TMOD	162	581	3.60
reticulon 1	RTN1	60	215	3.59
neuromedin B	NMB	53	190	3.58
collectin sub-family member 12	COLEC12	89	320	3.58
calcium channel, voltage-dependent, P/Q type, alpha 1A subunit	CACNA1A	63	223	3.57
Sam68-like phosphotyrosine protein, T-STAR		116	410	3.54
LIM domain protein		56	199	3.54

bridging integrator 1	BIN1	332	1152	3.47
sequestosome 1	SQSTM1	618	2141	3.46
apolipoprotein E	APOE	71	243	3.42
vascular endothelial growth factor	VEGF	312	1064	3.42
hypothetical protein FLJ22195		36	122	3.42
deleted in bladder cancer chromosome region candidate 1	DBCCR1	42	143	3.40
KIAA1277 protein		29	100	3.40
mannose-P-dolichol utilization defect 1	MPDU1	44	151	3.40
src homology three (SH3) and cysteine rich domain	STAC	111	372	3.35
matrix metalloproteinase 11 (stromelysin 3)	MMP11	64	212	3.32
pyruvate kinase, muscle	PKM2	519	1720	3.32
chromosome 1 open reading frame 21	C1orf21	69	227	3.31
brain-specific angiogenesis inhibitor 2	BAI2	55	181	3.30
mitogen-activated protein kinase kinase kinase 14	MAP3K14	49	161	3.28
slug homolog, zinc finger protein (chicken)	SLUG	222	726	3.27
regulator of G-protein signalling 2, 24kD	RGS2	977	3196	3.27
adipose differentiation-related protein	ADFP	250	816	3.27

histone deacetylase 5	HDAC5	96	311	3.25
cyclic AMP phosphoprotein, 19 kD		68	221	3.25
microtubule-associated protein tau	MAPT	37	119	3.23
transmembrane 4 superfamily member (tetraspan NET-7)		53	171	3.23
microfibrillar-associated protein 2	MFAP2	153	490	3.21
nuclear receptor subfamily 1, group D, member 1	NR1D1	139	447	3.21
cytokine inducible SH2-containing protein	CISH	67	214	3.20
sialyltransferase 4A (beta-galactosidase alpha-2,3-sialytransferase)	SIAT4A	27	87	3.19
hypothetical protein FLJ10633		133	425	3.19
hypothetical protein FLJ11736		31	99	3.19
tumour protein p53 (Li-Fraumeni syndrome)	TP53	79	251	3.19
solute carrier family 16 (monocarboxylic acid transporters), member 1	SLC16A1	42	134	3.18
protein tyrosine phosphatase, receptor type, D	PTPRD	28	89	3.17
vascular endothelial growth factor	VEGF	84	267	3.16
BCL2/adenovirus E1B 19kD interacting protein 3	BNIP3	164	518	3.16

matrix metalloproteinase 9 (gelatinase B, 92kD gelatinase, 92kD type IV collagenase)	MMP9	29	91	3.16
Rag D protein		58	182	3.15
pleckstrin homology-like domain, family A, member 1	PHLDA1	27	86	3.14
damage-specific DNA binding protein 2 (48kD)	DDB2	135	422	3.13
aldolase C, fructose-bisphosphate	ALDOC	77	241	3.13
amiloride-sensitive cation channel 2, neuronal	ACCN2	27	85	3.13
IGF-II mRNA-binding protein 2		62	193	3.12
bromodomain adjacent to zinc finger domain, 1A	BAZ1A	38	118	3.11
nuclear factor of activated T-cells, cytoplasmic, calcineurin-dependent 4	NFATC4	34	104	3.11
synuclein, alpha (non A4 component of amyloid precursor)	SNCA	73	228	3.11
vascular Rab-GAP/TBC-containing		186	577	3.10
glutamyl aminopeptidase (aminopeptidase A)	ENPEP	86	264	3.08
glutamate-cysteine ligase, modifier subunit	GCLM	61	187	3.08
hypothetical protein DKFZp434P2235		107	330	3.08
cysteine and glycine-rich protein 2	CSRP2	197	605	3.07

KIAA1277 protein	KIAA1277	51	156	3.07
cysteine and glycine-rich protein 2	CSRP2	218	665	3.06
collagen, type XIV, alpha 1 (undulin)	COL14A1	71	215	3.05
heterogeneous nuclear ribonucleoprotein L	HNRPL	47	143	3.04
endothelin receptor type A	EDNRA	151	454	3.02
gemin 6		35	106	3.02
tumour necrosis factor receptor superfamily, member 6	TNFRSF6	155	466	3.01
lifeguard		31	92	3.00
BTB and CNC homology 1, basic leucine zipper transcription factor 2	BACH2	84	251	2.99
synuclein, alpha interacting protein (synphilin)	SNCAIP	322	961	2.98
NAD(P)H dehydrogenase, quinone 1	NQO1	113	338	2.98
hypothetical protein FLJ20373		153	456	2.98
thymosin, beta, identified in neuroblastoma cells		35	104	2.98
vascular endothelial growth factor	VEGF	69	205	2.97
KIAA1025 protein		94	277	2.96
cAMP response element-binding protein CRE-BPa		27	80	2.96

chromosome 20 open reading frame 180	C20orf180	80	236	2.96
hypoxanthine phosphoribosyltransferase 1 (Lesch-Nyhan syndrome)	HPRT1	32	94	2.95
transferrin receptor (p90, CD71)	TFRC	223	652	2.92
protein tyrosine phosphatase type IVA, member 1	PTP4A1	38	112	2.92
hypothetical protein FLJ10847		50	147	2.92
superoxide dismutase 3, extracellular	SOD3	330	961	2.92
solute carrier family 16 (monocarboxylic acid transporters), member 3	SLC16A3	50	144	2.89
guanidinoacetate N-methyltransferase	GAMT	28	81	2.89
transferrin receptor (p90, CD71)	TFRC	231	665	2.88
Ets2 repressor factor	ERF	38	109	2.86
SEC14-like 1 (S. cerevisiae)	SEC14L1	41	118	2.85
activated p21cdc42Hs kinase		83	235	2.85
nucleolar protein 3 (apoptosis repressor with CARD domain)	NOL3	62	175	2.85
matrix metalloproteinase 14 (membrane-inserted)	MMP14	34	98	2.85

mesenchymal stem cell protein DSC43		44	125	2.84
phosphoglycerate dehydrogenase	PHGDH	90	255	2.84
hypothetical protein MGC5618		82	232	2.84
cytochrome P450 retinoid metabolizing protein		53	149	2.83
phosphofructokinase, platelet	PFKP	530	1499	2.83
MYC-associated zinc finger protein (purine-binding transcription factor)	MAZ	32	91	2.81
glutamyl aminopeptidase (aminopeptidase A)	ENPEP	65	181	2.81
mitochondrial ribosomal protein L2	MRPL2	62	173	2.80
cytochrome P450, subfamily I (dioxin-inducible), polypeptide 1 (glaucoma 3, primary infantile)	CYP1B1	173	483	2.80
calcium/calmodulin-dependent protein kinase I	CAMK1	71	198	2.79
protocadherin gamma subfamily C, 3	PCDHGC3	43	119	2.78
PET112-like (yeast)	PET112L	33	92	2.78
syntaxin 1A (brain)	STX1A	42	117	2.77
ATP-binding cassette, sub-family B (MDR/TAP), member 6	ABCB6	61	167	2.76
Pirin		91	250	2.76

KIAA0876 protein		50	137	2.76
prohibitin	PHB	145	398	2.75
sirtuin silent mating type information regulation 2 homolog 6 (S. cerevisiae)	SIRT6	47	130	2.75
ATPase, Na+/K+ transporting, beta 1 polypeptide	ATP1B1	454	1248	2.75
prostaglandin-endoperoxide synthase 1 (prostaglandin G/H synthase and cyclooxygenase)	PTGS1	58	160	2.74
synuclein, alpha (non A4 component of amyloid precursor)	SNCA	34	93	2.74
G protein-coupled receptor 56	GPR56	92	251	2.73
A kinase (PRKA) anchor protein 10	AKAP10	26	71	2.71
BTG family, member 3	BTG3	309	838	2.71
HSPC157 protein		33	90	2.71
KIAA1030 protein		68	183	2.70
solute carrier family 8 (sodium-calcium exchanger), member 2	SLC8A2	25	68	2.70
S164 protein		43	117	2.69
prostaglandin I2 (prostacyclin) synthase	PTGIS	71	190	2.68

cytochrome P450, subfamily I (dioxin-inducible), polypeptide 1 (glaucoma 3, primary infantile)	CYP1B1	124	331	2.67
SRY (sex determining region Y)-box 4	SOX4	111	296	2.67
deformed epidermal autoregulatory factor 1 (Drosophila)	DEAF1	89	238	2.66
fibrillin 2 (congenital contractural arachnodactyly)	FBN2	66	176	2.66
carnitine palmitoyltransferase I, muscle	CPT1B	27	72	2.66
fatty acid binding protein 3, muscle and heart (mammary-derived growth inhibitor)	FABP3	43	113	2.66
similar to H2A histone family, member A (H. sapiens)		79	208	2.65
protein kinase C, beta 1	PRKCB1	85	226	2.65
macrophage migration inhibitory factor (glycosylation-inhibiting factor)	MIF	842	2225	2.64
NADPH oxidase, EF hand calcium-binding domain 5	NOX5	26	69	2.63
chromosome 21 open reading frame 45	C21orf45	36	95	2.63
collagen, type VII, alpha 1 (epidermolysis bullosa, dystrophic, dominant and recessive)	COL7A1	32	83	2.62
hypothetical protein FLJ12929		58	152	2.62

carbonic anhydrase XI	CA11	84	218	2.61
hypothetical protein FLJ20113		28	72	2.61
KIAA0346 protein		29	77	2.61
cerebellin 1 precursor	CBLN1	26	67	2.60
PRO0641 protein		32	83	2.60
KIAA0411 gene product		45	117	2.60
TAF15 RNA polymerase II, TATA box binding protein (TBP)-associated factor, 68 kD	TAF15	77	200	2.60
protein predicted by clone 23627		76	196	2.60
phosphogluconate dehydrogenase	PGD	84	218	2.59
CDC28 protein kinase 2	CKS2	31	80	2.58
fibrinogen-like 2	FGL2	243	628	2.58
hypothetical protein FLJ20984		182	470	2.58
receptor tyrosine kinase-like orphan receptor 1	ROR1	69	178	2.57
B-cell CLL/lymphoma 2	BCL2	216	557	2.57
hypothetical protein FLJ20539		69	177	2.57
hypothetical protein FLJ10254		43	111	2.57

KIAA0712 gene product		30	76	2.56
TERA protein		426	1092	2.56
A kinase (PRKA) anchor protein 1	AKAP1	279	715	2.56
glioma pathogenesis-related protein		130	333	2.56
spondin 2, extracellular matrix protein	SPON2	407	1039	2.55
hypothetical protein PP1044		382	975	2.55
solute carrier family 2 (facilitated glucose transporter), member 1	SLC2A1	89	228	2.55
triosephosphate isomerase 1	TPI1	1148	2931	2.55
MAP/microtubule affinity-regulating kinase like 1	MARKL1	51	131	2.55
jun D proto-oncogene	JUND	86	219	2.55
KIAA0552 gene product		58	148	2.55
ankyrin 3, node of Ranvier (ankyrin G)	ANK3	158	401	2.54
proprotein convertase subtilisin/kexin type 7	PCSK7	28	70	2.54
CCAAT/enhancer binding protein (C/EBP), alpha	CEBPA	45	114	2.54
protocadherin gamma subfamily A, 11	PCDHGA11	40	100	2.53
putative T1/ST2 receptor binding protein		84	213	2.53

mitogen-activated protein kinase 7	MAPK7	47	117	2.52
hypothetical protein		46	115	2.52
hypothetical protein FLJ21324		236	594	2.52
solute carrier family 6 (neurotransmitter transporter, creatine), member 8	SLC6A8	145	365	2.52
ELKL motif kinase	EMK1	31	79	2.51
synuclein, alpha (non A4 component of amyloid precursor)	SNCA	37	93	2.51
tyrosine 3-monooxygenase/tryptophan 5-monooxygenase activation protein, epsilon polypeptide	YWHAE	76	191	2.51
small nuclear RNA activating complex, polypeptide 2, 45kD	SNAPC2	54	135	2.50
ligase I, DNA, ATP-dependent	LIG1	29	73	2.50
epithelial membrane protein 3	EMP3	336	838	2.49
putative DNA/chromatin binding motif		73	181	2.49
CSR1 protein		222	553	2.49
matrix metalloproteinase 2 (gelatinase A, 72kD gelatinase, 72kD type IV collagenase)	MMP2	741	1843	2.49
CGI-130 protein		385	959	2.49

hypothetical protein FLJ20707		46	115	2.49
procollagen-proline, 2-oxoglutarate 4-dioxygenase (proline 4-hydroxylase), alpha polypeptide I	P4HA1	213	528	2.49
ALL1-fused gene from chromosome 1q		253	627	2.48
connexin-36		25	62	2.47
cell division cycle 34	CDC34	179	441	2.46
guanine nucleotide binding protein 4	GNG4	26	63	2.46
zinc-finger protein DZIP1		71	174	2.46
KIAA0195 gene product		74	182	2.46
glucose-6-phosphate dehydrogenase	G6PD	77	189	2.46
x 009 protein		44	107	2.45
kinesin family member 5C	KIF5C	105	258	2.45
heparan sulfate (glucosamine) 3-O-sulfotransferase 2	HS3ST2	36	87	2.45
nucleosomal binding protein 1	NSBP1	32	78	2.45
special AT-rich sequence binding protein 1 (binds to nuclear matrix/scaffold-associating DNA's)	SATB1	145	355	2.44
phosphatidylinositol-4-phosphate 5-kinase, type I, alpha	PIP5K1A	58	141	2.44

transcription factor 3 (E2A immunoglobulin enhancer binding factors E12/E47)	TCF3	35	85	2.43
transmembrane protein 2	TMEM2	44	107	2.43
pyruvate dehydrogenase phosphatase		45	109	2.43
hypothetical protein FLJ10493		29	71	2.42
carbonyl reductase 1	CBR1	169	409	2.42
6-phosphofructo-2-kinase/fructose-2,6-biphosphatase 3	PFKFB3	102	246	2.42
matrix metalloproteinase 14 (membrane-inserted)	MMP14	134	323	2.41
ESTs, Weakly similar to AF208855 1 BM-013 [H.sapiens]		38	91	2.41
hypothetical protein FLJ11160		48	114	2.39
KIAA0717 protein		39	94	2.39
chromosome 21 open reading frame 91	C21orf91	30	72	2.39
eukaryotic translation initiation factor 5A	EIF5A	101	240	2.39
ortholog of rat pippin		143	341	2.38
low density lipoprotein-related protein 1 (alpha-2-macroglobulin receptor)	LRP1	101	241	2.38
hypothetical protein FLJ13848		45	106	2.38

TYRO3 protein tyrosine kinase	TYRO3	93	220	2.38
leukocyte receptor cluster (LRC) member 4		70	167	2.37
collagen, type IV, alpha 6	COL4A6	265	628	2.37
ATPase, H+ transporting, lysosomal (vacuolar proton pump), member D	ATP6D	567	1341	2.37
myo-inositol 1-phosphate synthase A1		191	453	2.37
pellino homolog 2 (Drosophila)	PELI2	79	187	2.36
secreted frizzled-related protein 4	SFRP4	100	236	2.36
tumour necrosis factor receptor superfamily, member 10b	TNFRSF10B	80	189	2.36
cell cycle progression 2 protein		26	62	2.36
KIAA0712 gene product		79	186	2.36
protein phosphatase 2A, regulatory subunit B' (PR 53)	PPP2R4	159	373	2.36
inhibitor of DNA binding 4, dominant negative helix-loop-helix protein	ID4	209	491	2.35
ATP-binding cassette, sub-family C (CFTR/MRP), member 1	ABCC1	62	145	2.35
hypothetical protein		259	609	2.35

DNA-dependent protein kinase catalytic subunit-interacting protein 2		51	120	2.35
KIAA0144 gene product		133	312	2.34
hypothetical protein FLJ23312		46	108	2.34
partner of RAC1 (arfaptin 2)		124	290	2.34
endothelin receptor type A	EDNRA	701	1639	2.34
low density lipoprotein-related protein 1 (alpha-2-macroglobulin receptor)	LRP1	187	436	2.33
tubulin, alpha 1 (testis specific)	TUBA1	287	669	2.33
F-box protein FBG4		49	115	2.33
heparan sulfate 2-O-sulfotransferase 1	HS2ST1	90	210	2.32
eukaryotic translation initiation factor 5A	EIF5A	86	199	2.31
cytochrome P450, subfamily I (dioxin-inducible), polypeptide 1 (glaucoma 3, primary infantile)	CYP1B1	457	1055	2.31
DKFZP566C0424 protein		85	196	2.31
Wilms tumour associated protein		98	226	2.31
ATPase, Na+/K+ transporting, beta 1 polypeptide	ATP1B1	425	980	2.31

chromobox homolog 6	CBX6	617	1423	2.30
hypothetical protein AF311304		47	108	2.30
integrin, beta 3 (platelet glycoprotein IIIa, antigen CD61)	ITGB3	38	87	2.29
GATA binding protein 6	GATA6	163	374	2.29
cyclin-E binding protein 1		135	308	2.29
MAGE-E1 protein		76	173	2.28
hypothetical protein FLJ12484		51	117	2.28
SCO cytochrome oxidase deficient homolog 2 (yeast)	SCO2	36	83	2.28
hypothetical protein 384D8_6		26	60	2.27
mitogen-activated protein kinase 8 interacting protein 1	MAPK8IP1	32	73	2.27
PHD finger protein 1	PHF1	85	192	2.27
ring finger protein 24	RNF24	86	196	2.27
putative DNA binding protein		27	61	2.26
ubiquinol-cytochrome c reductase binding protein	UQCRB	55	124	2.26
p21 (CDKN1A)-activated kinase 3	PAK3	56	127	2.26
nucleoporin 62kD	NUP62	46	103	2.26
procollagen-proline, 2-oxoglutarate 4-dioxygenase (proline				

4-hydroxylase), alpha polypeptide II				
hypothetical protein DKFZp547M136 similar to widely-interspaced zinc finger motifs		30	67	2.25
epoxide hydrolase 1, microsomal (xenobiotic)	EPHX1	770	1733	2.25
bone gamma-carboxyglutamate (gla) protein (osteocalcin)	BGLAP	34	77	2.25
ATPase, H+ transporting, lysosomal (vacuolar proton pump), alpha polypeptide, 70kD, isoform 1	ATP6A1	38	85	2.25
protein phosphatase 1, regulatory (inhibitor) subunit 3C	PPP1R3C	729	1638	2.25
retinol binding protein 4, plasma	RBP4	25	57	2.25
monocyte to macrophage differentiation-associated	MMD	133	300	2.25
hypothetical protein FLJ20550	FLJ20550	76	172	2.24
hypothetical protein FLJ20294		48	108	2.24
reticulon 2	RTN2	63	142	2.24
reticulon 2	RTN2	119	266	2.24
cAMP responsive element modulator	CREM	78	175	2.24
adenylate kinase 3	AK3	120	269	2.24
trichorhinophalangeal syndrome I	TRPS1	95	212	2.24

fibroblast growth factor receptor 1 (fms-related tyrosine kinase 2, Pfeiffer syndrome)	FGFR1	26	58	2.24
hypothetical protein FLJ20624		37	84	2.23
ferritin, heavy polypeptide 1	FTH1	3070	6845	2.23
carbohydrate (N-acetylglucosamine-6-O) sulfotransferase 2	CHST2	50	111	2.23
LIM domains containing 1	LIMD1	44	97	2.23
cytoplasmic linker 2	CYLN2	81	181	2.23
procollagen-lysine, 2-oxoglutarate 5-dioxygenase (lysine hydroxylase) 2	PLOD2	186	414	2.22
H2B histone family, member Q	H2BFQ	47	105	2.22
secreted frizzled-related protein 1	SFRP1	52	116	2.22
TSC-22-like		53	117	2.22
TGFB-induced factor (TALE family homeobox)	TGIF	145	323	2.22
neuro-oncological ventral antigen 1	NOVA1	66	147	2.22
four and a half LIM domains 3	FHL3	78	172	2.22
NGFI-A binding protein 2 (EGR1 binding protein 2)	NAB2	91	202	2.22
SRY (sex determining region Y)-box 4	SOX4	470	1036	2.21

dystrobrevin, alpha	DTNA	40	89	2.21
hypothetical protein FLJ10628		79	174	2.20
dopamine receptor D2	DRD2	31	68	2.20
carnitine palmitoyltransferase I, muscle	CPT1B	31	69	2.20
DKFZP434N014 protein	DKFZP434N014	30	66	2.20
CK2 interacting protein 1; HQ0024c protein		155	340	2.20
GLI-Kruppel family member GLI3 (Greig cephalopolysyndactyly syndrome)	GLI3	179	392	2.19
transforming growth factor, beta receptor III (betaglycan, 300kD)	TGFBR3	460	1008	2.19
anti-oxidant protein 2		745	1630	2.19
KIAA1361 protein		115	251	2.19
hypothetical protein		28	62	2.19
amiloride-sensitive cation channel 3, testis	ACCN3	25	56	2.19
PRO0457 protein		31	67	2.18
visinin-like 1	VSNL1	52	114	2.18
apolipoprotein L, 2	APOL2	33	72	2.18

HCNP protein; XPA-binding protein 2		42	90	2.18
myeloid leukemia factor 1	MLF1	52	113	2.17
protein phosphatase 2A, regulatory subunit B' (PR 53)	PPP2R4	158	343	2.17
gem (nuclear organelle) associated protein 4	GEMIN4	34	73	2.16
ribosomal protein S10-like	RPS10L	258	557	2.16
KIAA0076 gene product		36	77	2.16
RNA binding motif protein 8A	RBM8A	31	68	2.16
programmed cell death 4 (neoplastic transformation inhibitor)	PDCD4	86	185	2.16
Cdc42 effector protein 4; binder of Rho GTPases 4		137	294	2.16
hypothetical protein		39	83	2.15
histone deacetylase 9		96	208	2.15
Rag D protein		36	78	2.15
chondroitin sulfate proteoglycan 4 (melanoma-associated)	CSPG4	38	82	2.15
interleukin enhancer binding factor 3, 90kD	ILF3	99	212	2.15
downstream neighbor of SON	DONSON	80	171	2.15
olfactomedin 1	OLFM1	132	283	2.15

chromosome 21 open reading frame 2	C21orf2	30	65	2.15
DKFZP586N0721 protein		147	317	2.15
carbonic anhydrase IV	CA4	26	56	2.15
leucine-rich and death domain containing	LRDD	40	85	2.15
growth arrest and DNA-damage-inducible, gamma	GADD45G	42	91	2.15
hypothetical protein FLJ13373		26	56	2.14
spermine synthase	SMS	135	288	2.14
carbonyl reductase 3	CBR3	114	245	2.14
hypothetical protein MGC3035		189	405	2.14
estrogen receptor 1	ESR1	43	92	2.14
adrenomedullin	ADM	73	157	2.14
KIAA0876 protein		101	216	2.14
alveolar soft part sarcoma chromosome region, candidate 1	ASPSCR1	43	92	2.14
prostaglandin-endoperoxide synthase 1 (prostaglandin G/H synthase and cyclooxygenase)	PTGS1	68	145	2.13
cell division cycle 2, G1 to S and G2 to M	CDC2	31	67	2.13
hypothetical protein FLJ12800		34	73	2.13

dishevelled, dsh homolog 2 (Drosophila)	DVL2	32	69	2.13
KIAA0363 protein		39	83	2.13
hypothetical protein FLJ20043		230	488	2.13
U2 small nuclear ribonucleoprotein auxiliary factor (65kD)		174	370	2.12
calcium channel, voltage-dependent, beta 3 subunit	CACNB3	113	241	2.12
phosphofructokinase, liver	PFKL	126	267	2.12
hypothetical protein FLJ20604		90	190	2.12
centaurin, delta 1	CENTD1	69	147	2.12
chitinase 3-like 2	CHI3L2	27	57	2.12
hypothetical protein MGC17330		185	393	2.12
protein tyrosine phosphatase type IVA, member 1	PTP4A1	128	271	2.12
creatine kinase, mitochondrial 2 (sarcomeric)	CKMT2	26	56	2.12
jerky (mouse) homolog	JRK	67	142	2.12
KIAA0945 protein		68	145	2.11
C-terminal binding protein 1	CTBP1	172	364	2.11
pleckstrin homology-like domain, family A, member 3	PHLDA3	119	250	2.11
5-hydroxytryptamine (serotonin) receptor 2B	HTR2B	91	192	2.11

kaptin (actin binding protein)	KPTN	48	100	2.11
ring finger protein 24	RNF24	59	125	2.11
ELK1, member of ETS oncogene family	ELK1	31	65	2.11
uridine phosphorylase	UP	31	64	2.11
spastic paraplegia 7, paraplegin (pure and complicated autosomal recessive)	SPG7	146	307	2.11
hypothetical protein FLJ22195		106	224	2.10
thousand and one amino acid protein kinase		36	76	2.10
parathyroid hormone receptor 1	PTHR1	79	167	2.10
aldolase A, fructose-bisphosphate	ALDOA	1826	3839	2.10
uncharacterized hematopoietic stem/progenitor cells protein MDS032		49	102	2.10
interleukin 11 receptor, alpha	IL11RA	147	307	2.09
hypothetical protein FLJ20244		67	140	2.09
carcinoembryonic antigen-related cell adhesion molecule 1 (biliary glycoprotein)	CEACAM1	27	57	2.08
chromobox homolog 4 (Pc class homolog, Drosophila)	CBX4	31	65	2.08

Ras-GTPase activating protein SH3 domain-binding protein 2		38	79	2.08
KIAA0138 gene product		38	78	2.08
transcription factor 3 (E2A immunoglobulin enhancer binding factors E12/E47)	TCF3	86	180	2.08
phosphatidylinositol 4-kinase, catalytic, beta polypeptide	PIK4CB	66	138	2.08
KIAA0682 gene product		36	74	2.08
KIAA0677 gene product		63	130	2.08
PDZ domain containing guanine nucleotide exchange factor(GEF)1		74	153	2.07
hook2 protein		83	173	2.07
KIAA0557 protein		34	71	2.07
pim-1 oncogene	PIM1	89	185	2.07
chromosome 16 open reading frame 7	C16orf7	37	77	2.07
topoisomerase (DNA) I	TOP1	25	52	2.07
Homo sapiens mRNA; cDNA DKFZp564O1763 (from clone DKFZp564O1763)		33	67	2.07

C/EBP-induced protein		306	634	2.07
high-mobility group 20B	HMG20B	63	131	2.07
casein kinase 1, gamma 2	CSNK1G2	118	244	2.07
pleckstrin homology-like domain, family A, member 1	PHLDA1	30	62	2.07
secreted frizzled-related protein 1	SFRP1	200	411	2.06
myoglobin	MB	28	57	2.06
MAD, mothers against decapentaplegic homolog 3 (Drosophila)	MADH3	41	85	2.06
RNA polymerase I 16 kDa subunit		396	813	2.05
c-src tyrosine kinase	CSK	119	243	2.05
amyloid beta (A4) precursor protein-binding, family A, member 2 binding protein	APBA2BP	65	134	2.05
zinc finger protein 278	ZNF278	53	109	2.05
eukaryotic translation elongation factor 1 delta (guanine nucleotide exchange protein)	EEF1D	846	1733	2.05
hypothetical protein FLJ11323		60	122	2.05
early growth response 2 (Krox-20 homolog, Drosophila)	EGR2	31	63	2.04

p53 regulated PA26 nuclear protein		249	509	2.04
postmeiotic segregation increased 2-like 11	PMS2L11	95	193	2.04
contactin associated protein 1	CNTNAP1	186	378	2.04
ESTs, Weakly similar to dJ309K20.4 [H.sapiens]		37	75	2.04
a disintegrin and metalloproteinase domain 19 (meltrin beta)	ADAM19	87	176	2.04
zinc finger protein 212	ZNF212	82	166	2.03
hepcidin antimicrobial peptide	HAMP	26	52	2.03
adenylate kinase 1	AK1	279	568	2.03
ATP-binding cassette, sub-family A (ABC1), member 1	ABCA1	83	169	2.03
glycine receptor, beta	GLRB	63	129	2.03
hypothetical protein FLJ11807		42	85	2.03
calcium channel, voltage-dependent, beta 3 subunit	CACNB3	110	224	2.03
cyclic AMP phosphoprotein, 19 kD		63	128	2.03
RNA polymerase I transcription factor RRN3		35	70	2.03
stratifin	SFN	54	109	2.03
guanine nucleotide binding protein (G protein), beta 5	GNB5	98	200	2.03
KIAA1449 protein		50	101	2.03

HSPC002 protein		73	149	2.03
discs, large (Drosophila) homolog 3 (neuroendocrine-dlg)	DLG3	26	53	2.02
hypothetical protein FLJ22059		32	65	2.02
G protein-coupled receptor kinase-interactor 1	GIT1	68	137	2.02
modulator recognition factor I		111	223	2.02
smoothened homolog (Drosophila)	SMOH	69	139	2.02
serine protease inhibitor, Kazal type, 5	SPINK5	53	108	2.02
chromosome 5 open reading frame 6	C5orf6	229	461	2.02
pannexin 1	PANX1	71	143	2.02
H2A histone family, member O	H2AFO	50	100	2.02
tumour necrosis factor receptor superfamily, member 6b, decoy	TNFRSF6B	31	62	2.02
androgen receptor	AR	114	230	2.02
scaffold attachment factor B	SAFB	29	58	2.02
stress 70 protein chaperone, microsome-associated, 60kD	STCH	73	147	2.01
carcinoembryonic antigen-related cell adhesion molecule 1 (biliary glycoprotein)	CEACAM1	62	125	2.01

ceroid-lipofuscinosis, neuronal 3, juvenile (Batten, Spielmeyer-Vogt disease)	CLN3	96	193	2.01
solute carrier family 4, anion exchanger, member 2	SLC4A2	81	164	2.01
KIAA0557 protein	KIAA0557	62	124	2.01
poly(A) binding protein, nuclear 1	PABPN1	107	215	2.01
chromosome 10 open reading frame 2	C10orf2	38	77	2.01
protein tyrosine phosphatase type IVA, member 1	PTP4A1	46	92	2.01
platelet-activating factor acetylhydrolase, isoform Ib, gamma subunit (29kD)	PAFAH1B3	29	58	2.00
KIAA0672 gene product		44	88	2.00
mitochondrial ribosomal protein L19	MRPL19	25	50	2.00
EphB4	EPHB4	64	129	2.00
Wolf-Hirschhorn syndrome candidate 2	WHSC2	61	122	2.00
plasminogen activator, urokinase	PLAU	165	88	0.53
hippocalcin-like 1	HPCAL1	205	109	0.53
ras homolog gene family, member D	ARHD	73	39	0.53
interferon induced transmembrane protein 2 (1-8D)	IFITM2	3782	2000	0.53

putative UDP-GalNAc:polypeptide N-acetylgalactosaminyltransferase T9		167	88	0.53
DKFZP564F0522 protein		678	358	0.53
hypothetical protein FLJ20731		89	47	0.53
solute carrier family 21 (prostaglandin transporter), member 2	SLC21A2	923	487	0.53
complement component 6	C6	55	29	0.53
acyloxyacyl hydrolase (neutrophil)	AOAH	53	28	0.53
TNF-induced protein		167	88	0.53
hypothetical protein from clone 643		148	78	0.53
ferredoxin 1	FDX1	72	38	0.53
desmoplakin (DPI, DPII)	DSP	65	34	0.53
growth differentiation factor 3	GDF3	49	26	0.53
inositol 1,4,5-triphosphate receptor, type 3	ITPR3	68	36	0.53
epithelial membrane protein 1	EMP1	416	219	0.53
Ras association (RalGDS/AF-6) domain family 1	RASSF1	136	72	0.52
phospholipase C, gamma 2 (phosphatidylinositol-specific)	PLCG2	171	90	0.52

muscleblind-like (Drosophila)	MBNL	1220	639	0.52
DnaJ (Hsp40) homolog, subfamily B, member 4	DNAJB4	224	117	0.52
peripheral myelin protein 22	PMP22	1683	881	0.52
ribosomal protein S6 kinase, 90kD, polypeptide 2	RPS6KA2	384	201	0.52
glypican 4	GPC4	170	89	0.52
microtubule-actin crosslinking factor 1	MACF1	1142	597	0.52
tumour suppressor deleted in oral cancer-related 1		117	61	0.52
erythrocyte membrane protein band 4.1-like 2	EPB41L2	613	320	0.52
tropomyosin 1 (alpha)	TPM1	6327	3295	0.52
DKFZp434J1813 protein		92	48	0.52
endoglin (Osler-Rendu-Weber syndrome 1)	ENG	714	371	0.52
phosphatase and tensin homolog (mutated in multiple advanced cancers 1)	PTEN	279	145	0.52
putative protein kinase NY-REN-64 antigen		62	32	0.52
fumarate hydratase	FH	457	237	0.52
Cdc42 guanine nucleotide exchange factor (GEF) 9	ARHGEF9	165	85	0.52
inositol 1,4,5-triphosphate receptor, type 2	ITPR2	78	40	0.52

EMILIN-like protein EndoGlyx-1		392	203	0.52
melanoma cell adhesion molecule	MCAM	781	405	0.52
microtubule-actin crosslinking factor 1	MACF1	3071	1591	0.52
DKFZP564O123 protein		217	112	0.52
erythrocyte membrane protein band 4.1-like 3	EPB41L3	139	72	0.52
solute carrier family 29 (nucleoside transporters), member 1	SLC29A1	206	107	0.52
myomesin 1 (skelemin) (185kD)	MYOM1	70	36	0.52
apolipoprotein L, 1	APOL1	192	99	0.52
ATPase, Na+/K+ transporting, alpha 2 (+) polypeptide	ATP1A2	130	67	0.52
integrin, beta 4	ITGB4	200	104	0.52
protein kinase, AMP-activated, beta 1 non-catalytic subunit	PRKAB1	127	66	0.52
nuclear receptor subfamily 3, group C, member 1	NR3C1	738	381	0.52
lectin, galactoside-binding, soluble, 8 (galectin 8)	LGALS8	290	150	0.52
dual specificity phosphatase 14	DUSP14	375	194	0.52
cyclin D binding myb-like transcription factor 1	DMTF1	255	132	0.52
hypothetical protein		789	407	0.52
midline 1 (Opitz/BBB syndrome)	MID1	466	240	0.52

integrin, alpha 6	ITGA6	248	127	0.51
calcium channel, voltage-dependent, beta 2 subunit	CACNB2	77	39	0.51
muscleblind-like (Drosophila)	MBNL	277	142	0.51
interleukin 2 receptor, gamma (severe combined immunodeficiency)	IL2RG	82	42	0.51
chromosome 20 open reading frame 35	C20orf35	578	296	0.51
p300/CBP-associated factor	PCAF	182	93	0.51
multiple PDZ domain protein	MPDZ	277	142	0.51
ubiquitin specific protease 18	USP18	51	26	0.51
caspase 1, apoptosis-related cysteine protease (interleukin 1, beta, convertase)	CASP1	86	44	0.51
heme binding protein 1	HEBP1	829	424	0.51
synapsin I	SYN1	50	26	0.51
KDEL (Lys-Asp-Glu-Leu) endoplasmic reticulum protein retention receptor 3	KDELR3	270	138	0.51
annexin A11	ANXA11	753	385	0.51
myozenin 1	MYOZ1	70	36	0.51

PRKC, apoptosis, WT1, regulator	PAWR	593	302	0.51
hypothetical protein FLJ12150		194	99	0.51
pyruvate dehydrogenase (lipoamide) beta	PDHB	406	206	0.51
hypothetical protein MGC5149		569	289	0.51
complement component 3a receptor 1	C3AR1	194	98	0.51
degenerative spermatocyte homolog, lipid desaturase (Drosophila)	DEGS	489	248	0.51
selectin P (granule membrane protein 140kD, antigen CD62)	SELP	458	232	0.51
for protein disulfide isomerase-related		350	177	0.51
mitogen-activated protein kinase 10	MAPK10	367	186	0.51
CGI-109 protein		266	135	0.51
major histocompatibility complex, class I, E	HLA-E	1504	761	0.51
eukaryotic translation initiation factor 3, subunit 8 (110kD)	EIF3S8	1127	570	0.51
phosphoprotein enriched in astrocytes 15	PEA15	2191	1107	0.51
heptacellular carcinoma novel gene-3 protein		160	81	0.51
tumour rejection antigen (gp96) 1	TRA1	554	280	0.51

phosphodiesterase 10A	PDE10A	167	84	0.51
solute carrier family 2 (facilitated glucose transporter), member 3	SLC2A3	78	40	0.51
CD59 antigen p18-20	CD59	1718	868	0.51
butyrophilin, subfamily 3, member A3	BTN3A3	651	329	0.50
GTP-binding protein Rho7		62	31	0.50
myxovirus (influenza virus) resistance 2 (mouse)	MX2	90	46	0.50
potassium large conductance calcium-activated channel, subfamily M, beta member 1	KCNMB1	1696	854	0.50
ribokinase		50	25	0.50
homeo box B7	HOXB7	166	84	0.50
OLF-1/EBF associated zinc finger gene		293	147	0.50
phospholipase A2, group IIA (platelets, synovial fluid)	PLA2G2A	53	27	0.50
dimethylarginine dimethylaminohydrolase 2	DDAH2	491	246	0.50
SWAP-70 protein		247	123	0.50
adenylate cyclase 2 (brain)	ADCY2	225	112	0.50
major histocompatibility complex, class II, DR beta 5	HLA-DRB5	2362	1178	0.50

fer-1-like 3, myoferlin (C. elegans)	FER1L3	1089	543	0.50
TNF receptor-associated factor 5	TRAF5	717	357	0.50
dimethylarginine dimethylaminohydrolase 2	DDAH2	386	192	0.50
phosphorylase, glycogen; liver (Hers disease, glycogen storage disease type VI)	PYGL	132	65	0.50
hypothetical protein MGC11256		356	177	0.50
integrin-linked kinase	ILK	2496	1239	0.50
hypothetical protein FLJ20075		61	30	0.50
methyl-CpG binding domain protein 2	MBD2	515	256	0.50
L-3-hydroxyacyl-Coenzyme A dehydrogenase, short chain	HADHSC	599	297	0.50
tubulin, beta, 4		565	280	0.50
epithelial membrane protein 1	EMP1	295	146	0.50
ankyrin repeat domain 6	ANKRD6	105	52	0.50
major histocompatibility complex, class II, DP alpha 1	HLA-DPA1	1333	660	0.50
cystatin C (amyloid angiopathy and cerebral hemorrhage)	CST3	2286	1131	0.49
homeo box B2	HOXB2	364	180	0.49
hypothetical protein FLJ22471		1007	498	0.49

hypothetical protein FLJ20037		526	260	0.49
arachidonate 5-lipoxygenase	ALOX5	58	29	0.49
LIM domain only 4	LMO4	381	188	0.49
slit homolog 3 (Drosophila)	SLIT3	459	226	0.49
HIV-1 Tat interactive protein 2, 30 kD	HTATIP2	53	26	0.49
hypothetical protein		146	72	0.49
reticulocalbin 2, EF-hand calcium binding domain	RCN2	399	197	0.49
carboxypeptidase A3 (mast cell)	CPA3	277	136	0.49
F-box and leucine-rich repeat protein 5	FBXL5	529	260	0.49
Dmx-like 1	DMXL1	212	104	0.49
RAB33B, member RAS oncogene family	RAB33B	116	57	0.49
KIAA0475 gene product		387	190	0.49
hypothetical protein PRO0082		123	60	0.49
thymidine kinase 2, mitochondrial	TK2	161	79	0.49
delta sleep inducing peptide, immunoreactor	DSIPI	1071	525	0.49
hypothetical protein FLJ20568	FLJ20568	534	262	0.49
serum deprivation response (phosphatidylserine binding				

protein)				
aquaporin 1 (channel-forming integral protein, 28kD)	AQP1	1501	735	0.49
hypothetical protein PRO2032		632	309	0.49
epidermal growth factor receptor	EGFR	310	152	0.49
tight junction protein 1 (zona occludens 1)	TJP1	1230	601	0.49
fibulin 1	FBLN1	1050	512	0.49
target of myb1-like 1 (chicken)	TOM1L1	77	38	0.49
KIAA0941 protein		384	187	0.49
amyloid beta (A4) precursor protein-binding, family B, member 2 (Fe65-like)	APBB2	78	38	0.49
ATP-binding cassette, sub-family C (CFTR/MRP), member 4	ABCC4	83	41	0.49
serine (or cysteine) proteinase inhibitor, clade B (ovalbumin), member 9	SERPINB9	114	55	0.49
ADP-ribosylation factor-like 4	ARL4	201	98	0.49
MHC class I polypeptide-related sequence A	MICA	142	69	0.49
monokine induced by gamma interferon	MIG	93	45	0.49

fatty acid binding protein 5 (psoriasis-associated)	FABP5	130	63	0.49
myristoylated alanine-rich protein kinase C substrate	MARCKS	221	107	0.49
presenilin 2 (Alzheimer disease 4)	PSEN2	125	61	0.49
CS box-containing WD protein		471	228	0.49
claudin 17	CLDN17	64	31	0.48
solute carrier family 24 (sodium/potassium/calcium exchanger), member 1	SLC24A1	76	37	0.48
paraneoplastic antigen		96	46	0.48
interleukin 6 (interferon, beta 2)	IL6	57	28	0.48
ecotropic viral integration site 2B	EVI2B	78	37	0.48
FBJ murine osteosarcoma viral oncogene homolog B	FOSB	291	140	0.48
zinc finger protein 106		743	357	0.48
major histocompatibility complex, class II, DR alpha	HLA-DRA	1808	869	0.48
Cdc42 effector protein 3		417	201	0.48
claudin 5 (transmembrane protein deleted in velocardiofacial syndrome)	CLDN5	594	285	0.48
homeo box B7	HOXB7	65	31	0.48

UDP-glucose pyrophosphorylase 2	UGP2	1844	882	0.48
chromosome 21 open reading frame 7	C21orf7	99	47	0.48
3'-phosphoadenosine 5'-phosphosulfate synthase 2	PAPSS2	172	82	0.48
lectin, galactoside-binding, soluble, 8 (galectin 8)	LGALS8	132	63	0.48
Gardner-Rasheed feline sarcoma viral (v-fgr) oncogene homolog	FGR	96	46	0.48
carboxypeptidase E	CPE	488	232	0.48
complement component 1, s subcomponent	C1S	2313	1102	0.48
integrin, beta 4	ITGB4	54	26	0.48
hexabrachion (tenascin C, cytotactin)	HXB	1515	721	0.48
KIAA0746 protein		85	41	0.48
transmembrane 4 superfamily member (tetraspan NET-2)		106	51	0.48
hypothetical SBBI03 protein		117	55	0.47
integrin, alpha 7	ITGA7	514	244	0.47
phosphoinositide-3-kinase, catalytic, delta polypeptide	PIK3CD	132	62	0.47
single Ig IL-1R-related molecule		99	47	0.47
aspartylglucosaminidase	AGA	80	38	0.47

aldehyde dehydrogenase 1 family, member B1	ALDH1B1	84	40	0.47
fibronectin leucine rich transmembrane protein 2	FLRT2	275	130	0.47
hypothetical protein PRO2900		63	30	0.47
cell death regulator aven		254	120	0.47
histidine decarboxylase	HDC	73	35	0.47
CUG triplet repeat, RNA binding protein 2	CUGBP2	126	59	0.47
chromosome 1 open reading frame 17	C1orf17	76	36	0.47
GATA binding protein 2	GATA2	251	118	0.47
hemochromatosis	HFE	153	72	0.47
tight junction protein 2 (zona occludens 2)	TJP2	285	134	0.47
PTPL1-associated RhoGAP 1		591	277	0.47
thrombospondin 3	THBS3	202	95	0.47
CD59 antigen p18-20	CD59	1986	930	0.47
glypican 3	GPC3	56	26	0.47
cytidine monophosphate-N-acetylneuraminic acid hydroxylase	CMAH	104	49	0.47
homeo box C10	HOXC10	72	34	0.47

hypothetical protein FLJ10044		904	422	0.47
hypothetical protein FLJ12668		61	29	0.47
protein tyrosine phosphatase, non-receptor type 21	PTPN21	71	33	0.47
EphA3	EPHA3	125	58	0.47
septin 6		214	99	0.47
transmembrane 6 superfamily member 1	TM6SF1	127	59	0.46
nuclear transcription factor Y, beta	NFYB	109	50	0.46
deoxyribonuclease I-like 1	DNASE1L1	185	86	0.46
CGI-06 protein		603	280	0.46
LPAP for lysophosphatidic acid phosphatase		154	72	0.46
bone morphogenetic protein 6	BMP6	104	48	0.46
laminin, alpha 3 (nicein (150kD), kalinin (165kD), BM600 (150kD), epilegrin)	LAMA3	246	114	0.46
SH3-domain binding protein 4	SH3BP4	483	223	0.46
integrin, alpha 3 (antigen CD49C, alpha 3 subunit of VLA-3 receptor)	ITGA3	199	92	0.46
KIAA0870 protein		178	82	0.46

retinol binding protein 1, cellular	RBP1	422	194	0.46
KIAA0790 protein	KIAA0790	635	292	0.46
ectonucleoside triphosphate diphosphohydrolase 1	ENTPD1	1096	504	0.46
protein kinase, AMP-activated, beta 1 non-catalytic subunit	PRKAB1	104	48	0.46
heat shock 70kD protein 1A	HSPA1A	1140	524	0.46
sema domain, immunoglobulin domain (Ig), short basic domain, secreted, (semaphorin) 3F	SEMA3F	345	158	0.46
nuclear factor I/B	NFIB	1084	497	0.46
insulin-like growth factor 1 (somatomedin C)	IGF1	329	151	0.46
butyrophilin, subfamily 3, member A3	BTN3A3	134	62	0.46
nipsnap homolog 1 (C. elegans)	NIPSNAP1	269	123	0.46
3-oxoacid CoA transferase	OXCT	476	217	0.46
F-box and leucine-rich repeat protein 5	FBXL5	336	153	0.45
elastin (supravalvular aortic stenosis, Williams-Beuren syndrome)	ELN	128	58	0.45
nuclear receptor subfamily 3, group C, member 1	NR3C1	456	207	0.45
chromosome 18 open reading frame 1	C18orf1	97	44	0.45

myxovirus (influenza virus) resistance 1, interferon-inducible protein p78 (mouse)	MX1	248	113	0.45
solute carrier family 7 (cationic amino acid transporter, y+ system), member 4	SLC7A4	101	46	0.45
KIAA0237 gene product		119	54	0.45
epithelial V-like antigen 1	EVA1	57	26	0.45
dual specificity phosphatase 1	DUSP1	2903	1315	0.45
KIAA1058 protein		250	113	0.45
biotinidase	BTD	115	52	0.45
SBBI31 protein		76	34	0.45
phosphotriesterase related	PTER	59	27	0.45
hypothetical protein FLJ20515		79	36	0.45
rTS beta protein		170	77	0.45
prostaglandin E receptor 3 (subtype EP3)	PTGER3	274	123	0.45
aspartylglucosaminidase	AGA	82	37	0.45
junctional adhesion molecule 2	JAM2	618	278	0.45
KIAA0680 gene product		448	200	0.45

protein tyrosine phosphatase, receptor type, C	PTPRC	64	29	0.45
macrophage lectin 2 (calcium dependent)		57	26	0.45
cytoskeleton-associated protein 4	CKAP4	920	411	0.45
actin related protein 2/3 complex, subunit 1B (41 kD)	ARPC1B	648	289	0.45
KIAA0680 gene product		429	191	0.45
ribonuclease, RNase A family, 1 (pancreatic)	RNASE1	1075	479	0.45
oxysterol binding protein-like 10	OSBPL10	259	115	0.45
phosphoprotein enriched in astrocytes 15	PEA15	1167	519	0.44
inositol 1,4,5-triphosphate receptor, type 2	ITPR2	62	27	0.44
protein C receptor, endothelial (EPCR)	PROCR	209	92	0.44
cyclin-dependent kinase 8	CDK8	172	76	0.44
fibrillin 1 (Marfan syndrome)	FBN1	349	154	0.44
phospholipase C, beta 4	PLCB4	176	78	0.44
F-box only protein 9	FBXO9	602	265	0.44
ectodermal-neural cortex (with BTB-like domain)	ENC1	273	120	0.44
KIAA0427 gene product		195	86	0.44
Kallmann syndrome 1 sequence	KAL1	110	48	0.44

phosphatidylinositol glycan, class K	PIGK	222	98	0.44
calcitonin receptor-like	CALCRL	294	129	0.44
growth arrest and DNA-damage-inducible, beta	GADD45B	346	151	0.44
deleted in liver cancer 1	DLC1	1185	518	0.44
protein tyrosine phosphatase, receptor type, E	PTPRE	186	81	0.44
nephroblastoma overexpressed gene	NOV	277	120	0.44
HSPC019 protein		266	116	0.44
fibulin 5	FBLN5	769	334	0.43
N-acetyltransferase 1 (arylamine N-acetyltransferase)	NAT1	101	44	0.43
a disintegrin-like and metalloprotease (reprolysin type) with thrombospondin type 1 motif, 2	ADAMTS2	112	49	0.43
core-binding factor, runt domain, alpha subunit 2; translocated to, 3	CBFA2T3	102	44	0.43
hypothetical protein		340	147	0.43
neurotrophin 3	NTF3	63	27	0.43
likely ortholog of mouse zinc finger homeodomain 4		125	54	0.43
RGC32 protein		519	223	0.43

small inducible cytokine A2 (monocyte chemotactic protein 1)	SCYA2	164	70	0.43
Sac domain-containing inositol phosphatase 2		363	155	0.43
hypothetical protein FLJ10261		98	42	0.43
guanylate cyclase 1, soluble, beta 3	GUCY1B3	349	149	0.43
C-type (calcium dependent, carbohydrate-recognition domain) lectin, superfamily member 12	CLECSF12	64	27	0.43
cathepsin C	CTSC	391	166	0.43
protein tyrosine phosphatase, receptor type, M	PTPRM	562	239	0.43
phosphatidic acid phosphatase type 2B	PPAP2B	1174	499	0.42
minor histocompatibility antigen HA-1		74	31	0.42
hypothetical protein SMAP31		693	294	0.42
ectodermal-neural cortex (with BTB-like domain)	ENC1	61	26	0.42
hemoglobin, gamma G	HBG2	95	40	0.42
sushi-repeat-containing protein, X chromosome	SRPX	640	271	0.42
muscleblind-like (Drosophila)	MBNL	1990	841	0.42
SWAP-70 protein		244	103	0.42

lumican	LUM	1010	426	0.42
hypothetical protein FLJ21212		60	25	0.42
hypothetical protein, expressed in osteoblast		204	86	0.42
hypothetical protein FLJ11715		96	41	0.42
transmembrane 4 superfamily member 1	TM4SF1	418	176	0.42
DKFZP564J102 protein		107	45	0.42
monoglyceride lipase	MGLL	588	248	0.42
KIAA0443 gene product		491	206	0.42
RAS (RAD and GEM)-like GTP-binding	REM	150	63	0.42
D component of complement (adipsin)	DF	69	29	0.42
flavin containing monooxygenase 2	FMO2	160	67	0.42
frizzled homolog 1 (Drosophila)	FZD1	181	76	0.42
KIAA0427 gene product		85	36	0.42
tropomyosin 1 (alpha)	TPM1	167	70	0.42
tensin	TNS	178	74	0.42
KIAA0768 protein		84	35	0.42
exostoses (multiple) 1	EXT1	374	156	0.42

hypothetical protein FLJ10718		227	95	0.42
ATP-binding cassette, sub-family A (ABC1), member 3	ABCA3	83	35	0.42
RAN binding protein 17	RANBP17	61	25	0.42
absent in melanoma 1	AIM1	150	62	0.42
myelin protein zero (Charcot-Marie-Tooth neuropathy 1B)	MPZ	73	30	0.42
cysteine-rich protein 1 (intestinal)	CRIP1	304	126	0.42
KIAA1026 protein		182	76	0.42
tetranectin (plasminogen binding protein)	TNA	644	268	0.42
CUG triplet repeat, RNA binding protein 2	CUGBP2	139	58	0.42
guanine nucleotide exchange factor for Rap1; M-Ras-regulated GEF		277	115	0.42
insulin-like growth factor 1 (somatomedin C)	IGF1	183	76	0.41
related RAS viral (r-ras) oncogene homolog 2	RRAS2	158	66	0.41
manic fringe homolog (Drosophila)	MFNG	62	26	0.41
cysteine-rich motor neuron 1	CRIM1	241	100	0.41
carboxypeptidase, vitellogenic-like	CPVL	149	62	0.41
v-fos FBJ murine osteosarcoma viral oncogene homolog	FOS	1488	615	0.41

mitogen-activated protein kinase 9	MAPK9	221	91	0.41
tyrosylprotein sulfotransferase 2	TPST2	212	88	0.41
hypothetical protein FLJ22029		145	60	0.41
neurocalcin delta		135	55	0.41
tumour necrosis factor (ligand) superfamily, member 10	TNFSF10	206	84	0.41
Chediak-Higashi syndrome 1	CHS1	216	88	0.41
protein tyrosine phosphatase, receptor type, B	PTPRB	358	146	0.41
G protein-coupled receptor 48	GPR48	97	39	0.41
hypothetical protein FLJ10970		66	27	0.40
hypothetical protein FLJ10948		501	202	0.40
ribonuclease, RNase A family, 4	RNASE4	315	127	0.40
hypothetical protein FLJ11275		81	32	0.40
hypothetical protein FLJ10298		227	91	0.40
leukotriene C4 synthase	LTC4S	75	30	0.40
3'-phosphoadenosine 5'-phosphosulfate synthase 2	PAPSS2	96	39	0.40
tubulin, beta polypeptide	TUBB	89	36	0.40
insulin induced protein 2		358	144	0.40

mucin 1, transmembrane	MUC1	125	50	0.40
gap junction protein, alpha 1, 43kD (connexin 43)	GJA1	1100	439	0.40
chromosome 8 open reading frame 1	C8orf1	114	45	0.40
tryptase beta 2	TPSB2	212	84	0.40
mucosa associated lymphoid tissue lymphoma translocation gene 1	MALT1	79	31	0.39
KIAA0747 protein		469	185	0.39
decay accelerating factor for complement (CD55, Cromer blood group system)	DAF	98	38	0.39
hypothetical protein FLJ11082		108	42	0.39
hypothetical protein PP1665		161	63	0.39
RAB27A, member RAS oncogene family	RAB27A	186	73	0.39
steroid sulfatase (microsomal), arylsulfatase C, isozyme S	STS	74	29	0.39
transmembrane 4 superfamily member 1	TM4SF1	1540	604	0.39
LIM homeobox protein 6		385	151	0.39
TEK tyrosine kinase, endothelial (venous malformations, multiple cutaneous and mucosal)	TEK	228	89	0.39

cysteine-rich, angiogenic inducer, 61	CYR61	1007	394	0.39
chromosome 6 open reading frame 34	C6orf34	641	250	0.39
antigen identified by monoclonal antibody MRC OX-2	MOX2	147	57	0.39
nuclear receptor subfamily 2, group F, member 2	NR2F2	995	388	0.39
cystatin F (leukocystatin)	CST7	66	26	0.39
cysteine-rich motor neuron 1	CRIM1	572	223	0.39
hypothetical protein MGC5363		502	195	0.39
hypothetical protein FLJ22297		100	39	0.39
Wolfram syndrome 1 (wolframin)	WFS1	665	258	0.39
cellular retinoic acid binding protein 2	CRABP2	144	56	0.39
myosin 5C	MYO5C	433	167	0.39
cat eye syndrome chromosome region, candidate 1	CECR1	79	30	0.39
GTP cyclohydrolase 1 (dopa-responsive dystonia)	GCH1	84	32	0.38
hypothetical protein FLJ12428		361	138	0.38
hypothetical protein FLJ10781		210	80	0.38
polycystic kidney disease 2 (autosomal dominant)	PKD2	1521	579	0.38
Cbp/p300-interacting transactivator, with Glu/Asp-rich				

carboxy-terminal domain, 2				
hydroxyprostaglandin dehydrogenase 15-(NAD)	HPGD	176	66	0.38
trefoil factor 3 (intestinal)	TFF3	103	39	0.38
follistatin-like 1	FSTL1	3521	1327	0.38
synaptogyrin 2	SYNGR2	475	179	0.38
hypothetical protein FLJ23056		151	57	0.37
phospholipase C, beta 4	PLCB4	74	27	0.37
tumour necrosis factor (ligand) superfamily, member 10	TNFSF10	704	262	0.37
transducin-like enhancer of split 2, homolog of Drosophila E(sp1)	TLE2	620	230	0.37
periplakin	PPL	107	40	0.37
hydroxysteroid (11-beta) dehydrogenase 1	HSD11B1	146	54	0.37
cysteine-rich protein 2	CRIP2	527	195	0.37
vascular endothelial growth factor C	VEGFC	280	104	0.37
phosphorylase, glycogen; brain	PYGB	528	195	0.37
DKFZP566D213 protein		132	49	0.37
villin 2 (ezrin)	VIL2	114	42	0.37

FERM, RhoGEF (ARHGEF) and pleckstrin domain protein 1 (chondrocyte-derived)	FARP1	525	194	0.37
prostaglandin E receptor 3 (subtype EP3)	PTGER3	987	363	0.37
EGF-containing fibulin-like extracellular matrix protein 1	EFEMP1	512	188	0.37
prostaglandin E receptor 3 (subtype EP3)	PTGER3	1001	366	0.37
steroid sulfatase (microsomal), arylsulfatase C, isozyme S	STS	164	59	0.36
phosphodiesterase 4B, cAMP-specific (phosphodiesterase E4 dunce homolog, Drosophila)	PDE4B	77	28	0.36
prostaglandin E receptor 3 (subtype EP3)	PTGER3	960	347	0.36
proprotein convertase subtilisin/kexin type 5	PCSK5	99	36	0.36
single Ig IL-1R-related molecule	SIGIRR	247	89	0.36
I factor (complement)	IF	249	89	0.36
cysteine-rich, angiogenic inducer, 61	CYR61	1391	497	0.36
heat shock 70kD protein 6 (HSP70B')	HSPA6	137	49	0.36
fibrillin 1 (Marfan syndrome)	FBN1	1748	623	0.36
hypothetical protein CG003		473	168	0.36
dystrophin (muscular dystrophy, Duchenne and Becker				

types)				
heat shock 70kD protein 1A	HSPA1A	2623	927	0.35
transcription elongation factor A (SII)-like 1	TCEAL1	647	226	0.35
hypothetical protein MGC10848		395	137	0.35
myosin regulatory light chain interacting protein		641	223	0.35
met proto-oncogene (hepatocyte growth factor receptor)	MET	216	75	0.35
protein tyrosine phosphatase-like (proline instead of catalytic arginine), member a	PTPLA	456	158	0.35
hypothetical protein FLJ21313		171	59	0.35
Kruppel-like factor 4 (gut)	KLF4	216	75	0.35
Down syndrome critical region gene 1-like 1	DSCR1L1	346	119	0.34
CEGP1 protein		131	45	0.34
nitric oxide synthase 3 (endothelial cell)	NOS3	74	25	0.34
nicotinamide N-methyltransferase	NNMT	328	112	0.34
colony stimulating factor 2 receptor, beta, low-affinity (granulocyte-macrophage)	CSF2RB	107	36	0.34
hepatocellular carcinoma-associated antigen 112		272	92	0.34

coagulation factor II (thrombin) receptor	F2R	141	48	0.34
nuclear receptor subfamily 3, group C, member 2	NR3C2	159	54	0.34
p53-induced protein PIGPC1		140	47	0.34
microtubule-associated protein like echinoderm EMAP		124	42	0.34
Nijmegen breakage syndrome 1 (nibrin)	NBS1	199	67	0.34
latent transforming growth factor beta binding protein 2	LTBP2	1490	501	0.34
melanoma cell adhesion molecule	MCAM	396	133	0.34
DKFZP586F1018 protein		116	39	0.33
hydroxyprostaglandin dehydrogenase 15-(NAD)	HPGD	128	43	0.33
RAS guanyl releasing protein 2 (calcium and DAG-regulated)	RASGRP2	87	29	0.33
amine oxidase, copper containing 3 (vascular adhesion protein 1)	AOC3	702	234	0.33
hypothetical protein FLJ22690		432	144	0.33
EGF-containing fibulin-like extracellular matrix protein 1	EFEMP1	3011	1002	0.33
insulin-like growth factor 2 (somatomedin A)	IGF2	943	314	0.33
FAT tumour suppressor homolog 1 (Drosophila)	FAT	453	151	0.33

adipose specific 2		433	144	0.33
matrix metalloproteinase 19	MMP19	78	26	0.33
solute carrier family 22 (extraneuronal monoamine transporter), member 3	SLC22A3	301	99	0.33
hypothetical protein		567	186	0.33
serine protease inhibitor, Kunitz type, 2	SPINT2	126	41	0.33
hypothetical protein FLJ13612		481	157	0.33
neurexin 3	NRXN3	89	29	0.32
SPRY domain-containing SOCS box protein SSB-1		138	45	0.32
frizzled-related protein	FRZB	250	81	0.32
core-binding factor, runt domain, alpha subunit 2; translocated to, 1; cyclin D-related	CBFA2T1	113	37	0.32
TGFB inducible early growth response 2	TIEG2	295	95	0.32
chondroitin sulfate proteoglycan 2 (versican)	CSPG2	894	286	0.32
dipeptidylpeptidase VI	DPP6	322	102	0.32
ornithine decarboxylase 1	ODC1	1321	416	0.31
KIAA0475 gene product		379	119	0.31

decay accelerating factor for complement (CD55, Cromer blood group system)	DAF	128	40	0.31
ras homolog gene family, member E	ARHE	1279	401	0.31
hypothetical protein FLJ14054		601	188	0.31
serine (or cysteine) proteinase inhibitor, clade B (ovalbumin), member 1	SERPINB1	86	27	0.31
t-complex-associated-testis-expressed 1-like	TCTE1L	1171	364	0.31
tenascin XB	TNXB	105	33	0.31
glycoprotein A repetitions predominant	GARP	311	96	0.31
transcription elongation factor B (SIII), polypeptide 3 (110kD, elongin A)	TCEB3	289	89	0.31
KIAA0193 gene product		677	208	0.31
extracellular matrix protein 2, female organ and adipocyte specific	ECM2	340	104	0.31
glutaminase	GLS	135	41	0.31
interleukin 1 receptor, type I	IL1R1	607	185	0.31
fibromodulin	FMOD	774	236	0.31

neuroepithelial cell transforming gene 1	NET1	458	140	0.31
nidogen (enactin)	NID	215	66	0.30
insulin-like growth factor binding protein 6	IGFBP6	549	167	0.30
follistatin-like 3 (secreted glycoprotein)	FSTL3	231	70	0.30
myristoylated alanine-rich protein kinase C substrate	MARCKS	737	224	0.30
guanosine monophosphate reductase	GMPR	121	37	0.30
calcitonin receptor-like	CALCRL	309	94	0.30
glutathione S-transferase M5	GSTM5	181	55	0.30
peptidylprolyl isomerase C (cyclophilin C)	PPIC	369	111	0.30
dimethylarginine dimethylaminohydrolase 1	DDAH1	932	281	0.30
hypothetical protein DKFZp566J091		1326	400	0.30
myosin, light polypeptide 2, regulatory, cardiac, slow	MYL2	93	28	0.30
serum-inducible kinase		276	83	0.30
glutaredoxin (thioltransferase)	GLRX	226	68	0.30
ectonucleotide pyrophosphatase/phosphodiesterase 4 (putative function)	ENPP4	175	52	0.30
uncharacterized bone marrow protein BM046		143	43	0.30

platelet-derived growth factor receptor-like	PDGFRL	182	54	0.30
meningioma (disrupted in balanced translocation) 1	MN1	132	39	0.30
antigen identified by monoclonal antibody MRC OX-2	MOX2	489	145	0.30
KIAA0022 gene product		541	161	0.30
tenascin XB	TNXB	1149	341	0.30
cysteine dioxygenase, type I	CDO1	96	29	0.30
hypothetical protein FLJ20909		86	26	0.30
tubulin, beta polypeptide	TUBB	1100	324	0.30
serine (or cysteine) proteinase inhibitor, clade A (alpha-1 antiproteinase, antitrypsin), member 1	SERPINA1	132	39	0.29
platelet/endothelial cell adhesion molecule (CD31 antigen)	PECAM1	811	239	0.29
tenascin XB	TNXB	946	276	0.29
pre-alpha (globulin) inhibitor, H3 polypeptide	ITIH3	87	25	0.29
1,2-alpha-mannosidase IC		256	74	0.29
B cell RAG associated protein		265	76	0.29
KIAA0537 gene product		899	256	0.28
deafness, autosomal dominant 5	DFNA5	696	197	0.28

calsequestrin 2 (cardiac muscle)	CASQ2	154	44	0.28
purinergic receptor P2X, ligand-gated ion channel, 1	P2RX1	160	45	0.28
hypothetical protein FLJ20568		229	65	0.28
phosphodiesterase 4D interacting protein (myomegalin)	PDE4DIP	249	70	0.28
betaine-homocysteine methyltransferase 2	BHMT2	129	36	0.28
annexin A1	ANXA1	1647	459	0.28
von Willebrand factor	VWF	2585	718	0.28
CUG triplet repeat, RNA binding protein 2	CUGBP2	1234	342	0.28
hyaluronoglucosaminidase 1	HYAL1	99	27	0.28
BENE protein		285	79	0.28
steroid sulfatase (microsomal), arylsulfatase C, isozyme S	STS	174	48	0.28
chondroitin sulfate proteoglycan 2 (versican)	CSPG2	1193	329	0.28
hypothetical protein FLJ11088		149	41	0.27
dual specificity phosphatase 1	DUSP1	93	25	0.27
nicotinamide N-methyltransferase	NNMT	225	61	0.27
solute carrier family 2 (facilitated glucose transporter), member 10	SLC2A10	193	52	0.27

hypothetical protein FLJ13078		245	66	0.27
frizzled-related protein	FRZB	415	112	0.27
insulin-like growth factor 2 (somatomedin A)	IGF2	148	40	0.27
phospholipase C, epsilon	PLCE	226	60	0.27
CTP synthase	CTPS	662	177	0.27
chimerin (chimaerin) 1	CHN1	260	69	0.27
Ras association (RalGDS/AF-6) domain family 2	RASSF2	614	162	0.26
thrombospondin 4	THBS4	764	201	0.26
nuclear receptor subfamily 2, group F, member 2	NR2F2	2002	524	0.26
slit homolog 3 (Drosophila)	SLIT3	611	160	0.26
regulator of Fas-induced apoptosis		122	32	0.26
dynein, cytoplasmic, intermediate polypeptide 1	DNCI1	121	31	0.26
insulin-like growth factor 1 (somatomedin C)	IGF1	853	220	0.26
apolipoprotein D	APOD	886	229	0.26
hypothetical protein DKFZp434B044		723	186	0.26
Thy-1 cell surface antigen	THY1	551	141	0.26
downregulated in ovarian cancer 1		2690	689	0.26

complement-c1q tumour necrosis factor-related protein; likely ortholog of mouse CORS26		188	48	0.26
neuroepithelial cell transforming gene 1	NET1	781	200	0.26
actin binding LIM protein	ABLIM	1069	271	0.25
diphtheria toxin receptor (heparin-binding epidermal growth factor-like growth factor)	DTR	406	103	0.25
hypothetical protein FLJ11110		439	110	0.25
KIAA0938 protein		160	40	0.25
CGI-44 protein; sulfide dehydrogenase like (yeast)		520	130	0.25
matrix metalloproteinase 7 (matrilysin, uterine)	MMP7	261	65	0.25
Thy-1 cell surface antigen	THY1	479	118	0.25
platelet/endothelial cell adhesion molecule (CD31 antigen)	PECAM1	659	163	0.25
type I transmembrane protein Fn14		450	111	0.25
regulator of G-protein signalling 4	RGS4	246	61	0.25
protein S (alpha)	PROS1	877	216	0.25
glutathione peroxidase 3 (plasma)	GPX3	1278	313	0.25
diphtheria toxin receptor (heparin-binding epidermal growth				

factor-like growth factor)				
immunoglobulin lambda locus	IGL	172	42	0.24
cathepsin Z	CTSZ	243	59	0.24
chondroitin sulfate proteoglycan 2 (versican)	CSPG2	234	56	0.24
chemokine (C-X3-C) receptor 1	CX3CR1	461	110	0.24
procollagen C-endopeptidase enhancer	PCOLCE	427	101	0.24
coxsackie virus and adenovirus receptor	CXADR	590	139	0.24
MCF.2 cell line derived transforming sequence-like	MCF2L	145	34	0.24
hypothetical protein FLJ23356		123	29	0.23
thrombomodulin	THBD	375	86	0.23
core-binding factor, runt domain, alpha subunit 2; translocated to, 1; cyclin D-related	CBFA2T1	359	82	0.23
carboxypeptidase E	CPE	1458	333	0.23
phosphatidylserine-specific phospholipase A1alpha		120	27	0.23
hypothetical protein PP1665	PP1665	335	75	0.23
chondroitin sulfate proteoglycan 2 (versican)	CSPG2	176	40	0.22
hypothetical protein FLJ22662		283	64	0.22

serine (or cysteine) proteinase inhibitor, clade G (C1 inhibitor), member 1, (angioedema, hereditary)	SERPING1	1716	383	0.22
platelet/endothelial cell adhesion molecule (CD31 antigen)	PECAM1	1872	417	0.22
forkhead box C1	FOXC1	133	30	0.22
serum/glucocorticoid regulated kinase	SGK	748	166	0.22
osteoblast specific factor 2 (fasciclin I-like)		785	174	0.22
sema domain, immunoglobulin domain (Ig), short basic domain, secreted, (semaphorin) 3B	SEMA3B	196	43	0.22
NADPH oxidase 4	NOX4	170	37	0.22
KIAA0977 protein		239	52	0.22
FERM, RhoGEF (ARHGEF) and pleckstrin domain protein 1 (chondrocyte-derived)	FARP1	382	83	0.22
glycoprotein M6A	GPM6A	180	39	0.22
transforming growth factor, beta-induced, 68kD	TGFBI	2386	513	0.22
regulator of G-protein signalling 4	RGS4	126	27	0.21
kallikrein 6 (neurosin, zyme)	KLK6	146	30	0.21
mesenchyme homeo box 1	MEOX1	192	40	0.21

G protein-coupled receptor		343	70	0.20
hypothetical protein LOC57333	LOC57333	159	32	0.20
angiotensin receptor-like 1	AGTRL1	476	97	0.20
tuftelin 1	TUFT1	314	64	0.20
activated leucocyte cell adhesion molecule	ALCAM	1375	277	0.20
synaptotagmin I	SYT1	255	51	0.20
collagen, type XVI, alpha 1	COL16A1	1180	236	0.20
laminin, alpha 2 (merosin, congenital muscular dystrophy)	LAMA2	203	40	0.20
Leman coiled-coil protein		793	156	0.20
peptidylprolyl isomerase C (cyclophilin C)	PPIC	717	141	0.20
LR8 protein		248	48	0.20
5' nucleotidase (CD73)	NT5	529	103	0.20
slit homolog 2 (Drosophila)	SLIT2	888	171	0.19
ubiquitin carboxyl-terminal esterase L1 (ubiquitin thiolesterase)	UCHL1	209	40	0.19
glutaminase	GLS	417	79	0.19
thrombomodulin	THBD	190	36	0.19

hypothetical protein similar to small G proteins, especially RAP-2A		1068	194	0.18
Arg/Abl-interacting protein ArgBP2		632	114	0.18
latent transforming growth factor beta binding protein 1	LTBP1	1355	242	0.18
thrombospondin 1	THBS1	315	56	0.18
integrin beta 1 binding protein (melusin) 2	ITGB1BP2	280	49	0.18
hypothetical protein similar to small G proteins, especially RAP-2A		450	79	0.18
S100 calcium binding protein A4	S100A4	867	152	0.17
glutaminase	GLS	1052	184	0.17
KIAA1102 protein		195	33	0.17
collagen, type XV, alpha 1	COL15A1	2111	342	0.16
lysyl oxidase	LOX	166	27	0.16
dual adaptor of phosphotyrosine and 3-phosphoinositides	DAPP1	525	84	0.16
activated leucocyte cell adhesion molecule	ALCAM	431	69	0.16
connective tissue growth factor	CTGF	3466	552	0.16
neuropeptide Y receptor Y1	NPY1R	381	58	0.15

chromosome 18 open reading frame 1	C18orf1	169	26	0.15
Purkinje cell protein 4	PCP4	2239	340	0.15
DKFZP586L151 protein		466	69	0.15
natriuretic peptide receptor A/guanylate cyclase A (atrionatriuretic peptide receptor A)	NPR1	401	59	0.15
5-hydroxytryptamine (serotonin) receptor 2A	HTR2A	479	71	0.15
zinc finger protein 185 (LIM domain)	ZNF185	403	58	0.14
nidogen (enactin)	NID	415	60	0.14
scrapie responsive protein 1		2315	326	0.14
myelin basic protein	MBP	210	30	0.14
KIAA1102 protein		839	113	0.13
hemoglobin, alpha 2	HBA2	4710	614	0.13
thrombospondin 1	THBS1	619	80	0.13
inhibin, beta A (activin A, activin AB alpha polypeptide)	INHBA	707	91	0.13
immunoglobulin heavy constant gamma 3 (G3m marker)	IGHG3	312	40	0.13
death-associated protein kinase 1	DAPK1	624	79	0.13
hemoglobin, alpha 1	HBA1	3249	410	0.13

glycoprotein M6A	GPM6A	210	26	0.13
complement component 4A	C4A	546	68	0.13
latent transforming growth factor beta binding protein 1	LTBP1	417	52	0.12
Duffy blood group	FY	1674	204	0.12
KIAA1102 protein		680	83	0.12
lysyl oxidase-like 1	LOXL1	1041	126	0.12
proline arginine-rich end leucine-rich repeat protein	PRELP	1417	171	0.12
thrombospondin 1	THBS1	640	77	0.12
KIAA0977 protein		322	38	0.12
keratin 18	KRT18	498	59	0.12
WAP four-disulfide core domain 1	WFDC1	629	70	0.11
immunoglobulin lambda joining 3	IGLJ3	310	34	0.11
Microfibril-associated glycoprotein-2		2113	224	0.11
hemoglobin, beta	HBB	3820	371	0.10
H factor (complement)-like 2	HFL2	389	38	0.10
hemoglobin, alpha 2	HBA2	3324	315	0.09
insulin-like growth factor binding protein 2 (36kD)	IGFBP2	3426	304	0.09

elastin (supravalvular aortic stenosis, Williams-Beuren syndrome)	ELN	767	59	0.08
alcohol dehydrogenase IB (class I), beta polypeptide	ADH1B	1126	71	0.06
dermatopontin	DPT	420	26	0.06
aldehyde dehydrogenase 1 family, member A1	ALDH1A1	547	33	0.06
complement component 3	C3	576	33	0.06
complement component 7	C7	1525	87	0.06
alcohol dehydrogenase IB (class I), beta polypeptide	ADH1B	570	30	0.05
retinoic acid receptor responder (tazarotene induced) 2	RARRES2	618	29	0.05
oxytocin receptor	OXTR	1282	42	0.03